

Investigation of the In-Plane Cyclic Behaviour of Masonry Infill Walls Strengthened With Textile Reinforced Mortar

THESIS

Submitted in partial fulfillment of the requirements for the degree of

DOCTOR OF PHILOSOPHY

by

M. JAYA KUMAR BHASKAR

Under the supervision of

Prof. Dipendu Bhunia

Professor, Department of Civil Engineering

BITS Pilani, Pilani Campus, Rajasthan – 333031, India

&

Dr. Lampros Koutas

Assistant Professor, Department of Civil Engineering

University of Thessaly, Pedion Areos, Volos, GR – 38334, Greece



BITS Pilani
Pilani | Dubai | Goa | Hyderabad

BIRLA INSTITUTE OF TECHNOLOGY AND SCIENCE (BITS), PILANI

2024



Birla Institute of Technology & Science, Pilani

Pilani Campus

CERTIFICATE

This is to certify that the thesis entitled, “**Investigation of the In-Plane Cyclic Behaviour of Masonry Infill Walls Strengthened with Textile Reinforced Mortar**”, submitted by **M. Jaya Kumar Bhaskar**, ID No **2018PHXF0420P** for the award of Ph.D. degree of the Institute embodies original work done by him under our supervision.

Signature of the Supervisor

Name: **Dipendu Bhunia**

Designation: Professor

University: BITS Pilani

Signature of the Co-Supervisor

Name: **Lampros Koutas**

Designation: Assistant Professor

University: University of Thessaly

ACKNOWLEDGEMENTS

I take this opportunity with great pleasure to thank Prof. Dipendu Bhunia, Department of Civil Engineering, BITS Pilani and Dr. Lampros Koutas, Assistant Professor, Department of Civil Engineering, University of Thessaly, Greece for guiding me in defining my objectives and providing with a platform and to work on. In particular, I am grateful to the Department of Civil Engineering, BITS Pilani for having sponsored the research undertaken.

I sincerely thank Prof. Shamsheer Bahadur Singh and Dr. Rajesh Kumar, my Doctoral Advisory Committee members, for their suggestions during the course of the research. I also thank Prof. Anupam Singhal (Head, Department of Civil Engineering, BITS Pilani) and Prof. Anshuman, Professor, former Head of Department, Department of Civil Engineering, BITS Pilani for the patronage and encouragement given by them throughout the project period. I thank the lab in-charge Dr. Subhasis Pradhan and former lab in-charge Dr. S. N. Patel for their continuous support and encouragement throughout to conduct the experiment whenever required.

For moral support and emotional support, I will always remain in debt to the entire staff of the Department of Civil Engineering, BITS Pilani. I thank the Institute for all the support and all of its faculty members at the Department of Civil Engineering who delivered lectures on new avenues in Civil Engineering that gave me confidence to work in the field I have chosen. I thank and sincerely appreciate various staff members of all the laboratories in the Civil Department for their guidance.

This thesis would not have been possible without the confidence, endurance, and support of my mother Smt. Vani Satyanarayana who has given her love, teachings and moral support in every way that has brought me this far in life. Finally, I thank my father, sister, and friends who have been a source of encouragement. Last but not least, I want to mention my wife Priyanka Roy, whose continuous help and support has inspired me to reach my goal effortlessly

JAYA KUMAR BHASKAR

ABSTRACT

Masonry infill walls (MIW) are the most popular building elements commonly used in low-rise to medium-rise reinforced concrete (RC) structures all over the globe including seismically active regions. Nevertheless, these structures usually employ the infill panels as either non-structural elements, non-load bearing walls, or partition walls that carry their self-weight whereas the surrounding RC frame is designed as a structural member that carries lateral and gravity loads. However, the vulnerability of MIW when subjected to lateral forces has substantial implications for life safety and has a significant impact on the building's functional progress due to their brittle nature. As non-structural components, MIW modifies the structure's dynamic behavioral characteristics such as deformation resisting capacity, strength, stiffness, and natural frequency, leading to differences in overall structural performance. In spite of having significant stiffness contribution to the structural system, the fundamental nature of infills being brittle, the seismic behaviour of the surrounding RC frame is impacted mostly in a negative manner. The insight obtained from previous studies has proven that RC structures with MIW have many unintended effects during seismic activities such as the effect of soft-story, short-column effect, torsional effect, and in-plane (IP)/out-of-plane (OOP) collapse. In addition to this, if an opening is present in an infill wall, the behaviour of the structure will be considerably modified when subjected to lateral forces. To examine the changes that occur in the performance of the infill systems with openings under lateral forces require laboratory experiments designed realistically (closer to practical cases). Furthermore, textile reinforced mortar (TRM) composites are retrofitting techniques used for strengthening masonry structures giving them the required strength and stability to withstand external forces. Unfortunately, most of the previous research on frames with infills concentrated either on the most basic structural setup of infill panels without openings strengthened with TRM or with openings but without strengthening the infill panels. This thesis discusses the experiments and numerical simulations along with a parametrical study conducted on MIW combining the afore-mentioned two factors i.e., openings and strengthening to study the difference in the behavioral pattern of the system and the effectiveness of TRM.

For this purpose, initially, a numerical validation study is conducted which includes the process of simulation of the experimental campaign carried out at Wellington Institute of Technology by [N. Ismail et. al. (2018)]. This analysis is carried out for the following reasons: (i) to quantitatively measure the agreement between the predictions provided by the numerical

model and the practicals represented by observations in experiments through models and provide empirical formulations and, (ii) to understand the techniques and logics behind conducting an experiment on MIW in a laboratory with different materials and check the performance under lateral loading conditions.

Next, two 2/5th scaled, single-bay single-story MIW with RC frame test specimens having an aspect ratio (the length-to-height ratio of the infill wall) of 1.56 were constructed for this study. One specimen served as a conventional specimen unreinforced specimen (URS), and the other had an AR-resistant glass fiber TRM grid retrofitted into the wall, double reinforced specimen (DRS). The surrounding RC frame is made to be more similar to the practical scenario by applying ductile detailing which is common for both the specimens. Burnt clay red brick units that had a nominal compression strength of 6.83 MPa were set in a running stack bond pattern using a cement-sand mortar. With a volumetric ratio of 1:3, the brick-and-mortar layers were kept at a consistent thickness of around 12 mm in both the bed and head joints. A lintel beam is provided exactly above the opening by maintaining its configurations (dimension and reinforcement) and properties (grade of steel and concrete) standard in the experimental tests. A concrete mix having a nominal strength of 20 MPa was adopted to build the frames of the test specimens. Both beam and column had main reinforcement with steel rebars of 12 mm nominal diameter, while the shear reinforcement was provided with a nominal diameter of 8 mm. To prevent joint failure at the beam-column connection, top longitudinal reinforcing bars from the beam were extended inside the column with an embedment length of 450 mm while the bottom rebars were bent upside into the column at both ends. The foundation beam, intended as a doubly reinforced section and purposefully made robust has two bars of 12 mm diameter in the compression zone and three bars of 16 mm diameter in the tension zone, with a 20 mm clear cover on all sides. 10 mm stirrups placed with center spacings of 200 mm on both ends and 170 mm in the midspan are tied around the bars. To represent a permanent rigid connection, column longitudinal bars with a development length of 500 mm were also extended into the foundation beam. The test specimens with utmost care were placed on a strong floor, which was provided with a rigid connection by grouting six anchor bars to the floor through the foundation beam. The specimens were tested under quasi-static reversed cyclic lateral loading that was controlled by sinusoidal displacement.

Regarding numerical analysis, the study elaborated on the development of a numerical model to simulate the non-linear structural cyclic behaviour of the infill wall with an RC frame.

The numerical analysis was carried out in the finite element (FE) software ABAQUS using a simplified micro-model approach. The concrete damage plasticity (CDP) model was used to simulate the non-linear behaviour of the masonry blocks and concrete. The numerical model was performed using a non-linear structural cyclic analysis of the tested specimen, which was retrofitted. In other words, the experimental tests were validated in the software ABAQUS along with a parametric study conducted to determine the significance of the full-bond scenario between the RC frame infilled with masonry and the TRM considering: (1) the location of the strengthening material on the specimen and (2) the number of layers of the strengthening material. In particular, the lateral load-displacement relationships of test specimens were numerically simulated and validated against the experimental results.

Concerning the results, it was found in the experimental investigation that significant differences in the damage patterns, resisting the deformation capacity, lateral stiffness and strength, and energy dissipation capacity were observed in the two specimens. The results showed that the URS produced 65.73% less lateral strength and stiffness and a 58.88% increase in the maximum deflection compared to the DRS specimen. This indicates that the presence of TRM significantly increased the infill wall system's lateral stiffness and strength and decreased the frame's deflection when subjected to lateral forces. The numerical validation exhibited that the model can precisely simulate the performance and predict the capacity of retrofitted masonry-infilled RC constructions. The results of observations are discussed in the form of load-displacement hysteresis loops and excursion curves. Regarding the parametric study, all retrofitted wall specimens showed a considerable improvement in the in-plane performance; some features of the wall's behaviour were found to be strongly influenced by the parameters under examination.

The suggested strengthening technique significantly increased the infill walls' capacity by up to 66% to support in-plane loads. TRM has generally been successful in improving the seismic performance of RC frames with burnt clay red brick masonry infills that are seismically vulnerable. There was a noticeable delay in the onset of cracking and damage, and the ultimate gain in lateral strength was between 50 and 70 percent. The numerical results thus show great agreement with the experimental results and the significant effectiveness of TRM.

Keywords: Unreinforced masonry, textile reinforced mortar, in-plane behaviour, concrete damage plasticity, ABAQUS, opening, quasi-static load, energy dissipation

TABLE OF CONTENTS

ACKNOWLEDGEMENTS	i
ABSTRACT	iii
TABLE OF CONTENTS	vi
LIST OF FIGURES	xiii
LIST OF TABLES	xx
ABBREVIATIONS	xxi
1 INTRODUCTION	1
1.1 Background	1
1.2 Walls	5
1.2.1 Types of Walls	5
1.2.2 Wall Openings	6
1.3 Building Materials	6
1.3.1 Bricks	6
1.3.2 Composition of Bricks	6
1.4 Masonry Infill Walls (MIW)	7
1.4.1 Types of Masonry Construction	8
1.4.2 Modes of Failure of MIW	8
1.4.3 Prevention of Failures of MIW	9
1.5 Seismic strengthening of masonry structures	10
1.5.1 Repointing Technique	11
1.5.2 Centre core Technique	12
1.5.3 Fiber Reinforced Polymer (FRP)	12
1.5.4 Textile Reinforced Mortar (TRM)	14
1.6 Comparison of Testing Methods	15
1.6.1 Monotonic Loading	16
1.6.2 Cyclic Loading	16
1.7 Aims of the Research	16

1.8	Organization of the Thesis	17
1.9	Contribution of the Thesis	18
2	LITERATURE REVIEW	20
2.1	Overview	20
2.2	Research & Development on Masonry Infilled RC Frames	21
2.3	Experimental Work	21
2.3.1	Out-of-Plane Loading	21
2.3.2	In-Plane Loading	27
2.3.3	Masonry Infill Walls Strengthened with Textile Reinforced Mortar	44
2.4	Numerical Work	46
2.5	Analytical Work	58
2.6	Fragility Functions for Masonry Infill Walls	82
2.7	Gaps in Literature and Need for Research	91
2.8	Scope of Present Study	92
	IDENTIFICATION AND EVALUATION OF FACTORS	
3	INFLUENCING THE PERFORMANCE OF MASONRY INFILL WALL (MIW)	94
3.1	Introduction	94
3.1.1	Objectives	95
3.2	Database of Past Test Used in Validation (Ismail et al., 2018)	95
3.2.1	Brief Review of the Experimental Test	95
3.3	Numerical Analysis	98
3.3.1	Numerical Simulation Approach	101
3.3.2	Interface Simulation between Expanded Bricks	104
3.3.3	Plastic Response of the Joint Interfaces	105
3.3.4	Loading and Meshing	105
3.4	Results and Discussion	106

3.5	Expression to Determine the Specimen Load Carrying Capacity	113
3.6	Summary	118
	EXPERIMENTAL INVESTIGATION OF NON-DUCTILE	
4	REINFORCED CONCRETE (RC) FRAMES WITH MASONRY	119
	INFILL WALL (MIW) WITHOUT OPENING	
4.1	Outline	119
	4.1.1 Objectives	119
4.2	Test Program and Methodology	120
	4.2.1 Configuration of the Non-Ductile RC Frame	120
	4.2.2 Configuration of the Infill Wall	122
4.3	Test Setup And Instrumentation	124
4.4	Experimental Results	125
	4.4.1 Failure Mode	125
4.5	Numerical Work	126
	4.5.1 Numerical Simulation Approach	126
	4.5.2 Numerical Simulation	127
4.6	Results and Discussion	129
	4.6.1 Strength and Displacement Ductility Ratio	130
4.7	Summary	132
	EXPERIMENTAL INVESTIGATION OF DUCTILE REINFORCED	
5	CONCRETE (RC) FRAMES WITH MASONRY INFILL WALL (MIW)	135
	WITH OPENING	
5.1	Introduction	135
	5.1.1 Objectives	135
5.2	Test program and Methodology	136
	5.2.1 Materials	136
	5.2.2 Test Specimen Preparation	138
	5.2.3 Frame Configurations	138

5.2.4	Brick Panel Configurations and Construction	140
5.3	Application of TRM System on the Masonry Wall	141
5.4	Strengthening of Specimens	143
5.4.1	Application of Fiber to the Specimen	143
5.4.2	Strengthening Procedure	144
5.5	Test Setup and Instrumentation	145
5.6	Loading Regime	148
5.7	Experimental Results	149
5.7.1	Experimental Phenomena and Load-Deformation Curves	149
5.7.2	Energy Dissipation	151
5.7.3	Hysteresis Behaviour	151
5.7.4	Stiffness Degradation	153
5.8	Summary	155
6	NUMERICAL VALIDATION AND PARAMETRIC STUDY OF TEXTILE REINFORCED MORTAR (TRM) STRENGTHENED MASONRY INFILL WALL (MIW) WITH OPENINGS	157
6.1	Overview	157
6.1.1	Objectives	157
6.2	Numerical Analysis	158
6.2.1	Numerical Simulation Approach	158
6.2.2	Constitutive Model	159
6.2.3	Concrete Damage Plasticity (CDP) Model	159
6.2.3.1	CDP Model Under Uniaxial Cyclic Loading	160
6.3	Validation of the Experimental Study	162
6.3.1	Material Properties	162
6.3.2	Interface Simulation between Expanded Bricks	163
6.3.3	Model Development in ABAQUS	166
6.4	Parametric Study	168

6.5	Results & Comparison	171
6.5.1	Stiffness and Energy Dissipation	175
6.6	Expression to Determine the Load-Carrying Capacity of the Specimen	177
6.7	Cost Analysis	180
6.7.1	Quantification of the Test Specimen	181
6.7.2	Costs Quantification of MIW Strengthening Using TRM	184
6.8	Summary	185
7	CONCLUSIONS AND FUTURE STUDY	188
7.1	Conclusions	187
7.2	Contributions of the Research Conducted	192
7.3	Limitations of the Research Conducted	192
7.2	Scope of Future Work	193
	REFERENCES	194
	LIST OF PUBLICATIONS	221
	APPENDICES	223
A.1	Appendix - 1 - Design axial load carrying capacity of the column	223
A.2	Appendix – 2 - Ductility of the unreinforced and reinforced frames	224
A.3	Design Report - Design of Loading Frame to Mount Actuator	225
I	Drawing and Design Details	226
II	SKETCHUP Make - Whole Experimental Setup in Laboratory	227
1	Loading Frame Before the Installation of the Actuator - Top View	227
2	Loading Frame After the Installation of the Actuator (Experimental Setup) - Top View	228
3	Loading Frame After the Installation of the Actuator - Bottom View	229
III	AUTOCAD	230
1	Existing Loading Frame In Laboratory	230

1.1	Existing Loading Frame In Laboratory – Top View	231
1.2	Existing Loading Frame In Laboratory – Front View	232
1.3	Existing Loading Frame In Laboratory – Side View	233
2	Experimental Setup In Laboratory	234
2.1	Experimental Setup In Laboratory – Top View	235
2.2	Experimental Setup In Laboratory – Front View	236
2.3	Experimental Setup In Laboratory – Side View	237
3	Dimensions of Typical Masonry Infill Wall (MIW)	238
4	Loading Frame Dimensions	239
5	Plate Girder Dimensions	240
6	Column Dimensions	241
7	Test Specimen Setup	242
8	Extra Column Below Beam (At Back of the Actuator)	243
9	Extra Column Below Actuator (At Front of the Actuator)	244
10	Mounting Plate	245
11	Support to Resist Translation of MIW	246
12	Lateral Support at The Bottom of Both the Columns	247
13	Rear Support at The Back of the Actuator	248
14	Split Level Dimensions	249
15	Actuator Details	250
IV	STAAD Pro. - Design of Loading Frame	255
1	Skeleton Structure	256
2	Dimensions of the Structure	257
3	Material Properties of the Members	258
4	Rendered View of the Structure	259
5	Loading on the Structure	260
6	Design Input for the Steel	261
7	Design Input for the Concrete	262

8	Support Reactions	263
9	Shear Force Diagrams	264
10	Bending Moment Diagram	265
11	Displacement or Deflection or Elastic Curve	266
12	Steel Design Output	267
13	Concrete Design Output	269
14	Steel Take-Off Output	271
BIOGRAPHIES		273

LIST OF FIGURES

Figure 1.1	Adverse effects of earthquakes on masonry infilled RC buildings.....	2
Figure 1.1(a)	Soft storey failure.....	2
Figure 1.1(b)	In-plane failure.....	2
Figure 1.1(c)	Out-of-plane failure.....	2
Figure 1.2	Share of economic damage caused by natural disasters by continent.....	3
Figure 1.3	Strongest Earthquakes Worldwide.....	3
Figure 1.4	Construction of a typical MIW structure.....	6
Figure 1.5	Dimension of a typical burnt red clay brick.....	6
Figure 1.6	Masonry infill wall.....	8
Figure 1.7	Confined masonry wall.....	8
Figure 1.8(a)	CC and DC modes of failure of MIW.....	10
Figure 1.8(b)	SS, FF, and DK modes of failure of MIW.....	10
Figure 1.9	Repointing technique.....	13
Figure 1.10	Centre core technique.....	13
Figure 1.11	FRP wrapping around MIW.....	13
Figure 1.12	Textile reinforced mortar (TRM)	13
Figure 2.1	Main modeling approaches for masonry structures.....	48
Figure 2.2	Expanded brick unit.....	48
Figure 2.3	A beam element subjected to shear and axial deformation.....	59
Figure 2.4	The effective width of the diagonal strut.....	62
Figure 2.5	Variation of ratio w/d_m for infilled frames as a function of the parameter λ_h	63
Figure 2.6	Ratio w/d_m for framed masonry structures.....	63
Figure 2.7	Unreinforced masonry wall support configurations.....	64
Figure 2.8	Idealized non-linear single-degree-of-freedom model.....	64
Figure 2.9	Inertia forces and reactions on rigid URM walls.....	65
Figure 2.9(a)	Parapet Wall at incipient Rocking and Point of Instability.....	65

Figure 2.9(b)	Simply Supported Wall at Incipient Rocking and Point of Instability.....	65
Figure 2.10	Infill panel separation into two diagonal regions.....	66
Figure 2.11	Selected failure mechanisms.....	67
Figure 2.12	Force diagrams for mechanisms 1.....	69
Figure 2.13	Force diagrams for mechanisms 2.....	69
Figure 2.14	Force diagrams for mechanisms 3.....	69
Figure 2.15	Force diagrams for mechanisms 4.....	69
Figure 2.16	Force diagrams for mechanisms 5.....	70
Figure 2.17	Macro-model for the simulation of an infill masonry panel and force-displacement monotonic behaviour curve.....	70
Figure 3.1	Test setup details (all dimensions in mm).....	97
Figure 3.2	Reinforcement details (all dimensions in mm).....	97
Figure 3.3	Failure surface of CDP model in plane stress.....	99
Figure 3.4	Compression stress-strain properties.....	101
Figure 3.5	Tension stress-strain properties.....	101
Figure 3.6	Bare frame dimensions.....	102
Figure 3.7	Infill frame dimensions	102
Figure 3.8	Diagonal length (D3) dimensions.....	102
Figure 3.9	Diagonal length (D6) dimensions	102
Figure 3.10	Applied displacement time history.....	104
Figure 3.11	Traction separation response of brick wall joint interfaces in tension and shear.....	104
Figure 3.12	Meshing of the bare frame.....	106
Figure 3.13(a)	Meshing of half brick.....	106
Figure 3.13(b)	Meshing of full brick.....	106
Figure 3.14	Meshing of fiber.....	106
Figure 3.15(a)	Experimental BF-1 results.....	107
Figure 3.15(b)	Numerical BF-1 results.....	107

Figure 3.16(a)	Experimental IF-2 results.....	108
Figure 3.16(b)	Numerical IF-2 results.....	108
Figure 3.17(a)	Experimental RFG-D3-3 results.....	108
Figure 3.17(b)	Numerical RFG-D3-3 results.....	108
Figure 3.18(a)	Experimental RFG-D6-4 results.....	108
Figure 3.18(b)	Numerical RFG-D6-4 results.....	108
Figure 3.19(a)	Experimental RFC-D3-5 results.....	109
Figure 3.19(b)	Numerical RFC-D3-5 results.....	109
Figure 3.20(a)	Experimental RFC-D6-6 results.....	109
Figure 3.20(b)	Numerical RFC-D6-6 results.....	109
Figure 3.21(a)	Experimental RFB-D3-7 results.....	109
Figure 3.21(b)	Numerical RFB-D3-7 results.....	109
Figure 3.22(a)	Experimental RFB-D6-8 results.....	110
Figure 3.22(b)	Numerical RFB-D6-8 results.....	110
Figure 3.23(a)	Experi. BF-1 hysteresis curve.....	111
Figure 3.23(b)	Numerical BF-1 hysteresis curve.....	111
Figure 3.24(a)	Experi. IF-2 hysteresis curve.....	111
Figure 3.24(b)	Numerical IF-2 hysteresis curve.....	111
Figure 3.25(a)	Experi. RFG-D3-3 hysteresis curve.....	111
Figure 3.25(b)	Numerical RFG-D3-3 hysteresis curve.....	111
Figure 3.26(a)	Experi. RFG-D6-4 hysteresis curve.....	112
Figure 3.26(b)	Numerical RFG-D6-4 hysteresis curve.....	112
Figure 3.27(a)	Experi. RFC-D3-5 hysteresis curve.....	112
Figure 3.27(b)	Numerical RFC-D3-5 hysteresis curve.....	112
Figure 3.28(a)	Experi. RFC-D6-6 hysteresis curve.....	112
Figure 3.28(b)	Numerical RFC-D6-6 hysteresis curve.....	112
Figure 3.29(a)	Experi. RFB-D3-7 hysteresis curve.....	113
Figure 3.29(b)	Numerical RFB-D3-7 hysteresis curve.....	113

Figure 3.30(a)	Experi. RFB-D6-8 hysteresis curve.....	113
Figure 3.30(b)	Numerical RFB-D6-8 hysteresis curve.....	113
Figure 3.31	Maximum excursion curves for both experimental and numerical analyses.....	117
Figure 4.1	Test frame details (all dimensions in mm).....	121
Figure 4.2	Reinforcement details.....	121
Figure 4.3(a)	Beam c.s.a.....	121
Figure 4.3(b)	Column c.s.a.....	121
Figure 4.3(c)	Foundation c.s.a.....	121
Figure 4.4(a)	Front face (F.F.) of the specimen.....	122
Figure 4.4(b)	Back face (B.F.) of the specimen.....	122
Figure 4.5	Dimension details of the specimen.....	122
Figure 4.6	Construction of the test specimen.....	122
Figure 4.7	Graphical representation of the Test Setup.....	123
Figure 4.8	Test setup in the laboratory.....	123
Figure 4.9	Instrumentation details.....	124
Figure 4.10	Applied loading protocol.....	124
Figure 4.11(a)	Diagonal tension cracks at the joint.....	126
Figure 4.11(b)	Failure at the end of the test.....	126
Figure 4.12	Dimensions of RC frame model.....	128
Figure 4.13	Assembly of the full model.....	128
Figure 4.14	Meshing of full model.....	128
Figure 4.15	Failure of specimen – Experimental.....	129
Figure 4.16	Failure of specimen – Numerical.....	129
Figure 4.17	Hysteresis curve – Experimental.....	130
Figure 4.18	Hysteresis curve – Numerical.....	130
Figure 4.19	Envelope curve.....	131
Figure 5.1	Reinforcement details (all dimensions in mm).....	139

Figure 5.2(a)	Beam cross-section.....	139
Figure 5.2(b)	Column cross-section.....	139
Figure 5.2(c)	Foundation cross-section.....	139
Figure 5.3(a)	Front face (F.F.) of the test specimen.....	140
Figure 5.3(b)	Back face (B.F.) of the test specimen.....	140
Figure 5.4(a)	Schematic geometry of the MIW.....	142
Figure 5.4(b)	Application of TRM on the top face.....	142
Figure 5.4(c)	Application of TRM on the left face.....	142
Figure 5.4(d)	Application of TRM on the right face.....	142
Figure 5.5	Graphical example of full-surface application of TRM in the experimental procedure.....	142
Figure 5.6(a)	Preparing the surface of the specimen.....	145
Figure 5.6(b)	Cutting of fiber.....	145
Figure 5.6(c)	Mixing of plaster.....	145
Figure 5.6(d)	Applying the plaster 1 st layer.....	145
Figure 5.6(e)	Placing the 1 st layer of TRM fiber.....	145
Figure 5.6(f)	Specimen after placing two layers of the TRM.....	145
Figure 5.7	Test setup details.....	146
Figure 5.8	Isometric view of the test setup.....	146
Figure 5.9	Instrumentation details.....	148
Figure 5.10	Applied loading protocol.....	148
Figure 5.11(a)	Hysteresis curve for URS specimen.....	149
Figure 5.11(b)	Hysteresis curve for DRS specimen.....	149
Figure 5.12(a)	Initial cracks in the URS specimen.....	150
Figure 5.12(b)	Initial cracks in the DRS specimen.....	150
Figure 5.13(a)	Final cracks in the URS specimen.....	150
Figure 5.13(b)	Final cracks in the DRS specimen.....	150
Figure 5.14	Dissipation capacity area.....	152

Figure 5.15	Maximum excursion curve.....	152
Figure 5.16	Energy dissipation – Experimental results.....	154
Figure 5.17	Stiffness degradation – Experimental results.....	154
Figure 6.1	Concrete elastic modulus recovery shown under tension-compression stress transition.....	161
Figure 6.2	CDP model's tensile stress-strain curve.....	162
Figure 6.3	CDP model's compressive stress-strain curve.....	162
Figure 6.4	RC frame dimensions	165
Figure 6.5	Modeling of TRM.....	165
Figure 6.6	Infill frame.....	165
Figure 6.7	Meshing of the model.....	165
Figure 6.8	Configurations of the strengthened specimens to summarize the various parameters considered.....	170
Figure 6.9	Envelope curves of URS and DRS	172
Figure 6.10	Envelope curves of all numerical models.....	172
Figure 6.11	Failure patterns of the bare frame (BF).....	172
Figure 6.12	Failure patterns of the conventional/unretrofitted specimen (URS).....	172
Figure 6.13	Failure patterns of SRS-F1.....	173
Figure 6.14	Failure patterns of SRS-B1.....	173
Figure 6.15	Failure patterns of SRS-F2.....	173
Figure 6.16	Failure patterns of SRS-B2.....	173
Figure 6.17	Failure patterns of SRS-FIB1.....	173
Figure 6.18	Failure patterns of DRS.....	173
Figure 6.19	Hysteresis Curve of the BF.....	174
Figure 6.20	Hysteresis Curve of URS.....	174
Figure 6.21	Hysteresis Curve of SRS-F1.....	174
Figure 6.22	Hysteresis Curve of SRS-B1.....	174
Figure 6.23	Hysteresis Curve of SRS-F2.....	175

Figure 6.24	Hysteresis Curve of SRS-B2.....	175
Figure 6.25	Hysteresis Curve of SRS-F1B1.....	175
Figure 6.26	Hysteresis Curve of DRS.....	175
Figure 6.27	Stiffness degradation of URS and DRS	176
Figure 6.28	Stiffness degradation of all numerical models.....	176
Figure 6.29	Energy dissipation of URS and DRS	176
Figure 6.30	Energy dissipation of all numerical models.....	176
Figure 6.31	Load carrying capacity of the models determined using numerical models.	180
Figure 6.31	Relative component costs.....	183
Figure 6.33	Cost comparison of MIW strengthened with TRM considering different parameters.....	185

LIST OF TABLES

Table 1.1 Summary of classification of bricks.....	7
Table 2.1. Summary of the literature review on the out-of-plane testing on MIW.....	23
Table 2.2. Summary of the literature review on the in-plane testing on MIW.....	28
Table 2.3. Summary of the literature review on the numerical analysis on MIW.....	52
Table 2.4. Analytical prediction of lateral resistance and stiffness.....	68
Table 2.5. Summary of the literature review on the analytical study on MIW.....	74
Table 2.6. Summary of the literature review on the fragility functions for MIW.....	86
Table 3.1. Specifications for the specimen (N. Ismail et al., 2018).....	96
Table 3.2. Input parameters for Concrete Damage Plasticity.....	100
Table 3.3. Materials' mechanical characteristics for the numerical simulations.....	103
Table 3.4. Mechanical properties of the fibers for the numerical simulations.....	104
Table 3.5. Experimental, numerical, and analytical results of all the specimens.....	117
Table 4.1. Experimentally determined material properties of steel rebar.....	127
Table 4.2. Experimental and Numerical results.....	132
Table 5.1. Experimentally determined material properties of steel rebar.....	137
Table 5.2. Experimental results of URS and DRS.....	154
Table 6.1. Mechanical properties of all elements.....	163
Table 6.2. Calibration of model parameters.....	168
Table 6.3. Experimental, numerical, and analytical results of all the models.....	179
Table 6.4. Cost of construction materials before and after Covid-19.....	181
Table 6.5. Cost estimation for construction materials.....	182
Table 6.6. Transportation, workmanship, and other costs	183
Table 6.7. Costs of Reduced Scale and Full-Scale Specimen Strengthened with TRM.....	184

ABBREVIATIONS

AAC	Autoclaved aerated concrete
ATC	Applied technology council
C3D8R	Continuum, 3D, 8-node, reduced integration element
CDP	Concrete damaged plasticity
CFRP	Carbon fiber reinforced polymers
DMEM	Discrete macro-element method
DRS	Double retrofitted specimen
ECC	Engineered cementitious composite
EDR	Equivalent damping ratio
EVDC	Equivalent viscous damping coefficient
FEM	Finite element model
FEMA	Federal emergency management agency
FRCM	Fiber reinforced cementitious matrix
FRP	Fiber reinforced polymers
GFRP	Glass fiber reinforced polymers
HCB	Hollow concrete block
IMG	Inorganic matrix-grid
IP	In-plane
LVDT	Linear variable differential transformer
MIW	Masonry infill walls
NSM	Near surface mounted
OOP	Out-of-plane
OPC	Ordinary Portland cement
PCMs	Phase change materials
PT-MWs	Post-tensioned masonry walls
RC	Reinforced concrete
RCC	Reinforced cement concrete

RIW	Resilient infill wall
S4R	Reduced integration
SDOF	Single degree of freedom
SG	Strain gauge
TRM	Textile reinforced mortar
URM	Unreinforced masonry
URMIW	Unreinforced masonry infill walls
URS	Unretrofitted specimen
WWM	Welded wire mesh
XFEM	Extended finite element method
XPS	Extruded polystyrene sheets
3D	Three dimensional

CHAPTER 1

INTRODUCTION

1.1. BACKGROUND

Masonry infill walls (MIW) are frequently employed as internal and external partition walls in reinforced concrete (RC) frames, which are one of the most commonly used structural systems worldwide. In the structural analysis and seismic design process, infill walls are often disregarded since they are generally categorized as non-structural components (Elouali, 2008). In doing so, their stiffness and strength contribution, as well as their interaction with the load-bearing elements of the frame (i.e. beams, columns), are fully neglected. Thus, the actual performance of infilled RC frames will differ from the expected performance based on the structural analyses. Under seismic forces, they can interact with the surrounding frames and alter the behaviour of the RC frame in terms of load-resisting mechanism and failure pattern. The particular function that masonry walls play during an earthquake is complicated and not well known, making the topic of how infills influence an RC structure's performance during a seismic event challenging to understand. From the available published experimental and numerical data, it can be observed that MIW can have a significant effect on the structural performance of RC frames under seismic actions. Even light to moderate earthquake shaking/acceleration or drift levels can cause damage to the infill walls and this damage may result in life safety hazards, immediate evacuation, and loss of function of buildings, limiting the use of internal spaces. In many cases, the influence of the infill panels was shown to be the reason for extensive damage or even the buildings' collapse. Based on these factors, it is not surprising that, over the past six decades, an increasing interest has been observed concerning the investigation of the effect of infill walls on the seismic performance of infilled frames.

Masonry walls have been a fundamental element of construction since the inception of civilization due to its economic aspects, ease of construction, low maintenance, durable and aesthetic purposes. This is because of its crucial function in separating the interior from outside spaces, offering security, and protecting from adverse ecological repercussions. Because of these essential purposes, brick walls are used in almost all structures, including the most sophisticated ones in modern cities. In order to brace low-rise and medium-rise structures

against in-plane lateral stresses brought on by wind or earthquakes (Block & Block, 2023), this approach has shown to be both effective and efficient. However in the past few years, several studies have been conducted on soft-story failure, in-plane (IP) and out-of-plane (OOP) damages as a result of its inadequate performance during an earthquake, as seen in Figure 1.1 (a)-(c) (Adem et. al., 2013).



Figure 1.1. Adverse effects of earthquakes on masonry infilled RC buildings (Adem et. al., 2013)

Among the most destructive natural calamities are earthquakes. Earthquakes that are innocuous often occur in several US locations. Large-scale earthquakes have historically caused the most catastrophic loss of life and physical infrastructure. They have also had a profoundly negative economic impact on the places they strike. Approximately 500,000 earthquakes occur worldwide each year, with many of them being felt (AlKhaldi, 2024). Figure 1.2 shows the share of economic damage caused by natural disasters by continent (Statista, 2024), from which it is evident that, America suffers the highest percentage share of economic loss (69.6%) caused by the natural disasters in a single year 2022, followed by Asia which has an economic loss of 21.8%. Both Africa and Oceania share the same amount of economic loss of 3.8% whereas the continent that suffered least economic losses is Europe which is 0.1% which is almost 200 times less in terms of percentage compared to America. Some of the strongest earthquakes occurred worldwide according to the measurements recorded by the Richter Scale in the year 2023 is shown in Figure 1.3 (Statista, 2024).

Some examples of earthquake events around the world includes in the places such as the moderate earthquake struck the Turkish region of Kutahya on May 19, 2011 (Adem et. al., 2013). The strongest earthquakes that have affected Albania in the last 40 years are with a

magnitude of 5.6 foreshock occurred on September 21, 2019, Durrës and on November 26, 2019, an earthquake with a magnitude of 6.4 occurred to the north of Durrës, the second-largest city in Albania and a port city on the Adriatic coast. (Andonov et al., 2022).

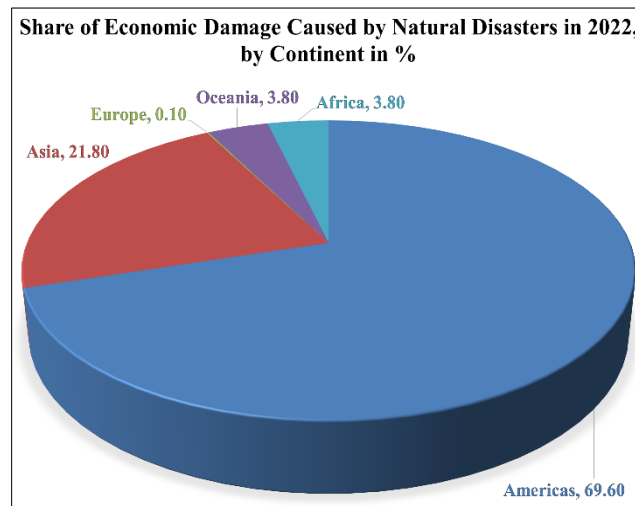


Figure 1.2. Share of economic damage caused by natural disasters by continent (Andonov et al., 2022)

The Indian subcontinent has had some of the largest earthquakes in history, with magnitudes greater than 8.0. For example, within a brief period of around 50 years, four of major earthquakes took place: Assam earthquake of 1897 (magnitude = 8.7), Bihar-Nepal earthquake of 1934 (magnitude = 8.4), Kangra earthquake of 1905 (magnitude = 8.6) and the Assam-Tibet earthquake of 1950 (magnitude = 8.7) (Pribadiet. al., 2014).

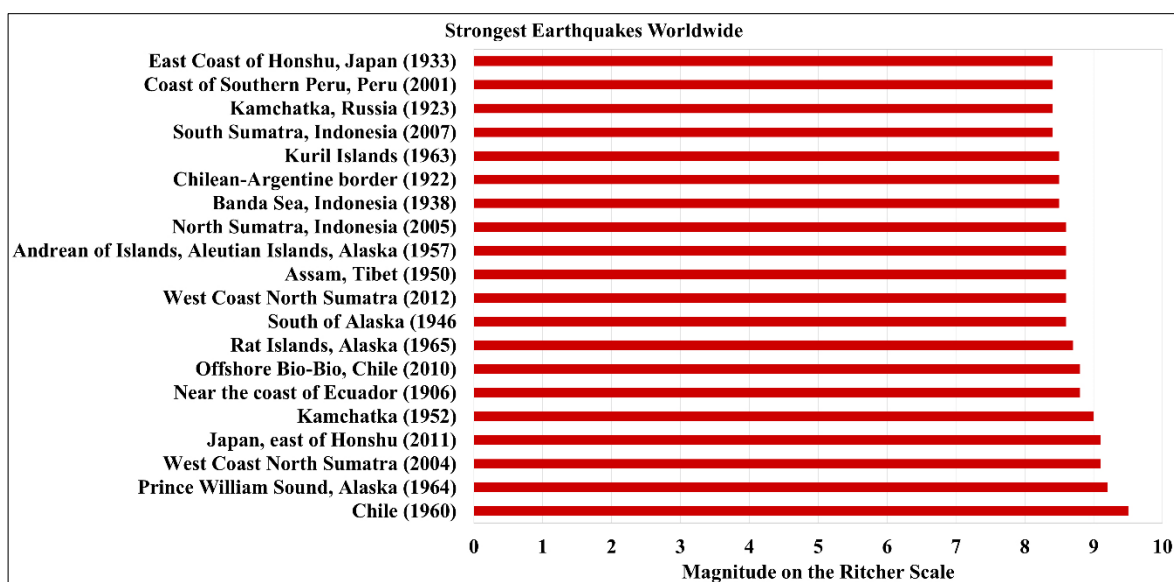


Figure 1.3. Strongest Earthquakes Worldwide (Andonov et al., 2022)

Building performance during mild, moderate, and severe earthquakes has been observed, and these observations have helped to expand our understanding of the seismic behaviour of structures, particularly with regard to identifying appropriate and inappropriate designs and earthquake load-resisting systems. The behaviour of the RC constructions is determined by the stiffness, strength, ductility, and energy-dissipation properties of the structural parts, amid other characteristics (Rodrigues et al., 2018). Each structural part and the connections and interactions between them give the structure its structural strength (Fardis & Panagiotakos, 2007). The load redistribution capacity of the highly redundant buildings regulates their reaction. The buildings may fail if certain elements fail, and the remaining members cannot withstand considerable deformations before collapse. Certain structural elements' inadequate strength capability can be explained by the fact that they are subjected to seismic loading demands much higher than the values considered during their design. To provide sufficient stiffness, strength, and ductility to the elements and, consequently, the global structure, the structures should be constructed in accordance with the predicted seismic demands specified by the current codes. It is necessary to consider non-structural features like the MIW and secondary RC structural elements while performing the seismic design of RC structures. Some international codes, for example (BS EN 1998-1 :2004 EN 1998-1 :2004 (E), 2011) regard infill panels as non-structural components and assign little emphasis on how they behave during earthquakes or affect how the structure responds. Usually ignored is their contribution to the seismic structural reaction. The 2015 Nepalese earthquake provided evidence that infill walls frequently impact how RC buildings respond to seismic activity (Arede, 2017). They improve the overall structural performance in terms of stiffness, strength, and energy dissipation. They induce more significant seismic loadings than anticipated during the design process by altering buildings' natural periods and vibration modes (Rodrigues et al., 2018). However, their distribution, both in-plan and in-elevation, may adversely impact the overall structural response (Trapani et al., 2018). Including infill walls in a RC building can amplify failure mechanisms that the structural components were not intended to sustain and decrease the building's capacity for deformation (Misir, 2015).

Its structural behaviour is dependent on each of its constituent parts since it is a dual system. The advantageous confinement effects of the concrete frame, which in turn strengthens the frame to produce a shear-resisting element, strengthens the infill panel. Because of its restricting action, the frame keeps the infill from disintegrating after its initial cracking, and

the infill keeps stiffening the frame. Together, these factors provide a system that combines the surrounding frame's ductility with a high degree of infill strength and stiffness.

Vulnerability studies are very important to evaluate seismic risk and their application is particularly interesting in urban areas located in low to moderate seismic hazard regions where the increase of the population and the absence of adequate seismic-resistant prescriptions for buildings increment the seismic risk. Very often, in these areas, a large number of RC frame structures have been designed mainly for gravity loads, or their lateral resistance has been determined without adequate seismic-resistant considerations or according to old seismic codes, in which ductile detailing is not explicitly required. It is very likely that these buildings, when subjected to a maximum credible seismic event, suffer more damage than reasonable. Therefore, it became a necessary job for earthquake engineers to design earthquake-resistant buildings in such a way that the whole structure contributes to seismic safety.

1.2. WALLS

Brickwork is regularly framed by spreading various interlocking units bound together by mortar. The dry-set masonry depends on the friction between the units to forestall movement and does not need mortar. Brick masonry is vital in compression, however less viable at opposing horizontal loading or tension forces.

1.2.1. Types of Walls

The wall is a construction characterizing an accurate region and giving security and haven. There are different sorts of walls utilized in the development of structures shown underneath.

- a) **Load Bearing** – the walls that carry the imposed load and their self-weight are the load-bearing walls. These walls can be classified as exterior or enclosing walls.
- b) **Non-Load Bearing** – the walls that do not carry the imposed load but carry the gravity load are named the non-bearing wall. An example is partition walls.
- c) **Masonry infill walls** – the structural elements are constructed first, and the brick wall panels fill the open rectangular spaces between the lower and higher beams and side columns.
- d) **Confined walls** – the walls are constructed first using masonry units, and then the walls are enclosed (confined) by erecting concrete columns and beams (Brzev, 2007).

1.2.2. Wall Openings

The critical parameter that alters the performance of a wall under lateral loads is the openings provided in the wall. Therefore, the consideration of openings in the design of barriers is of utmost importance. The different types of wall openings available are doors, windows, and ventilators. Many researchers study the performance of walls subjected to lateral loads with and without openings. Figure 1.4 shows some examples of walls with openings.



Figure 1.4. Construction of a typical MIW structure

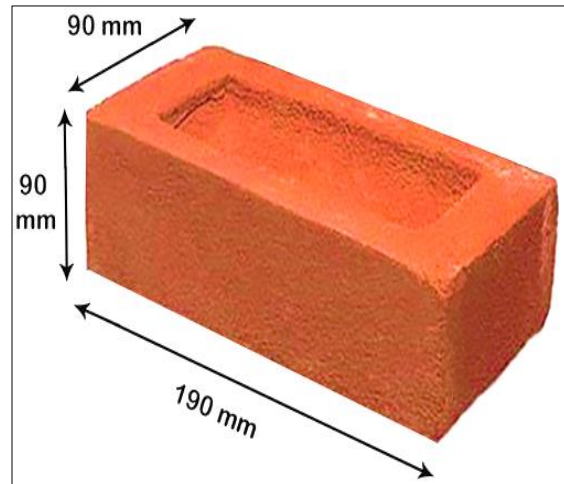


Figure 1.5. Dimensions of a typical burnt red clay brick

1.3. BUILDING MATERIALS

1.3.1. Bricks

Brick is one of the oldest building materials used for construction purposes – bricks for constructing shelter dates to 7000 B.C. Since then, bricks have been the most famous building material until today. Bricks (Figure 1.5) the materials manufactured artificially using natural resources such as clay heated and moulded in uniform shape and size. There are four classes of bricks based on their compressive strength (IS 1077 : 1992 (Reaffirmed 2002), 2007). The details of the different classes of bricks are given in Table 1.1.

1.3.2. Composition of Bricks

Bricks are not naturally available material. The manufacturing takes place artificially, either manually or mechanically. Later, Romans invented firebricks in 3500 B.C. They just eliminated the long and tedious process of hardening the bricks under warm temperatures and

manufactured bricks in different shapes according to the requirement of wooden moulds. In the medieval period, clay became the most crucial ingredient in the making of bricks. In 1666, the city of London was majorly decorated with brickwork structures. The majority of the skyscrapers in the United States of America use bricks or terracotta (Brick, 2023).

Table 1.1. Summary of classification of bricks

Class	Crushing strength (N/mm²)	Water absorption (%)	Colour	Uses
Class I	≥ 10	12 to 15	Deep Red	Load-bearing masonry structures
Class II	≥ 7	16 to 20 (22 max.)	Reddish Orange	Exterior walls and flooring
Class III	3.5 to 7	22 to 24 (24 max.)	Reddish Yellow	Partition or parapet walls
Class IV	≤ 3.5	No limit	Dark Reddish Brown	Temporary structures

The bricks consist of primarily five constituents, namely, silica, alumina, lime, iron oxide, and magnesia in different proportions. Each component has another purpose that forms the end product brick. Hence, it can be a great brick if its excellent properties such as the shape and size of the brick are uniform with straight and sharp edges, deep red with the surface texture being rough so that binding action with the mortar will be proper. The hardness should be so that no mark should be visible if nails scratch the brick, and it should make a clear metallic sound when it pounded on each other, which is the soundness of the brick. Most importantly, the brick should not contain any impurities in the form of stones grits, etc.

1.4. MASONRY INFILL WALLS (MIW)

Masonry construction is a process that utilizes singular units such as bricks, stone, etc. bound along with different types of mortar such as cement-sand mortar, lime mortar, gauged mortar, etc. Even though it is amazingly durable, masonry does, in any case, wear out after some time and regularly needs repair or restoration.

1.4.1. Types of Masonry Construction

The construction of masonry walls is done in two different ways. One method includes filling the space between the upper and lower beams and columns with brick walls with/without openings (being optional). These structures are known as masonry infill walls (Figure 1.6). In the second method, the brick wall is constructed first by leaving the required amount of gap to construct vertical compression members, called tie columns joined with tie beams. These structures are known as confined masonry walls (Figure 1.7).

In this thesis, the study focuses only on the research and development of masonry infill walls, which will be discussed in the following sections.



Figure 1.6. Masonry infill wall



Figure 1.7. Confined masonry wall

1.4.2. Modes of Failure of MIW

Building performance during mild, moderate, and severe earthquakes has been observed, and this observation has helped to expand our understanding of the seismic behaviour of structures, particularly with regard to identifying appropriate and inappropriate designs and earthquake load-resisting systems. The RC structures' behaviour depends on the structural elements' stiffness, strength, ductility, and energy-dissipation characteristics, among other factors (Rodrigues et al., 2018). The building's structural strength is provided by each structural member and the interaction and connection between them (Fardis & Panagiotakos, 2007). Since the buildings are structures with a high degree of redundancy, their response is controlled by the loading redistribution capacity, which can fail if some of the members reach the failure, and the remaining ones cannot accommodate significant deformations before failure. The

insufficient strength capacity of some structural members can be justified by being subjected to seismic loading demands significantly higher than the values considered during their design process. The structures should be designed according to the expected seismic demands prescribed by the modern codes to ensure adequate stiffness, strength, and ductility to the elements and, consequently, the global structure. The seismic design of RC structures needs to be performed by considering the RC structural elements secondary elements and non-structural elements like the masonry infill walls. Some international codes like (BS EN 1998-1 :2004 EN 1998-1 :2004 (E), 2011) consider the infill panels as non-structural elements and provide low importance to their seismic behaviour and participation in the response of the building. Their contribution to the seismic structure response is usually disregarded. The Nepalese earthquake in 2015 evidenced that the infill walls often play an essential role in the seismic response of the RC structures (Arede, 2017). They provide an increment of stiffness, strength, and energy dissipation to the global structure. They change the natural periods and vibration modes of structures, attracting higher seismic loadings than those expected during the design process (Rodrigues et al., 2018). Nevertheless, their in-plan and in-elevation distribution can also affect negatively the global structural response (Trapani et al., 2018). The infill walls presence reduces the building's deformation capacity and can potentiate failure mechanisms that the structural members were not designed to support (Misir, 2015).

The infills have a beneficial influence on the performance of the existing non-ductile RC frames if properly designed for heavy seismic forces (Armin Mehrabi et al., 1996). However, its unsatisfactory performance during an event earthquake led to several studies over the past few years such as Corner Crushing (CC) mode, Diagonal Compression (DC) mode, Sliding Shear (SS) mode, Diagonal Cracking (DK) mode, Frame Failure (FF) mode are some of the examples for performance failure of MIW, as represented in Figure 1.8 (a)-(b) (P. G. and C. Z. C. Asteris, 2011).

1.4.3. Prevention of Failures of MIW

The fundamental purpose of seismic strengthening is to enhance the overall structural performance and increase the resistance to deformation when subjected to lateral loadings. There are two safeguarding strategies for the masonry system against the effect of the earthquake. One is to protect the structure from seismic forces, and the other is to enhance the strength of the existing systems to withstand seismic loads. The two ways of retrofitting a structure are by using additional components and additional adhesives.

Seismic analysis of the existing structure is proper if the soil under the construction is in good condition so that fewer seismic forces will be transferred to the superstructure. The structural engineers estimate the capacity of the structure for strengthening by considering the type of construction materials, loads acting on the structure, and the geometric aspects of deteriorated structures. All kinds of failure modes must be considered during the strengthening process.

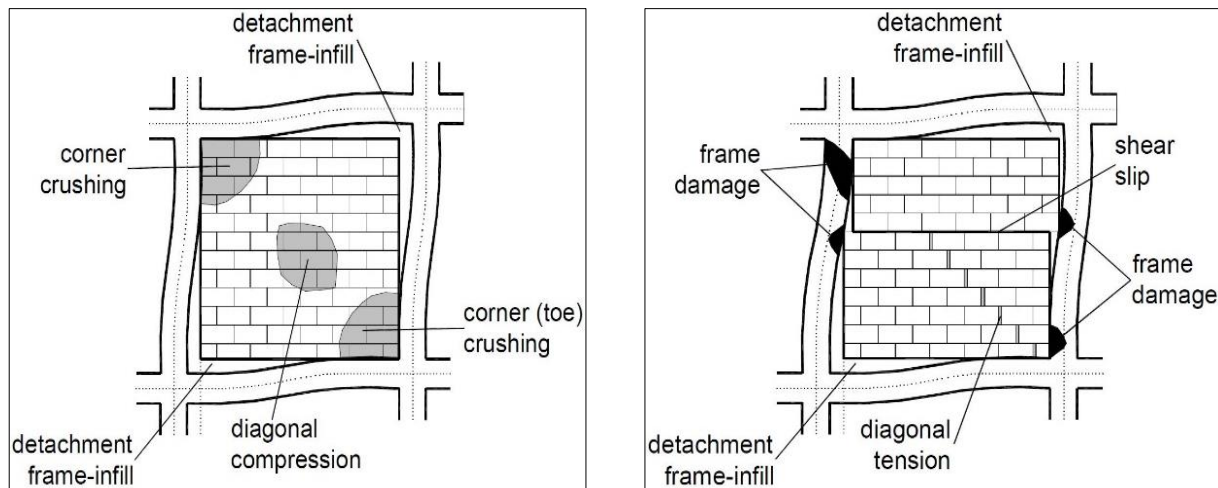


Figure 1.8 (a) CC and DC modes of failures Figure 1.8 (b) SS, FF, and DK modes of failures

The selection of the strengthening technique should be according to the design and condition of the existing structure, knowing the overall characteristics of the system in detail for the selection process of a particular strengthening method. The basic parameters such as deformation capacity, dissipating energy capacity, shear capacity, stiffness, and strength properties are considered. The other consideration factors are the economic aspects, aesthetic views, etc. In addition to all these mentioned, other details include the foundation design, seismic zone, and earthquake records in that zone.

1.5. SEISMIC STRENGTHENING OF MASONRY STRUCTURES

Seismically strengthening the structure represents improving each structural as well as non-structural member's strength, such as beams, columns, and walls individually. There are various techniques to retrofit these members. The strengthening methods are two types based on the location of the strengthening material on the MIW; intrinsic and extrinsic. The former method consists of dowel bars, vertical and horizontal reinforcement, and the center core technique whereas the latter technique consists of various methods such as repointing

technique, welded wire mesh (WWM), fiber reinforced polymer (FRP) jacketing, steel bracing, and textile reinforced mortar (TRM).

1.5.1. Repointing Technique

The repointing technique is a popular method in strengthening the masonry walls among the available traditional retrofitting methods. This method's general procedure follows to eradicate the defective portion and substitute those with similar elements to rehabilitate the previously lost strength of the wall. In such cases, this method is more productive when the mortar is eroded over time or notches included in the bonds, (Jaime et al., 2019).

The filling of the bed joint between the bricks in a brick wall is called the pointing method. This method accomplishes the ongoing work by disseminating the mortar in the bed joint with the masonry wall face or separately when the exterior part of the mortar in the bed joint is left broken. The primary factor contributing to the brick wall's aesthetic appearance is the pattern of the mortar joints, uniformity, and the sequence of laying, significantly when the sizes of the bricks vary. The mortar joint contributes to the aesthetic aspect of a masonry wall. It favors keeping the structure dry mainly in two ways, i.e., by not letting the atmospheric moisture penetrate through the wall and allowing the already present humidity inside the wall to dissipate into the dry weather. There is a possibility that rainwater may penetrate through the wall through the tiny cracks between the mortar joints and the bricks. The water must escape back into the environment after the rain stops to avoid moisture entering the wall. The best way to achieve this is through permeable mortar bed joints. If hardened cement mixes with the mortar, it may not release moisture, and it may stagnate in the bricks, which increases the chances of damage caused by to crystallization of soluble salts, (Chuang & Zhuge, 2005).

Repointing can improve the aesthetic appearance as well as the durability of the brick masonry. It may affect the brickwork if it is not done correctly, sometimes leading to unrecoverable damage. It is most suitable on the exposed face of the brick wall of the structure. The principle of the repointing technique is that the bed joint mortar should be a little weaker than the bricks, for example, if the mortar is stronger than the brick masonry then, the wall will be in the danger zone where the permeability occurs, preventing the moisture content evaporating through the bed joints. Due to this, cement-based mortars started declining; instead, lime-based mortars came into the limelight, strictly following the principle. The type of mortars that can be advantageous for the repointing techniques are lime-based mortars. Two

types of lime are easy to use in mortars, i.e., non-hydraulic lime and natural hydraulic lime. After completing the repointing process (Figure 1.9), the wall is safeguarded from temperature variations such as rain, sunlight, and heavy winds to prevent any damage. It should be maintained under damp conditions using jute bags or thick mats to allow the mortar to set. Finally, the cannon is ready for the final step, finishing while still in damp condition. Proper maintenance is necessary until the curing of mortar is complete enough to resist any kind of damage caused by the variation in temperature.

1.5.2. Centre Core Technique

This technique follows a method in which holes (cores) are drilled vertically along the height through the masonry brick wall through which reinforcement bars are embedded through the brick wall into the basement of the wall as shown in Figure 1.10. The diameter of this core varies between 100 to 150 mm depending on the type and size of the wall. The cores are drilled using the oil-well drilling technique. This dry process may release large debris that can be removed manually or using any mechanical instrument such as a vacuum cleaner. The most common reinforcement used is solid steel bars placed at the center of the drilled hole and usually filled with a pump using sand grout throughout the cavity under pressure. This technique will help in filling out the voids along with the height of the drilled core. The bonding between the inner surface of the grout with the rebar and the outer surface of the grout to the masonry makes it a homogeneous compound better than the core itself. This method helps the masonry infill wall to resist both the in-plane loading and the out-of-plane loading. However, this method has the disadvantage of creating a large amount of disturbance/noise during the process. The geometry of the wall is not changed overall since it is one of the non-destructive testing methods (Breiholz, 1993).

1.5.3. Fiber Reinforced Polymer (FRP)

Many existing structures built with masonry are vulnerable to seismic forces both in the in-plane and out-of-plane directions. Hence, these structures need retrofitting to resist these loads to avoid damage or collapse, resulting in property loss or life loss. Available techniques for strengthening masonry infills more often have disadvantages such as corrosion, heavy weight, uneconomical, requiring skilled labours, and is time-consuming. To overcome these limitations, materials such as fiber-reinforced polymer (FRP) are developed as a strengthening material. Due to its lightweight in nature and minor time-consuming procedure, it has gained

significant popularity. FRP is available in many types and many forms as well. The different fibers available are carbon fiber, glass fiber, and basalt fiber in various forms, such as chopped fibers and woven fibers (Masuelli, 2013).



Figure 1.9. Repointing technique

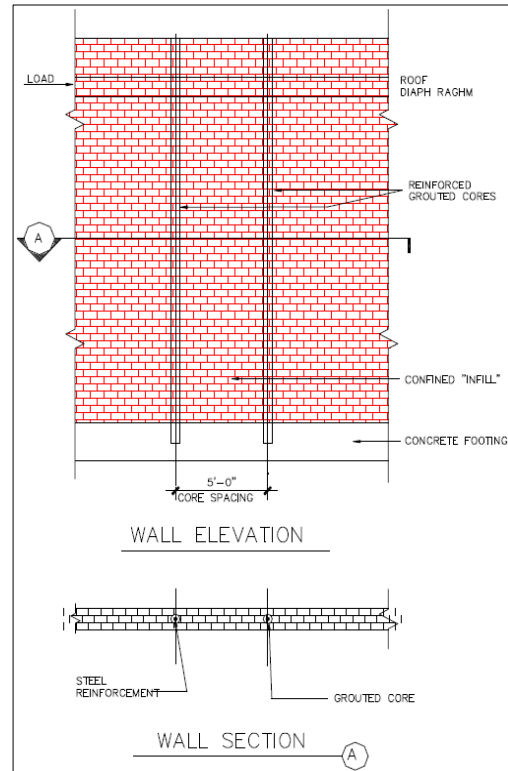


Figure 1.10. Centre core technique

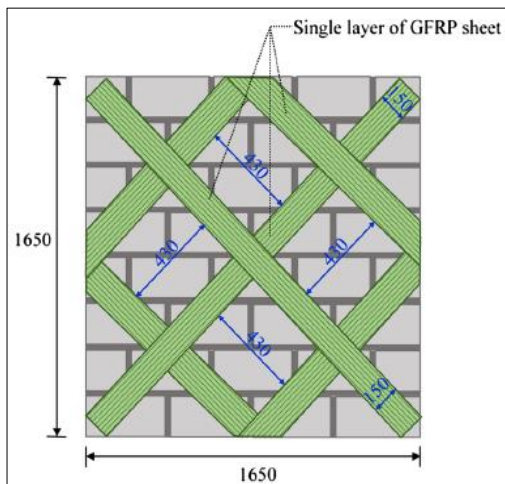


Figure 1.11. FRP wrapping around MIW (Elsanadedy et al., 2016)



Figure 1.12. Textile reinforced mortar (TRM)

Fibre Reinforced Polymers (FRP) has broad applications, including aerospace, automotive, marine, and construction industries. FRP is a composite material made of a

polymer matrix reinforced with fibers. The fibers used are usually carbon, basalt, glass, or aramid, although other fibers such as paper, wood, or asbestos are sometimes functional.

The polymer is usually epoxy, vinyl ester, or polyester thermosetting plastic, and phenol-formaldehyde resins are still available. As shown in Figure 1.11, the applicability of FRP to concrete or masonry structures as a substitute for steel bracing or pre-stressing tendons has been actively studied in numerous research laboratories and professional organizations worldwide. FRP strengthening offers several advantages: corrosion resistance, nonmagnetic properties, high tensile strength, lightweight, and ease of handling. They also have poor resistance to fire and when exposed to high temperatures (Tetta & Bournas, 2016). They lose significant strength upon bending, and they are sensitive to stress-rupture effects. Moreover, regarding the economic aspect, either considered cost per unit weight or based on force carrying capacity, is high compared to conventional strengthening methods. One of the disadvantages of using FRP solutions is the high costs associated, which makes this solution impracticable for the large majority of the building's owners (Shrivastava et al., 2009).

1.5.4. Textile Reinforced Mortar (TRM)

It is known as textile-reinforced mortar (TRM) or fiber reinforced cementitious matrix (FRCM) or textile-reinforced concrete (TRC), in international literature (Figure 1.12). Multi-axial fabrics are helpful in combination with fine-grained concrete in a newly developed material. The new TRM externally bonded composite strengthening system combines high-performance sprayable mortar with any fiber grid that creates a thin structural layer without significantly altering the structure's weight or volume (Naaman, 2010).

TRM is being built as a revolutionary alternative to conventional strengthening methods, at the same time giving the RC structures the required strength and stability to withstand external forces. These fibers are too soft to add directly to concrete, so they apply a coating to stiffen after being woven together. The fibers in the weave are adjusted for maximum tenacity to perform optimally in the concrete. These individual fibers form the basis of the concrete; up to 50,000 are combined to create a yarn. It is then processed on an automated loom to produce woven mesh. The new concrete's textile interior emerges from a myriad of fine threads. Another coating is put into the mesh that increases stability then, within a few minutes, the piece is cut to the required length (Naaman, 2010).

Earthquake-resistant structures are designed to protect buildings from earthquakes. While no structure can be entirely immune to damage from earthquakes, the goal of earthquake-resistant construction is to erect structures that fare better during seismic activity than their conventional counterparts. According to (Dr. Sudhir K Jain, n.d.), masonry infills hold considerable in-plane stiffness and strength and contribute to the overall stiffness and stability. The infills show a lesser effect on the structure if openings are present. However, these infills pose the hazard of out-of-plane collapse, which means structural engineers should design the buildings in such a way that the loss of life should be maintained minimum by preventing the destruction of the buildings against major earthquakes, same time limiting the loss of functionality to more frequent ones.

Strengthening RC frame structures generally increases the resistance and deformation capacity of the frame itself for the system to satisfy the levels of performance according to the codal provisions. Another possible way to improve the resistance of existing structures under lateral loads is to convert the infill walls into a more stable source of resistance over the whole spectrum of structural response through a significant and indemnified contribution to the structure's strength/stiffness (Curbach & Jesse, n.d.).

1.6. COMPARISON OF TESTING METHODS

The general aim of cyclic testing, which may include any method of testing where the structure is subjected to repeated reversals of loading direction, is to study the seismic performance of structural systems. Such tests can be further categorized according to the loading rate as either quasi-static or dynamic.

Quasi-static cyclic tests involve administering a cyclic loading pattern at a slow rate, usually in displacement control. The primary advantage of this mode of testing is to allow the load versus displacement (hysteresis) behaviour to be studied under predefined displacement at sequentially increasing levels, with multiple cycles at each level of displacement. This can be used to quantify the system's cyclic load-displacement envelope as well as its degradation and energy dissipation characteristics.

Dynamic shake table testing is fundamentally different from quasi-static loading because it subjects the structure to a series of accelerations. Whilst this mode of testing does not afford the same level of control over the imposed structural deformations, it does recreate the true dynamic nature of the seismic response by incorporating inertial and viscous damping

forces. It also allows the structure to be subjected to realistic earthquake motions. A further aspect of shake table testing is that the structure is inherently subjected to loading spatially distributed according to its mass, which is an experiment considered in quasi-static testing if it is to be used for seismic resistance assessment.

(G. Calvi, et. al., 1996) provide a good discussion of the relative merits of the different testing methods concerning masonry structures. He notes that since URM exhibits rate-dependent behaviour whereby crack propagation can occur during the application of a constant load, quasi-static tests tend to indicate lower load resistance than dynamic tests and are thus generally considered to be conservative for seismic assessment. Furthermore, he and other researchers (for example, (Daniel Abrams, 1996) have also argued that since typical displacement histories used in quasi-static cyclic tests involve a large number of displacement cycles, which are more severe than monotonic or random earthquake histories, quasi-static cyclic tests tend to be even further conservative in terms of the measured strength for structural systems such as URM, where degradation is affected by the number of cycles.

1.6.1. Monotonic Loading

According to the literature survey, in the past four decades, a substantial amount of monotonic testing has been performed on masonry walls, with significant contributions made in Europe, Canada, and the Asian countries. The general aim of these studies has been to measure the static load capacity of various types of wall configurations in response to a uniformly distributed pressure, typically considering different strengthening materials.

1.6.2 Cyclic Loading

Whilst a relatively large amount of work has been performed involving monotonic loading (as reported in Section 3.2.1), only a handful of studies have administered cyclic loading, be it quasi-static or dynamic. Furthermore, the majority of such studies have focused only on vertically spanning walls. (mentioned in Chapter 2, Section 2.5).

1.7. AIMS OF THE RESEARCH

The proposed study will explore the field of seismic performance of masonry infill walls strengthened with textile-reinforced mortar. The objective of the research is to investigate scientifically and systematically the behavior and dynamic response of the same by

implementing new strengthening techniques to improve the performance when subjected to severe seismic conditions.

The following specific objectives are set up to be achieved through the course of this study:

1. To identify and evaluate the factors influencing the performance of masonry infill walls (MIW).
2. To evaluate the cyclic behavior such as the development of cracks, ultimate strength, and deformation capacity of the MIW.
3. To carry out the parametric study by considering the opening in the infill wall, the location of strengthening material on MIW, and number of strengthening material layers used that affect the response of the seismic performance of the structure.
4. To develop empirical expression to depict the lateral load carrying capacity of MIW and validate the obtained results using numerical methods and to report the cost analysis for different scales of the specimen.

1.8. ORGANIZATION OF THE THESIS

In this thesis, the response of ductile-detailed RC frames including MIW consisting of central door openings strengthened with TRM was tested by in-plane cyclic load to evaluate the effectiveness of TRM as a strengthening material in contributing to the maximum load-carrying capacity and deflection-resisting phenomena of the MIW. Hence, to achieve the aforementioned objectives, the content of this thesis is divided into three parts: Part I reports on the numerical validation work undertaken which includes Chapter 3. Part II reports the associated experimental numerical and analytical methodologies that includes Chapters 4, 5, 6, and 7. Part III includes various supporting appendices relating to the work carried out.

Chapter 1 introduces MIW and TRM members including other strengthening methods, as well as outlines the purpose of this study.

Chapter 2 contains a comprehensive literature review of the previous research.

Chapter 3 explains the numerical validation study conducted to measure the agreement between the outcomes of the simulated model and the observations/results of the experiments.

Chapter 4 & 5 reports experimental tests performed where the testing of one specimen without ductile detailing and opening is explained in Chapter 4; two 1:2.5 scaled walls with opening and ductile detailing subjected to quasi-static cyclic loading strengthened with TRM is explained in Chapter 5. The experimental results are presented at the end of the Chapters.

Chapter 6 is dedicated to the specific numerical validation model used in this research to represent the infill walls. Next, a parametric study was conducted to determine the significance of the full-bond scenario between the RC frame infilled with masonry and the TRM and an analytical model is developed to predict the wall's load-carrying capacity by assuming that the masonry possesses zero bond strength. The resulting approach is based primarily on the geometrical properties of the wall. The numerical results are presented at the end of the Chapter. Also, the cost analysis of different scales of the test specimens are reported after the numerical results.

The outputs of the analyses are shown in terms of load-displacement hysteresis graphs, maximum excursion graphs, stiffness degradation, and energy dissipation capacity graphs.

Chapter 7 concludes this thesis by summarizing its main outcomes and providing recommendations for future research.

1.9. CONTRIBUTION OF THE THESIS

This thesis contributes to three categories, i.e., experimental work, numerical work, and analytical work. The experiment is conducted on two 1:2.5 scale specimens to understand the cyclic performance of MIW under lateral loading conditions with one of the specimens with seismic retrofitting using TRM, which proved to increase the load carrying capacity and resisting deflection of the masonry wall specimen. Numerical simulation provides the validation of the experimental hysteresis behaviour. Finally, cost analysis for reduced scale and full-scale models is provided to compare the rates, which lets the users/customers select the configuration of the TRM according to their requirements and also depending on the seismic hazard of the particular area.

CHAPTER 2

LITERATURE REVIEW

2.1. OVERVIEW

Related studies were recognized through various bibliographies such as Science Direct, ASCE, Springer, Earthquake Spectra, Wiley, Taylor & Francis, etc., to conduct an organized review, published from 1971 until 2024. References for this study were selected based on the fundamental requirement such that they provide (a) the material and mechanical property tests; and (b) the details of the strengthening materials. Indeed, it was considered suitable to incorporate these works because of the profoundly important and various data on this subject. All these records were segregated using Mendeley Desktop (version 1.19.4). Following this task, titles, and year of publication of the articles were filtered to eliminate the irrelevant papers. The titles of each journal were read with utmost care and were categorized based on the type of work carried out by the authors. Initially, they were segregated based on the type of loading (out-of-plane (OOP) and in-plane (IP) load) and strengthening method. Later, it was even more segregated based on the numerical or experimental tests carried out. Full articles related to the selected titles/work were scrutinized thoroughly and complemented the mentioned criterion in the ultimate bibliography.

The parameters considered while gathering the information regarding the methods of strengthening and retrofitting of masonry infill wall (MIW) were (a) technical parameters of the strengthening material, (b) specifications regarding strengthening strategies of MIW, (c) failure pattern of strengthened MIW (d) effect of strengthening material on MIW. As this research topic consists of several parameters, systematic evaluation was contemplated as the appropriate practice as far as this topic is concerned.

Although most of the literature concludes that infills increase the overall lateral stiffness of the whole structure, still researchers and scientists does not considering the infills in the seismic design of reinforced concrete (RC) structures (Stavridis et al., 2011). In a few cases, a small gap pertains between the infill wall and the bounding structural system, and in other cases, innovative strengthening methods of MIW are practiced. In contrast, strengthening existing MIW constructions is a bit complicated due to the absence of the technical details of

the structure, such as the type of masonry units used for building the wall, which leads to the unpredictability of selecting a suitable strengthening technique to adopt for the masonry structure.

2.2. RESEARCH & DEVELOPMENT ON MASONRY STRUCTURES

Several researchers have carried out and performed studies on MIW for decades. Studies showed that MIWs contribute to the resistance of lateral forces such as seismic actions. Hence, the presence of infills serves the purpose of its presence in the overall structure. The masonry infills can also be strengthened with various materials to increase the tensile capacity, as the material is brittle in nature. Research on MIW is not a contemporary topic as it was started a few decades back and is continuing. The research on MIW is divided into three categories, i.e., experimental work, numerical work, and analytical work, as discussed in the following sections.

2.3. EXPERIMENTAL WORK

Researchers performed and are still performing several experiments to investigate the effect of numerous parameters on the performance of reinforced concrete masonry infill frames. An extensive review of these works has led to the compilation of a database incorporating the references segregated year-wise in ascending order, from oldest publication to the recent (1988 to 2023). Table 2.1 and 2.2 summarizes the main aspects of the published test data (OOP and IP loads, respectively), including the type of masonry blocks, type of strengthening material, parameters considered, and the strengthening contribution along with the failure modes.

2.3.1. Out-of-Plane Loading

(Drysdale & Essawy, 1988) tested 21 full-scale MIW with concrete blocks by applying uniformly distributed load (UDL) perpendicular to the wall plane with simple support conditions on four sides of the border. The bending strength used was extracted from the results of the tests in which bending strength was removed from the test performed on masonry assemblages. Load for initial cracking and failure load were examined. (R Ehsani et al., 1999) investigated three unreinforced masonry (URM) infill walls retrofitted with composite strips with five reinforcement ratios & 2 different glass fabric composite densities by applying OOP cyclic loading. Results concluded that URM walls retrofitted with composite strips are effective

alternate strengthening techniques. (Papanicolaou et al., 2008) compared the performance of textile reinforced mortar (TRM) overlays and fiber reinforced polymer (FRP) overlays as a strengthening material or near surface mounted (NSM) reinforcements. The parameters considered were motor-based vs resin-based matrix materials, the number of layers of TRM, and the orientation of moment vector concerning bed joints, and concluded that TRM is advantageous over FRP in terms of strength & deformability. In other words, TRM is a promising solution for strengthening MIW under OOP. (Babaeidarabad et al., 2014) conducted OOP experimental tests on nine clay brick MIW in which three specimens were without strengthening and six were with strengthening, with fiber reinforced cementitious matrix (FRCM) having one and four reinforcement fabrics. The behaviour of the infill wall in terms of both stiffness and flexural capacity was a significant improvement. Also neglecting the arching effect, an analysis was carried out, and was compared with experimental data.

(Elsanadedy et al., 2016) conducted an experimental and analytical study on the OOP flexural performance of six URM infill walls constructed with hollow concrete blocks externally bonded with glass fiber reinforced polymer (GFRP) composites that were loaded to failure using an airbag and a loading frame by considering FRP reinforcement ratio and stiffness as main parameters. The conclusion derived was that FRP effectively enhances the load-carrying capacity and the OOP deformation-resisting capacity of URM walls. (D'Ambra et al., 2018) performed experiments on full-scale clay infill walls strengthened with basalt grid with inorganic matrix used to strengthen pre-damaged walls and constructed walls to study the effectiveness of FRCM to regain the capacity of pre-damaged walls & to enhance the overall performance of a non-damaged wall. (Padalu et al., 2018b) examined different parameters such as loading direction, reinforcement ratio, and effect of shear span by conducting experiments on 8 URM and 28 welded wire mesh (WWM) reinforcement-strengthened wall specimens and concluded that these characteristics of the latter are much higher than the former specimens. (Kariou et al., 2018a) suggested TRM has a significant effect on the load-carrying capacity of MIW by testing 18 specimens divided in equal numbers into single-wythe & double wythe walls, investigating key parameters such as textile reinforcement ratio, textile material, and textile material coating of textile reinforcements with epoxy resin & the wall thickness. (Verderame, et al., 2019) performed experiments on URM and RM infill frames by using OOP lateral loading. These specimens are compared with the other two models, which were strengthened using FRCM and FRP. The results showed that the FRCM gave three times the strength, whereas FRP gave two times the strength of the specimen without support.

Table 2.1. Summary of the literature review on the out-of-plane testing on MIW

Authors	Brick Unit Used (size in mm)	Details of Strengthening Material	Parameters Considered	Strengthening Contribution	Failure Mode
(B. P. Sinha, M. D. Loftus, 1979)		Filling of vertical joints	Different aspect ratio	Increase in flexural capacity	
(Drysdale & Essawy, 1988)	Concrete block		Simple support conditions on all four boundaries		Initial cracking
(R Ehsani et al., 1999)	Unreinforced brick walls	Vertical composite strips	Reinforcement ratios and different glass fabric composite densities	Capable of dissipating some energy.	Tensile failure, delamination
(Papanicolaou et al., 2008)	Fired clay brick, ridge-faced, 6-hole, horizontally perforated clay bricks	TRM or FRP jackets in comparison to NSM strips	Mortar-based vs resin-based matrix materials, number of layers, orientation of the moment vector w.r.t. the bed joints	TRM overlays provide a substantial gain in strength and deformability	Damage in the masonry
(Babaeidarabad et al., 2014)	Clay brick	FRP, FRCM	Strengthening material	Flexural capacity and stiffness	Flexural failure and shear failure in the substrate material

Authors	Brick Unit Used (size in mm)	Details of Strengthening Material	Parameters Considered	Strengthening Contribution	Failure Mode
(Elsanadedy et al., 2016)	Hollow concrete block	FRP, GFRP	FRP reinforcement ratio and stiffness	Upgrading the load-carrying capacity, enhancing the ductility capacity	FRP debonding
(Gattesco & Boem, 2017)	Solid brick, 250 mm thick, rubble stone and cobblestones, 400 mm thick	GFRP meshes	Types of masonry and failure mode	Resist OOP bending moments almost 4-5 times greater than those of plain specimens	Collapse occurred abruptly, almost at mid-height of the sample, at the interface between mortar joint and masonry units
(Shermi & Dubey, 2017)	Brick of size 230 x 110 x 70	WWM	Three-point loading method	Enhanced the flexural strength and ductility of masonry.	Flexure cracks, ductile failure.
(Kariou et al., 2018b)	Solid clay bricks 215 x 102.5 x 65	TRM	Textile reinforcement ratio, textile material, coating of the textile reinforcement with epoxy resin, and wall thickness	Increase the load-bearing capacity	Textile rupture, slippage of the textile fibers, shear failure of the masonry wall
(D'Ambra et al., 2018)	Clay brick	Composite basalt grid with inorganic matrix FRCM	Damaged wall and not pre-damaged wall	Prevent a brittle failure, ultimate load doubled	Shear sliding at higher displacement levels

Authors	Brick Unit Used (size in mm)	Details of Strengthening Material	Parameters Considered	Strengthening Contribution	Failure Mode
(Fagone & Ranocchiali, 2018)		CFRP Composite Materials	Influence of spike anchors on the load-bearing capacity and dissipation of the capability of the reinforcements	Increase of F_1 and F_{max} , spike anchors effectively increase strength and dissipative power of CFRP reinforcement sheets	Cracks pattern in the central portion because of masonry compressive failure, detachment of the reinforcement from the substrate
(Padalu et al., 2018a)	Solid clay brick units 229 x 109 x 72	WWM reinforcement	Loading direction, reinforcement ratio, and effect of shear span	Enhances the flexural strength of the wallets deformability and energy absorption capacity	Failure of URM wallets is sudden and brittle, debonding of bed-joints at the interface with mortar.
(Verderame, Balsamo, et al., 2019)	Clay hollow units 250 x 250 x 80	FRCM and FRP	Unreinforced and reinforced one-way spanning masonry infills	Increment of the OOP strength	Combined flexural and arching mechanism
(Anić et al., 2021)	Hollow clay masonry blocks	Non-contact optical techniques to measure contour strains and deformations	With and without window and door openings	High stability, no cracks occurred in the frame, except in the infill wall and the lower beam	Debonding of the infill from the frame, fall out of parts of infill walls due to inertia

Authors	Brick Unit Used (size in mm)	Details of Strengthening Material	Parameters Considered	Strengthening Contribution	Failure Mode
(Furtado et al., 2018)		uniform OOP pressure applied by airbags	Gravity load and panel support condition	The arching mechanism provided the sufficient capacity to not occur the panel collapse	
(Milanesi et al., 2021)	Hollowed lightweight tongue and groove clay blocks, 235 x 350 x 235		Codified applications		Vertical arching mechanism with an asymmetrical behaviour, uplift, and torsional rotation at top, and shear failure or crushing of the units at bottom course
(Hwang et al., 2022)	Concrete bricks 190 × 90 × 57		Rocking and toe crushing strengths based on the elasticity and plasticity theorems of concrete		Rocking rotation and then ultimately failed with compressive toe-crushing
(Gkournelos et al., 2023)	Square masonry assemblages 450 × 450 × 120	TRM	Expanded polystyrene boards were used for thermal insulation	TRM-based strengthening scheme can improve the OOP response of MIW both in terms of strength and stiffness	Local crushing

The main goal of (Furtado et al., 2020) is to contribute to increasing the understanding regarding the infill panels' OOP behaviour and evaluate the influence of different variables in the panel's performance, and the second goal is to perform a comparative study between these two specimens with the other three tests already tested. (Milanesi et al., 2021) discussed the OOP resistance of strong clay masonry infills built-in full adherence with the frame and proposed some new formulations to better estimate these values according to the experimental evidence. (Hwang et al., 2022) tested two full-scale unreinforced masonry (URM) walls under constant axial stress and cyclic OOP lateral loads and proposed mathematical models to predict the rocking and toe-crushing strengths based on the elasticity and plasticity theorems of concrete. (Baek et al., 2024) presented a series of combined IP and OOP shake table tests conducted on a 60%-scaled 2-storey infilled RC building with parameters being the presence of openings in the MIW and the effect of bi-directional dynamic shaking to the latter. The evolution of damage exhibited significant variations between the two directions of the building.

2.3.2. In-Plane Loading

(Parisi et al., 2011) studied the behaviour of MIW with openings in the form of doors subjected to IP loads. The damaged specimen is further applied with cyclic displacement-controlled force repaired with inorganic matrix-grid (IMG) composites. (Redmond et al., 2016) proposed a method to account for the connection of the dowels between the infills and the reinforced concrete frame that forms a hybrid concrete-masonry structure that can elevate the seismic performance of the unreinforced infilled masonry structures. (Dautaj et al., 2019) carried out an experimental study on five MIRC frames with different upper and lower story heights of MIW to determine the shear resistance capacity using a newly proposed method that offers a promising approach to designing RC infill frames. (Niasar et al., 2020) constructed resilient infill wall (RIW) whose performance was enhanced by using metal connectors and conducted cyclic IP tests to compare the damage evolution and hysteric performance of the same, successfully concluded that the understanding of RIW is much better in terms of initial stiffness, storey drift ratios, and has been shown deterioration of strength. (Niasar et al., 2020) tested the efficacy of engineered cementitious composite (ECC) on URM under IP loading by constructing three specimens among which the first one is a reference wall, the second one is strengthened with ECC. Finally, the third was damaged and then retrofitted with ECC as in the case of the previous specimen and observed a hike in terms of energy dissipation capacity and shear strength in the second specimen and 115% and 330% in the third specimen.

Table 2.2. Summary of the literature review on the in-plane testing on MIW

Reference	Frame	Openings	Specimen Properties							Strengthening Material	Results	
			Scale	Overall Dim (mm)	Wall	Bricks		Mortar			Contribution of Strengthening Material	Failure Mode
					Aspect Ratio (L/H)	Type	Comp Strength (MPa)	Type/Ratio	Comp Strength (MPa)			
(Dawe & Seah, n.d.)	Steel frame	Doorway	-	3600 x 2800	1.19	Hollow concrete blocks	27 - 34	Type S	22	Masonry infilled in steel frames	Specimens consisting of a panel in a hinge frame with a 20 mm gap between the upper edge of the panel and the roof beam	Failure of the compression diagonal at ultimate load occurred as localized crushing of infill at the loaded comers
(Armin B. Mehrabi, et.al., 1996)	RC frame	No	1:02	3302 x 1955.8	1.5	Hollow and solid concrete blocks	2.39	Masonry mortar	-	Strong and weak panels	Strong frame and strong panel	Flexural, Mid-height horizontal crack, diagonal crack, horizontal slip, corner crushing
(Erdem et al., 2006)	RC frame	No	1:03	4310 x 2695	1 (second storey) & 1.5 (first storey)	Hollow clay block	7.8	Not Mentioned	2.6	RC infill & Carbon fiber reinforced polymer (CFRP)	Both strengthened frames behaved similarly under reversed cyclic lateral loading.	

Reference	Frame	Openings	Specimen Properties							Strengthening Material	Results	
			Scale	Overall Dim (mm)	Wall	Bricks		Mortar			Contribution of Strengthening Material	Failure Mode
					Aspect Ratio (L/H)	Type	Comp Strength (MPa)	Type/Ratio	Comp Strength (MPa)			
(Anil & Altin, 2007)	Ductile RC frame	Partial infills	1:03	1500 x 1050	Four different aspect ratios	RC partial infills	Not Mentioned	Not Mentioned	Not Mentioned	Dowels	Specimens with partial infill walls both connected to the column and beams of the frame	Column mechanism, Shear sliding, Web crushing, Short column failure, Column failure
(Almusallam & Al-salloum, 2007)	RC frame	No	1:02	2900 x 1950	1.35	Hollow concrete block	7.1	Not Mentioned	Not Mentioned	Glass Fiber reinforced polymers	GFRP sheets enhance the strength	Debonding of the FRP sheets
(Kakaletsis & Karayannis, 2008)	RC frame	Window and door	1:03	1500 x 1000	1.5	Clay brick and vitrified ceramic brick	3.10 & 26.4	Type M1 mortar/ 1:1:6	1.53 & 1.75	Clay brick and vitrified ceramic brick infill types	Strong infills	Plastic hinges, internal strut crushing, shear sliding at joints, shear sliding crack, corner rocking crushing
(Altin et al., 2010)	Ductile RC frame	No	1:03	1500 x 900	1.73	Hollow clay tiles, (masonry clay units)	6.6	Masonry mortar	4.2	Reinforced plaster	Mesh-reinforced high-strength plaster layer	Shear failure

Reference	Frame	Openings	Specimen Properties							Strengthening Material	Results	
			Scale	Overall Dim (mm)	Wall	Bricks		Mortar			Contribution of Strengthening Material	Failure Mode
					Aspect Ratio (L/H)	Type	Comp Strength (MPa)	Type/Ratio	Comp Strength (MPa)			
(Vladimir G. Haach Graça Vasconcelos and Paulo B. Lourenço, 2010)	-	No	1:02	Refer paper	0.67	Concrete blocks	12.1	Cement - sand mortar (1:3)	-	Innovative system for RC MIW based on the combination of vertical and horizontal trussed reinforcement	Presence of horizontal reinforcement	Mixed shear-flexure failure mode.
(Tasnimi & Mohebkah, 2011)	Steel frame	Window & door	1:01	2400 x 1870	1.25	Solid clay bricks	7.63	Cement-sand mortar/ 1:3	10.1	Steel frames with clay brick masonry infill having openings	Frames with solid infills	Diagonal tension or toe-crushing
(Augenti et al., 2011)	-	Door	1:01	5100 x 3620	1.35 & 1.7	Tuff masonry	4.13	Hydraulic mortar (1:6.25)	3.96	Inorganic matrix grid strengthening system	IMG strengthening system	Piers' rocking was more evident and diagonal shear cracking
(Zovkic, J., Sigmund, V., &	RC frame	No	01:2.5	2200 x 1500	1.38	Perforated clay bricks, lightweight	10, 5, 2.5	Lime cement mortar (1:1:5) &	5 & 12	High-strength and medium-strength perforated clay	Composite 'framed wall' structure	Sliding shear failure

Reference	Frame	Openings	Specimen Properties							Strengthening Material	Results	
			Scale	Overall Dim (mm)	Wall	Bricks		Mortar			Contribution of Strengthening Material	Failure Mode
					Aspect Ratio (L/H)	Type	Comp Strength (MPa)	Type/Ratio	Comp Strength (MPa)			
Guljas, 2012)						AAC blocks		Glue mortar		bricks, low-strength lightweight AAC blocks		
(L. Koutas et al., 2014)	Masonry wallets and RC prisms	No		400 x 400 & 600 x 500		Perforated, fired clay bricks	4.4	Rapid hardening cement mortar (1:0.5:4 & 1:2:5)	23.6, 9.4, 6.1	TRM jacketing	Anchors developed in this study enable the transfer of substantial tensile forces between masonry and concrete	Anchor debonding in the region over the concrete followed by anchor rupture
(Abdel-hafez et al., 2015)	RC frame,	No		1500 x 1600		Fired silt bricks	7.35			GFRP sheets, steel rebar impeded in the frame, plastering, and ferrocement mesh	Ferrocement strengthening method	Flexural nature
(L. Koutas et al., 2015)	RC frames	No	2:03	2730 x 2000		Perforated, fired clay bricks	11.3	Rapid hardening sulfur	12.6 and 13.3 MPa	TRM jacketing	TRM jacketing	Shear failure

Reference	Frame	Openings	Specimen Properties							Strengthening Material	Results	
			Scale	Overall Dim (mm)	Wall	Bricks		Mortar			Contribution of Strengthening Material	Failure Mode
					Aspect Ratio (L/H)	Type	Comp Strength (MPa)	Type/Ratio	Comp Strength (MPa)			
									mortar (1:1:5)			
(Jiang et al., 2015)	RC moment-resisting frames	No	1:01	6040 x 3175		Aerated concrete blocks	3.8	Cement mortar	3.11	MIW and flexible connection, MIW and rigid connection, and without infill wall	Infill wall with a rigid connection	Diagonal crack, horizontal slip, corner crushing
(Schwarz et al., 2015)	RC frames	Window	1:02	2045 x 1400		Autoclave-cured aerated concrete block	3.3	Cement mortar	8.3	AAC Masonry Infill Walls	Refer paper	Shear failure in the column
(Sassun et al., 2016)	RC frame	No	1:01			Concrete masonry unit	13.8 & 24.1	Portland cement sand mix / 1:3		hybrid concrete-masonry structure	A method is proposed to account for the dowel connections and the partially reinforced infill when designing hybrid concrete-	OOP failure

Reference	Frame	Openings	Specimen Properties							Strengthening Material	Results	
			Scale	Overall Dim (mm)	Wall	Bricks		Mortar			Contribution of Strengthening Material	Failure Mode
					Aspect Ratio (L/H)	Type	Comp Strength (MPa)	Type/Ratio	Comp Strength (MPa)			
											masonry structures in earthquake zones	
(Hassanli et al., 2016)		No		1400 x 2000		Concrete masonry unit	19.5 +/- 0.9	Portland cement lime type N (1:1:6)		Unbonded post-tensioned masonry walls (PT-MWs)	Doubling the total initial PT forces in the bars & using bonded horizontal steel	Major diagonal shear crack
(Dutu et al., 2016)	Timber frame	No	1:01	2760 x 2380		Japanese brick	57.6	Cement lime mortar (1:2:6)	4.8	Timber frames with masonry infills,	Good IP behavior of the timber-framed masonry system	Shear sliding failure
(Najif Ismail & Ingham, 2016)		-	1:01	4424 x 2652		Solid clay brick	39.4 & 21.3	Hydraulic cement mortar (1:2:9)	1.3 & 1.4	URM walls are strengthened using two different types of polymer TRM	TRM strengthening	Rupture of textile rovings spanning masonry cracks, shear failure
(Zhou et al., 2017)	Wood frame	No		2440 x 2800 wood & 1400 x		Hollow masonry blocks		Type S		Wood–Masonry Hybrid Wall		Brittle

Reference	Frame	Openings	Specimen Properties							Strengthening Material	Results	
			Scale	Overall Dim (mm)	Wall	Bricks		Mortar			Contribution of Strengthening Material	Failure Mode
					Aspect Ratio (L/H)	Type	Comp Strength (MPa)	Type/Ratio	Comp Strength (MPa)			
				2800 masonry								
(Leal G. et al., 2017)	RC frame	No	1:02	3750 x 1650		Clay bricks				Confining elements and horizontal reinforcement	Use of horizontal reinforcement	Sliding of the infill wall and diagonal tension in the beam-column connection of the frame
(N. Ismail et al., 2018b)	RC frame	No	2:03	2730 × 2000	1.36	Hollow Concrete masonry	7.23	Masonry	4.53	Basalt, Carbon, Glass Fiber	Increase in IP Strength and Ductility capacity	Main damage patterns observed in FRCM strengthened test frames were distributed cracking in the surface of the FRCM matrix, without any signs of fiber slippage/rupture

Reference	Frame	Openings	Specimen Properties							Strengthening Material	Results	
			Scale	Overall Dim (mm)	Wall	Bricks		Mortar			Contribution of Strengthening Material	Failure Mode
					Aspect Ratio (L/H)	Type	Comp Strength (MPa)	Type/Ratio	Comp Strength (MPa)			
(Akhoundi et al., 2018)	RC frame	No	1:03	2735 × 1875	1.55	Perforated clay brick	10	Premixed mortar	5	Composite rods, glass fibers	Increased the IP behavior of the infilled frame, namely the initial stiffness and lateral strength.	A smeared cracking pattern is observed in the mortar layers of the specimen strengthened with the commercial glass fiber mesh. The cracks developed mostly along the diagonals and some horizontal cracks at the level of the upper and bottom interfaces between the masonry infill
(Nadège et al., 2018)	RC frame	No	1:01	1630 × 1410	0.817	Hollow clay bricks		Cement mortar		FRP-composites or	TRC contribute more effectively	Macro cracks, concentrated in

Reference	Frame	Openings	Specimen Properties							Strengthening Material	Results	
			Scale	Overall Dim (mm)	Wall	Bricks		Mortar			Contribution of Strengthening Material	Failure Mode
					Aspect Ratio (L/H)	Type	Comp Strength (MPa)	Type/Ratio	Comp Strength (MPa)			
										TRC-composites	to an increase in ductility than FRP-composites, but FRP-reinforcements have proved in delaying the onset of damage	unreinforced zones
(Morandi et al., 2018)	RC frame	Door	1:01	4920 × 3330	1.43	Tongue and Groove Clay units	9.81	Cement mortar	7.68	Clay Bricks	Increased the IP behavior of the infilled frame's initial stiffness and lateral strength.	
(Cyclic et al., 2019)	RC frame	Door	1:04	1150 × 950	1.2	Solid clay bricks	10.9	Cement mortar / 1: 0.5		Solid clay bricks	The ductility of the RC frame was reduced by the presence of a central opening	Shear cracks in solid infill came across in the central part of the panel, whereas infill with an opening was dominated

Reference	Frame	Openings	Specimen Properties							Strengthening Material	Results	
			Scale	Overall Dim (mm)	Wall	Bricks		Mortar			Contribution of Strengthening Material	Failure Mode
					Aspect Ratio (L/H)	Type	Comp Strength (MPa)	Type/Ratio	Comp Strength (MPa)			
												at the corners of the opening.
(Liu et al., 2019)	RC frame	No	1:01	2240 × 1350	2	Recycled concrete Hollow blocks	10	Cement mortar	10	Recycled concrete Hollow blocks	Improves the strength and energy dissipation capacity of the RCHB masonry structure	Diagonal cracks and horizontal cracks widened rapidly and linked together to form a large “X” shape crack under cyclic loading.
(L. Wang et al., 2019)	RC and PC frame	Door	1:02	2500 × 1515	1.55	Porous brick	15.9	Cement mortar	6	Porous Bricks	MIW with an opening ratio of 27.8% could increase the lateral load resistance and initial stiffness of PC frames by 63.0% and 124.2%, respectively	No shear crack occurred at the beam-column joints. Wide diagonal stepped cracks occurred at the left panel and some of the bricks collapsed.

Reference	Frame	Openings	Specimen Properties							Strengthening Material	Results	
			Scale	Overall Dim (mm)	Wall	Bricks		Mortar			Contribution of Strengthening Material	Failure Mode
					Aspect Ratio (L/H)	Type	Comp Strength (MPa)	Type/Ratio	Comp Strength (MPa)			
(Maheri et al., 2019)	RC frame	No	1:01	1590 × 1560	1.164	Hollow Concrete masonry	20.63	Cement mortar	11.6	Concrete with steel mesh	Increasing the concrete layer thickness and compressive strength decreases ductility while increasing the reinforcing steel ratio	Diagonal shear failure of the wall is the predominant mode of failure under IP loading
(Do et al., 2019)	RC frame	No	1:01	3000 × 2250	1.25	Hollow clay bricks	4.1					
(Dautaj et al., 2019)	RC frame	No	2:03	2600 × 2200	1.18	Hollow brick masonry		Cement mortar		Hollow brick masonry	Increase in stiffness	After the masonry degraded, plastic hinges developed in discreet locations at the top and bottom of the columns

Reference	Frame	Openings	Specimen Properties							Strengthening Material	Results	
			Scale	Overall Dim (mm)	Wall	Bricks		Mortar			Contribution of Strengthening Material	Failure Mode
					Aspect Ratio (L/H)	Type	Comp Strength (MPa)	Type/Ratio	Comp Strength (MPa)			
(Esposito & Rots, 2020)	Masonry wall	No	1:01	2760 × 1100	2.5	Calcium Silicate Bricks	13.26	Cement mortar 2.8: 1	7.57	Calcium silicate brick masonry	Increase in IP Strength	Slender walls fail in flexure governing, and shear failure occurs for low slender ratios.
(Niasar et al., 2020)	Masonry wall	No	1:02	2000 × 1400	1.43	Solid clay bricks	20	Cement mortar	9.6	Engineered cementitious composites	Increase in shear strength and energy dissipation	Cracks occurred at the top of the steel rebar dowels in the retrofitted walls
(Niu et al., 2020)	RC frame	No	1:01	1610 × 906	1.81	Clay bricks	13.4	Cement mortar	10	Confined masonry	As chloride corrosion cycles increased, the time of primary horizontal cracks at the brick wall was formed early, which reduced the bond strength between brick and mortar.	

Reference	Frame	Openings	Specimen Properties							Strengthening Material	Results	
			Scale	Overall Dim (mm)	Wall	Bricks		Mortar			Contribution of Strengthening Material	Failure Mode
					Aspect Ratio (L/H)	Type	Comp Strength (MPa)	Type/Ratio	Comp Strength (MPa)			
(da Porto et al., 2020)	RC-frame	Door	1:01	4500 × 3000	1.56	Robust clay bricks	13.5	Cement mortar	10	Robust clay bricks with reinforcement in both vertical and horizontal	Overall performance of robust clay MIW systems is adequate, reinforcement reduces damage and increases ductility	More moderate and uniform damage pattern and a limited toe crushing close to the masonry corner
(Zuo et al., 2021)	Steel Frame	Door and window	1:02	2478 × 2450	0.9	Solid clay bricks	14.95	Cement mortar	4.84	Solid clay bricks	The infills can greatly improve the load-carrying and energy-dissipation capacities	The crushing failure of infill piers
(Shah et al., 2021)	RC frame	No	1:01	1080 × 1080	0.875	Solid clay bricks		Cement mortar		Solid clay bricks	Increase in stiffness and capacity	
(Lu & Zha, 2021)	RC frame	No	1:01	4000 × 3000	1.32	Hollow Concrete masonry	10	Cement mortar	10	Novel resilient infill	Reduces infill damage and improves energy dissipation capacity	Damage is initiated by the yielding of the metal connectors.

Reference	Frame	Openings	Specimen Properties							Strengthening Material	Results	
			Scale	Overall Dim (mm)	Wall	Bricks		Mortar			Contribution of Strengthening Material	Failure Mode
					Aspect Ratio (L/H)	Type	Comp Strength (MPa)	Type/Ratio	Comp Strength (MPa)			
												Subsequently, the wall cracks, the mortar and bricks begin to fall off, finally the wall collapses
(Furtado et al., 2021)	RC frame	Window	1:01	4800 × 2800	1.82	Hollow clay bricks	10	Cement mortar	5	TRM	TRM increased the initial stiffness, maximum peak strength, and energy dissipation capacity	Diagonal cracking is visible from the wall's top right. Apart from the plaster cracking, it also introduced some damage to the textile mesh
(Lyu, Deng, Han, et al., 2022)	RC frame	No	1:01	4700 × 3000	1.95	Hollow clay bricks	5.52	Cement mortar	3.2	High ductile concrete	Restrained crack development and prevented brittle failure of the MIW	Crushing failure occurred in the infill wall corner.

Reference	Frame	Openings	Specimen Properties							Strengthening Material	Results	
			Scale	Overall Dim (mm)	Wall	Bricks		Mortar			Contribution of Strengthening Material	Failure Mode
					Aspect Ratio (L/H)	Type	Comp Strength (MPa)	Type/Ratio	Comp Strength (MPa)			
(Lyu, Deng, Ma, et al., 2022)	RC frame	No	1:01	4700 × 3000	1.95	AAC blocks	5.52	Cement mortar	5	High ductile concrete with anchor plates	Enhance the deformation and energy dissipation capacities of the AAC-infilled frame	Frame-infills retrofitted with plaster layers showed brittle failure
(Kabas & Kusain, 2023)	RC frame	Window and door	1:03	1500 × 1300	1.1	Hollow clay bricks	7.2	Cement mortar	3.5	Carbon fiber-reinforced polymer	CFRP strips increased the ultimate load capacity, initial stiffness, displacement ductility, and energy dissipation capacity values of the masonry infilled frame systems	In the strengthened specimens, the infill walls collapsed not due to shear cracks but due to crushing bricks in areas with no CFRP strips or at the corners of the RC frame
(F. Wang, 2023)	RC frame	No	1:01	3600 × 2650	1.15	Hollow Brick masonry		Tsirco-Poly-122		FRCM with phase change materials	Reduces infill damage and improves energy	Fiber rupture of the fabric and fragmentation of

Reference	Frame	Openings	Specimen Properties							Strengthening Material	Results	
			Scale	Overall Dim (mm)	Wall	Bricks		Mortar			Contribution of Strengthening Material	Failure Mode
					Aspect Ratio (L/H)	Type	Comp Strength (MPa)	Type/Ratio	Comp Strength (MPa)			
								commercial mortar		(PCMs) and Extruded polystyrene sheets (XPS)	dissipation Capacity and ductility	the matrix, brick Crushing at the corners at different levels
(Smiraldo et al., 2023)	RC frame	No	1:01	4900 × 2750	1.83	Hollow clay bricks	7.2	Cement mortar	6.4	Laminated Timber panels	Increase in maximum base shear capacity, displacement capacity, and rotational capacity	Bending of the RC columns, and yielding of the fasteners, with a few of them snapping after yielding
(K. S. Sreekeshava, Hugo Rodrigues, 2023)	RC frame	No	1:02	2100 × 1400	1.36	Solid clay bricks	7.6	Cement mortar / 1: 6	5.02	Geo fabric	Increase in load-carrying capacity and ductility	No crack was observed in the geo-fabric, but masonry failure was observed in a stepped pattern in unreinforced regions

Six half-scale testing specimens, including three unreinforced concrete block masonry walls (URM) and three confined walls, were tested by (M. Deng et al., 2020) under IP cyclic loading to investigate their seismic performance before and after the upgrade. The test results indicated that these configurations significantly increased the lateral shear strength, stiffness, and energy dissipation capacity of the URM walls, and changed the brittle failure mode into a ductile mode. (Roosta and Liu, 2021) presented an experimental study on the IP behaviour of a masonry infilled frame system assessing the effects of several design parameters on the behaviour of this type of infilled frame and assessing its performance against its infilled RC frame counterparts. (Azmat et al., 2022) investigated the influence of full-scale brick MIW on the seismic performance of RC frames and found that the infill walls improve the RC frame performance in terms of strength and stiffness. (F. Wang, 2023) focused on the development of an FRCM system in combination with phase change materials (PCMs) and extruded polystyrene sheets (XPS) to achieve adequate mechanical and thermal properties for RC and masonry structures. The IP behaviour of five FRCM-strengthened RC frames with hollow-brick wall infill was tested under cyclic loading to investigate the improvement in earthquake resistance. (Kabas & Kusain, 2023) examined the general load-displacement behaviour of RC frames with opening MIW in different sizes and locations under lateral earthquake loading. The strengthening method developed with anchored carbon fiber reinforced polymers (CFRP) strips increased the ultimate load capacity, initial stiffness, displacement ductility ratio, and dissipating capacity values of the masonry infilled frame systems with opening by an average of 72%, 11%, 13%, and 10%, respectively.

2.3.3. Masonry Infill Walls Strengthened with Textile Reinforced Mortar

Grids for TRM applications are often constructed using carbon fibers, individually treated basalt fibers, and glass fibers that are resistant to alkalis. The application of TRM in concrete and masonry projects has been documented on several occasions (L. N. Koutas et al., 2019). These fabrics are warp-knitted fabrics, which are manufactured for applications in civil engineering, which have the inlay yarns are spread throughout the textile in two orthogonal directions, which are 0° straight yarns in the longitudinal direction and 90° straight yarns in the transverse direction. The inlay yarns are sometimes placed diagonally and are also consecutive yarns oriented at a 45° angle in the warp-knitted fabric (Gries et al., 2016). The most recent cutting-edge research indicates that TRM is useful for fortifying masonry and concrete constructions. Five FRCM-enhanced RC frames with hollow-brick wall infill were investigated

by (F. Wang, 2023) for their IP behaviour to look at the improvement in earthquake resistance under cyclic loading. Ultimately, it was demonstrated that the mechanical and seismic performance of RC frames filled with masonry could be significantly improved by using this innovative integrated technique. (C. Filippou et al., 2022) carried out an extensive review of masonry walls retrofitted with TRM both experimental and numerical studies available and suggested that TRM reduces the vulnerability of collapse criteria if the guidelines apply to the surrounding RC frame, suggested that lack of specified criteria for infill walls within RC frames leads to the inapplicability of this method on existing structures. (Sagar et al., 2019) evaluated the two modes of fabric application namely direct application and sandwich application to strengthen the masonry-infilled RC frames where the former method proved to be more effective than the latter method. (L. N. Koutas & Bournas, 2019) determined that the behavior of MIW retrofitted with carbon-fiber TRM jackets was drastically improved when subjected to OOP loads where the thickness of the wall and the infill-frame interaction have pivotal roles in the behavior of the wall. (Ismail et al., 2018b) presented an overview expertly conducted on the efficiency of three kinds of FRCM, namely basalt, carbon, and glass, to resist the critical shear damage in unreinforced hollow concrete block (HCB) masonry, which altered the failure mode from sliding bed joint brittle mode to gradual diagonal cracking on toe crushing. Observations indicated that FRCM rupture and debonding did not occur. In addition, other parameters such as shear strength, toughness modulus, and energy deformation capacity considerably increased with FRCM.

(Carozzi et al., 2018) presented the performance of ancient masonry structures strengthened with TRM systems with different glass fiber grids and a NSM system. (Triantafillou et al., 2018) tested a system combining both TRM and thermal insulation, which turned out to be a highly effective technique in increasing the IP resistance of masonry wall. (Bilotta et al., 2017) presented the results of tensile and bond tests of FRCM systems bonded to masonry specimens and were monitored by the digital image correlation (DIC) technique. (Carozzi & Poggi, 2015) investigated five different types of FRCM materials made with different fiber grids for masonry strengthening. (L. Koutas et al., 2015) examined the significance of the textile reinforced mortar (TRM) jacketing retrofitting scheme of a three-story reinforced concrete frame and concluded that the infill full-face application of TRM needs support by proper frame-infill connection to obtain the optimistic output. (Jiang et al., 2015) performed full-scale reversed cyclic in plane and OOP test on URM walls strengthened with polymer TRM, which were constructed using vintage solid clay bricks and low-strength

hydraulic cement mortar to repeat the similar properties of ancient masonry material. The observations concluded that the strength increased from 128% to 136% when URM tested IP loads and 575% to 789% under OOP loading. (L. Koutas et al., 2014) concluded that the ultimate flexural or shear capacity, stiffness, and performance of concrete members could be increased by strengthening those with TRM. (Bournas & Triantafillou, 2008) compared experimentally the effectiveness of TRM jackets and FRP jackets as a means of confining RC columns with lap splices at their base and concluded that TRM jackets enhanced the lateral strength (25.6%) and deformation capacity (64.7%) under cyclic loads.

2.4. NUMERICAL WORK

Several numerical investigations were performed to investigate the effect of numerous parameters on the performance of reinforced concrete masonry infill frames. The references are segregated year-wise, from oldest publication to the recent (1996 to 2023) and summarized in tabular form in Table 2.3.

Experimental research provides accurate results but on the other side also has a few disadvantages in the form of the economic aspect, space occupation to conduct tests, and time-consuming setup of the test such as mounting the types of equipment like actuators, sensing meters like strain gauges, linear variable differential transformer (LVDT), Data Acquisition System, slow motion cameras to capture the crack propagation. Hence, to overcome these limitations involved in conducting the experimental tests, the best-suited alternative is numerical simulation or modeling, which becomes crucial for evaluating seismic behavior and undertaking parametric studies. Numerical modeling encoded in computer programs has become increasingly employed to predict the behavior of masonry-infilled frames as computing capability has advanced over the previous two decades. The finite element method (FEM) has been widely employed by researchers to comprehend the performance of infilled RC frame systems under seismic loading.

Simulation of masonry walls can be implemented in three ways: micro modeling, simplified micro modeling, and macro modeling, micro modeling of infill walls, involves modeling masonry units, mortar joints, and the frame wall interface separately, as well as their relative constitutive models. In the simplified micro-modeling method, the thickness of the brick units is increased on all sides to half the thickness of the mortar. Macro models follow a simple simulation technique in which the whole masonry wall including the brick units and

mortar is modeled as a solo panel, anyhow that can only predict appropriate results. The micro modeling approach delivers more accurate results, which also involves huge storage, and space for data, and is time-consuming. Hence, many researchers conducting numerical simulations on the study of the performance of MIW during seismic activities usually prefer a simplified micro modeling approach so that few idealizations (such as not considering the thickness of mortar, increasing the thickness of the brick unit) can be assumed to extract the desired output.

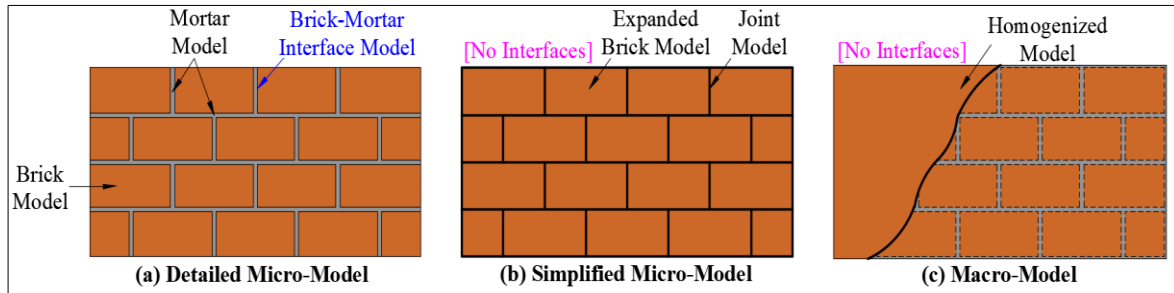
The mentioned modeling techniques, shown in Figure 2.1, can be selected, depending on the degree of accuracy and simplicity desired (Lourenço, 1996):

- In detailed micro-modeling, the continuum elements represent the units and mortar in the joints while the unit-mortar interface is represented by discontinuous elements.
- In simplified micro-modeling, the continuum elements represent the expanded units (Figure 2.2).
- In macro modeling, the behavior of mortar joints and the unit-mortar interface is grouped in discontinuous elements in macro-modeling; and units, mortar, and the unit-mortar interface are discarded in the continuum.

As mentioned previously, numerical modeling encoded in computer programs has become increasingly employed to predict the behavior of masonry-infilled frames as computing capability has advanced over the previous two decades. Since FEM was employed in this work, the following literature review will focus on FEM investigations in brick-infilled frames. (X. Wang et al., 2017) investigated the effect of TRM on the non-linear response and failure modes of masonry walls by developing a model using the DIANA finite element analysis (FEA) software. Mortar elements were modeled by implementing a total strain rotating crack material model. For infill wall elements, a softening anisotropic elastoplastic continuum model was applied (Hill type criterion for compression and Rankine type yield criterion for tension). (Furtado et al., 2021) evaluated the impact of the openings and the use of textile-reinforced mortar strengthening along with the slenderness of MIW constructed with horizontal hollow clay bricks. The numerical validation of the experimental study was carried out using the software Open Sees that concluded that IP maximum strength and energy dissipation capacity were decreased by the openings by roughly 40% and 18%, respectively.

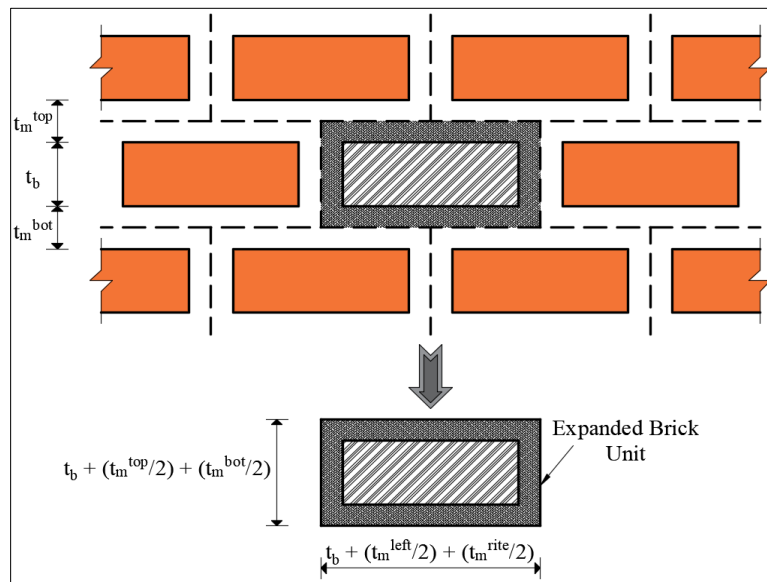
(Ademovi et al., 2023) examined the seismic response of a typical Austro-Hungarian masonry building in Sarajevo in modeling scenarios with various horizontal diaphragm typologies and found that the stiffness of the diaphragm and its method of connection to load-

bearing walls determine how well the diaphragm can improve the seismic behaviour of such buildings. The IP shear behaviour of URM wallettes built with Sarooj mortar and retrofitted with NSM-GFRP bars is examined by (Soleymani et al., 2024) through experimental and computational research. The test results demonstrated that the wall's IP shear strength was greatly boosted using the epoxy filled joint (EFJ) approach.



(a) Macro modeling; (b) meso modeling; (c) detailed micro modeling.

Figure 2.1. Main modeling approaches for masonry structures



t_b = thickness of mortar; t_m = thickness of brick unit; t_m^{top} = thickness of mortar above the brick; t_m^{bot} = thickness of mortar below the brick.

Figure 2.2. Expanded brick unit (Kouris et al., 2020)

(Kareem et al., 2022) use nonlinear three-dimensional (3-D) solid finite elements to represent the frame, and the discrete macro-element method (DMEM) model, or macro-elements, is used to simulate the infills. In contrast to other models, this one makes use of 2D continuum contact components to simulate the shear behavior between the frame and infill, which heavily influences the lateral resistance. (Basili et al., 2016) proposed a two-dimensional

modeling approach using MIDAS FEA software to analyze the IP shear behavior of tuff stone masonry panels retrofitted with a basalt textile reinforced mortar (BTRM) system. Isotropic continuum elements were used to model the infill wall, but different non-linear functions were used for the tensile and compressive behavior of the infill wall. The tension elastic-brittle material model for textile reinforcement is employed for the BTRM strengthening and the mortar. A perfect bond is assumed between the TRM system and the masonry wall. (C. A. Filippou et al., 2020) conducted a numerical study to simulate the IP behavior of RCFMI, which was experimentally studied by (L. Koutas et al., 2015), by developing a two-dimensional finite element model using DIANA FEA. They used a smear-cracked approach constitutive model to precisely model the characterization of the nonlinear response of concrete, masonry infill, and TRM. (L. Koutas et al., 2015) developed a numerical model to simulate the nonlinear performance of the concrete masonry-infilled RC frames subjected to IP lateral forces. FEM ABAQUS was used, and the modeling of the behavior of masonry and concrete blocks was carried out using the concrete damaged plasticity (CDP) model. (Nasiri & Liu, 2017a) studied the effect of infill isolators significantly affecting a structure's natural period, stiffness, and strength, when subjected to seismic ground vibrations by considering various layers of carbon fiber reinforced polymer (CFRP) to strengthen the MIW, then simulated in ABAQUS.

(Fallahi et al., 2018) Implemented a micro-modeling approach to numerically model to comprehend the complex hysteretic behavior of the unreinforced masonry panels made up of soft brick subjected to lateral loads and determined that the aspect ratio (Height/Length of the wall has the greatest influence on the failure type. (Vemuri et al., 2018) selected the micro-modeling approach to study the behavior of solid brick masonry subjected to lateral loads. (Shah et al., 2021) numerically analyzed the experiments conducted by (Augenti et al., 2011) using a finite element micro-model of the masonry walls with TRM using DIANA FEA software. Isotropic continuum elements are used for modeling the brick units, mortar joints, and their interface. TRM was modeled as a grid reinforcement embedded in the mortar elements. A smear crack model based on the Rankine yield criterion for tension and the Von-Mises criterion for compression was used for the infill wall and mortar joint elements. (Parisi et al., 2011) uses the micro-modeling technique to construct an infill wall in ABAQUS by applying the actual earthquake excitation that took place in Iraq to analyze the contribution of MIW in the seismic behavior of reinforced concrete frames. (Augenti et al., 2011) proposed a simplified micro model to establish an effective way to model the 3-D nonlinear behavior of brickwork under monotonic in-plane, OOP, and cyclic loads using the extended finite element

method (XFEM) and plasticity-based constitutive models. The analysis is carried out utilizing the Newton Raphson technique in Abaqus 6.13, which has captured the non-linear behavior and failure mechanisms of masonry under both vertical and horizontal loads with some published experimental investigations in comparison. The significance of the presence of openings is modeled by (Shawkat & Rahman, 2017) using ABAQUS whose results displayed that the amount of area of the openings and the capacity of the wall in resisting lateral loads are not in proportion to each other. (Abdulla et al., 2017) in ABAQUS, developed a three-dimensional micro-model for similar specimens of the previous study but under diagonal compression loading. The brick units and mortar joints are represented by eight-node quadrilateral elements. A multi-directional Drucker-Prager and Mohr-Coulomb strength criterion supplemented Concrete Damage Plasticity model is implemented for these elements. A perfect bond is assumed between the TRM system and the cementitious matrix, which embedded the strengthening material modeled as a truss reinforcement. The primary objective of (Meillyta, 2012) is to find suitable numerical constitutive models and elaborate their efficiencies as an interface model to take into consideration the shearing, residual shear strength, and joint opening and closing under cyclic shear stresses in conventional combinations of concrete blocks and mortar joints.

(Kostinakis & Athanatopoulou, 2020) aimed to propose a multi-strut large-scale model suited for simulating the long-term force-displacement behaviour of infilled frames with various opening configurations. The outcomes show that the extent and spot of the opening have considerable repercussions on both the inclination and the effective width of the struts. (Nasiri & Liu, 2017a) proposed an attributed study concerned with developing a numerical model for simulating the nonlinear behaviour of the concrete masonry infilled R.C. frames subjected to IP lateral loading. The ABAQUS FEM software was incorporated into the modeling. FEM results of this study conveyed that the dilatancy of mortar should be considered in the numerical models. (Mohammed Ashraf Nazief, 2014) proposed an FE technique to model masonry infilled frames using the simplified micro-modeling approach and observed that the best location for an opening in an infill wall is where the interference with the developed compression strut is minimal. (Koutromanos et al., 2011) studied the nonlinear FE models to simulate the behaviour of masonry-infilled RC frames under cyclic lateral loading. The finite element models presented here can accurately reproduce the infilled frames' load-displacement response, crack patterns, and failure mechanisms. (Stavridis & Shing, 2010) proposed the initiation of nonlinear FEM models for determining the seismic performance of

masonry structures. The proposed modeling approach can understand various failure processes, and infilled RC frames show the load-displacement reactions. et. al., 2009) prepared single brick walls and eccentrically braced frames (EBF) with infilled walls and were analyzed by the FEA Diana software. The stiffness of the braced frames with infill walls showed better yield strength but on the other hand, the frame deteriorated due to plastic behaviour. (Al-Chaar, 2008) discovered a modeling technique that addresses masonry discontinuities by adding interface components for the masonry joints. Additionally, following a thorough evaluation of the literature, the selected constitutive material models' capabilities were illustrated. The experimental results are concisely summarized, and a constitutive model is presented by (Mehrabi & Benson Shing, 1997) for the general modeling of masonry mortar joints and cementitious interfaces. The models eventually can be used for numerical parametric studies to extrapolate existing experimental results to develop comprehensive design guidelines. The development of the hysteretic model and the definitions of the control parameters, which can be determined using any suitable theoretical model for masonry infills, has been carried out by (B. A. Madan et al., 1997). The proposed macro-model is better suited for representing the behaviour of infills in nonlinear time history analysis of large or complex structures with multiple components, particularly in cases where the focus is on evaluating the inelastic structural response.

To explore the bi-directional loading behavior of fully and partially grouted masonry shear walls, researchers used the Concrete Damaged Plasticity (CDP) model in ABAQUS. Although prior numerical studies have demonstrated the ability of FE models to simulate masonry infills or masonry shear walls, these models have some limitations. The 2D models were unable to capture several elements of infilled frames, such as non-typical geometric properties, stress concentration, local reinforcement effects, and OOP behavior, despite their ease of use. There is frequently a paucity of information supplied on the input material parameters for current 3-D model studies, making it impossible for others to recreate the model and accompanying results. Furthermore, because these models were calibrated using test results for a single type of brick infill and bounding frame, their efficacy for a wide variety of material and geometric factors was not examined.

Table 2.3 summarizes the main aspects of the published data on the numerical analyses, including the type of masonry blocks, type of strengthening material, parameters considered, and the strengthening contribution along with the failure modes.

Table 2.3. Summary of the literature review on the numerical analysis on MIW

Authors	Brick Unit Used (size in mm)	Details of Strengthening Material	Parameters Considered	Strengthening Contribution	Failure Mode
(A. Madan et al., 1997)	Clay bricks		Drift analysis and base shear		Cyclic lateral loading
(Mehrabi & Benson Shing, 1997)	Hollow and solid concrete masonry blocks		Compressive, shear and tensile strength, elastic and shear modulus		Lateral and horizontal loads
(Kaushik et al., 2007)	Burnt clay solid bricks		Compressive, shear and tensile strength, elastic and shear modulus		Crushing failure
(Al-Chaar, 2008)	Hollow concrete blocks		Compressive, shear and tensile strength, elastic and shear modulus		Cyclic lateral loads
(Amir Saedi Daryan, Masood Ziaei, Ali Golafshar, 2009)	Concrete blocks	Link Beams	Compressive, shear and tensile strength, elastic and shear modulus	Dissipation of a large amount of energy during earthquake	Dynamic loading
(Stavridis & Shing, 2010)	Empty frame, hollow and solid concrete masonry blocks		Compressive, shear and tensile strength, elastic and shear modulus	Increase in strength	Horizontal sliding, diagonal crack, panel crushing
(Vladimir G. Haach Graça Vasconcelos)		Prefabricated Steel Truss Reinforcement	Compressive, shear and tensile strength,		Shear-flexure failure

Authors	Brick Unit Used (size in mm)	Details of Strengthening Material	Parameters Considered	Strengthening Contribution	Failure Mode
and Paulo B. Lourenço, 2010)			elastic and shear modulus		
(Koutromanos et al., 2011)			Drift analysis and base shear		Lateral loading
(Rai et al., 2011)	Burnt clay bricks		Compressive, shear and tensile strength, elastic and shear modulus	Response of the system gets reduced	Seismic failure
(Meillyta, 2012)	Clay brick and concrete blocks		Compressive, shear and tensile strength, elastic and shear modulus		Shear failure
(Torrise, G S Crisafulli, F J, 2012)			Compressive, shear and tensile strength		Lateral loading
(Zhai et al., 2012)	Concrete blocks		Compressive, shear and tensile strength, elastic and shear modulus		Dynamic loading
(Kai et al., 2013)		A coefficient-based method will be used for the design	Peak ground accelerations	Technique used can be suitably adopted	Seismic failure
(Mohyeddin et al., 2013)			Compressive, shear and tensile strength, elastic and shear modulus		Dynamic loading failure (in plane and out of plane)

Authors	Brick Unit Used (size in mm)	Details of Strengthening Material	Parameters Considered	Strengthening Contribution	Failure Mode
(X. Chen & Liu, 2015)			Compressive, shear and tensile strength, elastic and shear modulus		Diagonal tensile cracking as well as crushing
(Mohammed Ashraf Nazief, 2014)	Hollow concrete blocks		Compressive, shear and tensile strength, elastic and shear modulus		Sliding shear failure
(Karimi et al., 2016)	Clay bricks		Compressive, shear and cyclic loading		Seismic failure
(G. Wang et al., 2017)	Solid clay bricks	Precast concrete columns and beams	Compressive, shear and tensile strength, elastic and shear modulus	Increase in strength	Shear failure
(Maidiawati & Sanada, 2017)			Compressive, shear and tensile strength, elastic and shear modulus	Increased survival time during ground motion	Seismic loading
(H. Deng & Sun, 2016)			Shear strength parameters	Increased survival time of the structure	Seismic failure
(Chungman et al., 2016)	Concrete bricks		Compressive, shear and tensile strength, elastic and shear modulus		Diagonal cracking
(Rahgozar & Hosseini, 2017)	Clay bricks	Mortars including mud,	Compressive, shear and tensile strength,	Improved structural performance	Shear failure

Authors	Brick Unit Used (size in mm)	Details of Strengthening Material	Parameters Considered	Strengthening Contribution	Failure Mode
		lime–mud, and lime–sand	elastic and shear modulus		
(De Risi et al., 2017)	Clay bricks		Lateral and horizontal loads, displacement	Technique used can be suitably adopted	Shear failure
(Ali . Laftah. Abbas and Maan. H. Saeed, 2017)			Lateral and horizontal loads, displacement		Dynamic loading failure
(Khatewada & Jiang, 2017)			Compressive, shear and tensile strength, elastic and shear modulus		
(Nasiri & Liu, 2017b)			Compressive, shear and tensile strength, elastic and shear modulus		Seismic loading failure
(Shawkat & Rahman, 2017)	Concrete masonry blocks		Compressive, shear and tensile strength, elastic and shear modulus		Seismic loading
(De Angelis & Pecce, 2018)			Dynamic testing		Dynamic loading
(Liberatore et al., 2018)	Hollow and solid brick blocks		Cyclic loading test		Seismic failure
(Baghi et al., 2018)	Ceramic bricks		Lateral loading, compressive, shear		Seismic failure

Authors	Brick Unit Used (size in mm)	Details of Strengthening Material	Parameters Considered	Strengthening Contribution	Failure Mode
			and tensile strength, elastic and shear modulus		
(Nasiri & Liu, 2019)	Concrete masonry blocks		Dynamic loading tests		Dynamic loading failure
(Šipoš et al., 2018)			Compressive, shear and tensile strength, elastic and shear modulus	Increase in strength	Seismic failure
(Pantò et al., 2019)	Commercial vertical perforated masonry	Commercial vertical perforated masonry	Lateral loading, compressive, shear and tensile strength, elastic and shear modulus	Improved structural performance	Seismic failure
(Maheri et al., 2019)	Hollow concrete masonry blocks		Compressive, shear and tensile strength, elastic and shear modulus		Diagonal shear failure
(Khalilzadeh Vahidi & Moradi, 2019)			Compressive, shear and tensile strength, elastic and shear modulus		Seismic failure
(Verderame, Balsamo, Ricci, & Domenico, 2019)	Hollow clay bricks	FRP's & CFRP's	Lateral loading, compressive, shear and tensile strength, elastic and shear modulus	Improved structural performance	Dynamic loading

Authors	Brick Unit Used (size in mm)	Details of Strengthening Material	Parameters Considered	Strengthening Contribution	Failure Mode
(Di Domenico et al., 2021)	Hollow clay masonry blocks		Lateral loading, compressive, shear and tensile strength, elastic and shear modulus		Seismic failure
(Liberatore & AlShawa, 2021)	Solid or hollow clay bricks		Lateral loading, compressive, shear and tensile strength, elastic and shear modulus		Seismic failure
(Yekrangnia & Asteris, 2020a)			Compressive, shear and tensile strength, elastic and shear modulus	Improved structural performance	
(Jalaeefar & Zargar, 2020)			Compressive, shear and tensile strength, elastic and shear modulus		Seismic failure
(Niu et al., 2020)	Sintered ordinary brick		Lateral loading		Seismic loading
(Nyunn et al., 2020)			Lateral loading		Column failure at corner and exterior region
(Liberatore et al., 2020)	Clay bricks and concrete blocks		Compressive, shear and tensile strength, elastic and shear modulus		Seismic failure

2.5. ANALYTICAL WORK

An extensive review of analytical works has led to the compilation of a database incorporating the references segregated year-wise in ascending order, from (1971 to 2021).

(Mallick DV, Garg RP 1971) have considered the effect of most probable positions of openings on the lateral stiffness of infilled frames (Figure 2.3). It is recommended that the best position for door opening be located in the center of the lower half of the panel and to the center of the window. Using FEM stiffness has been calculated for MIW with openings. To derive the stiffness matrices, Airy's stress function, which fulfills a bi-harmonic equation with B.C., was introduced. By minimizing the energy for linear edge displacement, the stress pattern obtained is

$$\left. \begin{aligned} X &= A_1 + A_2Y + A_3X \\ Y &= A_3 + A_4X + A_5Y \\ XY &= A_5 - A_6Y - A_7X \end{aligned} \right\} \quad (1)$$

Stress components having seven coefficients for the accuracy of the solution are of the form

$$\left. \begin{aligned} U &= B_1 + B_2X + B_3Y + B_4XY \\ V &= B_5 + B_6X + B_7Y + B_8XY \end{aligned} \right\} \quad (2)$$

The stiffness matrix of a beam element subjected to shear and axial deformation

$$K'B = \begin{pmatrix} \frac{12EI}{l^3} & & & \\ & \frac{AE}{l} & & \\ & & \frac{12EI}{l^3} & \\ & & & \frac{AE}{l} \end{pmatrix} \quad \text{Symmetrical} \quad (3)$$

Smith's formula was used to determine the length of contact for the frame without shear connectors

$$\frac{\beta}{l} = \frac{\pi}{2\lambda l} \quad \text{where } \lambda = 4 \sqrt{\frac{E_o t}{4EI}} \quad (4)$$

The stiffness of MIW with shear connectors can be derived using

$$S = \frac{A+B+C}{C+(A+B)} \quad \text{where } A = \frac{htan^2\alpha}{aE_s}, B = \frac{d}{WtE_s\cos^2\alpha}, C = \frac{h^3(3h+21)}{(2E_sI(6h+1))} \quad (5)$$

Where h is the wall height, W is the weight, t is the thickness, and E_s is the modulus of elasticity.

(Saneinejad & Hobbs, 1995) have considered a new analysis method of steel frames with concrete MIW subjected to IP forces. Further model is analyzed for multi-story infilled frames as braced frames. (Moehle JP, 1996) seismic performance is considered to produce structures that satisfy the specific performance of the objectives. The probabilistic approach should be used to deal with the uncertainties in estimating the capacity and demands (Madan BA et al., 1997.) an equivalent strut approach is considered, and hysterical modelling is proposed for masonry infill panels in the non-linear analysis of frame structures. Dynamic analysis is done for a light-reinforced concrete structure to find the influence of masonry infill frames.

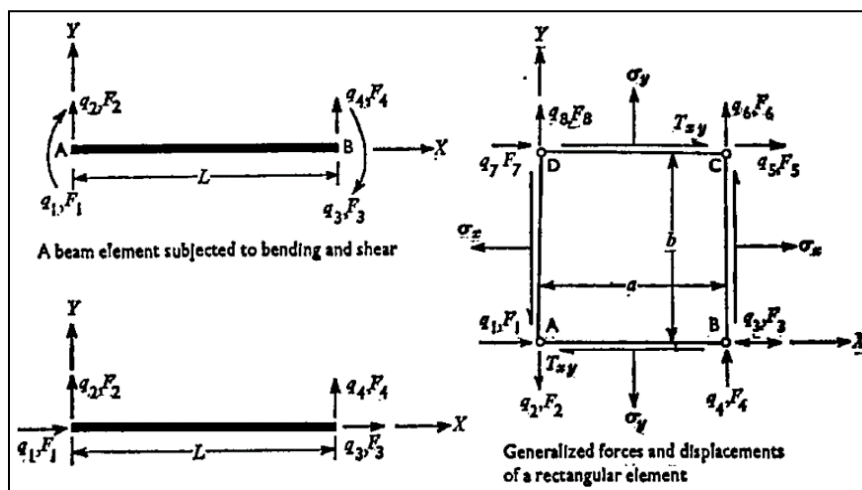


Figure 2.3. A beam element subjected to shear and axial deformation (Mallick DV, Garg RP 1971)

$$\text{Maximum lateral force } V_m = V_m^+ (V_m^-) \leq A_d f_m' \cos \theta \leq \frac{v t l'}{(1 - 0.45 \tan \theta) \cos \theta} \leq \frac{0.83 t l'}{\cos \theta} \quad (6)$$

$$\text{Displacement } u_m = u_m^+ (u_m^-) = \frac{\epsilon' m L_d}{\cos \theta} \quad (7)$$

$$\text{Where } A_d = (1 - \alpha_c) \alpha_c t h' \frac{\alpha_c}{f_c} + \alpha_b t l' \frac{\tau_b}{f_c} \leq \frac{0.5 t h' f_a}{f_c \cos \theta} \quad (8)$$

$$L_d = \sqrt{(1 - \alpha_c)^2 h'^2 + l'^2} \quad (9)$$

Where V_m is the maximum lateral force, U_m is the displacement, L_d is the lateral length.

The initial stiffness of the wall can be determined by

$$K_o = 2 \left(\frac{V_m}{u_m} \right) \quad (10)$$

$$V_y^+ (V_y^-) = \frac{V_m - \alpha K_o u_m}{(1 - \alpha)} \quad (11)$$

$$u_y^+(u_y^-) = \frac{V_m - \alpha K_o u_m}{K_o(1 - \alpha)} \quad (12)$$

K_o is the stiffness of the wall, V_m and U_m are the maximum lateral force and displacement.

The stiffness loss due to deformation is an important property of the hysteric model, including the control parameter η for Z , the hysteric parameter

$$dZ_i = \{A - |Z_i|^n [\beta \operatorname{sgn}(d\mu_i Z) + Y]\} \frac{d\mu_i}{\eta_i} \quad (13)$$

where $\eta_i = [s_k + \alpha(\mu_i - 1) + 1] / [s_k + \mu_i]$ for $\mu_i \geq 0$ (14)

The strength degradation is modelled reducing the yield force V_y from

$$V_y^k = V_y (1 - DI) \text{ where} \quad (15)$$

$$DI = \frac{\mu_{max} - 1}{\mu_c - 1} \left[1 - 0.25 s_{pl} \int \left(\frac{V}{V_y} \right) \frac{d\mu}{(\mu_c - 1)} \right]^{-s_{p2}} \quad (16)$$

Crack slip model $\mu = \mu_1 + \mu_2$ where μ_2 is displacement ductility component given by

$$d\mu_2 = a f(z) dz \quad (17)$$

$$f(z) = \exp\left(-\frac{[z - \check{z}]^2}{z_x^2}\right) \text{ where } -1 \leq z, \check{z} \leq 1 \quad (18)$$

$$\frac{dz}{d\mu} = \frac{[A - Z^n \{\beta \operatorname{sgn}(d\mu z) + \lambda\}]}{\eta \left[1 + a \exp\left(-\frac{[z - \check{z}]^2}{z_x^2}\right) (A - |Z|^n \{\beta \operatorname{sgn}(d\mu z) + \lambda\}) \right]} \quad (19)$$

(Yaw-Jeng Chiou, Jyh-Cherng Tzeng, 1999) a full-scale test verifies IP monotonic loading. Finally, after the analysis is completed, full-filled masonry walls show high stiffness, whereas the adjacent column fails with nearly uniform cracks. A complete first-order polynomial is chosen as the displacement function for the 2D block.

$$\begin{Bmatrix} u \\ v \end{Bmatrix} = \begin{bmatrix} 1 & 0 & -(y - y_o) & (x - x_o) & 0 \\ 0 & 1 & (x - x_o) & 0 & (x - x_o) \end{bmatrix} \begin{bmatrix} \frac{(y - y_o)}{2} \\ \frac{(x - x_o)}{2} \end{bmatrix} \begin{pmatrix} u_o \\ v_o \\ r_o \\ \varepsilon_x \\ \varepsilon_y \\ \gamma_{xy} \end{pmatrix} \quad (20)$$

$$\begin{Bmatrix} u \\ v \end{Bmatrix} = [T_i] [D_i] \quad (21)$$

Where u and v are the lateral force and displacement respectively.

The failure criteria for mortar are

a) Tensile failure –

$$\sigma \geq \sigma_t \quad (22)$$

$$d K^n \geq \sigma_t l \quad (23)$$

Where σ is the tensile stress and σ_t is the failure tensile stress

b) Shear failure –

$$\tau_f = \tau_o + \sigma_n \tan\varphi \quad (24)$$

$$\tau \geq \tau_o \pm \sigma_n \tan\varphi \quad (25)$$

$$s. K_s \geq \tau_o l \pm d K_n \tan\varphi \quad (26)$$

Where, τ_f is the shear failure and σ_n is the normal tensile stress

(Rodolico, 1985) carried out at the University of Adelaide and the University of Melbourne. The main objective of the research is to find the collapse behaviour of unreinforced masonry walls. Finally, the comparison of displacement-based analysis with time history analysis is made. The natural, highly non-linear system should be modelled as a primary linear single degree of freedom (SDOF) oscillator to apply T_{HA} to predict the semi-rigid rocking response of a URM wall. Doing this allows the utilization of time-stepping integration procedures, such as the Newmark constant-acceleration approximation. The modelling change is accomplished by the correlation of the individual framework dynamic equations of motion. Equation [27] addresses the generally acknowledged dynamic equation of action for a primary linear SDOF oscillator exposed to base excitation \ddot{a}_g where C is the corresponding damping coefficient, M is the framework mass, $v(t)$ the relocation reaction, and ω the framework average precise recurrence. Since for the SDOF oscillator, the framework recurrence ($f = \omega/2\pi$) is consistent. The single condition can portray assertive conduct. For semi-inflexible URM walls with the tri-straight, (F- Δ) rearrangements used to show the genuine non-direct bend, three states are needed to depict the unique behaviour with changing straight firmness segments. Equations [27-29] address the dynamic equation of motion where $v(t)$ is the removal reaction at either the mid-stature of an SS wall or at the wall top of a free-standing parapet wall.

(Crisafulli et al., 2000) it is seen that modelling a masonry structure is a complex issue because it shows a high non-linear behaviour (Figure 2.4). Different methods are considered, and further advantages and disadvantages of each of the methods are studied.

$$\ddot{v}(t) + \left[\frac{C}{M} \right]_{SDOF} \dot{v}(t) + [\omega^2]_{SDOF} v(t) = -[\ddot{a}_g]_{SDOF} \quad (27)$$

$$\ddot{v}(t) + \frac{3}{2} \left[\frac{C}{M} \right]_{EXP} \dot{v}(t) + \frac{3}{2} \left[\left(\frac{Re(1) + Ke(1)uy(2)}{Muy(1)} \right) \right]_{EXP} v(t) = -\frac{3}{2} [\ddot{a}_g]_{EXP} \text{ for } v(t) < u_y(1) \quad (28)$$

$$\ddot{v}(t) + \frac{3}{2} \left[\frac{C}{M} \right]_{EXP} \dot{v}(t) + \frac{3}{2} \left[\left(\frac{Re(1) + Ke(1)uy(2)}{Mv(t)} \right) \right]_{EXP} v(t) = -\frac{3}{2} [\ddot{a}_g]_{EXP} \text{ for } u_y(1) < v(t) < u_y(2) \quad (29)$$

$$\ddot{v}(t) + \frac{3}{2} \left[\frac{C}{M} \right]_{EXP} \dot{v}(t) + \frac{3}{2} \left[\left(\frac{Re(1) + Ke(1)v(t)}{Mv(t)} \right) \right]_{EXP} v(t) = -\frac{3}{2} [\ddot{a}_g]_{EXP} \text{ for } v(t) > u_y(2) \quad (30)$$

$$f_{SRR} = \frac{\sqrt{\frac{3}{2} \left[\left(\frac{Re(1) + Ke(1)uy(2)}{Mv(t)} \right) \right]_{SRR}}}{2\pi} u_y(1) < v(t) < u_y(2) \quad (31)$$

The first approximation to calculate the width of the equivalent strut in the lack of experimental data, assuming that:

$$w = \frac{d_m}{3} \quad (32)$$

where d_m is the diagonal length of the panel. Additional experimental information allowed a more refined evaluation of w , considering the ratio h_n/L_m , and a dimensionless parameter A_i (which takes account of the relative stiffness of the masonry panel to the frame) defined by:

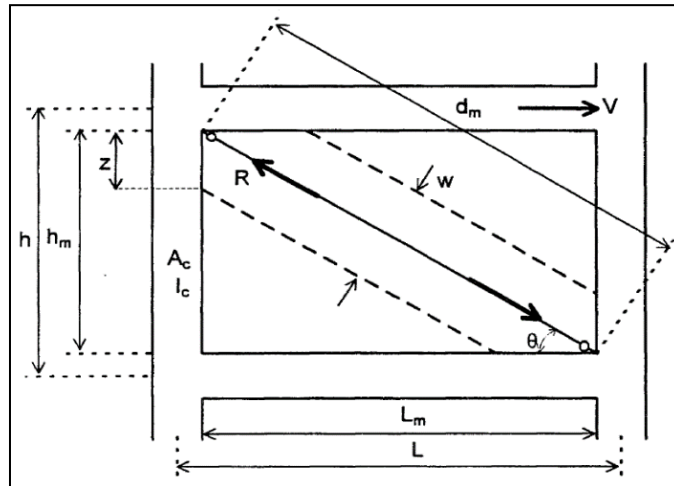


Figure 2.4. The effective width of the diagonal strut (Crisafulli et al., 2000)

$$\lambda_h = h^4 \sqrt{\frac{E_m t \sin 2\theta}{4E_c I_c h_m}} \quad (33)$$

t and h_m are the thickness and the height of the masonry panel, respectively, θ is the inclination of the diagonal of the panel, E_m and E_c are the modulus of elasticity of the masonry and the concrete, respectively, and I_c is the moment of inertia of the columns. The equation that is recommended for a lateral force level of 50% of the ultimate capacity is given by

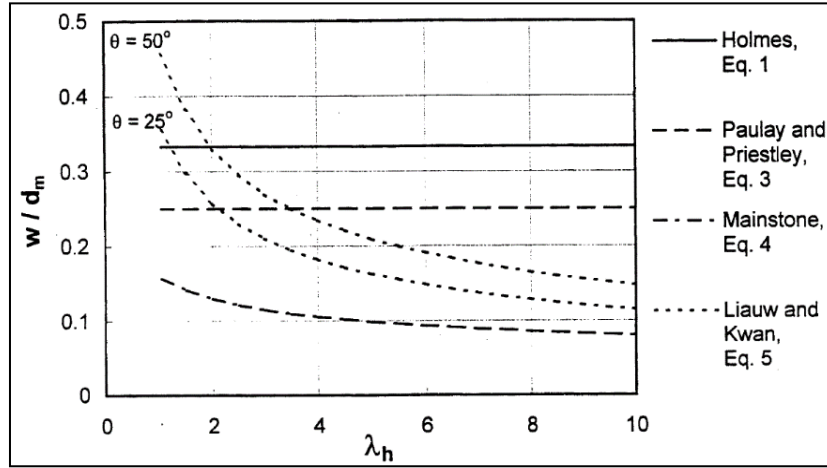


Figure 2.5. Variation of the ratio w/d_m for infilled frames as a function of the parameter λ_h (Crisafulli et al., 2000)

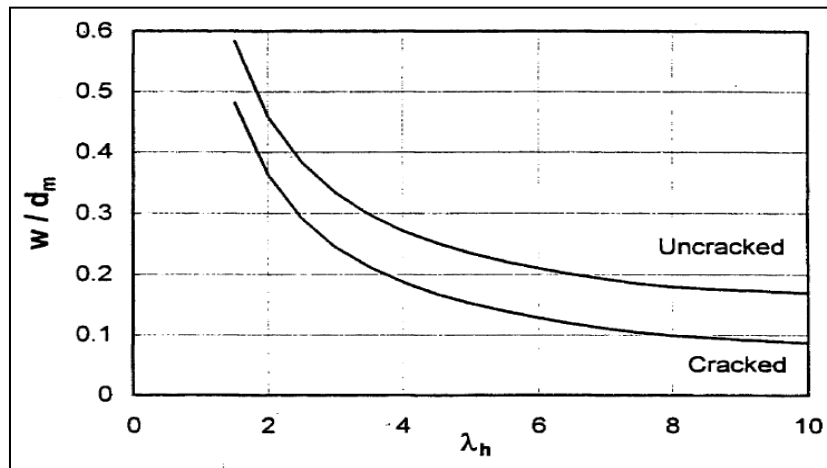


Figure 2.6. Ratio w/d_m for framed masonry structures (Crisafulli et al., 2000)

$$w = 0.25 d_m \quad (34)$$

Figure 2.5 illustrates the variation of the ratio w/d_m according to the previous expressions. Two sets of equations were proposed considering different states of the masonry infill

Uncracked panel:

$$\left. \begin{aligned} w &= \left(\frac{0.748}{\lambda_h} + 0.085 \right) d_m \quad \text{if } \lambda_h \leq 7.85 \\ w &= \left(\frac{0.393}{\lambda_h} + 0.130 \right) d_m \quad \text{if } \lambda_h > 7.85 \end{aligned} \right\} \quad (35a)$$

Cracked panel:

$$\left. \begin{aligned} w &= \left(\frac{0.707}{\lambda_h} + 0.010 \right) d_m \quad \text{if } \lambda_h \leq 7.85 \end{aligned} \right\}$$

$$w = \left(\frac{0.470}{\lambda_h} + 0.040 \right) d_m \text{ if } \lambda_h > 7.85 \quad (35b)$$

The modulus E_m calculates parameter A.11, corresponding to the considered state (uncracked or cracked masonry). These equations are plotted in Figure 2.6 as a function of the parameter λ_h . The principal advantage of the approach is the distinction between the uncracked and cracked stages. The comparison of Eqs. 35a and 35b indicate that w reduces significantly after cracking to a value ranging from 50% to 80% of the initial width. The higher reductions occur for large values of the parameter λ_h because the influence of the infill panel in the system's response is more remarkable in these cases. (Doherty et al., 2002) a newly developed displacement-based method for the seismic assessment of URM walls in one-way vertical bending for application to walls (as shown in Figure 2.7) in two-way bending is done the results are tabulated. The single-degree-of-freedom idealization of URM walls is shown in Figure 2.8.

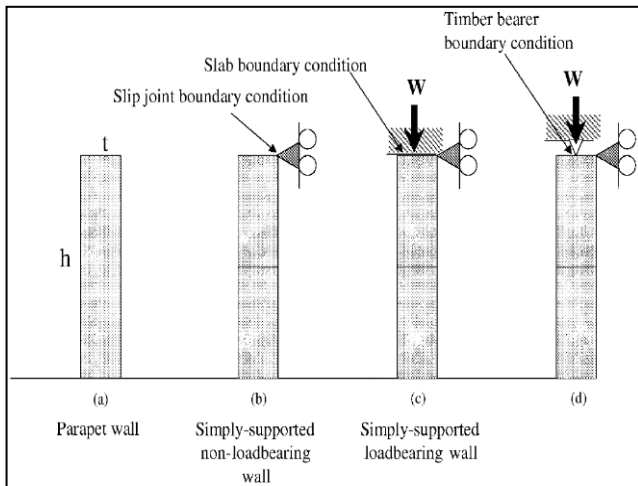


Figure 2.7. Unreinforced masonry wall support configurations (Doherty et al., 2002)

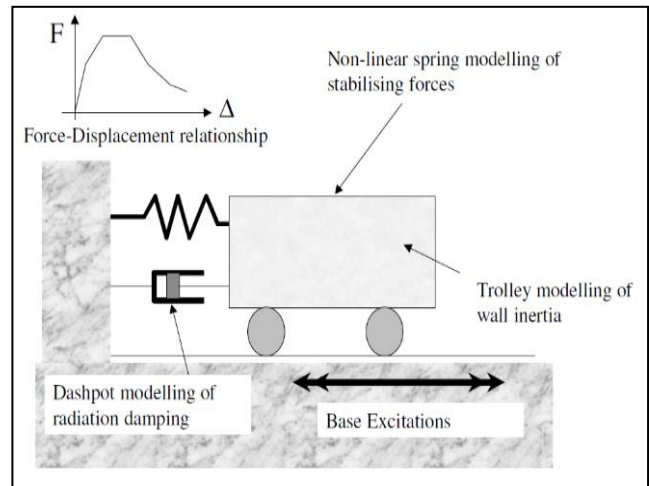


Figure 2.8. Idealized non-linear single-degree-of-freedom model (Doherty et al., 2002)

The computed displacement, velocity, and acceleration of the lumped mass are defined as the effective displacement, velocity, and acceleration, respectively. The equation of motion of the lumped mass SDOF system can, therefore, be expressed as follows

$$M_e \ddot{a}_e(t) + C v_e(t) + F(\Delta_e(t)) = -M_e a_g(t) \quad (36)$$

where $a_e(t)$ is the effective acceleration, $a_g(t)$ the acceleration at wall supports, $v_e(t)$ the effective velocity, $\Delta_e(t)$ the effective displacement, C the viscous damping coefficient and $F(\Delta_e(t))$ the non-linear spring force which can be expressed as a function of $\Delta_e(t)$ (NB: $F(\Delta_e(t))$ is abbreviated hereafter as $F(\Delta_e)$).

The effective modal mass (M_e) is calculated by dividing the wall into several finite elements, each with mass (m_i) and displacement (δ_i), and applying Equation (2) which is defined as follows:

$$M_e = \frac{(\sum_{i=1}^n m_i \delta_i)^2}{\sum_{i=1}^n m_i \delta_i^2} \quad (37)$$

The effective mass for a wall with uniformly distributed mass for parapet walls and walls supported at their top and bottom has been calculated to be three-fourths of the total mass, based on standard integration techniques. Thus,

$$M_e = 3/4 M \quad \text{where } M \text{ is the total mass of the wall}$$

A similar expression, Equation (4), also derived using standard modal analysis procedures, defines the effective displacement (Δ_e) (Figure 2.9).

$$\Delta_e = \frac{\sum_{i=1}^n m_i \delta_i^2}{\sum_{i=1}^n m_i \delta_i} \quad (38)$$

It can be seen from Equation (4) that

$$M_e = 2/3 \Delta_t \quad \text{for a parapet wall and} \quad (39a)$$

$$M_e = 2/3 \Delta_m \quad \text{for a simply supported wall and} \quad (39b)$$

where Δ_t and Δ_m are the top-of-wall and mid-height wall displacements, respectively.

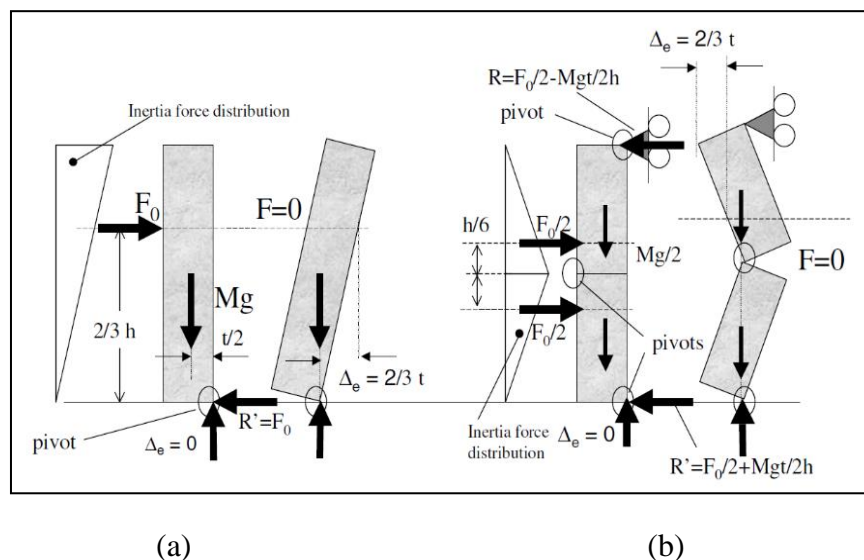


Figure 2.9. Inertia forces and reactions on rigid URM walls

(a) Parapet Wall at incipient Rocking and Point of Instability

(b) Simply Supported Wall at Incipient Rocking and Point of Instability

(El-Dakhakhni et al., 2003) Masonry infill frames are known for their stiffness, ductility, and strength of structure; in this paper, lateral stiffness, and lateral load capacity of concrete frame structures. This method can further be used in computer modelling, and non-linear analysis can also be performed. In the case of an unconfined panel, immediately after a diagonal crack develops within an infilled panel, the panel assumes itself confined inside the bounding frame and bearing against it over contact lengths, as shown in Figure 2.10.

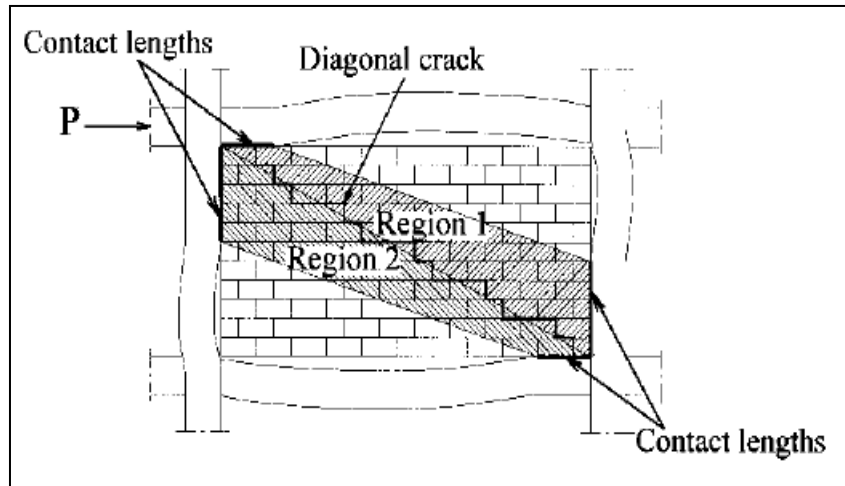


Figure 2.10. Infill panel separation into two diagonal regions (El-Dakhakhni et al., 2003)

The total diagonal struts area, A , is to be calculated by

$$A = \frac{(1-\alpha_c) \alpha_c ht}{\cos\theta} \quad (40)$$

The Young's modulus, E_u , of the panel in the diagonal direction using the following equation

$$E_\theta = \frac{1}{\frac{1}{E_o} \cos^4\theta + \left[-\frac{2\nu_o-90}{E_o} + \frac{1}{G}\right] \cos^2\theta \sin^2\theta + \frac{1}{E_{90}} \sin^4\theta} \quad (41)$$

(Kuzik et al., 2003) has studied the OOP behaviour of masonry walls reinforced with GFRP and subjected to cyclic loading. Simple model behaviour is taken for evaluation for strength and deformation characteristics. The amount of GFRP sheet reinforcement can be expressed as a reinforcement ratio (ρ_{GFRP}) in terms of the transformed section area as

$$\rho_{GFRP} = \frac{A_{GFRP} E_{GFRP}}{A_e E_m}$$

A_{GFRP} = area of the GFRP sheet reinforcement on one side of the wall

E_{GFRP} = modulus of elasticity of the GFRP sheet reinforcement on one side of the wall

E_m = prism modulus of elasticity of the masonry

Figure 2.11 shows the regression line plotted through the data and the resulting linear equation relating the two ratios.

The cracking moment can be explained by considering axial forces as

$$M_{cr}^f = \left(f_t + \frac{P}{A_e} \right) \cdot \left(\frac{2I^f g}{h} \right) \quad (42)$$

Where P is axial compressive force; A is the effective area of an uncracked cross-section; h is the total depth of the cross-section.

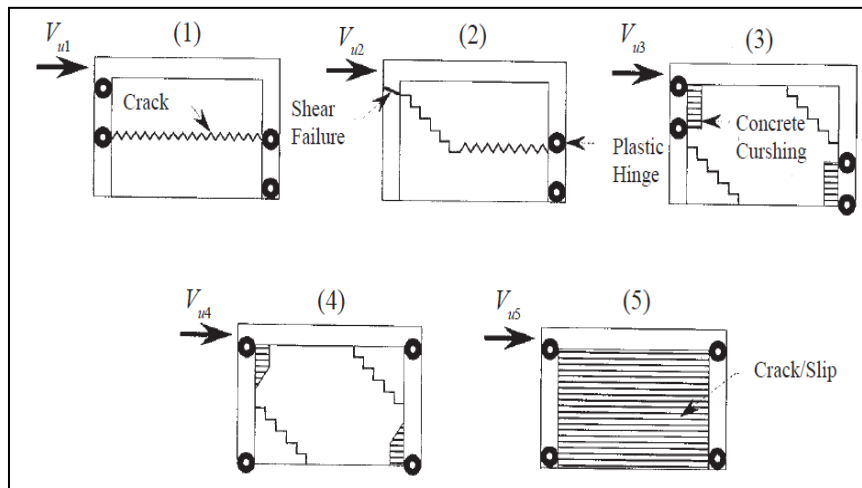


Figure 2.11. Selected failure mechanisms (Meharbi & Benson, 2003)

There are various numerical methods in the world. (Alwathaf et al., 2003) has reviewed conventional mortared and non-conventional mortarless interlocking blocks masonry. Also finally, different analytical methods for masonry joint analysis are reviewed. (Meharbi & Benson, 2003) simple techniques that can be used to evaluate the seismic performance of masonry-infilled reinforced concrete frames are presented. Response spectrum analysis is performed on the masonry structure, and results are evaluated. The selected failure mechanisms are displayed in Figure 2.11. (Simsir et al., 2004) OOP behaviour of unreinforced masonry structure is taken into consideration. Experimental results are compared with SDOF and MDOF. Two degrees of freedom are considered for dynamic stability. K. (Hwee Tan & H Patoary, 2004) thirty masonry walls were strengthened using three different fiber-reinforced polymers, with three anchorage methods, and were fabricated and tested under a concentrated load over a 100 mm square area. The test results were compared well with the analytical predictions. (Milani et al., 2006) the usage of a simplified homogenized technique is used for the analysis of masonry subjected to OOP loading. Efficient results are found in all the cases, indicating the proposed simple technique is sufficient for safety assessment for OOP-loaded

masonry panels. (Matjaz Dolsek, 2008) Four-storey reinforced concrete frame structures have been analyzed using the response spectrum method by inelastic approach. The provision of infills helps in resisting the loads and does not cause the failure of the columns. (Amato et al., 2008) due to masonry infills in the frame structure, infill behaviour switches from a strut element to a plate shell. The lateral stiffness of infill frames is evaluated.

Table 2.4. Analytical prediction of lateral resistance and stiffness

S.No.	Failure Mechanisms	Force Diagrams	Lateral resistance
1	Figure 2.11(1)	Figure 2.12	$V_{u1} = V_{wr} + F_{cc} + F_{ct}$ $F_{cc} = \frac{4M_{pc}}{h}$, $F_{ct} = \frac{4M_{pct}}{h}$
2	Figure 2.11 (2)	Figure 2.13	$V_{u2} = V'_{wr} + F_{cc} + V_{ct}$ $V'_{wr} = A_w \frac{\frac{\mu_r P}{A_w + 2 A_{ceq}}}{1 - 0.5 \mu_r \frac{h}{L}}$, $V_{ct} = 0.8V_{cs} + V_{cc}$
3	Figure 2.11 (3)	Figure 2.14	$V_{u3} = y f'_{mt} = m_c f'_{mthc}$ $m_c = \sqrt{\frac{4M_p}{f'_{mthc^2}}}$ $y = \sqrt{\frac{4M_{pc}}{f'_{mt}}}$
4	Figure 2.11 (4)	Figure 2.15	$V_{u4} = 0.67 f'_{m} \alpha h + 2F_c =$ $(m_c^2 + 0.67\alpha - 0.5\alpha^2) f'_{mth}$ $\alpha h = \pi^4 \sqrt{\frac{E_c I_c h}{4E_w t \sin 2\theta}}$
5	Figure 2.11 (5)	Figure 2.16	$V_{u5} = V_{wr} + F_f$ $F_f = \frac{4M_{pc}}{h}$

(P.G. Asteris, 2008) a different computer-based programming method is done to analyze single bay single storey masonry infilled RC frame when subjected to Lateral load. The difference in Magnitude and contact lengths has been clearly shown for different frame members. (Kaushik et al., 2008) A comparative study was carried out considering different models. After linear and non-linear analysis, it is found that the 3-strut model can estimate the force resultants in RC members with accuracy. In addition, a single strut model can be effectively used when masonry is discontinued in the first storey for parking space. (Stavridis, 2009) Unreinforced masonry panels are used for exterior or interior partitions in concrete frames, which are further subjected to shake table tests. This approach can be further used for the construction of simple struts in the construction of the entire structure.

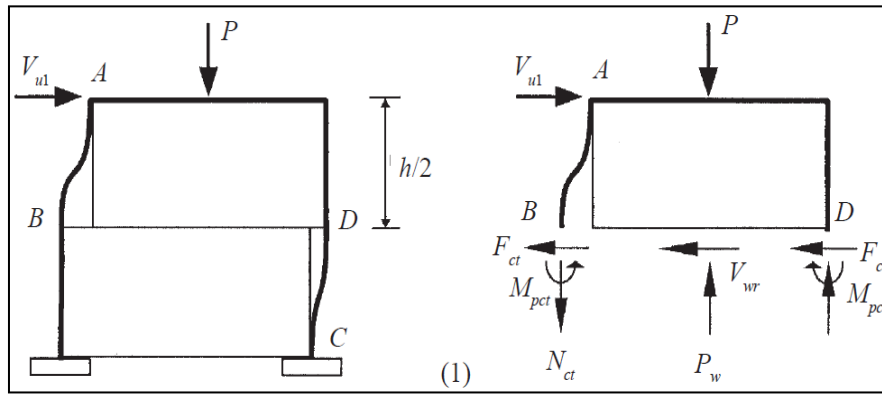


Figure 2.12. Force diagrams for mechanisms 1 (Meharbi & Benson, 2003)

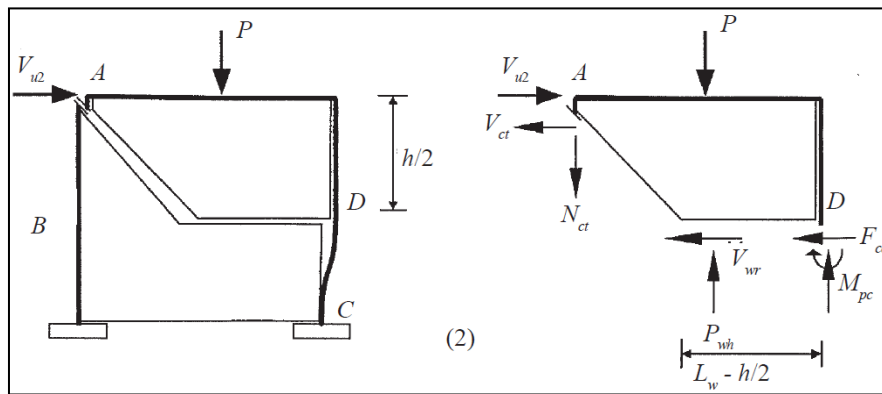


Figure 2.13. Force diagrams for mechanisms 2 (Meharbi & Benson, 2003)

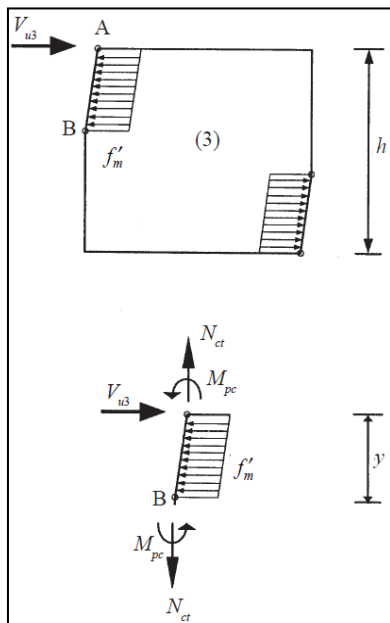


Figure 2.14. Force diagrams for mechanisms 3 (Meharbi & Benson, 2003)

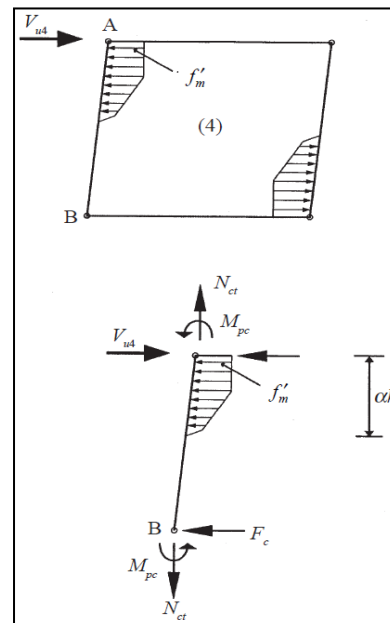


Figure 2.15. Force diagrams for mechanisms 4 (Meharbi & Benson, 2003)

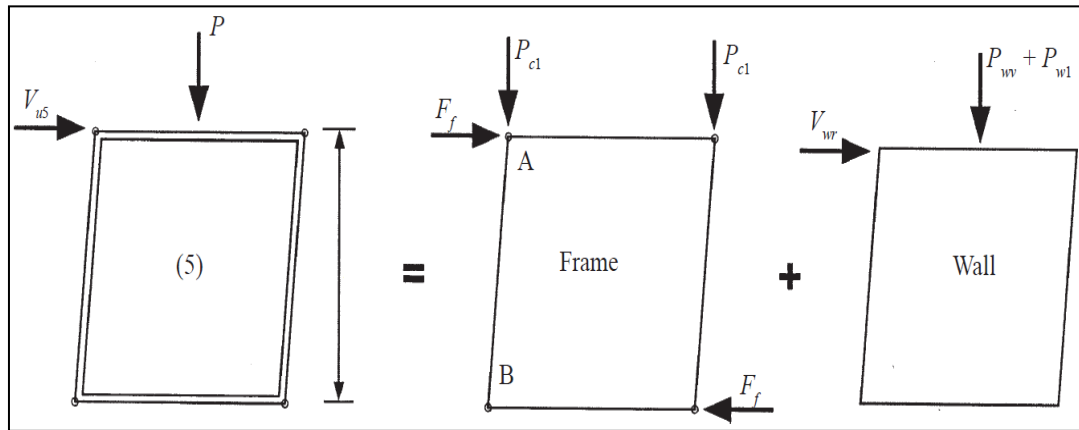


Figure 2.16. Force diagrams for mechanisms 5 (Meharbi & Benson, 2003)

(Panagiotis G. Asteris, et. al. 2011) When the structure is subjected to earthquake loads, the behaviour of infill frames will be affected. So, in this paper, the bi-diagonal compression strut model is considered for the analysis. Single bay and double bay are tested in different laboratories and a comparison of the results is done.

In the proposed infill board model, every masonry panel is characterized by considering four support strut-elements, with rigid behaviour and a center swagger component, where the nonlinear hysteretic conduct is concentrated (Figure 2.17). The stresses created in the focal component are simply of a tensile or compressive nature (H Rodrigues, H Varum, 2010).

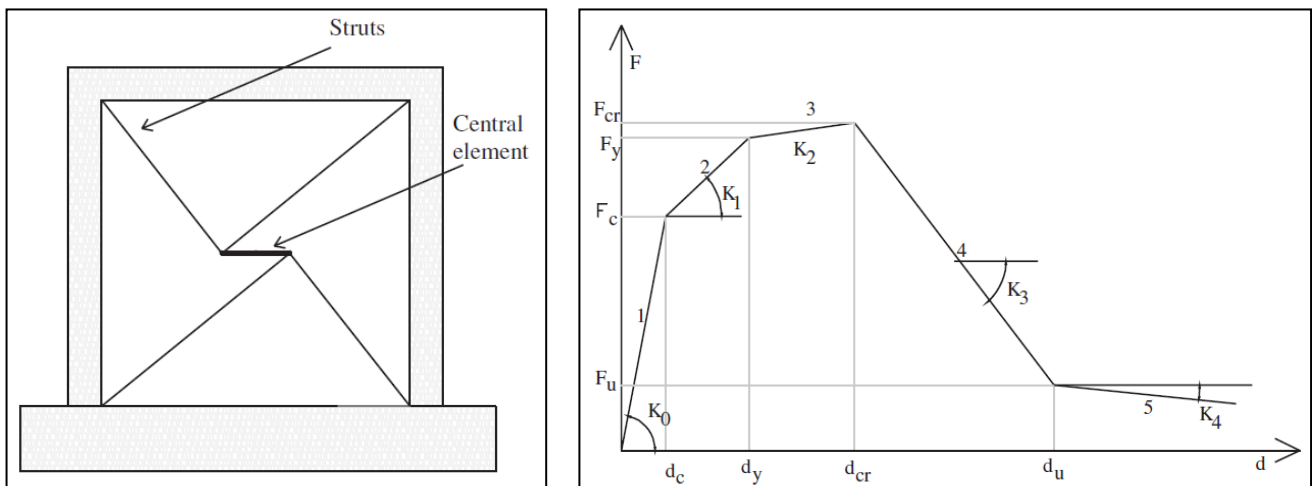


Figure 2.17. Macro-model for the simulation of an MIW panel and force-displacement monotonic behaviour curve (Hugo Rodrigues, Humberto Varum, 2010).

Nine parameters characterize the nonlinear behaviour by a multi-linear envelope curve (Figure 2.17), representing:

- (i) Cracking (cracking force, F_c ; cracking displacement, d_c)
- (ii) Yielding (yielding force, F_y ; yielding displacement, d_y)
- (iii) Maximum strength, corresponding to the beginning of crushing (F_{cr} ; and corresponding displacement, d_{cr})
- (iv) Residual strength (F_u) and corresponding displacement (d_u)
- (v) The fifth branch of the behaviour curve is defined by its stiffness (K_4).

A different behaviour curve can be defined for each loading direction, which allows for the consideration of non-symmetrical behaviour.

(Asteris P G et al., 2011) for achieving higher stiffness in the infilled frames, diagonal struts are provided. After the analysis, the validity of the proposed equations is verified by comparing the work done results by researchers against the achieved results. (Mohyeddirkermani, 2011) the exterior and interior walls are constructed using infill frames. When subjected to earthquake loads behaviour of such frames is evaluated. The structure is analyzed by using ANSYS software. The structure is analyzed both in plane and out of a plane for different drifts to check the behaviour of the buildings. (Kai et al., 2013) seismic fragility and spectral displacement are the parameters that are considered for low-rise and RC buildings. Coefficient-based methods obtain fragility curves after the shake load test. Spectral displacements are found to be within limits for low-rise buildings.

(Asteris P G et al., 2013) Since the behaviour of infilled frames under earthquake loads is different in each case, different micro models are considered for the analysis in this paper. Both advantages and disadvantages of each of the considered models are evaluated. (Caliò & Pantò, 2014) macro modelling technique is implemented, lumped plasticity beam-column elements model the frame members. This approach is evaluated by Non-Linear analysis performed on Infilled structures. (Yuen and Kuang, 2014) the response of IP and out of a plane is usually analyzed separately. The masonry infills, when subjected to OOP loading, are provided with diagonal thrust. In addition, IP loading reduces the load capacity of the RC frame by 50%. In addition, by providing anchorage, it stabilizes the forces against buckling. (Kumar et al., 2014) plasticity-based interface model is considered for masonry structures. The structure is further analyzed using ABAQUS software, and the results are validated by comparing with literature review with the experimental results. (Dolatshahi et al., 2015) different types of macro-elements are considered in unreinforced masonry structures and evaluated under seismic

loads. After the analysis, the derivation curve is compared with non-linear FEA. This curve is further used for the preliminary evaluation of URM walls for bi-directional loading. (Moretti, 2015) for the analysis of masonry structure is done by considering experimental, analytical, and code provisions. Different approaches for single strut members are made, and results are tabulated. (Yuen & Kuang, 2015) A unified analysis method with the damage-based modelling technique is proposed for numerical simulations of masonry-infilled reinforced concrete frame failure. Non-Linear behaviour of infilled frames was conducted by combining IP and OOP loading. (T.P. Ganesana, M. Lakshmipathy, V. Thirumurugan, 2015) properties of the frame, infills are the main factors of an infilled frame. Different members of different sizes are taken along with one 3D. The effectiveness of the cork is interface material is studied, and adaptive infilled frames are adapted. (Gattesco & Boem, 2015) the diagonal compression tests are compared with the IP behaviour of unreinforced masonry walls with GFRP-coated structures. The tensile strengths are compared with experimental results and from an analytical formulation. (Gattesco & Boem, 2015) the infilled structures are analyzed by various numerical procedures and are limited to the IP or OOP behaviour of masonry walls. In this paper, the experiment is done by considering extreme loading to address the gaps. The analysis was carried out using DIANA and ABAQUS software. (Lin et al., 2016) since there will be a decrease in the energy of masonry-infilled frames, a new dry-stacked panel (DSP) semi-interlocking masonry (SIM) infill panel has been provided. The constant friction part is verified to provide substantial energy dissipation and benefits such as ductility of the structure. (Miglietta et al., 2017) a branch of the FDEM software was developed at the University of Toronto and called it Y-Brick. It is presented and validated as a reliable tool to model the reverse cyclic behaviour of masonry structures by varying levels of complexity. Y-Brick is also shown to identify the position of the cracks that form in the structure.

(Pasca et al., 2017) the OOP response of infilled frames is considered for damage assessment of RC and steel buildings when subjected to seismic loads. After the analysis, the comparison between experimental and analytical values is made. (Abdulla et al., 2017) has chosen extended Finite element analysis, he has approached three-dimensional non-linear behaviour of masonry under monotonic in-plane, out-plane, and cyclic loads. Abaqus software is used for the analysis, followed by a numerical algorithm, i.e., the Newton Raphson method for employing user-defined subroutines. (Edri & Yankelevsky, 2017) URM structures, when subjected to OOP loading, incorporate large deflection and strains. A master has considered which has suitable geometry and material nonlinearity. The two experimental results, when

subjected to lateral loading, are compared with analytical model predictions. In both cases, results are within the limit and safe. (Dautaj & Kabashi, 2018) 7 RC frames with masonry infills are tested under cyclic loading. Based on the results achieved, a new macro model is framed to analyze the infill RC frames. Further, the model is used to predict the failure patterns of infilled RC frames. (Mazza & Donnici, 2018) Four diagonal OOP nonlinear beams and one horizontal IP truss are considered. After analyzing the numerical results of the OOP and IP models, cyclic tests for six-story RC-framed buildings are compared. Different displacement histories are considered, such as i) OP loading faster than IP, at the sixth storey; ii) equal IP and OP loading, at the third storey; iii) IP loading faster than OP, at the first storey. (Pradhan, 2018) a master macro model unreinforced masonry infill is considered under seismic action. Existing macro models are analyzed, and their advantages and disadvantages are reported. Using diagonal struts is complex for structural engineers to obtain the desired efficiency. The feasibility of the 3D frame structure is checked and adapted. (Mbewe & van Zijl, 2019) Seismic analysis infilled structures using strut models and pushover analysis have gained popularity. The results show a good correlation between experimental data and the proposed model. (Kostinakis & Athanatopoulou, 2020) the presence of infill frames in the masonry structure in RC buildings behave feasibly under seismic loads. However, the position of infilled frames irregularly in the structure results in adverse effects. Finally, it is concluded that the irregular placement of infill frames in the structure leads to significant seismic damage. (Xiaomin Wang et al., 2020) conducted Bidirectional seismic behaviour of MIW. After the analysis, a comparison of experimental and analytical data is done to predict the failure modes. Further, based on the slenderness ratio, and masonry strength on the OOP, the response of infill walls within the plane damage is explored. Finally, stability is obtained by reducing stiffness and strength in OOP. (Yekrangnia & Asteris, 2020b) has chosen multi strut macro model, which is capable of simulating the overall force-displacement behaviour of infilled frames with different configurations. The model is analyzed for different parameters and varying characteristics such as position, opening height to length ratio, etc. A reduction factor is proposed for better strength and stability. (Pohoryles & Bournas, 2020) using composite materials for IP retrofitting will reduce the risk of collapse of the infills. The stiffness of the material and angle are considered as the crucial factors. The comparison between the experimental and obtained strain is assessed using an empirical formula. (Gerson Moacyr Sisniegas Alva, Alessandro Onofre Rigão, João Kaminski Junior, 2021) seismic analysis is performed on RC buildings with masonry walls is considered. An equivalent strut on the seismic response is found which eases the complexity

of the structural engineers. Finally, the use of participating masonry walls is to be considered by engineers for better efficiency under seismic loads.

Concerning Table 2.5, the analytical studies carried out on masonry infill panels are summarized. For demonstrating infills, a few strategies have been created. They are assembled in two principle classes: macro-models and micro-models. The first depends on the equivalent strut method, and the second depends on the FEM. The principle benefits of macro modelling are computational effortlessness and underlying mechanical properties from masonry tests since the brickwork is a heterogeneous material. The dispersion of material properties of its constituent components is hard to anticipate. The single strut model is most generally utilized, as it is essential and most appropriate for large structures.

Table 2.5. Summary of the literature review on the analytical study on MIW

Authors	Brick Unit Used (size in mm)	Strengthening Material	Parameters Considered	Strengthening Contribution	Failure Mode
(Mallick DV & Garg RP, 1971)			Lateral stiffness of infilled frames		The door opening position can be best located in the center of the lower half of the panel and the center of the window.
(Saneinejad & Hobbs, 1995)			IP forces		Analysis of Multi-storey infilled frames as braced frames
(Jack P. Moehle, 1996)			Probabilistic approach		Uncertainties in estimating the capacity and demands
(A. Madan et al., 1997)			Non-linear analysis		Influence of masonry infill frames
(Yaw-Jeng Chiou, Jyh-Cherng Tzeng, 1999)	Brick		IP monotonic loading		Entire filled masonry walls show high stiffness, whereas the adjacent

Authors	Brick Unit Used (size in mm)	Strengthening Material	Parameters Considered	Strengthening Contribution	Failure Mode
					column fails with nearly uniform cracks
(Rodolico, 1985)			Collapse behaviour of unreinforced masonry walls		A comparison of displacement-based analysis with Time History analysis is made
(Crisafulli et al., 2000)			Non-linear behaviour		The advantages and disadvantages of each of the methods are studied.
(Doherty et al., 2002)			Seismic assessment		One-way vertical bending for application to walls in two-way bending is done.
(El-Dakhkhni et al., 2003)			Lateral stiffness and lateral load capacity		
(Kuzik et al., 2003)		GFRP Masonry walls	OOP behaviour		Simple model behaviour is taken for evaluation for strength and deformation characteristics.
(Alwathaf et al., 2003)	Masonry blocks		Conventional mortared and non-conventional mortar		Different analytical methods for masonry joint analysis are reviewed
(Meharbi & Benson, 2003)			Seismic performance		Response spectrum analysis is performed on the

Authors	Brick Unit Used (size in mm)	Strengthening Material	Parameters Considered	Strengthening Contribution	Failure Mode
					masonry structure, and results are evaluated.
(Simsir et al., 2004)			OOP behaviour		Experimental results are compared with SDOF and MDOF. Two degrees of freedom are considered for dynamic stability.
(Hwee Tan & H Patoary, 2004)		Fiber-Reinforced Polymers	Three anchorage methods		Results were compared well with the analytical predictions.
(Milani et al., 2006)			OOP loading		Efficient results are found in all the cases, indicating the proposed simple technique is sufficient for safety assessment for OOP-loaded masonry panels
(Matjaz Dolsek, 2008)			Response spectrum method		The provision of infills helps in resisting the loads and does not cause the failure of the columns.
(Amato et al., 2008)			Infill behaviour switches from a strut element to a plate shell		The lateral stiffness of infill frames is evaluated
(P.G. Asteris, 2008)			Lateral load		The difference in magnitude and contact lengths has been

Authors	Brick Unit Used (size in mm)	Strengthening Material	Parameters Considered	Strengthening Contribution	Failure Mode
					clearly shown for different frame members.
(Kaushik et al., 2008)			Linear and nonlinear analysis		The single strut model can be effectively used when masonry is discontinued in the first storey for parking space.
(Stavridis, 2009)			Shake table test		The approach can be further used to construct simple struts in the construction of the entire structure.
(Hugo Rodrigues, Humberto Varum, 2010)			Bi-diagonal compression strut model		Single bay and double bay are tested in different laboratories, and a comparison is made.
(Panagiotis G. Asteris, et. al., 2011)			Diagonal struts are provided		The validity of the proposed equations is verified by comparing the work done results by researchers against the achieved results
(Mohyeddin-kermani, 2011)			Earthquake loads behaviour		IP and OOP for different drifts to check the behaviour of the buildings.
(Kai et al., 2013)			Seismic fragility and spectral displacement		Spectral displacements are found to be within limits for low-rise buildings.

Authors	Brick Unit Used (size in mm)	Strengthening Material	Parameters Considered	Strengthening Contribution	Failure Mode
(P G Asteris et al., 2013)			Micro-models are considered		Both advantages and disadvantages of each of the considered models are evaluated.
(Caliò & Pantò, 2014)			Plasticity beam-column elements		This approach is evaluated by Non-Linear analysis performed on Infilled structures.
(Yuen & Kuang, 2014)			IP and OOP loading		By providing anchorage, it stabilizes the forces against buckling.
(Kumar et al., 2014)			Plasticity-based interface model		The results are validated by comparing with literature review with the experimental results.
(Dolatshahi et al., 2015)			Seismic loads		The curve is further used for the preliminary evaluation of URM walls for bidirectional loading.
(Moretti, 2015)			Experimental, analytical, and code provisions		Different approaches for single strut members are made, and results are tabulated.
(Yuen & Kuang, 2015)			Damage based modelling		Non-Linear behaviour of infilled frames was conducted by combining IP and OOP loading

Authors	Brick Unit Used (size in mm)	Strengthening Material	Parameters Considered	Strengthening Contribution	Failure Mode
(T.P. Ganesana, M. Lakshmiathy, V. Thirumurugan, 2015)			Infills are the main factors		The effectiveness of the cork is interface material is studied, and adaptive infilled frames are adapted.
(Gattesco & Boem, 2015)		GFRP	Diagonal compression and Plane behaviour		The tensile strengths are compared with experimental results and from an analytical formulation.
(Dolatshahi & Aref, 2015)			IP or OOP behaviour		The analysis was carried out using TNO DIANA and ABAQUS software.
(Lin et al., 2016)			Dry stacked panel (DSP) semi-interlocking masonry (SIM)		The constant friction part is verified to provide substantial energy dissipation and benefits such as ductility of the structure.
(Miglietta et al., 2017)			Cyclic behaviour		Y-Brick is also shown to identify the position of the cracks that form in the structure.
(Pasca et al., 2017)			Seismic loads		A comparison between experimental and analytical values is made.

Authors	Brick Unit Used (size in mm)	Strengthening Material	Parameters Considered	Strengthening Contribution	Failure Mode
(Abdulla et al., 2017)			Monotonic in-plane, out-plane, and cyclic loads.		Abaqus software is used for the analysis, followed by a numerical algorithm, i.e., the Newton Raphson method for employing user-defined subroutines.
(Edri & Yankelevsky, 2017)			OOP loading		The two experimental results, when subjected to lateral loading, are compared with analytical model predictions. In both cases, results are within the limit and safe.
(Dautaj & Kabashi, 2018)			Cyclic loading		The model is used to predict the failure patterns of infilled RC frames.
(Mazza & Donnici, 2018)			OOP and IP model		Different displacement histories are considered, such as i) OP loading faster than IP, at the sixth storey; ii) equal IP and OP loading, at the third storey; iii) IP loading faster than OP, at the first storey.
(Pradhan, 2018)			Seismic action		The feasibility of the 3D frame structure is checked and adapted.
(Mbewe & van Zijl, 2019)			Pushover analysis		The results show a good correlation between

Authors	Brick Unit Used (size in mm)	Strengthening Material	Parameters Considered	Strengthening Contribution	Failure Mode
					experimental data and the proposed model.
(Kostinakis & Athanatopoulou, 2020)			Seismic loads		It is concluded that the irregular placement of infill frames in the structure leads to severe seismic damage.
Jorge Varela-Rivera et. al.			OOP behaviour	Failure of the walls was from crushing of masonry is found by yield line	It is concluded that the bidirectional strut method is the best choice.
(Xiaomin Wang et al., 2020)			Bidirectional seismic behaviour		Stability is obtained by reducing stiffness and strength in OOP.
(Yekrangnia & Asteris, 2020b)			Simulating overall force-displacement behaviour		A reduction factor is proposed for better strength and stability.
(Pohoryles & Bournas, 2020)		Composite materials	Stiffness of the material and angle		The comparison between experimental and obtained strain is assessed using an empirical formula.
(Gerson Moacyr Sisniegas Alva, et. al., 2021)			Seismic response		The use of participating masonry walls is to be considered by engineers for better efficiency under seismic loads.

Consequently, R.C. frames with masonry infilled walls can be demonstrated as comparable supported casings with infill dividers supplanted by an identical corner-to-corner swagger, which can be utilized in a thorough nonlinear sucker investigation. The fundamental boundary of these struts is their equivalent width, which influences their stiffness and strength. There are new bricks known as Porotherm bricks developed considering the weight of the overall structure, from an economic point of view, especially in new masonry constructions. Still, there is secondary research to characterize the infill panels' behaviour with these masonry units.

The popular strengthening material for MIW GFRP is widely used on the MIW to increase the lateral resisting capacity against horizontal loads. As suggested by (Gattesco & Boem, 2015), the principal tensile strength f_t at the center of a sample square subjected to diagonal compression is calculated by using the formula (Equation 43)

$$f_t = \alpha \frac{P_{max}}{b.t} \quad (43)$$

P_{max} is the maximum load attained in the test, t and b are the thickness and the width of the specimen, respectively, and α is a coefficient assumed equal to 0.5. Then, a modification factor (β) (Equation 44) is defined as the ratio between the experimental resistance of RM wallets $P_{max(R)}$ and the preliminary analytical prediction ($P_{max(U)} + P_c$).

$$\beta = \frac{P_{max(R)}}{(P_{max(U)} + P_c)} \quad (44)$$

In addition, it is seen that masonry with similar mechanical characteristics and the coating is tested for the mortar range. The coefficient β is assumed as a linear trend function of the tensile strength of the mortar, with values decreasing as the mortar strength increases. From tendency curves, the values of the modification factor are calculated for each masonry type of structure. The relation between the resistance of RM specimens and the mortar coating resistance was derived analytically through the relationship as shown in Equation 45.

$$P'_{max(R)} = \beta' \cdot (P_{max(U)} + P_c) \quad (45)$$

2.6. FRAGILITY FUNCTIONS FOR MASONRY INFILL WALLS

An extensive review of the fragility functions for MIW has led to the compilation of a database incorporating the references segregated year-wise in ascending order, from (2013 to 2021).

(Grubišić et al., 2013) conducted deals with the seismic assessment of the masonry infilled walls with different infill conditions by utilizing fragility curves which assess the vulnerability of the structure during seismic activity. Results showed that the type of infill considerably affected the seismic response of the frame with the lowest probability of failure belonging to fully and partially infilled frame as compared to bare frame. (Nassirpour & D'Ayala, 2014) analyzed masonry-infilled RCC frames for spectral acceleration and displacement under seismic action using the coefficient-based method (CBM). The CBM is more advantageous than FEM in terms of complexity. The frames analyzed using CBM obtained fragility results which were in validation with the previous studies. (Cardone & Perrone, 2015) considered infilled frames with steel frames with different end conditions to determine their seismic response using fragility analysis. The results pointed out that the infilled frames with steel bracing performed better under simulated earthquake vibrations as compared to the bare frames with steel bracing. (Jong-Su Jeon, Ji-Hun Park, 2015) evaluated the damage potential of the non-structural component of the masonry-infilled RC frames with and without opening through fragility functions by utilizing the experimental results of previous studies. Further, the damage quantification was performed and the remedial measures were given based on fragility curves which indicated that the results can be directly incorporated performance assessment calculation tool. (Kai et al., 2013) estimated the seismic vulnerability of the lightly reinforced masonry-infilled wall through fragility analysis. The simulation was conducted by taking into account a non-linear push-over analysis. The masonry unit that was taken into account was either hollow or solid. The results concluded that RC frames with masonry infill improved the seismic response of the frames. (Sassun et al., 2016) examined the IP seismic performance of the masonry-infilled RC or steel frames. A non-linear analysis was implemented to obtain the results which concluded that low drift values such as 0.2% did not cause any serious damage to the structures until the drift values were as high as 2%. When the repair cost analysis was executed, it was concluded from the results that there is a reasonable correlation between Italian masonry infill repair cost estimates obtained using costing manuals and those obtained through consultation with the industry. (Eduardo Charters Morais, 2016) The probabilistic damage state estimation of unreinforced masonry infilled walls made with clay bricks in case of the occurrence of an earthquake using dynamic structural analysis was performed. The earthquake intensities were obtained through 50 selected seismic data matching the Komárom historical earthquake and incremental dynamic analysis was implemented. The results concluded that peasant houses were probably not made of clay

masonry when the 1763 Komárom historical earthquake occurred, and possibly made of adobe or srfal.

(Carlo Del Gaudio, et. al., 2017) conducted experimental investigation of RC frames infilled with clay brick masonry under seismic activity was executed and the results were then correlated with previous studies to obtain the fragility functions. (Chiozzi & Miranda, 2017) performed in the study deals with the development of fragility functions by incorporating 152 different masonry units from previous works which were strengthened with RCC or steel and infilled with either solid/hollow clay bricks or concrete blocks. The failure modes were identified according to the previous literature considered in the research. The results concluded that the type of masonry did not have any significant effects on fragility analysis. However, the compressive strength of the masonry influenced the performance of the building under seismic activity. (Gianni Blasi, Daniele Perrone, 2018) evaluated the seismic performance of the RC frames infilled with clay and concrete blocks using incremental dynamic analysis to develop fragility functions for the IP behaviour of the structure. The results concluded that seismic retrofitting techniques needed to be employed to prevent the seismic failure of the structures. (De Risi et al., 2018) carried out discussed the IP behaviour of the RC frames infilled with hollow clay bricks under earthquake activity. The analysis was conducted both experimentally and analytically to develop fragility functions and a new model is proposed. The results concluded that the proposed model was reliable in determining the key points at which losses occur during earthquakes. (Mohamed & Rom, 2002) conducted encompasses the non-linear dynamic analysis of the partially and fully infilled and soft-story RC framed structures with and without openings to develop fragility functions to evaluate seismic stability. A bare frame model was also analyzed for reference purposes. For the first three damage states i.e., slight, light, and moderate damage the bare frame and soft storey had a close performance while the performance of the partially infilled framed structure was closer to that of the fully infilled framed structure. (Gautam, 2018) executed determined the seismic vulnerability of the stone masonry houses in the village affected by the 2015 Gorkha earthquake sequence of Nepal. The fragility curves for seismic analysis were obtained from the 665,515 damage state conditions of the houses built in Nepal. The results highlighted that stone masonry houses in Nepal were highly vulnerable even in the case of low to moderate seismic activity. (Choudhury & Kaushik, 2019) found its background from the seismic events that occurred in the Mediterranean region. These regions are of high economic and social importance. The study executed analyzed masonry-infilled RC frames. The masonry units used were clay and concrete-type blocks. The

damage quantification was conducted concerning drift and seismic activity and the fragility curves were obtained. The results concluded that concrete blocks filled masonry frames performed better as compared to clay block-infilled masonry in case of drift capacity and seismic activity.

(Del Gaudio et al., 2019) investigated the seismic stability of the RC frames with partially and fully infilled conditions. A non-linear time history analysis was performed to develop fragility curves. The results showed that the epistemic uncertainty is significant only for higher damage states in any type of RC frame. On the other hand, the ground motion variability was found to be the major contributor to the total uncertainty in all the frames. (Carlo Del Gaudio, et al., 2019) evaluated structural and non-structural damage of the structures conducted by post-earthquake survey following the L'Aquila earthquake. For the analysis, a database of 32,520 residential masonry buildings was taken into account. The analysis showed that vulnerability was strongly related to the quality of the masonry units and the type of connections provided. (Xianxin Xie, Lingxin Zhang, 2020) conducted on nine fully infilled masonry RC frames subjected to quasi-static loading to develop their fragility functions and corresponding fragility curves. The results showed that maximum crack widths gave the smallest dispersion, whereas the skeleton curve-based methods generated excessive dispersions, and the phenomena-based method was shown to be self-contradictory in certain circumstances. (Trapani et al., 2020) conducted on unreinforced masonry-infilled units that were not subjected to prior IP damage to develop their fragility curves. An incremental dynamic analysis was performed to assess the OOP behaviour of masonry units based on 26 seismic data. The outcomes showed fragility curves which represented the possibility of exceedance of OOP failure at a given ground vibration as a function of a different combination of geometrical and mechanical parameters, IP damage level, and supporting conditions. (Khan et al., 2021) aimed at performing fragility assessment of RCC frames infilled with masonry blocks using linear and non-linear static and dynamic analysis. All the models were analyzed for plastic behaviour. The results concluded that the probability of exceedance of collapse for specific damage was under the limit. (Marco Nale, et al., 2021) evaluated the OOP failure mechanism of the unreinforced masonry infilled walls by developing the fragility curves using the multiple strip analysis method. The results concluded that the fragility functions developed in the study will help assess the damage conditions of unreinforced masonry units as well as the economic losses. (Gautam et al., 2021) concentrated on developing the fragility functions of the RCC framed infilled brick walls affected by the Gorkha earthquake that occurred in Nepal in 2015.

For the analysis purpose, 2196 damage data of the structures were collected based on a global and local level. The damage states were categorized into three types which were minor, major, and collapse. The conclusion that was arrived at from the fragility analysis was that even a moderate-intensity earthquake can cause serious damage to RC framed structures of Nepal which will lead to collapse. (Pradhan et al., 2021) developed a procedure to derive the fragility functions of the low-rise RC framed structures. The OOP fragility functions were developed using a probabilistic approach based on Monte Carlo Simulation. The results indicated that the OOP fragility of the infill walls increased as the level of IP damage increased.

Table 2.6. Summary of the literature review on the fragility functions for MIW

Authors	Brick Unit Used (size in mm)	Strengthening Material	Parameters Considered	Strengthening Contribution	Failure Mode
(Grubišić et al., 2013)	Not specified	RCC Frames	Pushover analysis on frames with and without masonry infills	Increase in the time takes for collapse	Light, moderate, extensive, and partial collapse
(Kai et al., 2013)		Masonry-infilled RCC frames	The coefficient-based method utilized for obtaining spectral accelerations	Increase in the lateral stiffness and capacity of the structure	
(Nassirpour & D'Ayala, 2014)	Clay bricks	Brick-infilled steel frame with and without opening	Pushover analysis on masonry infills with different end conditions	Increase in the lateral stiffness and capacity of the structure	Compression failure
(Cardone & Perrone, 2015)	Hollow clay bricks	RC frames with and without openings	Peak floor acceleration to identify OOP behaviour of infilled walls	Increase in the resistance to drift	Light cracking, corner crushing, extensive cracking, and collapse
(Jong-Su Jeon, Ji-Hun Park, 2015)	Hollow or solid brick	Masonry-infilled RCC frames	Non-linear pushover analysis	Increase in the lateral stiffness	Sliding shear, diagonal cracking, and corner crushing

Authors	Brick Unit Used (size in mm)	Strengthening Material	Parameters Considered	Strengthening Contribution	Failure Mode
				and capacity of the structure	
(Sassun et al., 2016)	Solid and hollow clay brick or concrete block	Masonry-infilled RCC frames	Non-linear structure analysis	Increase in the lateral stiffness and capacity of the structure	Combination of different failure modes - horizontal slip, diagonal cracking, corner crushing
(Eduardo Charters Morais, 2016)	Clay bricks	Unreinforced masonry infilled wall	Incremental dynamic analysis to simulate the IP shear behaviour of MIW		Compression failure
(Carlo Del Gaudio, Maria Teresa De Risia, Paolo Riccia, 2017)	Hollow clay bricks	Masonry-infilled RCC frames	IP behaviour analysis of infilled walls	Increase in the lateral stiffness and capacity of the structure	Combinations of various failures
(Chiozzi & Miranda, 2017)	Solid, hollow clay bricks and concrete blocks	Masonry-infilled RCC frames	IP behaviour analysis of infilled walls	Increase in the lateral stiffness and capacity of the structure	Combinations of various failures - hairline cracks in masonry up to 2 mm, significant cracks, (>2 mm), development of wide diagonal cracks (>4 mm)

Authors	Brick Unit Used (size in mm)	Strengthening Material	Parameters Considered	Strengthening Contribution	Failure Mode
(Gianni Blasi, Daniele Perrone, 2018)	Clay and concrete blocks	Masonry-infilled RCC frames	Fragility functions for the IP performance of masonry infills using incremental dynamic analysis	Increase in the lateral stiffness and capacity of the structure	Flexure and shear failures
(De Risi et al., 2018)	Hollow clay bricks	Masonry-infilled RCC frames	IP behaviour of frame under lateral load	Increase in the lateral stiffness and capacity of the structure	Sliding Shear, diagonal cracking and compression, corner crushing
(Mohamed & Rom, 2002)		Fully and partially infilled masonry RCC frames with and without openings	Non-linear dynamic analysis	Increase in the lateral stiffness and capacity of the structure	
(Gautam, 2018)	Stone Masonry	Masonry-infilled walls without any reinforcement	Peak ground acceleration and ground acceleration		Combinations of various damages observed
Carlo Del Gaudio et al.	Clay and concrete bricks	Masonry-infilled RCC frames	Damage and loss analysis due to drifts and seismic activity	Increase in the lateral stiffness and capacity of the structure	Combinations of failure according to the type of damage
(Choudhury & Kaushik, 2019)		Fully and partially infilled masonry RCC frames	Non-linear time history analysis	Increase in the lateral stiffness and capacity of the structure	Failure possibilities according to the type of damage

Authors	Brick Unit Used (size in mm)	Strengthening Material	Parameters Considered	Strengthening Contribution	Failure Mode
(Del Gaudio et al., 2019)					Failure possibilities according to the type of damage
(Xianxin Xie, Lingxin Zhang, 2020)	Clay and concrete bricks	Masonry-infilled RCC frames	Maximum crack widths, skeleton curve-based and phenomena-based methods	Increase in the lateral stiffness and capacity of the structure	Combinations of failure according to the type of damage
(F. Di Trapani, M. Malavisi, P.B. Shing, 2020)		Unreinforced masonry infilled wall	Incremental dynamic analysis to determine the OOP behaviour of MIW		A failure occurred according to damage conditions
(Khan et al., 2021)		Masonry-infilled RCC frames	Nonlinear static and dynamic analyses	Increase in the lateral stiffness and capacity of the structure	A failure occurred according to damage conditions
(Marco Nale, Fabio Minghini, Andrea Chiozzi, 2021)		Unreinforced masonry infilled wall	Multiple strip analysis for determining the OOP behaviour		OOP local failure
(Gautam et al., 2021)		Masonry-infilled RCC frames	Fragility analysis was conducted based on in-plane and OOP damages	Increase in the lateral stiffness and capacity of the structure	A failure occurred according to damage conditions

Authors	Brick Unit Used (size in mm)	Strengthening Material	Parameters Considered	Strengthening Contribution	Failure Mode
(Pradhan et al., 2021)		Masonry-infilled RCC frames	Monte Carlo simulations employing a numerical macro-model for the evaluation of the OOP capacity of infills	Increase in the lateral stiffness and capacity of the structure	OOP failure

From the literature carried out, it is clear that strengthening of MIW is necessary to prevent the failure of the wall against earthquake forces. There are various strengthening techniques available to fulfill the functional requirement. The popular approach is to provide reinforcement either in the vertical and horizontal direction or in both directions depending on the severity of the seismic attacks. The reinforcement bars are inserted into the base of the wall at the bottom and the beam on the top for vertical reinforcement and column-to-column for horizontal reinforcement. An alternative method is to provide perforated steel plates or steel braces on the surface of the wall. This method unintentionally adds extra weight to the existing structure, which also increased the overall cost of the whole system. The dowel bar system was then implemented, consisting of round steel bars inserted inside the wall so that half-length of the bar is penetrated inside the bounding frame. The remaining portion is inserted into the wall connecting both the structure and infill wall. This method has the disadvantage that the bar has more stiffness than the wall system, due to which cracks start propagating on the wall, which reduces the performance of the wall itself. The welded wire mesh (WWM), popularly known as ferrocement, was weightless and advantageous compared to previous methods. But the only disadvantage was the corrosion aspect as the mesh is mainly made up of steel. However, WWM is recommended for the improvement of ductility and ultimate failure loads of existing frames. Later, epoxy materials started gaining recognition as FRP overcame all these disadvantages. The various types of FRPs are carbon, basalt, and glass. Still, this method does not perform satisfactorily under elevated temperatures or aggressive environments. The experimental results showed that the lateral resistance of the infill wall increased when FRP was wrapped around MIW in any pattern. However, the experimental results displayed that the lateral resistance depends on the reinforcement ratio, specific aspect ratio, and fiber characteristics.

In contrast, the ultimate drifts were independent of reinforcement ratio and reinforcement type but dependent on the aspect ratio and the retrofitting configuration. The most recent upcoming strengthening material is a TRM that displayed better performance under elevated temperature, and UV radiation and was used where vapour permeability is required. The same types of fibers are present in TRM, too, but the manufacturing and implementation method differentiates both. The TRM is recommended to strengthen the newly constructed walls as well as repair the pre-damaged wall. FRCM helps regain the capacity of pre-damaged walls and enhances the non-damaged wall's overall performance. According to (Tetta & Bournas, 2016), TRM had the upper hand over FRP in strength and deformability, i.e. TRM is a promising solution for strengthening MIW under OOP loading conditions.

In addition to the strengthening material used, the type of masonry unit with which the wall is constructed also influences the overall performance of the infill system. The oldest known commonly used brick type is the burnt clay bricks, famous in many developing countries. Other types of bricks used to erect MIW are solid/hollow concrete blocks; autoclaved aerated blocks, interlocking blocks, and Porotherm bricks (for which research needs to be carried out). Considering the brittle nature of the infill materials, the tensile capacity should be enhanced by using additional materials or techniques that have been summarized in the above sections. In alternate cases, a small gap is provided between the infill walls and the bounding frame so that the deflection of the structure once loaded does not show more impact on the infill wall as in the case without the gaps being provided. The use of similar techniques is also allowed for different materials. Still, it is necessary to determine the perfect method to safeguard the infill wall through experimental tests or numerical simulations.

2.7. GAPS IN LITERATURE AND NEED FOR RESEARCH

After an exhaustive literature review, to plug the gaps in the research, the following research needs were identified

- Need for a detailed study on the behavioral aspects such as load carrying capacity, deflection resisting capacity, stiffness degradation, energy dissipation capacity, ductility behaviour of the MIW with central door opening with TRM strengthening.
- Need for the detailed study of TRM as a strengthening material, even though research on the same has been conducted from the past decade, still there are no codal provisions to be followed by the engineers.

- A combination of the above two factors has been discovered to be lacking in the literature carried out, which needs to be addressed as both the factors can impact the performance of MIW under lateral loading conditions to a larger extent.
- Numerical analysis needs to be conducted and propose suitable models for the MIW strengthened with TRM, which is not given focus in the past, and provide a significant material and interaction properties for the same.

2.8. SCOPE OF PRESENT STUDY

The MIW typology forming the main focus for this research is single-leaf, half-overlap stretcher bonded, burnt red clay brickwork, which has widespread prevalence in both new and existing Indian construction. While multi-leaf wall constructions with different kinds of brickwork (for example, lightweight blocks) are also common, it is beyond the scope of this thesis. Furthermore, as stated previously, single-bay, single storey walls with central door opening represent the main type of wall configuration considered in this work; although where forming a specific case of the developed methodology, TRM as a strengthening material was also considered. It is the author's intention that within this scope, the findings of this research are kept as general as possible, so that they may be applied toward the design of new buildings as well as the assessment of existing buildings alike.

CHAPTER 3

IDENTIFICATION AND EVALUATION OF FACTORS INFLUENCING THE PERFORMANCE OF MASONRY INFILL WALL (MIW)

3.1. INTRODUCTION

In this chapter, experimental test results reported at Wellington Institute of Technology (Ismail et al., 2018) were used to validate the adequacy of the finite modelling technique described in Section 3.2 in predicting the behaviour of masonry infill walls (MIW) without openings with/without fiber-reinforced cementitious mortar (FRCM) or Textile reinforced mortar (TRM). Experimental investigations were carried out on RC frames with solid infill walls (i.e., no openings) and infill walls strengthened with FRCM. The validation process carried out in this Chapter is of particular interest to find out how effectively the method can deal with the specific aspects of the tested walls, such as the material properties, interaction properties, application of FRCM layers and to suggest improvements and refinements to the method, if necessary in the finite element (FE) software ABAQUS.

This chapter is structured as follows: Section 3.2 briefs the experimental study conducted by (Ismail et al., 2018) at Wellington Institute of Technology. Section 3.3 provides the validation study of FE model discussed in Section 3.2 using ABAQUS software. Section 3.4 compares the results of both numerical predictions to experimentally measured values in terms of load capacity and deflection resisting capacity. Section 3.5 provides the proposed empirical expressions to determine the load carrying capacity of the MIW and provides a comparison among experimental, numerical, and analytical results of all the specimens.

The advancement of computers and software made it easier to forecast how buildings would behave. In any analysis, choosing a numerical model for simulation is a crucial step. A structure is categorized into a discrete count of components using the FEM, and it is from these elements that an approximate numerical solution is derived. The selection of relevant pieces with the proper material characteristic modeling determines how accurate the findings will be.

The structural evaluation of infilled frames has been simplified using parametric analyses and experimental results. The suggested numerical method may create strut models for a complete structure and predict structural performance, including stiffness, strength and deflection.

3.1.1. Objectives

The main objectives of this chapter are

- a. To identify and evaluate the factors such as material properties and interaction properties influencing the performance of masonry infill walls (MIW).
- b. To explore the numerical validation of the infill model with experimental data.
- c. To create a strut model for a complete structure and predict structural performance, including maximum deflection and ultimate strength.
- d. To provide an efficient method and an expression for evaluating the structural integrity of infilled frames.

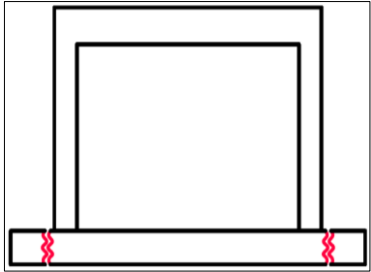
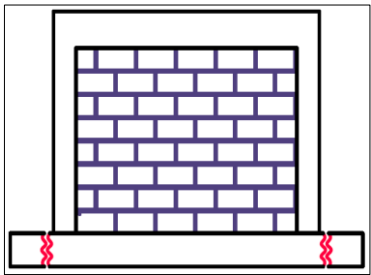
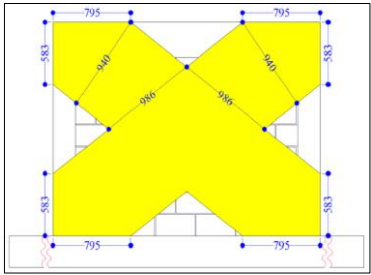
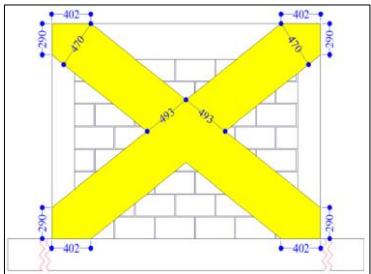
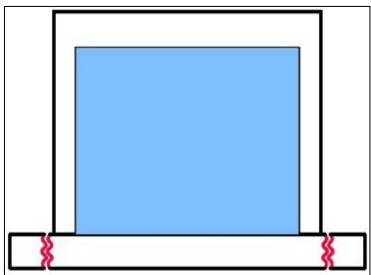
3.2 DATABASE OF PAST TEST USED IN VALIDATION (Ismail et al., 2018)

3.2.1. Brief Review of the Experimental Test

In order to validate the developed finite element technique, experimental test results available in (Ismail et al., 2018) were considered. The seismic performance of retrofitted FRCM systems on reinforced concrete frames with masonry infill (RCFMI) under cyclic IP loads was tested on these structures. For the benefit of the readers, a succinct summary of the tests carried out is provided in this section. However, readers are urged to consult (Ismail et al., 2018a) if they want any further details.

A total of nine 2/3 scaled single bay-single story RCFMIs representing a typical mid to high-raised building are constructed and tested. Ordinary moment resisting single bay reinforced concrete portal frame was selected as a prototype structure to replicate details prevalent in existing RCFMI buildings. The infill bay aspect ratio (infill length to infill height ratio) of 1.4 was selected, being typical in non-ductile RCFMI buildings. Considering the ratio of predicted lateral strength of the bare frame to that of the infill wall ($V_{\text{frame}}/V_{\text{infill}}$), the test frames were characterized to have a strong frame-weak infill configuration. Various configurations were included: a bare frame, an RCFMI, and seven RCFMIs retrofitted using FRCM made up of three fiber materials: aramid glass, carbon, and basalt. Table 3.1 provides specifics on the MIW frame's setup.

Table 3.1. Specifications for the specimen (Ismail et al., 2018a)

S. No.	Specimen Description	Type of Strengthening material used	Strengthening Configuration	Layout
1	Bare Frame (BF-1)	-	-	
2	Infill Wall (IF-2)	-	-	
3	Retrofitted (RFG-D3-3 RFC-D3-5 RFB-D3-7)	AR-Glass (RFG) and Carbon (RFC) and Basalt (RFB)	Cross-pattern pattern FRCM bands having a width equal to 1/3 of the diagonal length (D3)	
4	Retrofitted (RFG-D6-4 RFC-D6-6 RFB-D6-8)	AR-Glass (RFG) and Carbon (RFC) and Basalt (RFB)	Cross-pattern pattern FRCM bands having a width equal to 1/6 of the diagonal length (D6)	
5	Retrofitted (RFB-FU-9)	Basalt (RFB)	Full-face FRCM application (FU)	

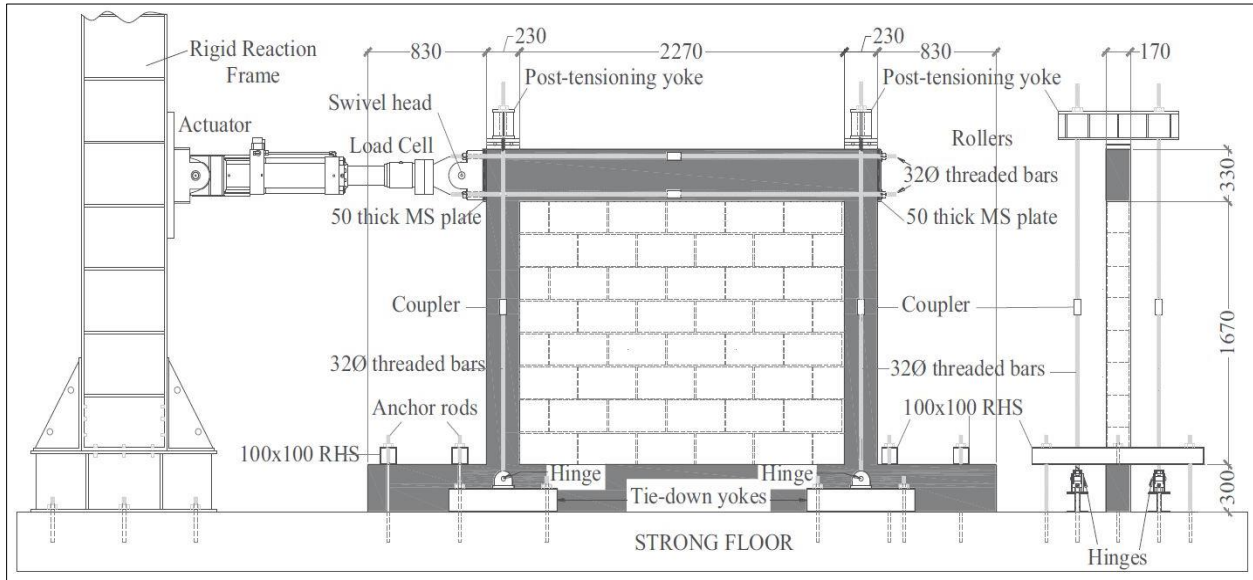


Figure 3.1. Test setup details (all dimensions in mm)

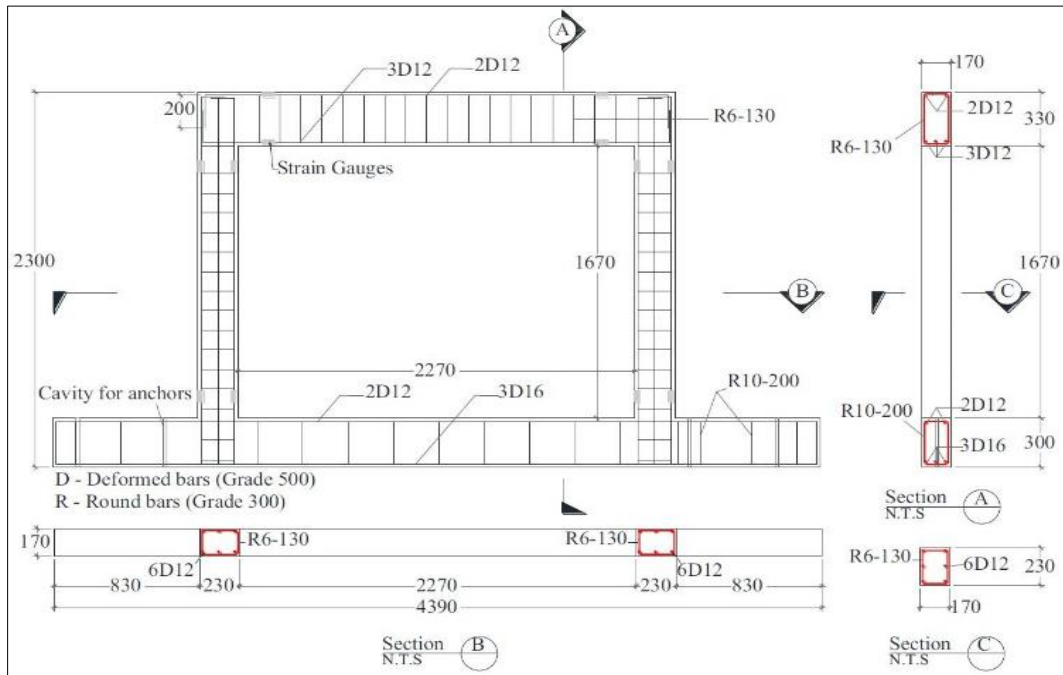


Figure 3.2. Reinforcement details (all dimensions in mm)

Three alternative fiber-reinforced cementitious matrix (FRCM) configurations, made of basalt, carbon, and glass, are used to carry out the strengthening strategy for the RCFMI frame. The first and second step involves applying the FRCM structure to the test specimen as a percentage of the diagonal length, using FRCM bands that are 1/3 the diagonal measurement wide (denoted as D3 in the literature) and with a width 1/6 of the diagonal length (denoted as D6 in the literature). The third procedure involves applying only basalt fabric FRCM to the whole face of the brick wall. For the building of the RC frame, a ready mixed concrete (RMC)

mixture having a nominal compressive strength of 25 MPa was utilized to construct the test specimens. The concrete masonry units had a nominal specified compression strength of 12 MPa and were 400 x 200 x 150 mm³ in size. Grade 500 deformed steel reinforcement bars with nominally specified diameter of 12 mm (D12) were used as longitudinal bars, whereas round steel reinforcement bars with nominal specified diameter of 6 mm and a yield strength of 300 MPa (R6) were used as transverse reinforcement. A cement-sand mortar having a volumetric ratio of 1:4 was used to lay hollow concrete masonry units in a staggered stack bond pattern. In both the bed and head joints, the masonry mortar layers were preserved to a constant thickness of 10 – 15 mm. The average concrete modulus of elasticity (E_c) was 23.8 GPa. The FRCM thickness was kept between 12 and 15 mm thick throughout. Figure 3.1 and Figure 3.2 (Ismail et al., 2018a) shows the overall geometry of the specimen and the adopted reinforcement details used in the numerical model, respectively.

Test frames were given the designations BF-N, IF-N, or RFX-Y-N, where B stands for "bare," I for "infilled," F for "frame," R for "retrofitted," and X represents the kind of fabric used (where B stands for basalt, C for carbon, and G for glass). Y represents the FRCM configuration applied to the test frame as a percentage of the diagonal length (where D3 denotes X-pattern FRCM bands with width equal to 1/3 of the diagonal length, D6 denotes cross-pattern FRCM bands with width equal to 1/6 of the diagonal length, and FU denotes full face FRCM application), and N denotes test number. These representations are given in detail in Table 3.1.

The experimental results are explained in the Section 3.5 along with the numerical outcomes making it easier for the comparison among the same.

3.3. NUMERICAL ANALYSIS

Conducting an experimental testing in a laboratory is costly and time-consuming; therefore, validation modeling was done instead. The implicit analysis approach and the program ABAQUS/Standard were used, and the C3D8R (Continuum-3D-8 node-reduced integration) element was chosen owing to its numerical efficiency. Many examples of the use of the finite element (FE) approach to creating two-dimensional (2D) models that replicate masonry reactions are stated in the literature (Chapter 2), while the use of 2D models to simulate masonry performance is widespread (Cavaleri & Di, 2019; Doudoumis, 2007; Haach et al., 2013) including the models which employ 2D components in 3D space. However, it is generally acknowledged that 3D FE models provide accurate simulation (Krueger et al., 2002).

Hence, 3D finite element model is employed in this masonry research because of the quick advancement of computer technology, which has made them less expensive to compute. Table 3.3 shows the values adopted in the numerical study.

Figure 3.3 depicts the yield surface under plane stress and deviatoric conditions. The yield line intercepting points at the major stress axes determine the material's uniaxial tension and compression strengths. The graph shows decreased tension and improved compression capacity under biaxial stress situations, and damage criteria. An input of the fracture energy as a material attribute can directly dictate the post-peak behavior under strain.

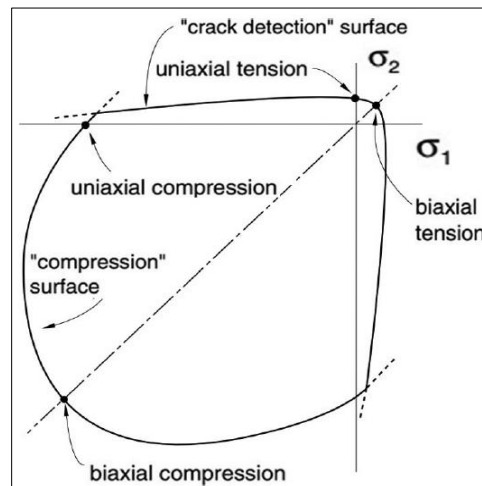


Figure 3.3. Failure surface of CDP model in plane stress (Lubliner J, Oliver J, 1988)

ABAQUS plastic-damage model is contingent on models that were suggested by (Lee & Fenves, 1998) and described in detail by (Scacco et al., 2020). The major features of the governing equations for the concrete damaged plasticity (CDP) model are given in this section.

The CDP model's elastic-plastic response is characterized based on the effective stress and the hardening factors.

$$\begin{aligned}
 \sigma &= D_0^{el}; (\varepsilon - \varepsilon^{pl}) \in \{ \sigma' \mid F(\sigma', \varepsilon^{pl}) \leq 0 \} \\
 \varepsilon^{pl} &= h(\sigma', \varepsilon^{pl}) \cdot \varepsilon^{pl} \\
 \varepsilon^{pl} &= \lambda \frac{\partial G(\sigma')}{\partial \sigma'}
 \end{aligned} \tag{1}$$

where λ and F obey the Kuhn-Tucker conditions:

$$\lambda \cdot F = 0; \lambda \geq 0 \text{ and } F \leq 0$$

The effective stress and the stiffness degradation variable, d ($'$, pl), are used to determine the Cauchy stress.

$$\sigma = (1 - d) \sigma' \quad (2)$$

Equation (1), which separates the constitutive principles for the elastic-plastic response from the stiffness degradation response, makes the model desirable for efficient numerical implementation. By allowing strains to exist outside the yield surface and applying a viscoplastic regularization, the inviscid model as it has been summarized above may be simply expanded to consider visco-plastic effects.

Assuming the ability to convert the uniaxial stress-strain curves into stress versus plastic strain curves of the kind.

$$\left. \begin{aligned} \sigma_t &= \sigma_t(\varepsilon_t^{pl}, \dot{\varepsilon}_t^{pl}, \theta, f_i), \\ \sigma_c &= \sigma_c(\varepsilon_c^{pl}, \dot{\varepsilon}_c^{pl}, \theta, f_i), \end{aligned} \right\} \quad (3)$$

Where tension and compression are denoted by the subscripts t and c, respectively;

$$\left. \begin{aligned} \dot{\varepsilon}_t^{pl} \text{ and } \dot{\varepsilon}_c^{pl} &= \text{the equivalent plastic strain rates,} \\ \left. \begin{aligned} \varepsilon_t^{pl} &= \int_0^t \dot{\varepsilon}_t^{pl} dt \\ \varepsilon_c^{pl} &= \int_0^t \dot{\varepsilon}_c^{pl} dt \end{aligned} \right\} &= \text{the equivalent plastic strains,} \\ \theta &= \text{the temperature,} \\ f_i, (i = 1,2,3\dots) &= \text{other predefined field variables.} \end{aligned} \right.$$

The effective plastic strain rates under uniaxial stress conditions are given as

$$\left. \begin{aligned} \dot{\varepsilon}_t^{pl} &= \dot{\varepsilon}_{11}^{pl} \text{ in uniaxial tension} \\ \dot{\varepsilon}_c^{pl} &= \dot{\varepsilon}_{11}^{pl} \text{ in uniaxial compression} \end{aligned} \right\} \quad (4)$$

Tension and compression responses of concrete under uniaxial force Figure 3.4 and 3.5.

Table 3.2. Input parameters for concrete damage plasticity

Dilatation Angle (ψ)	Flow Potential Eccentricity (e)	K_c	Viscosity Parameter
11°	0.1	0.67	0.00015

The viscosity parameter is often estimated to fall between 0.0001 and 0.0005. Following various sensitivity tests, a value of 0.00015 was found to be a reasonable

compromise for ensuring accurate findings and addressing convergence difficulties. Table 3.2 provides the numbers utilized in the analysis to determine the yield surface (Salehi & Nikghalb Rashti, 2018):

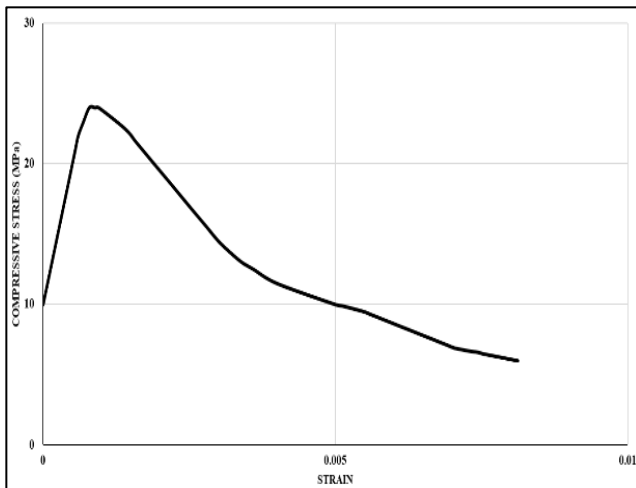


Figure 3.4. Compression stress-strain properties

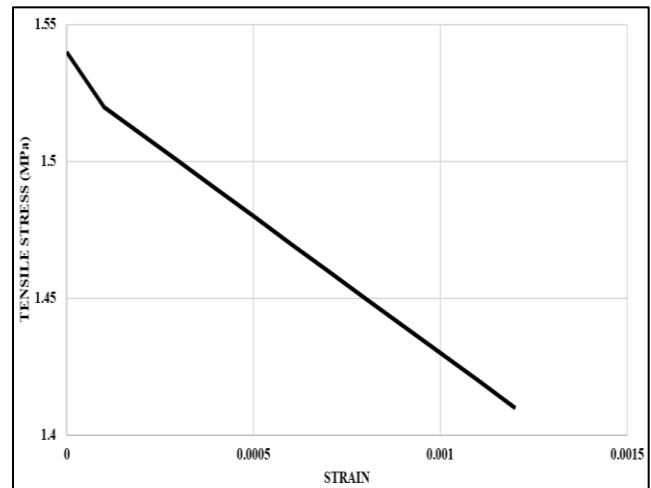


Figure 3.5. Tension stress-strain properties

3.3.1. Numerical Simulation Approach

This portion provides information on the implemented FE model, including model geometry, modeling methodology, and validation results. Using this modeling method, a parametric investigation of the behavior of RC frames with solid masonry infill walls was carried out after the accuracy of the numerical model was confirmed. Using the well-known FEA application ABAQUS, the masonry-infilled RC frame reinforced with FRCM was simulated in this study. Solid components were used to mimic RC frame members and concrete masonry units (CMU). In both the horizontal and vertical directions, the CMU dimensions were increased by the mortar joint's half thickness, resulting in expanded brick units (refer to Figure 2.2 in Chapter 2) that connect the separate CMUs and allow them to interact with one another. Even though it uses expanded brick units, the simplified micro-model was found to provide the required precision, and it is regarded as a more computer-efficient modeling approach than a full micro-modeling approach where mortar joints and brick units are simulated separately, as mentioned in Chapter 2.

Each part of the infilled frame is carefully modeled and explored in the parts that follow. Although ABAQUS offers general material constitutive and interfacial behaviour models for many different structural applications, the contribution of this study lies in the selection of appropriate models and crucial material parameters, as well as the execution of an accurate and

successful computational simulation of masonry infills surrounded by RC frame members with FRCM as a strengthening material.

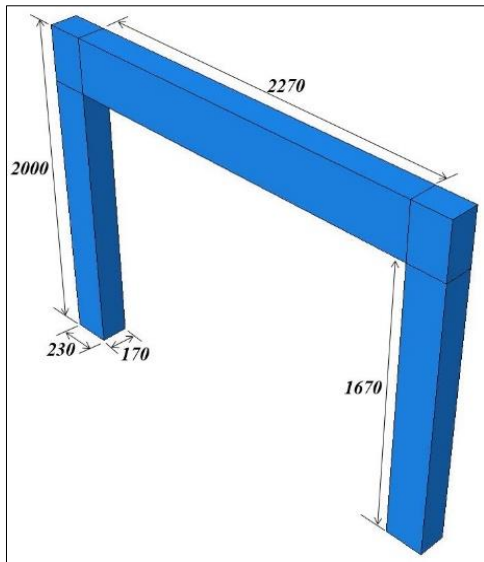


Fig 3.6. Bare frame dimensions

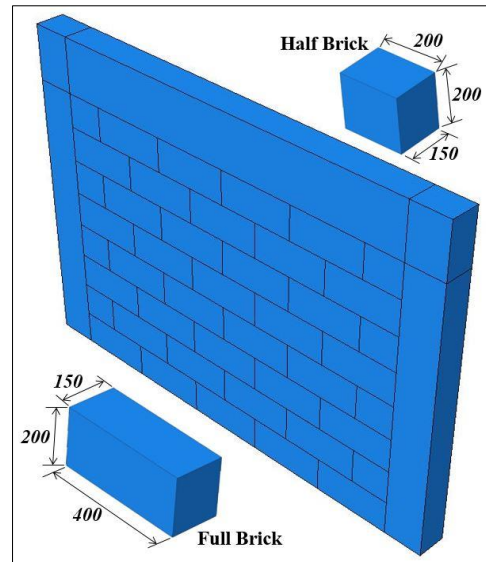


Figure 3.7. Infill frame dimensions

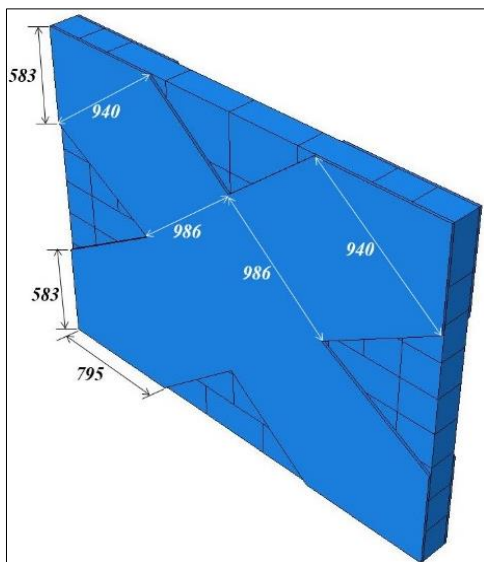


Figure 3.8. Diagonal length (D3) dimensions

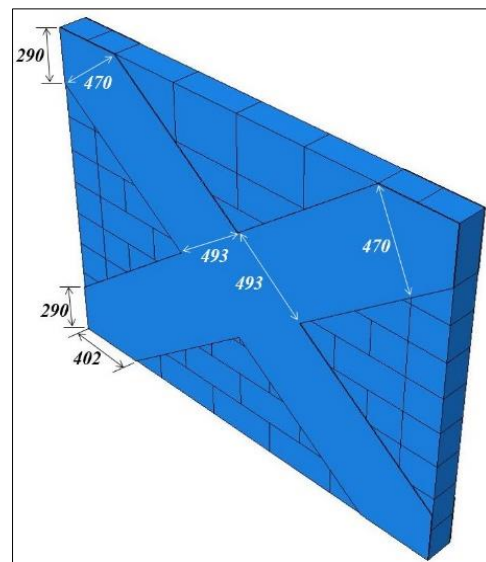


Figure 3.9. Diagonal length (D6) dimensions

Blocks, mortar, and reinforcement—all made of cementitious mortar and basalt fibers—are all meshed individually during the completely heterogeneous 3D process. For the mortar, bricks, and reinforcement matrix, linear 8-node brick components are utilized (Figure 3.6 - 3.9). As stated in (Scacco et al., 2020), a comprehensive application of FRCM reinforcement should include the complete modeling of the basalt grid, considering both its brittle behavior and the potential for fiber slippage inside the mortar. There are computational challenges, which necessitate model simplification. Again, in accordance with (Lee & Fenves,

1998), the mesh of the grid is modeled with a spacing of about 50 mm, with special attention paid to placing the truss through the respective nodes of the brick components.

Table 3.3. Materials' mechanical characteristics for the numerical simulations

Concrete		Steel	
Young's Modulus	23800 MPa	Young's Modulus	210000 MPa
Poisson's ratio	0.21	Poisson's ratio	0.33
Compression strength	25 MPa	Grade	Fe 500
Infills		FRCM	
Young's modulus	1900 MPa	Fabric density (γ_f)	420
Poisson's ratio	0.15	The cross-sectional area of fibers (A_f)	45.3
Dilation Angle	10	Fabric tensile rupture strength (F_{fu})	105
Eccentricity	0.1	Ultimate strain at rupture (ϵ_{fu})	>2.0
f_{bo}/f_{co}	1.16	Tensile elastic modulus (E_f)	32
Stiffness	0.66	Average compressive strength of FRCM matrix (f'_{cj})	43.1
Viscosity Parameter	0.015	No. of tests (C109 ASTM Standard)	15

An ABAQUS input that addresses the mesh sensitivity issue specific to a stress-strain input, the inclusion of reliable fracture energy, characterizes the inelastic behavior in tension under the post-peak range. The section that follows provides a sensitivity analysis of various fracture energy values applied to the unreinforced model. Parabolic softening is approximated by the stress-strain criterion used in ABAQUS to explain the inelastic behavior in compression.

Vertical compression and horizontal cyclic force are two separate types of loads that have been applied to the model. A force equal to 10% of the column's nominal axial load carrying capability, that is 60 kN axial load was applied on the head of each column to replicate the system's dead load. The joints between the beam and column were made stiff to prevent stress concentration. To closely resemble the experimental loading, a prescribed deformation load was also applied for the horizontal cyclic loading above each level. Cyclic loading was applied to the structure at the top beam-column joint level, which imparts lateral forces in the IP direction. The FEM analysis was conducted using the ABAQUS/Explicit software, with the

analysis type selected as dynamic explicit. The loading strategy is a displacement-control method used consistently for all specimens. The same loading process that is used in experimental campaign is employed for numerical analysis, as depicted in Figure 3.10.

Table 3.4. Mechanical properties of the fibers for the numerical simulations

Fabric Type	γ_f (g/m ²)	A_f (mm ² /m)	F_{fu} (kN/m)	ϵ_{fu} (%)	E_f (GPa)
Glass	420	45.3	105	>2.0	32
Carbon	170	48.0	240	2.0	252
Basalt	250	38.9	60	1.8	89

3.3.2. Interface simulation between expanded bricks

The surface-based cohesive contact model has been chosen as the interaction model between various blocks. The specification of the tensile strength and the softening behavior may be used to simulate the fracture between blocks. The compression between blocks is specified by the hard contact concept. Cohesive and friction models are the two types of shear models (Bertolesi et al., 2016).

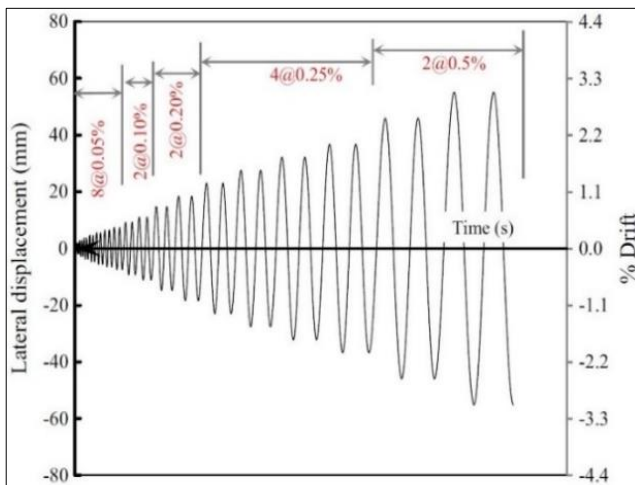


Figure 3.10. Applied displacement time history

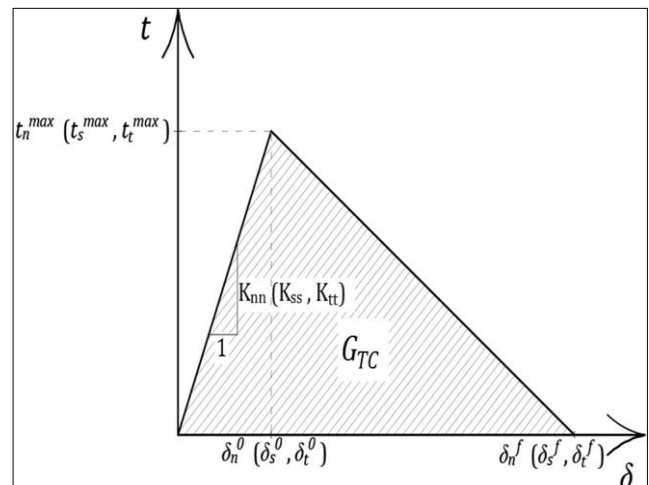


Figure 3.11. Traction separation response of brick wall joint interfaces in tension and shear

The general linear behavior is written in the form of an elastic stiffness matrix. The relation between the elastic stiffness matrix K , nominal traction vector t , and corresponding separation vector d , of the joint interfaces Figure 3.11 (Abdulla et al., 2017) is expressed as in Eq. (5).

$$\mathbf{t} = \begin{Bmatrix} t_n \\ t_s \\ t_t \end{Bmatrix} = \begin{bmatrix} K_{nn} & K_{ns} & K_{nt} \\ K_{sn} & K_{ss} & K_{st} \\ K_{tn} & K_{ts} & K_{tt} \end{bmatrix} \quad (5)$$

Under the same boundary conditions, the components of the stiffness matrix \mathbf{K} for joint interfaces in a simplified micromodel (interfaces between enlarged masonry units) ought to be identical to the stiffness of the original masonry joint interfaces (brick and mortar). The elasticity moduli of the mortar and unit, as well as the thickness of the mortar Equation's, are used to define the equivalent stiffness for joint interfaces. (2), and (3) (Lourenço, 1996).

$$k_n = \frac{E_u E_m}{h_m(E_u - E_m)}, \quad k_s = \frac{G_u G_m}{h_m(G_u - G_m)} \quad (6)$$

3.3.3. Plastic response of the joint interfaces

The damage initiate criterion (Eq. 7), and the damage development criterion (Eq. 8), comprise the surfaced-based cohesive contact model.

$$\left\{ \frac{t_n}{t_n^0} \right\}^2 + \left\{ \frac{t_s}{t_s^0} \right\} + \left\{ \frac{t_t}{t_t^0} \right\} = 1 \quad (7)$$

$$t_n = \begin{cases} (1 - D)\bar{t}_n, & \bar{t}_n \geq 0 \\ \bar{t}_n, & \text{Otherwise} \end{cases} \quad t_s = (1 - D)\bar{t}_s \quad t_t = (1 - D)\bar{t}_t \quad (8)$$

The normal and two shear tractions are represented by the symbols t_n t_s t_t . The letters n , s , and t stand in for the pertinent separations. The superscript zero indicates peak values. Pure normal slip or pure shear separation with zero normal separation does not produce cohesive forces in the normal direction because the traction-separation behaviour is decoupled in this scenario. The Macaulay bracket in Eq. (7) shows that the compressive stresses are not taken into account for the joints' typical direction fracture behaviour.

3.3.4. Loading and Meshing

In two steps, the numerical analysis was computed. The initial phase was applying the first vertical axial load. In the second stage, the horizontal IP cyclic load was slowly delivered while displacement was being controlled, keeping the imposed vertical compression stress constant. To preserve the identical boundary conditions as in the experiment, the vertical and OOP horizontal displacements and rotations around all axes were limited to the top of the wall. A mesh sensitivity analysis has been used to determine the size of the mesh. A three-dimensional element having dimensions of 50 x 50 x 50 mm has been used to simulate the RC frame, which comprises one beam and two columns. A whole brick unit (400 mm length, 200

mm height, and 150 mm thick) has been designed for research with 7 x 2 x 3 elements as opposed to the half brick unit width scenario, where each unit had a model with 3 x 2 x 3 sections. The mesh size utilized in ABAQUS for the RC frame, half brick unit width, entire masonry unit, and FRCM are shown in Figures 3.12 to 3.14.

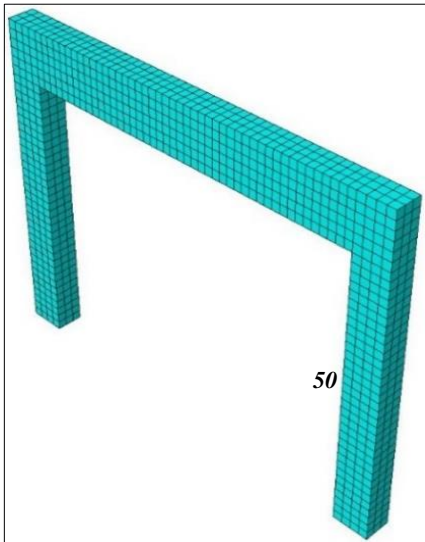


Fig 3.12. Meshing of the bare frame

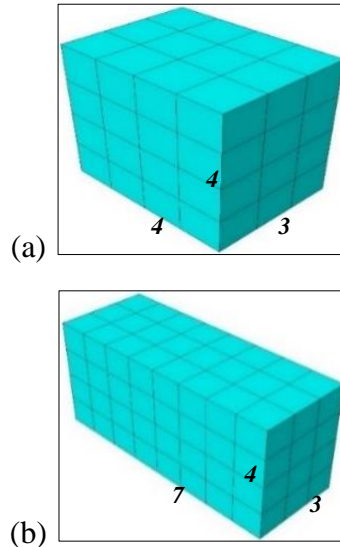


Fig 3.13. Meshing of (a) half brick and (b) full brick

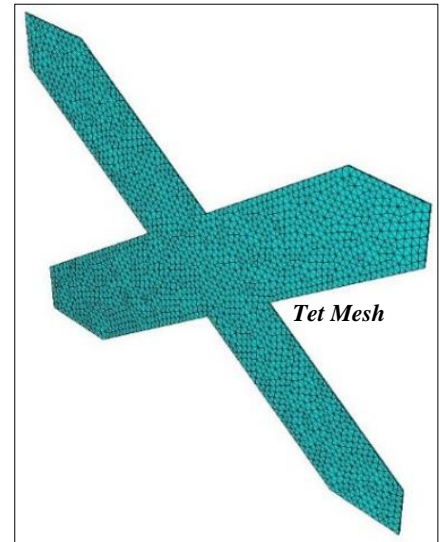


Figure 3.14. Meshing of fiber

Depending on the method used to conduct the numerical analysis, the actions (load or displacement) given to the model are either based on load control or displacement control. In all scenarios, the acts must be performed progressively. The effects of large displacement non-linear geometry were taken into account in all models. A broad non-linear static methodology was then used to solve the Newton-Raphson method's solution, which iteratively solves equilibrium in each increment. For the surface-based cohesive behaviour model to accurately predict the breakdown of masonry joints without experiencing numerical convergence issues, viscous regularization is necessary as a damage stabilizer. This is because masonry joints' softening and stiffness deterioration also induce numerical instability.

3.4. RESULTS AND DISCUSSION

In this section, the findings of the numerical analysis from the current investigation (Figure. 3.15b – 3.22b) before comparing them to the findings of the experimental (Figure. 3.15a – 3.22a) nonlinear structural cyclic analysis is quickly explained. In BF-1, a vertical bending crack was started from the tensile side of the beam close to the joint region, which is the potential hinge's location, although no fractures could be seen in the columns. In infill wall

IF-2, the upper part of the masonry wall system showed signs of stress creation; fractures had developed in the mortar joints of the wall. The columns showed no signs of breakdown or the formation of any plastic hinges, as could be seen in the bare frame. The loading joint underwent some stresses; however, the FRCM did not exhibit any delamination failure in the RFG-D3-3 model. In contrast, RFG-D6-4's left half-top region underwent a tremendous number of loads and deformations. Regarding RFC-D3-5, RFB-D3-7, and RFB-D6-8, both the left and right bottom corners of the masonry and frame underwent minor cracks. In the case of RFC-D6-6, cracks appeared on the left side of FRCM as well as in the bed joints. The hysteresis curves of the experiments are shown in Figure. 3.23a to 3.30a, and those obtained in the numerical analysis are presented in Figure. 3.23b to 3.30b. It can be seen that identical hysteresis graphs are created from the ABAQUS model simulations in agreement with the experimental data. One can see that the hysteresis curve for the BF-1 specifically matches the outcomes of the numerical analysis hysteresis curves.

The hysteresis graph of the IF-2, as illustrated in Figure 3.24b, exhibits the pinching effect. The experimental findings and the numerical analysis hysteresis curve correspond well. As indicated in Table 3.5, the maximum deformation values and the maximum load-bearing capacity are practically identical. The initial fracture in specimens RFB-D3-7 and RFC-D3-5 first manifested itself at a lateral drift of 0.5% (see Figure. 3.29a and 3.27a) at the left and the right base masonry and frame interfaces. Neither the face of the FRCM nor the wall had any visible fissures.

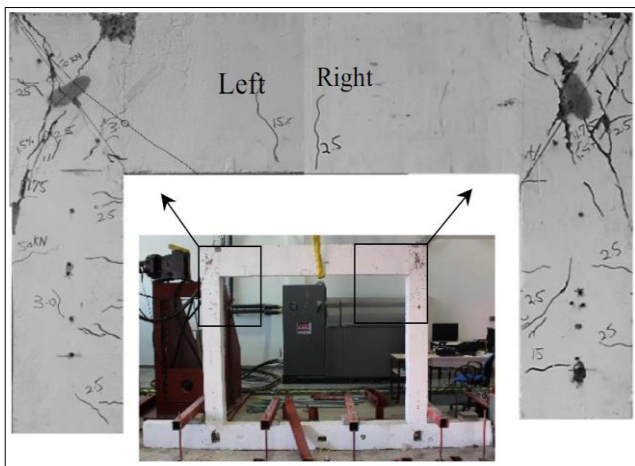


Figure 3.15a. Experimental BF-1 results

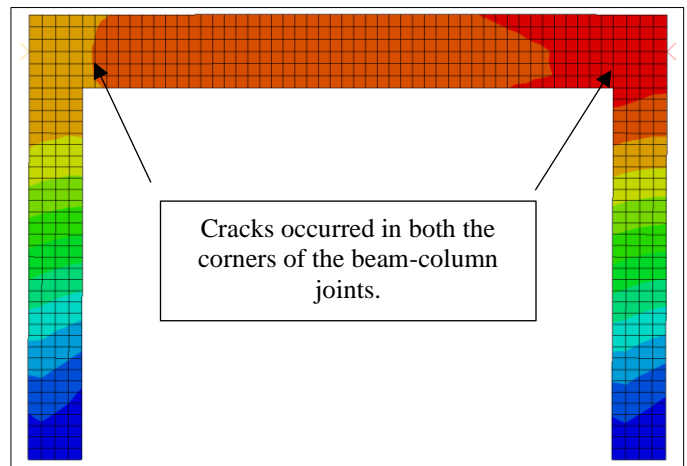


Figure 3.15b. Numerical BF-1 results

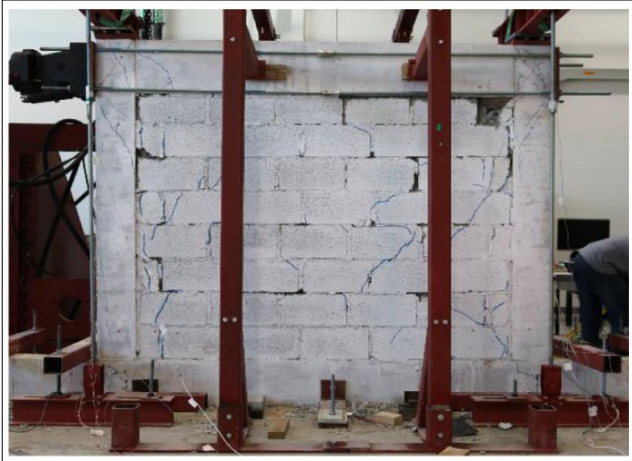


Figure 3.16a. Experimental IF-2 results

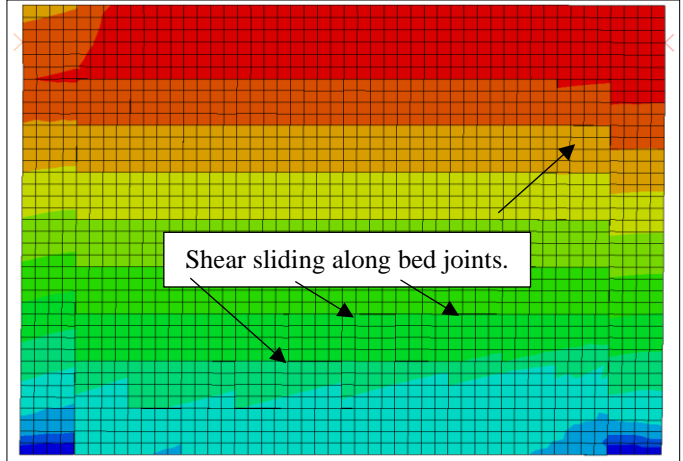


Figure 3.16b. Numerical IF-2 results

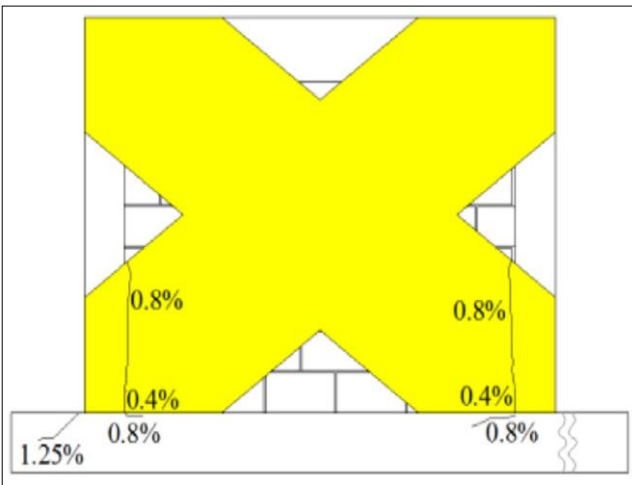


Figure 3.17a. Experimental RFG-D3-3 results

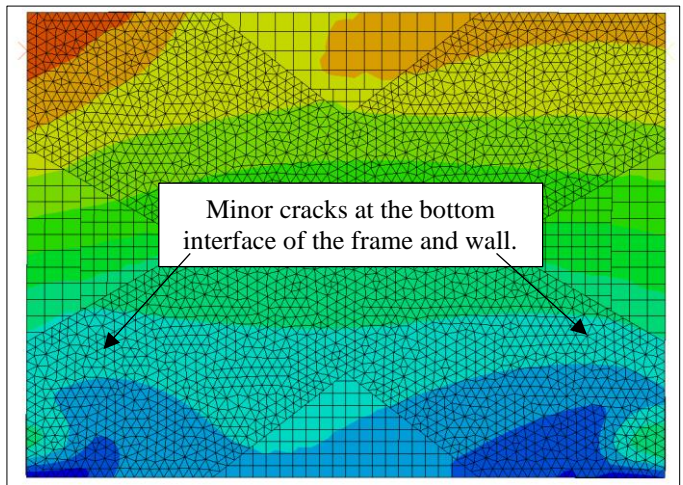


Figure 3.17b. Numerical RFG-D3-3 results

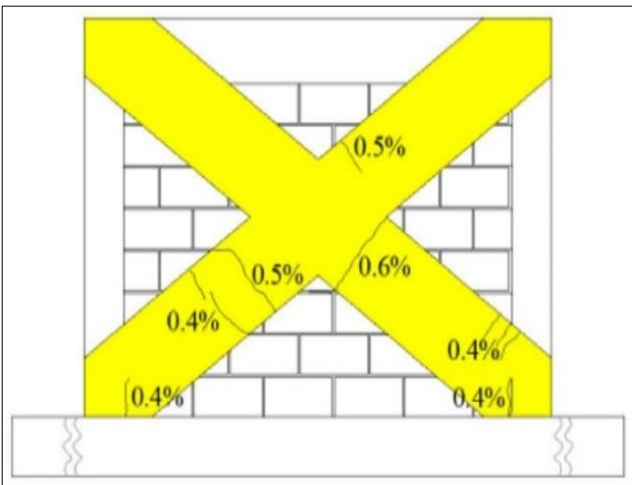


Figure 3.18a. Experimental RFG-D6-4 results

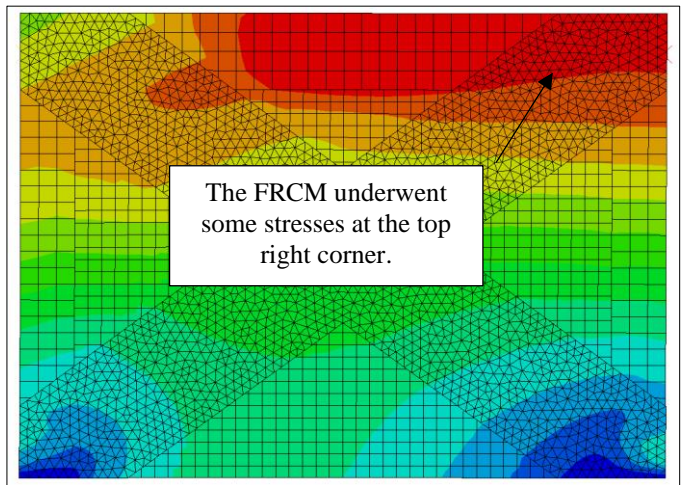


Figure 3.18b. Numerical RFG-D6-4 results

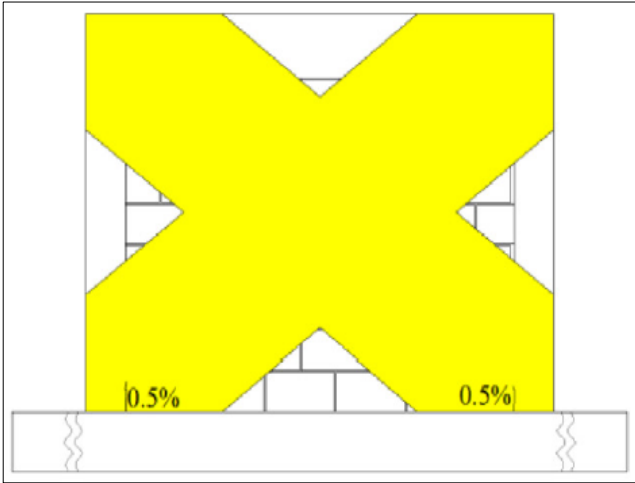


Figure 3.19a. Experimental RFC-D3-5 results

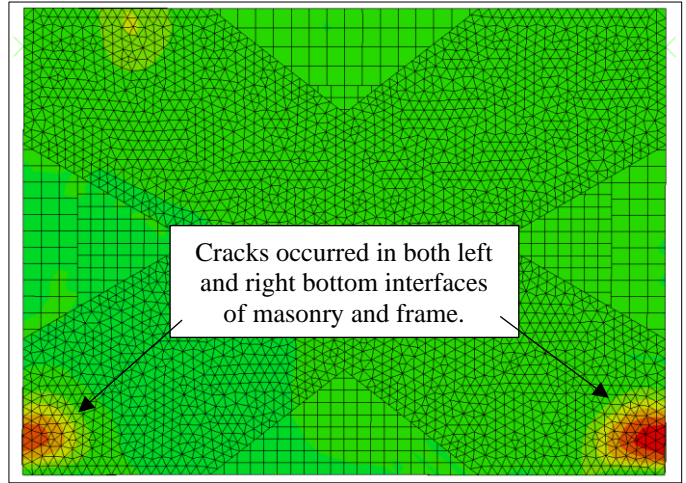


Figure 3.19b. Numerical RFC-D3-5 results

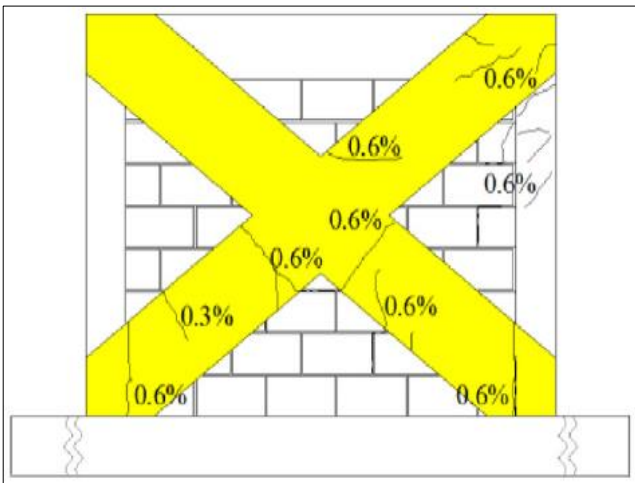


Figure 3.20a. Experimental RFC-D6-6 results

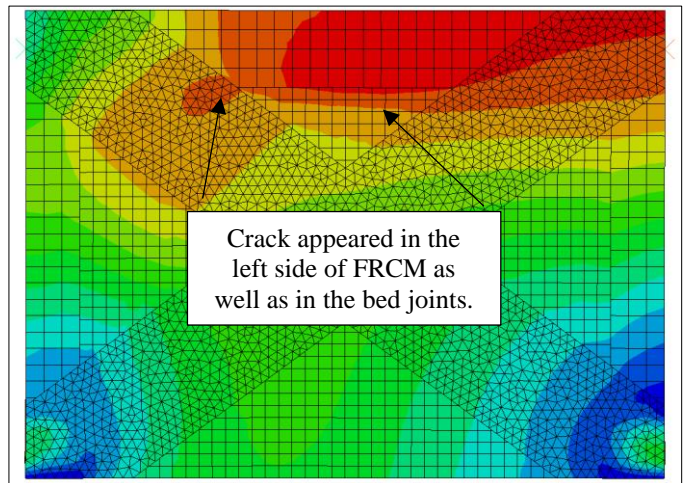


Figure 3.20b. Numerical RFC-D6-6 results

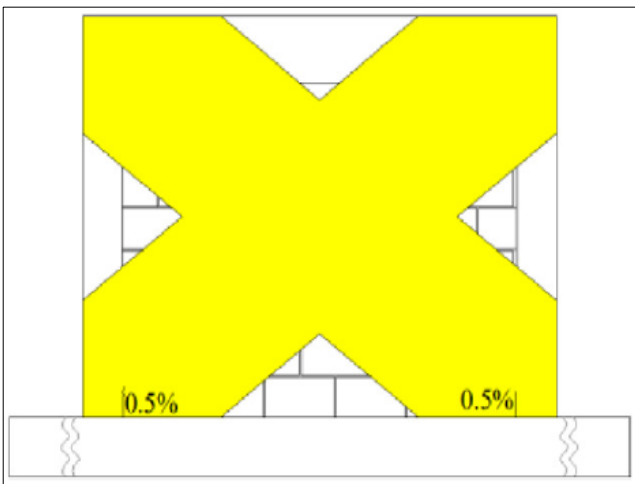


Figure 3.21a. Experimental RFB-D3-7 results

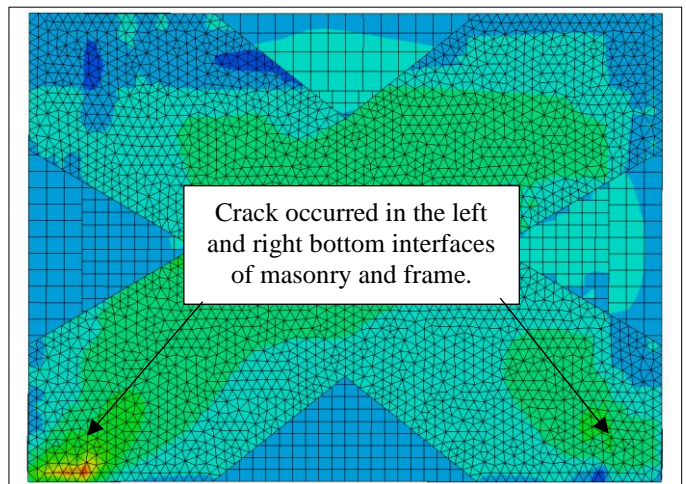


Figure 3.21b. Numerical RFB-D3-7 results

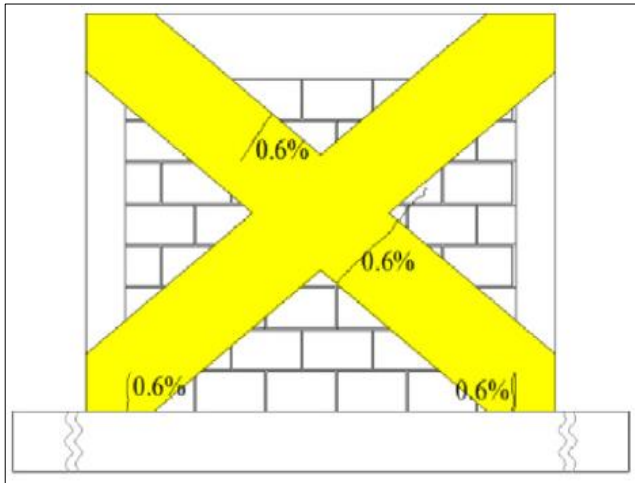


Figure 3.22a. Experimental RFB-D6-8 results

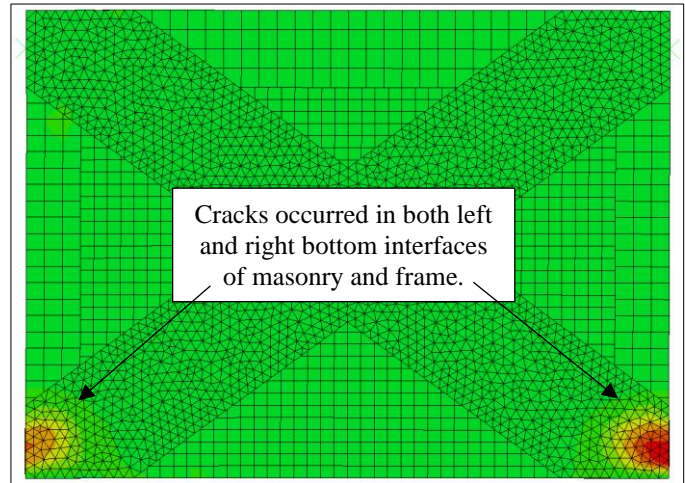


Figure 3.22b. Numerical RFB-D6-8 results

The first fracture in specimen RFC-D6-6 started to appear with a lateral drift of 0.3% on the left-hand side of FRCM. At a horizontal drift of 0.6%, a crack developed at the base of the masonry and the frame connection. More fractures developed at the FRCM and in the bed joints during the same drift (see Figure 3.26b). In the upper right section of the column, close to the presumed hinge point, shear cracking was also visible. Gravity force was applied to this frame before testing, and as a result, numerous pre-existing cracks worsened throughout the test. At a lateral drift of 0.6%, the specimen RFB-D6-8's left, and right bottom masonry and frame interfaces saw the emergence of the first fracture. The FRCM also experienced a few mild diagonal fractures at the same time (see Figure 3.30b). The figures of the load-bearing capacity determined from numerical analysis, apart from the bare frame, are marginally greater than the outcomes of the experiments. The numerical and analytical values, however, are invariably greater than the values found in the experimental findings when it comes to the values of the largest lateral displacement. In general, ABAQUS overestimates the ultimate lateral displacement and the maximum load-bearing capacity of the specimens by a maximum of 5% when compared to the experimental data. Infilled frames, on the other hand, show an inaccuracy of about 18.5%. This may be because the ABAQUS validation of the infill wall behavior used idealized assumptions, such as the smoothness of the brick surface, the lack of material flaws, and the total absence of mortar.

Once, the numerical outcomes were matched with the experimental results, analytical equations were proposed for the same specimens to determine the load-carrying capacity considering the geometry of the specimen, properties of the materials used such as bricks, concrete, strengthening material FRCM elaborated in the following section.

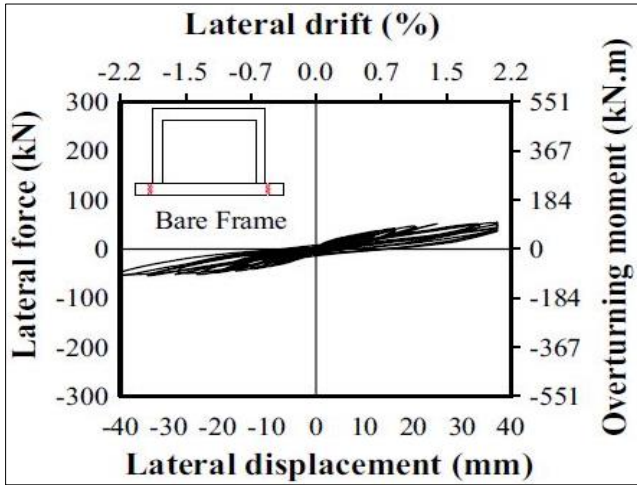


Figure 3.23a. Experi. BF-1 hysteresis curve

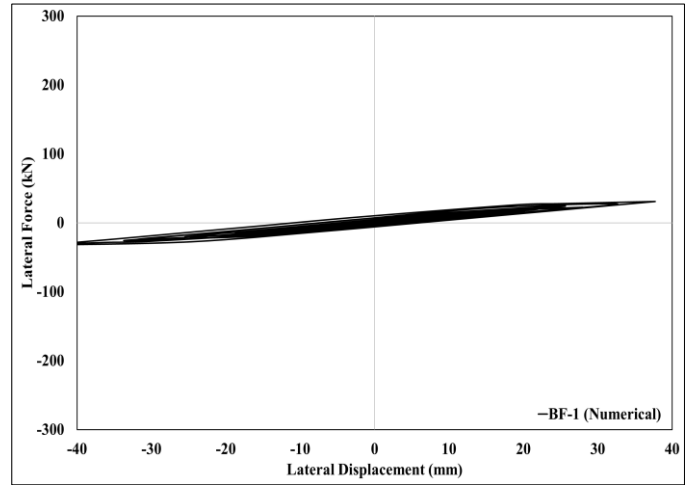


Figure 3.23b. Numerical BF-1 hysteresis curve

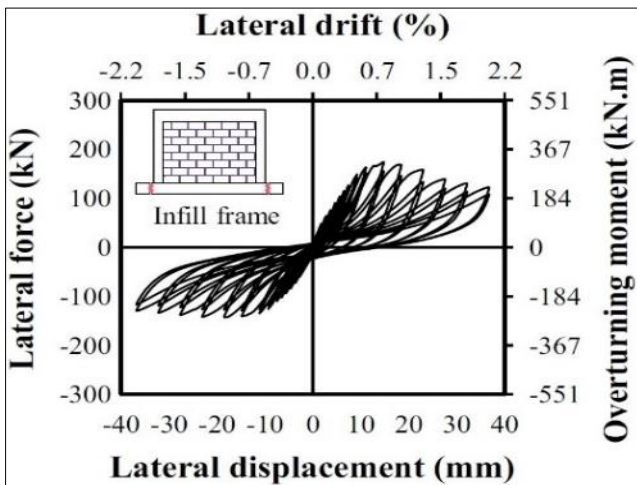


Figure 3.24a. Experi. IF-2 hysteresis curve

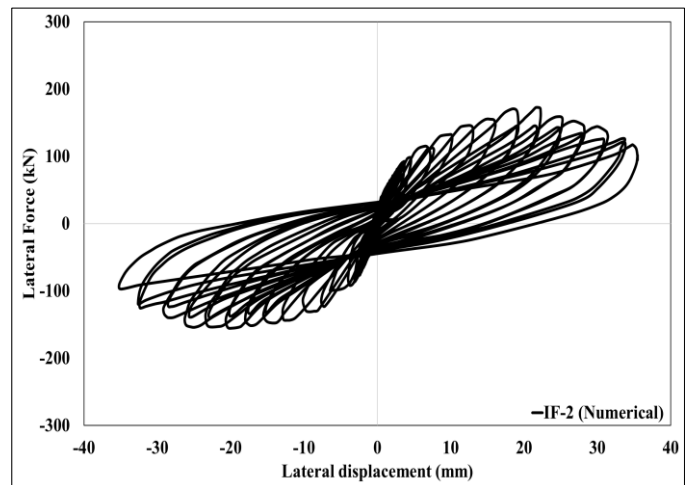


Figure 3.24b. Numerical IF-2 hysteresis curve

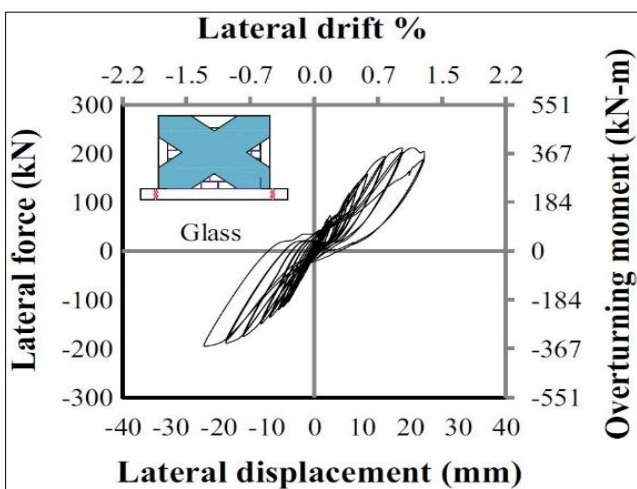


Figure 3.25a. Experi. RFG-D3-3 hysteresis curve

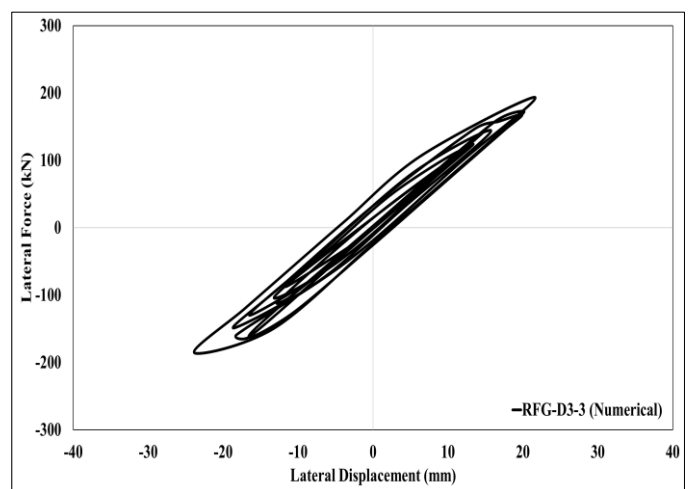


Figure 3.25b. Numerical RFG-D3-3 hysteresis curve

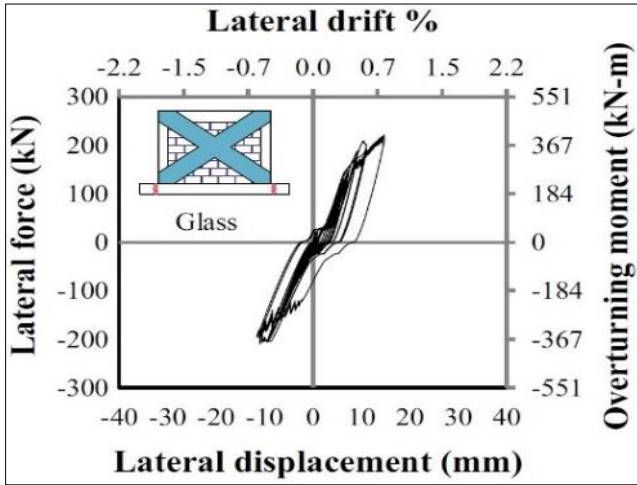


Figure 3.26a. Experi. RFG-D6-4 hysteresis curve

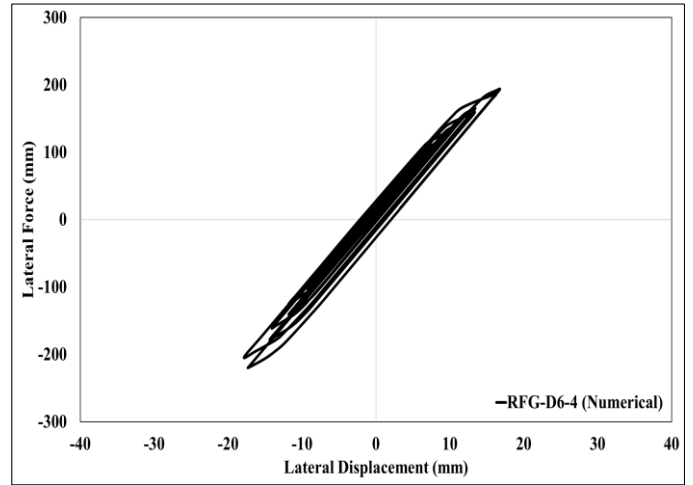


Figure 3.26b. Numerical RFG-D6-4 hysteresis curve

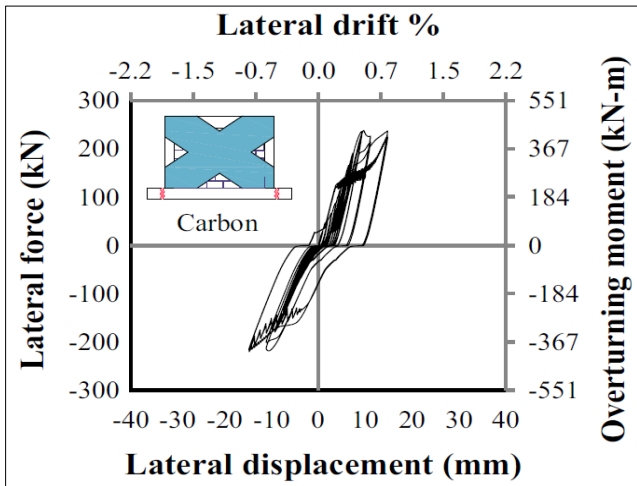


Figure 3.27a. Experi. RFC-D3-5 hysteresis curve

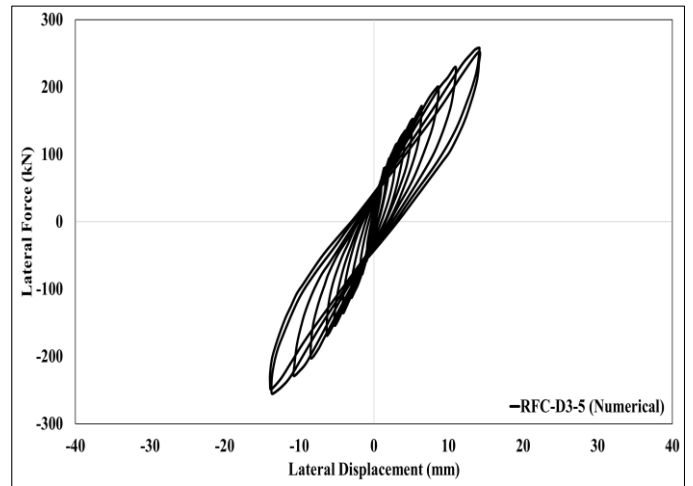


Figure 3.27b. Numerical RFC-D3-5 hysteresis curve

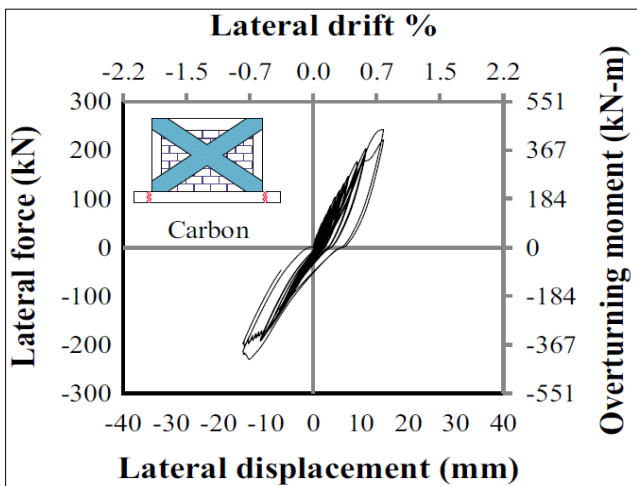


Figure 3.28a. Experi. RFC-D6-6 hysteresis curve

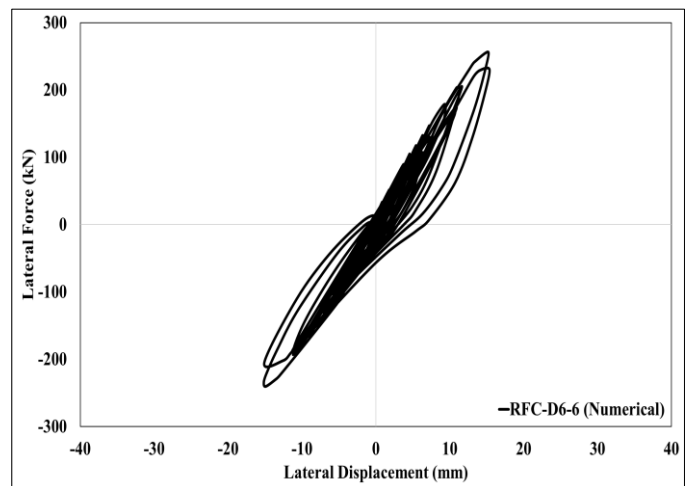


Figure 3.28b. Numerical RFC-D6-6 hysteresis curve

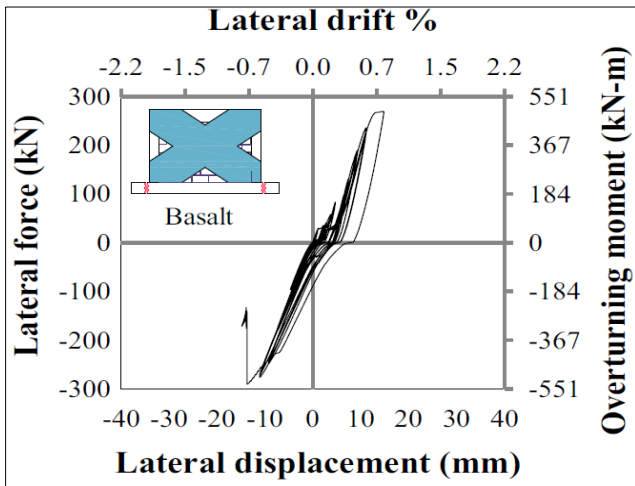


Figure 3.29a. Experi. RFB-D3-7 hysteresis curve

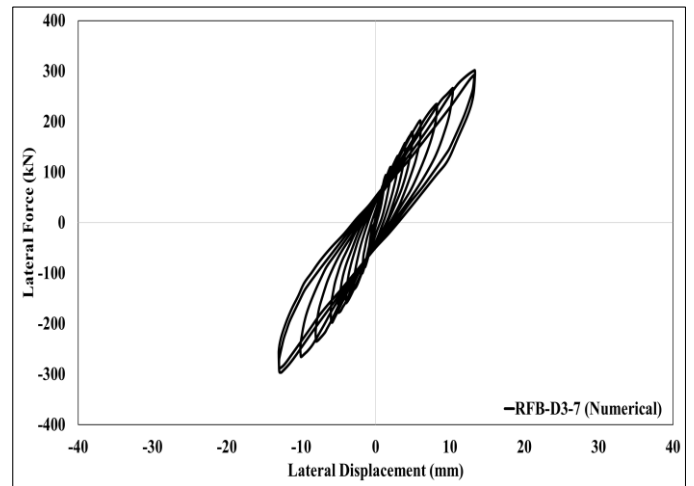


Figure 3.29b. Numerical RFB-D3-7 hysteresis curve

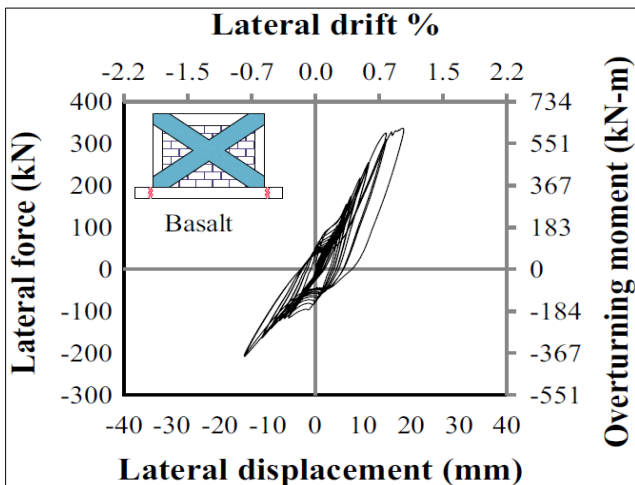


Figure 3.30a. Experi. RFB-D6-8 hysteresis curve

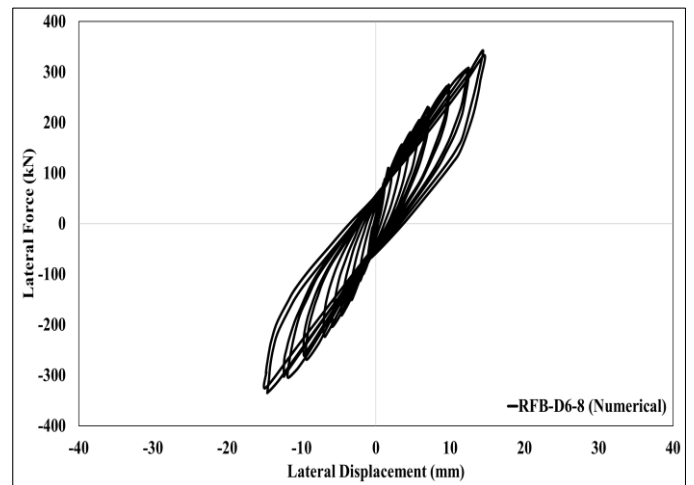


Figure 3.30b. Numerical RFB-D6-8 hysteresis curve

3.5. EXPRESSION TO DETERMINE THE LOAD CARRYING CAPACITY

To develop empirical equations for estimating the load-carrying capacities of the investigated test specimens, a systematic methodology involving experimental data and numerical simulations is typically adopted. A detailed breakdown of the methodology based on the study is as follows

A. Experimental Data Collection

Test specimens' preparation - Construct two 2/5th scaled, single-bay single-story MIW with RC frame test specimens. One specimen serves as an unreinforced specimen (URS), and the other as a double reinforced specimen (DRS) retrofitted with AR-resistant glass fiber TRM.

Material properties - Document properties of materials used (e.g., burnt clay red bricks, cement-sand mortar, concrete, steel reinforcement) to ensure accurate replication in numerical models.

Quasi-static reversed cyclic lateral loading - Apply this loading to the specimens and record the lateral load versus displacement data. Note differences in damage patterns, lateral strength, stiffness, and deflection between URS and DRS.

B. Numerical Simulation

Model development in ABAQUS - Use the finite element software ABAQUS to create a detailed numerical model of the RC frame with MIW.

Concrete damage plasticity (CDP) model - Employ this model to simulate the non-linear behavior of masonry blocks and concrete under cyclic loading.

Simplified Micro-model approach - This approach allows for the modeling of the interaction between the RC frame and infill wall, including TRM strengthening.

Model calibration and validation - Calibrate the numerical model using experimental results to ensure accuracy. Validate by comparing numerical results with experimental data, focusing on load-displacement hysteresis loops and excursion curves.

C. Parametric Study

Varying the parameters: Conducting a parametric study to explore the effects of:

- Type of TRM strengthening material.
- Pattern of TRM layers.
- Bonding scenarios between the RC frame and infill.

Simulate scenarios - Use the validated numerical model to simulate various scenarios, recording changes in lateral load-carrying capacity and displacement.

D. Development of Empirical Equations

Data analysis - Analyzing the experimental and numerical results to identify key trends and relationships. Focus on how variables such as TRM reinforcement, wall openings (if present), and material properties influence load-carrying capacity.

Regression analysis - Performing statistical regression analysis on the collected data to derive empirical relationships. Typically, the following steps are involved:

- Identify influencing factors - Determining the most significant factors affecting load-carrying capacity (e.g., TRM layers, wall openings).
- Formulate equation structure - Choosing an appropriate form for the empirical equation (e.g., linear, polynomial).

- Fit the model - Using regression techniques to fit the model to the experimental and numerical data, minimizing error terms.
- Validate the equation - Comparing the predictions of the empirical equation against independent data sets or additional experimental results to ensure reliability and accuracy.

E. Equation Formulation

Empirical formulation - Based on the regression analysis, formulating the empirical equations that can estimate the load-carrying capacities of MIW in RC frames. These equations typically take the form:

$$P = f (X_1, X_2, \dots, X_n)$$

$$P = f (X_1, X_2, \dots, X_n)$$

where P is the load-carrying capacity and X_1, X_2, \dots, X_n are the influencing factors (e.g., number of TRM layers, presence of openings, material properties).

F. Verification and Adjustment

Model refinement - Adjust the empirical equations as necessary based on further testing and feedback. Ensure that they account for all significant factors and interactions observed in the study.

Practical applicability - Ensure that the equations are practical and easy to use for engineers in the field. Simplify terms and coefficients for straightforward application in design and assessment.

The proposed empirical equations to determine the load-bearing capacity of the eight 2:3 scaled one-bay one-story reinforced concrete masonry (RCM) buildings including a bare frame (BF), an RCFMI (IF), and six RCFMIs that had been retrofitted with FRCM constructed using three different fiber materials: carbon, aramid glass, and basalt.

The following expression represents the bare frame (BF-1) load-bearing capacity:

$$\frac{(A_s - A_w) \times t_w \times \Delta \times f_{ck \text{ concrete}}}{\pi \times (E_{conc} - E_{brick}) \times 3.4} \quad (9)$$

The following expression represents the infill frame (IF-2) load-bearing capacity:

$$\frac{A_s \times t_w \times \Delta \times f_{ck \text{ brick}}}{\pi \times (E_{conc} - E_{brick}) \times 3.4} \quad (10)$$

The following expression represents the RFG-D3-3's load-bearing capacity:

$$\frac{1}{2\pi} \times \frac{A_s \times t_w \times \Delta \times f_{ck \text{ brick}} \times A_f}{(E_{conc} - E_{brick}) \times E_f \times 3.4} \times (D3) \quad (11)$$

The following expression represents the RFG-D6-4's load-bearing capacity:

$$\frac{1}{2\pi} \times \frac{A_s \times t_w \times \Delta \times f_{ck \text{ brick}} \times A_f}{(E_{conc} - E_{brick}) \times E_f \times 3.4} \times (D6 \times \varepsilon_{fu}) \quad (12)$$

The following expression represents the RFC-D3-5's load-bearing capacity:

$$\frac{1}{2\pi} \times \frac{A_s \times t_w \times \Delta \times f_{ck \text{ brick}} \times A_f}{(E_{conc} - E_{brick}) \times E_f \times 3.4} \times (D3 \times 13) \quad (13)$$

The following expression represents the RFC-D6-6's load-bearing capacity:

$$\frac{1}{2\pi} \times \frac{A_s \times t_w \times \Delta \times f_{ck \text{ brick}} \times A_f}{(E_{conc} - E_{brick}) \times E_f \times 3.4} \times (D6 \times 13 \times \varepsilon_{fu}) \quad (14)$$

The following expression represents the RFB-D3-7's load-bearing capacity:

$$\frac{1}{2\pi} \times \frac{A_s \times t_w \times \Delta \times f_{ck \text{ brick}} \times A_f}{(E_{conc} - E_{brick}) \times E_f \times 3.4} \times (D3 \times 7) \quad (15)$$

The following expression represents the RFB-D6-8's load-bearing capacity:

$$\frac{1}{2\pi} \times \frac{A_s \times t_w \times \Delta \times f_{ck \text{ brick}} \times A_f}{(E_{conc} - E_{brick}) \times E_f \times 3.4} \times (D6 \times 7 \times \varepsilon_{fu}) \quad (16)$$

Where, A_s = Area of the total specimen including (area of RC frame and area of infill wall); t_w = thickness of infill wall; Δ = maximum drift (%); E_{conc} = concrete elastic modulus; E_{brick} = infills elastic modulus; $f_{ck \text{ brick}}$ = infills compressive strength; A_f = cross-sectional area of fibers; E_f = tensile elastic modulus of the fibers; $D3$ = FRCM bands with a cross-pattern design that is 1/3 the width of the diagonal length; $D6$ = FRCM bands with a cross-pattern design that is 1/6 the width of the diagonal length; ε_{fu} = ultimate strain at rupture. Values are given in Tables 3.3 and 3.4.

The constants used in the empirical equations are the co-relation factors to adjust the units or dimensions of variables in the equation which are determined using linear regression analysis. These factors ensure that the equation is consistent and provides results in the desired units, which depends on the data provided by the manufacturer such as cross-sectional area (A_f), tensile elastic modulus of the fibers (E_f), and fabric tensile rupture strength (F_{fu}). For each test, backbone/envelope curves were plotted by interconnecting the highest excursion points of each cycle (Figure 3.31) which are useful in understanding the behaviour of a test specimen. It is easier to note the load carried by a specimen at a particular displacement to observe its each step behaviour under lateral loads. According to the hysteresis graphs acquired from the linear regression analysis conducted, the average value of the coefficient of

determination (R^2) is determined to be 0.894, which evaluates how well the numerical model predicts the results.

Table 3.5. Experimental, numerical, and analytical results of all the specimens

Specimen	Maximum Lateral Load (kN)			Max. Lateral Displacement (mm)		Maximum Drift (%)	
	Experiment	Numerical	Equation	Experiment	Numerical	Experiment	Numerical
BF-1	58	54	54.131	40	45	2.5	2.65
IF-2	168	186	162.475	38	39	2	2.13
RFG-D3-3	206	213	208.36	23	25	1.25	1.36
RFG-D6-4	221	227	219.72	17	18	0.8	0.98
RFC-D3-5	236	244	236.46	15	17	0.8	0.93
RFC-D6-6	231	237	232.29	16	18	0.8	0.98
RFB-D3-7	290	295	295.96	12	16	0.8	0.87
RFB-D6-8	335	336	339.19	20	21	0.8	0.89

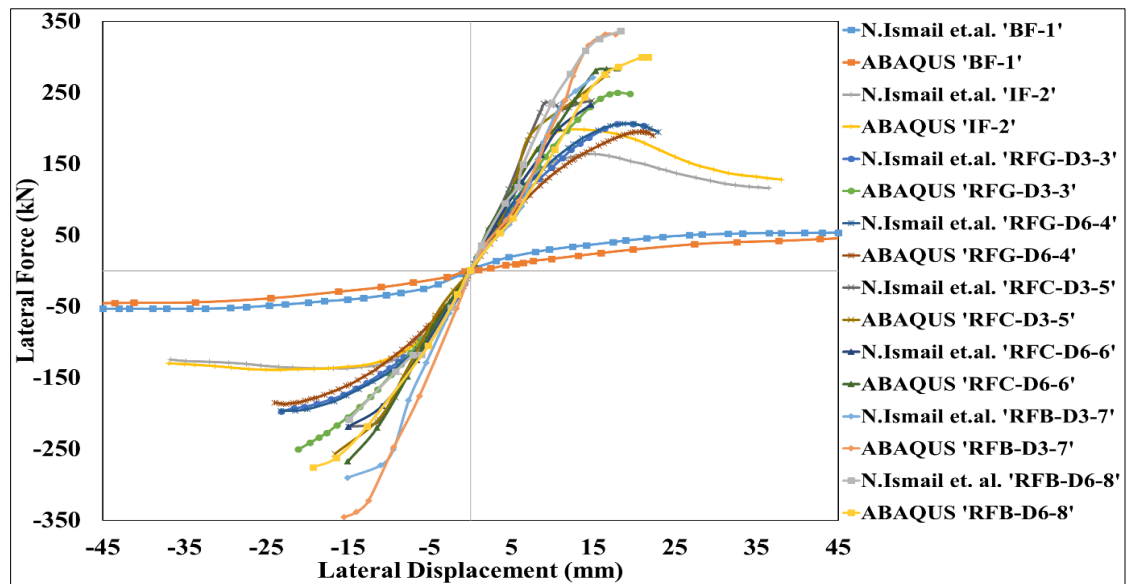


Figure 3.31. Maximum excursion curves for both experimental and numerical analyses

The variation in the values among the experimental values and the simulation values occurs because of the non-consideration of the practical imperfections of the construction materials in real situations. For instance, in the case of experimental testing, a few factors have to be considered such as the transportation of the materials, different workers involved, atmospheric conditions, material quality, construction quality, construction procedure, etc. because of which some imperfections in the material or the construction arises. These

imperfections are not involved in the numerical analyses where for example, the surfaces and the edges of the bricks are perfectly straight without the imperfections as mentioned earlier.

3.6. Summary

In this Chapter, the finite element technique proposed in Section 3.2 was validated against experimental observation from a major research program. Eight masonry infilled RC frames were considered in the validation. The experimental data included infilled frames of 2/3 scale and covered cases of infill walls constructed using concrete masonry units (CMU) strengthened with FRCM or TRM.

It was demonstrated that the developed finite element (FE) technique is capable of capturing the entire lateral load-lateral displacement history of masonry infilled RC frames up to failure with acceptable accuracy. In addition, the technique is capable of accurately predicting the failure mechanisms of the infill wall: sliding shear, failure patterns, and minor cracks on FRCM. Although ABAQUS offers general material constitutive and interfacial behaviour models for many different structural applications, the contribution of this study lies in identifying and the selection of appropriate models and crucial material parameters, as well as the execution of an accurate and successful computational interaction properties of masonry infills surrounded by RC frame members with FRCM as a strengthening material. Therefore, the identified and the evaluated factors that have been discussed in this Chapter (Section 3.3 and Section 3.5) are considered for the studies conducted in the following Chapters.

Based on the observations and the learnings from this Chapter, an experimental investigation is carried out (explained in Chapter 4) in which a 2/5th scale non-ductile RC frames with MIW without opening subjected to in-plane load. Various parameters considered for the purpose were different types of masonry unit (for example, material properties and compressive strength), different grades of concrete and steel. Because of space constraints and the limited capacity of the servo-hydraulic actuator (200 kN) available in the laboratory, the scale of the test specimen, compressive strength of the brick units, and grade of the concrete used were all reduced. These experiments were carried out at Pilani, a town in Rajasthan, India, a Moderate Risk Zone, using locally produced and accessible bricks with a compressive strength of 10.92 MPa. (Intensity VII) (Zone, 2023). Hence, consideration is required to safeguard these structures, as most of them are built using masonry units.

CHAPTER 4

EXPERIMENTAL INVESTIGATION OF NON-DUCTILE REINFORCED CONCRETE (RC) FRAMES WITH MASONRY INFILL WALL (MIW) WITHOUT OPENING

4.1. OUTLINE

This chapter illustrates the experimental study in which a 2/5th scale non-ductile reinforced concrete (RC) frames with masonry infill wall (MIW) without opening was subjected to quasi-static cyclic lateral loading that was controlled by sinusoidal displacement. The specimen was rigidly anchored to the ground at the foundation level and was provided customized out-of-plane resistance. The wall panel configurations are described in greater detail in the following sections. Parameters considered for the test included:

- (i) the thickness of the infill wall
- (ii) the RC frame without ductile detailing
- (iii) the class of the brick
- (iv) the infill wall without opening

4.1.1. Objectives

The main objectives of this Chapter are

- a. To record the load-displacement (P- Δ) behaviour of the walls
- b. To study the wall cracking patterns, measure their deformation profiles, and assess the accuracy of idealized failure mechanisms.

The outline of this chapter is as follows: Section 4.2 details about test program and methodology. Section 4.3 elaborates the test setup and instrumentation. Section 4.4 discusses the experimental results along with the failure modes of the specimen. Section 4.5 provides the validation study of the experimental investigation discussed in Section 4.4. Section 4.6 discusses the results and discussion. Section 4.7 summarizes the key observations and lessons derived from the experimental program.

The thesis concludes with appendices that give further support for the experimental investigation. The loading frame design specifications for mounting the actuator in the laboratory to conduct the experimental test are described in Appendix.

4.2. TEST PROGRAM AND METHODOLOGY

4.2.1. Configuration of the Non-Ductile RC Frame

Without considering the seismic detaining of the buildings, separate, one-story wall-type masonry specimens having 1:2.5 scale (aspect ratio defined as the ratio of the wall length up on the wall height that is 1.56) is created to replicate the features seen in the walls of the ground floors of typical two-story Indian homes now in existence to examine its seismic performance. In both the bed and head joints, mortar layer was maintained at a standard thickness of 12 mm using 1:3 mortar (Portland cement and sand). Figures 4.1 and 4.2 display the reinforcement details and construction of the test specimen, respectively. This aspect ratio (lesser than the dimensions of the specimen tested by (N. Ismail et al., 2018a) in Chapter 3) of the specimen is selected by considering the capacity of the actuator and the space available in the laboratory.

To guarantee uniformity, inspection procedures were followed while the mortar was being mixed. This involved batching the components in drums and making sure that all of the sand was completely air-dried before blending. Based on the expertise of the construction labourers, water was added to the cement and sand mixture within the mortar mixer to achieve the required workability. The dimensions of the beam cross-section (Figure 4.3(a)) are 240 mm x 185 mm, the cross-section of the column (Figure 4.3(b)) is 210 mm x 185 mm, and the foundation beam cross-section (Figure 4.3(c)) are 400 mm x 275 mm. The height of the column is 1200 mm. Two-legged stirrups with 8 mm diameter bars spaced at 120 mm center-to-center distance are linked to four bars with a 12 mm diameter reinforcement and a 10 mm clear cover on either side of the column. To meet the requirements for development length, the column's inner face reinforcement and peripheral face reinforcement are each inserted into the foundation to a depth of 500 mm and 165 mm on the inner and outer sides, respectively. The foundation plinth beam has two bars of 12 mm diameter in the compression zone and three bars of 16 mm diameter in the tension zone, with a 20 mm clear cover on both sides. To avoid damage, the foundation beam was purposely over-reinforced. Stirrups with a diameter of 10 mm and center-to-center spacings of 170 mm throughout the span were tied around the bars.

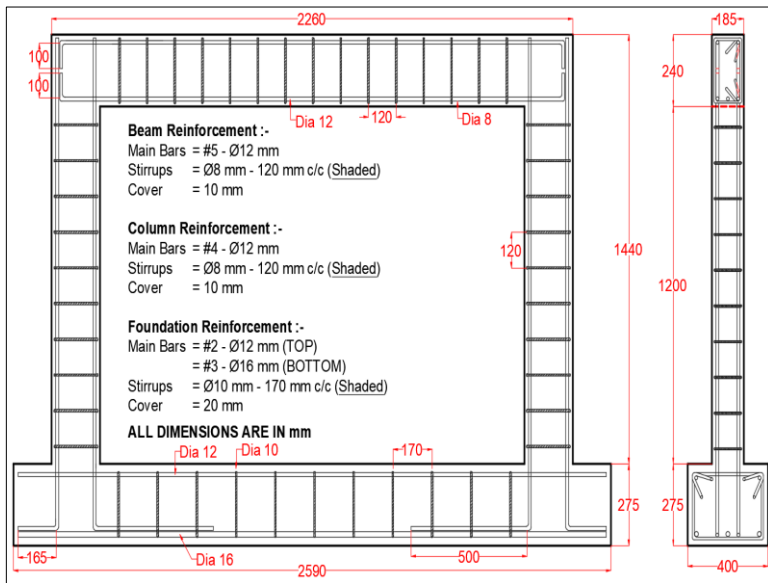


Figure 4.1. Test frame details (all dimensions in mm)



Figure 4.2. Reinforcement details

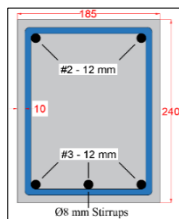


Figure 4.3(a) Beam c.s.a

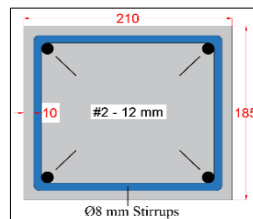


Figure 4.3(b) Column c.s.a

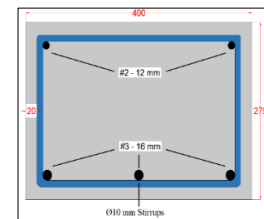


Figure 4.3(c) Foundation c.s.a

The concrete cover is 20 mm thick in the foundation beam and has a 10 mm thickness in the beam and columns. The foundation's rings and the hoops in the beam and column are separated by 170 mm and 120 mm, respectively. Burnt red clay bricks make up the infill wall; the major bricks are 200 mm by 110 mm by 80 mm. The concrete and masonry's material qualities were tested initially as a part of the experiments. The compressive strength of concrete is tested using three 150 mm cubes and three cylinders tested split-tensile procedure. The grade of concrete used was M20 whereas the cement grade was ordinary Portland cement (OPC 43).

4.2.2. Configuration of the Infill Wall

All brickwork used in this study, including the masonry panels and the small-scale material test specimens, were constructed by qualified bricklayers to ensure the best possible quality control. The burnt clay red masonry units were 228 x 114 x 80 mm³ (L x B x H) in dimension and had a nominal specified compressive strength of 10.92 MPa. Figure 4.5 depicts the dimensions of the specimen (total span of 2.26 mm and total height of 1.44 mm) that offers an aspect ratio of 1.56. The aspect ratio is the ratio of the length of the wall to the height of the

wall. The surrounding frame consists of a beam and two columns on the sides. The area between the columns was filled with a brick masonry wall that had a thickness of 114 mm. The entire wall was built of stretcher-bond, half-overlapped brickwork, which is generally adopted in Pilani, a town in Rajasthan, India. The half brick, also known as the half-bat, was made by cutting one end precisely above the middle of the full-length brick.

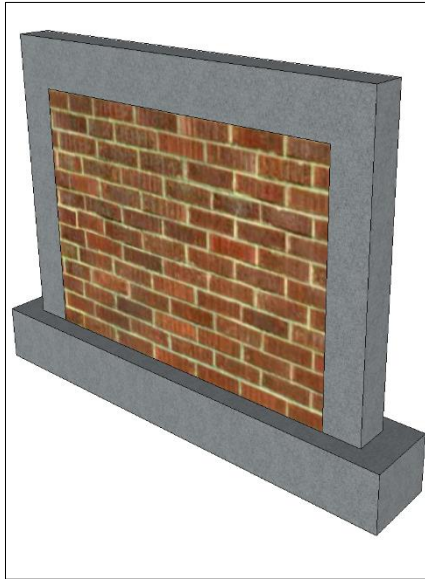


Figure 4.4(a) Front face (F.F.) of the specimen

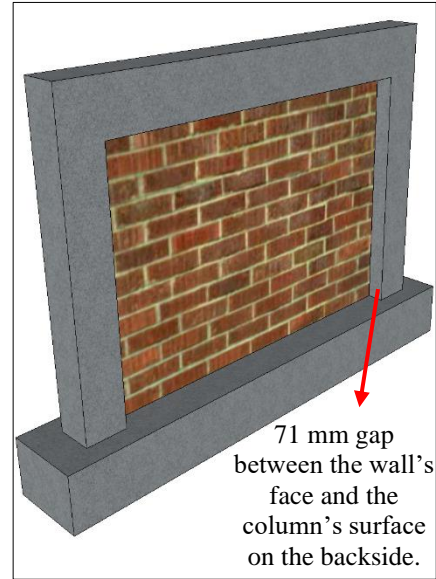


Figure 4.4(b) Back face (B.F.) of the specimen

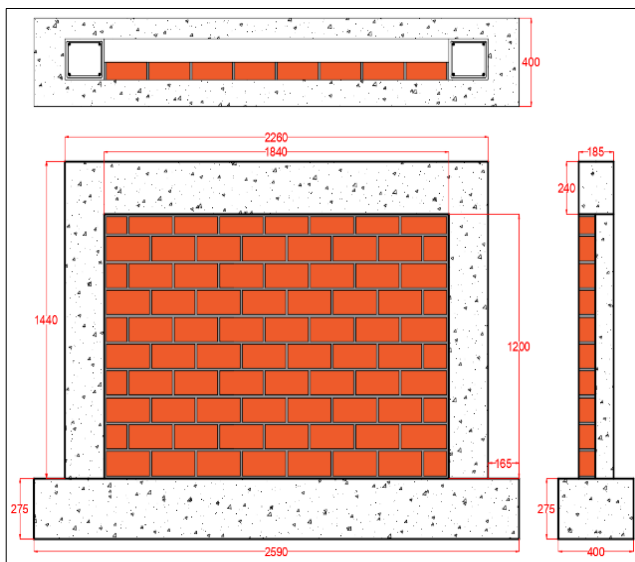


Figure 4.5. Dimension details of the specimen



Figure 4.6. Construction of the test specimen

To create a firm connection between the concrete and bricks, the inside of both of the surrounding frame's columns were pierced and made rough throughout their height using a trowel.

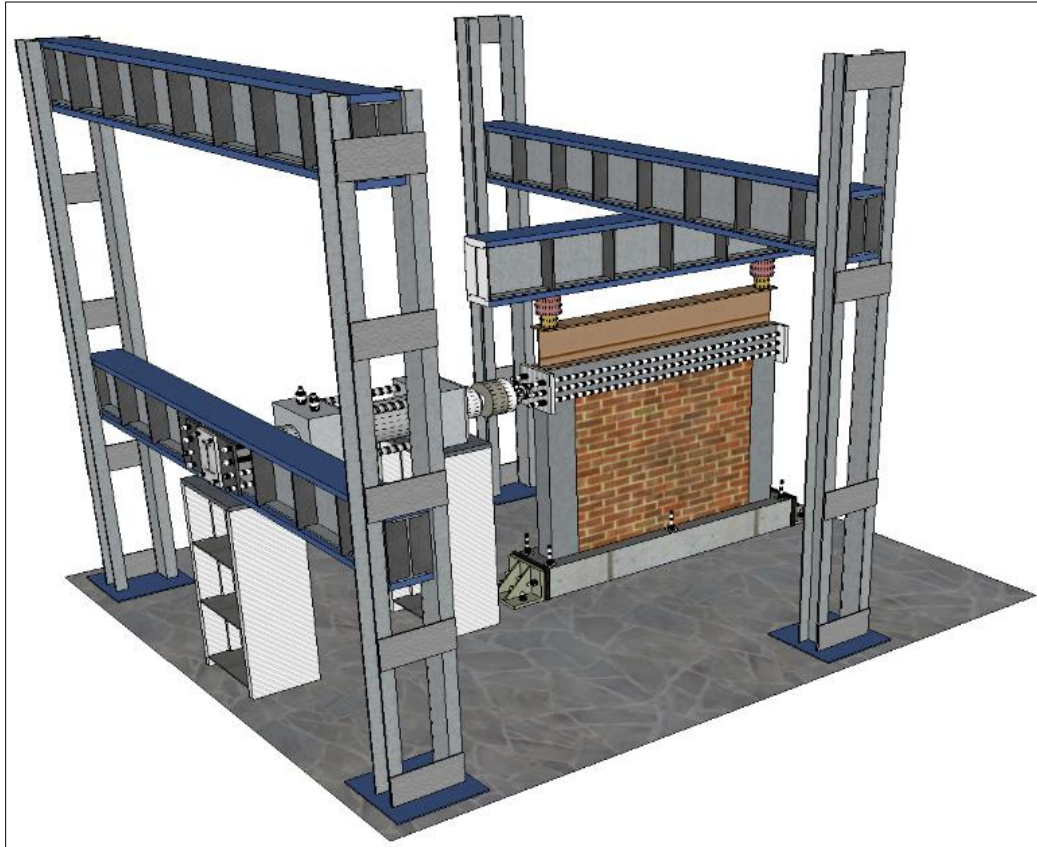


Figure 4.7. Graphical representation of the test setup



Figure 4.8. Test setup in the laboratory

As seen in Figure 4.4(a), the brick wall was positioned so that, on one side (front face (F.F.)), its face aligns with the column's surface and, on the other side (back face (B.F.)), there is a 71 mm gap. Finally, the specimen was wet cured for 21 days with wet burlap fabric, and then exposed to ambient conditions for a further seven days while the curing process continued.

4.3. TEST SETUP AND INSTRUMENTATION

According to Figure 4.7, the experiment setup comprises a reaction frame, displacement restrainers, two vertical jacks, a force transmission mechanism, and a horizontal servo-hydraulic actuator. Two vertical jacks are used to apply a steady axial load of 100 kN (50 kN each) to the frame columns. A low-friction plate system was used in the vertical jack's top portion to enable the jacks to retain the same horizontal displacement as the specimen while being loaded.

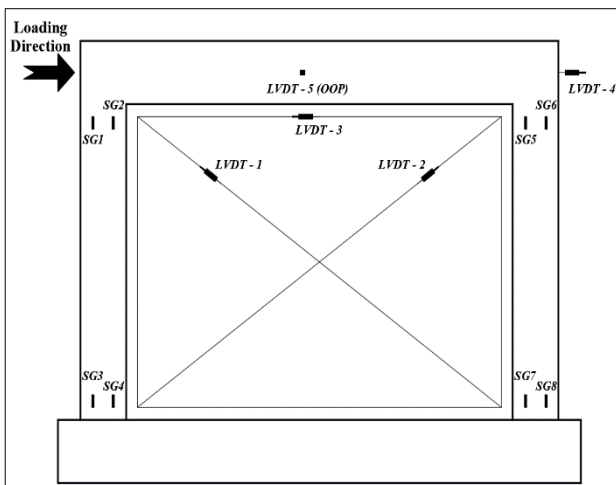


Figure 4.9. Instrumentation details

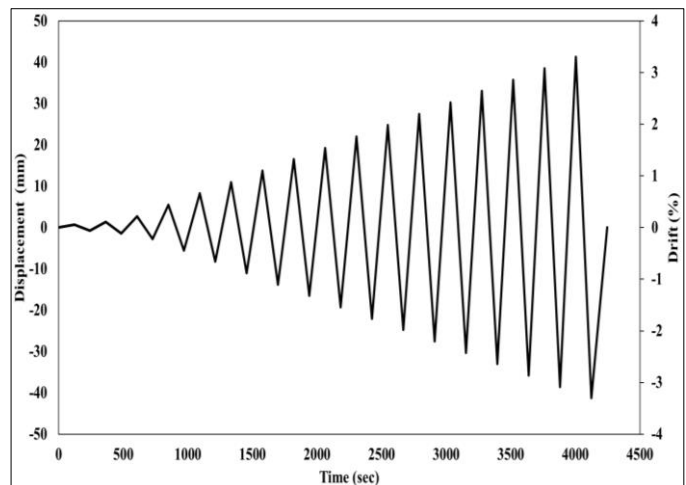


Figure 4.10. Applied loading protocol

On top of the specimen, a force transmission device (load cell) is installed. The horizontal hydraulic servo actuator is coupled to the force transmission device to apply the cyclic displacement load. A preload precedes the test. The frame columns are first subjected to a continuous vertical force and then subjected to a cyclic horizontal displacement with an amplitude of 0.5 mm to determine whether the loading devices are correctly attached, and the acquisition tools are operating as intended. One of the primary techniques used in cyclic loading testing is displacement loading that is used in this investigation. It is often used to examine the seismic performance of various building elements, including infilled frames, shear walls, beams, and columns. The test measures the horizontal displacement of the specimen and the strain on the steel bars. Figure 4.9 shows where the linear variable differential transformer

(LVDT) and strain gauges are situated to measure the displacements and the strains occurring during the test. The two displacement gauges at the top and bottom measure the specimen's horizontal displacement and remove any potential vertical or horizontal displacement of the ground beam during the loading process. The longitudinal bars and hoops at the ends of the beams and columns are where the strain gauges are positioned. In Figure 4.10, the loading protocol according to (ATC 24, 1992) is displayed.

4.4. EXPERIMENTAL RESULTS

The observed force-drift hysteretic data for both tests in Figs. 4.11 (a-b) show that the specimen reacted elastically before breaking when the horizontal loading magnitude was less than 50% of the ultimate load. The hysteretic loops of the specimen were slim and contained diminutive loops. Figure 4.11(b) displays the failure condition of the specimen at the end of testing. There is a very little amount of failure observed in the infill wall compared to the surrounding RC frame. This type of failure is categorized as a frame failure which implies the structural element RC frame is stronger than the non-structural component i.e. infill wall which should not be the actual failure condition. This is because the structural elements are designed to carry the loads whereas the non-structural elements are the ones which can carry only the gravity loads (as discussed in Chapter 1).

4.4.1. Failure Mode

Failure occurred along the wall/frame horizontal interfaces between beam and infill with shearing of the respective steel reinforcement at the loaded beam-column joint for the specimen. When failure occurred along the bottom horizontal interface, failure was also observed at the base of the columns and the adjacent corner of the wall with concrete pullout in the region. Diagonal tension cracks formed at the loaded joints in the specimen, which was first observed at a load 60 kN, whereas further diagonal cracking led to sudden crushing of the joint. Local failure of the columns finally occurred. Some cracking in the infill was observed at the bottom corner joint. The presence of axial compressive force in the columns of the frame would have eliminated the horizontal cracks in the column and might have also delayed the failure at the joints.

Hence, in the following experiments, the reinforcement configuration is modified by implementing the ductile detailing and designing according to IS 13920:2016. Additionally, the thickness of the infill wall is reduced by changing the orientation of the bricks during the

construction itself. It is done by considering the smallest dimension of the brick is selected as the total thickness of the masonry wall unlike in the present specimen in which the smallest dimension of the brick was the height of one bricklayer. Furthermore, the compressive strength of the bricks is reduced by selecting the second-class bricks according to the (IS 1077 : 1992 (Reaffirmed 2002), 2007).



Figure 4.11(a) Diagonal tension cracks at the joint



Figure 4.11(b) Failure at the end of the test

4.5. NUMERICAL WORK

This analysis chooses the same model for the numerical validation research described in the earlier parts concerning the experimental campaign. The validation study is necessary to shorten the experiment's duration, to save money and labour. The 28-day cure period can potentially be eliminated. If the laboratory test is successfully validated, the software's settings may be changed to provide a variety of outcomes by conveniently disregarding the components listed above that are involved in the experimental testing.

4.5.1. Numerical Simulation Approach

Details on the constructed finite element model (FEM), including the model geometry, modelling approach, and validation results, are presented in this part. In this work, the RC frame with brick infills was modelled using the well-known FEM programme ABAQUS. Masonry units and RC frame members were simulated using solid components. Expanded brick units (EBUs) are that have had their dimensions increased by the mortar joint's half thickness in horizontal and vertical directions to connect the separate bricks and allow them to interact with one another. The simplified micro-model, albeit employing larger brick units, offered the

necessary precision and is regarded as a more computing-efficient modelling technique than a detailed micro-modelling approach where mortar joints and the brick units are modelled independently. In the following sections, modeling of each component of the infilled frame is thoroughly discussed. Although ABAQUS provides general material constitutive and interfacial behaviour models for many different structural applications (Documentation, 2010), it should be noted that this study's contribution lies in the selection of appropriate models and critical material parameters, as well as the execution of a precise and successful computational simulation of masonry infills surrounded by RC frame members.

4.5.2. Numerical Simulation

Bricks and concrete were modelled using an 8-noded three-dimensional element with reduced integration (C3D8R). The bending impact of the rebars was not considered in this modelling; hence, the stirrups were modelled as rectangular structures without bending performance. The reinforcement was modelled using B31, a 3-dimensional beam with a linear (first-degree) function. The concrete served as the master surface, while the brick served as the slave surface, with the relationship between them being characterized by a tie constraint. It is important to remember that the bricks were created as a simplified micro model, necessitating separate construction of each. Concrete and rebar interaction was simulated using the embedded area.

Table 4.1. Mechanical properties of all elements

Concrete		Steel	
Young's Modulus	25000 MPa	Young's Modulus	210000 MPa
Poisson's ratio	0.17	Poisson's ratio	0.33
Compression strength	20 MPa	Grade	Fe 500
Infills		Concrete Damage Plasticity (CDP) Properties	
Young's modulus	12500 MPa	Dilation Angle	10
Poisson's ratio	0.15	Eccentricity	0.1
		f_{bo}/f_{co}	1.16
		Stiffness	0.66
		Viscosity Parameter	0.015

In addition, to replicate the strong foundation RC-beam plate used at the bottom of the frame in the experiment, all the nodes at the bases of both columns were restricted using coupling constraints to prevent translation and represented as a fixed connection. The vertical load was applied in the first step and the horizontal cyclic load was applied as the displacement controlled in the second step. To simulate the system's dead load, a force equal to 50 kN axial load was applied to the top of each column which adds up to 100 kN overall. The joints between the beam and column were made stiff to avoid stress concentration. To mimic the experimental loading as closely as possible, the horizontal cyclic loading at each level likewise received the required deformation load. The top beam-column joint level structure is subjected to cyclic loading using lateral forces in the in-plane direction. The loading approach is a displacement-control technique used uniformly on each specimen.

The horizontal in-plane cyclic load was incrementally applied under displacement control in the second step. At the same time, the imposed vertical compression stress was maintained constant, and the vertical and out-of-plane horizontal displacements and rotations about all axes were restrained at the top of the wall to maintain the same boundary conditions as in the experiment. It was assumed in the model that after the mortar joints crack, coulomb friction defined through a friction coefficient of 0.4 controls the interaction between the bricks itself and the brick infill and RC frame.

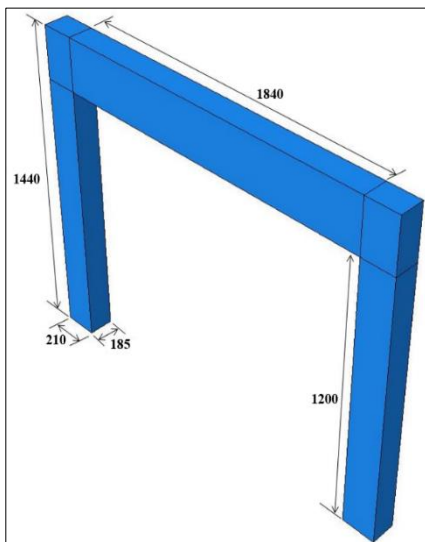


Figure 4.12. Dimensions of RC frame model

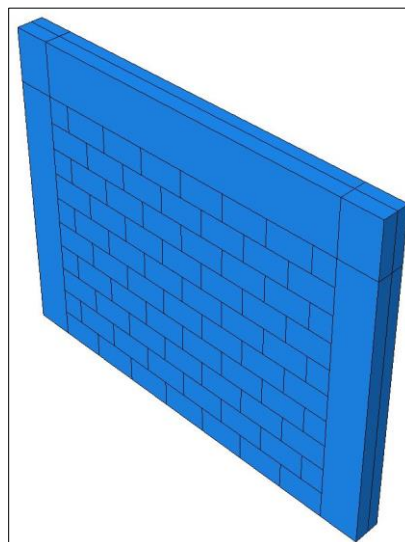


Figure 4.13. Assembly of the full model

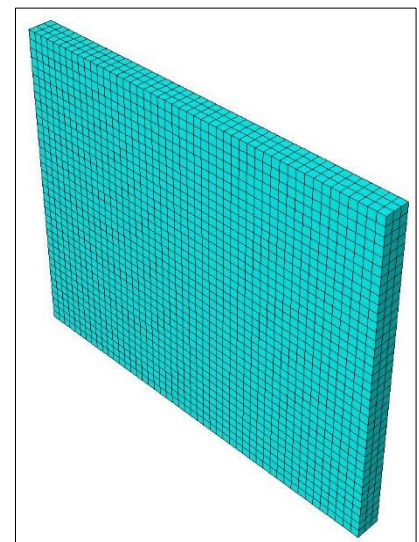


Figure 4.14. Meshing of full model

The accuracy of this interaction is affected by the mesh density, which in turn affects the capture of penetration or slippage between the surfaces required for interaction to take place. The discrepancy can be reduced by using a finer mesh and assuming a much higher contact stiffness or a smaller penetration tolerance value but all at the expense of a significant increase in computing time. Note that the ultimate capacity compares well with the experimental results, and it is deemed that the assumptions used in this study achieved a balance of reasonable accuracy and computing efficiency.

4.6. RESULTS AND DISCUSSION

Results of the experimental campaign on masonry-infilled RC frames are presented towards developing a new retrofitting strategy for newly constructed RC buildings. A reduced scale model of a single bay, single-story RC frame was constructed and tested after being infilled with masonry units. The structure responded to imposed drift demands of up to 0.7% satisfactorily, developing rapidly increasing cracking in the beam-column joints and, most importantly, exhibiting beam-column joint failure and it being separated due to weak bond between the infill wall and the frame and displaying significant amount of deflection at the top end. The phenomenon developed only along one of the frame's right side, causing the non-symmetry observed in the base shear-inter storey drift loops. Shear cracking at the column-beam zone and toe-crushing failure along the other corner of the infill wall was inferior.



Figure 4.15. Failure of specimen - Experimental

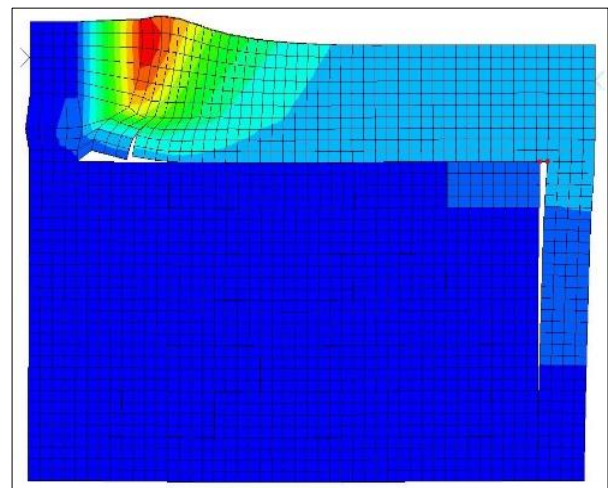


Figure 4.16. Failure of specimen - Numerical

First, the FE predicted damage during the in-plane loading stage is compared with the experimental results as shown in Figure 4.11. It can be seen that the FE model accurately predicted the in-plane cracking pattern of the MIW. Figure 4.15 depicts the specimen's damage

conditions upon failure. Plastic hinges formed at the beam's ends and the column's bottom, and the buckling of longitudinal steel bars at the bottom caused the specimen to collapse. At the ultimate limit condition, the specimens with infill walls also sustained significant damage. Further, it displays close-up images of the plastic hinges on the beam and column. The damage behaviour and failure pattern for the infill wall were comparable. The topmost corner mortar joint near the tie columns was first where horizontal fractures were noticed during the early loading phase. Concrete that had been crushed and spalled was observed at the column's bottom opposite corner. The infill wall is preserved except for the minor horizontal cracks in the highest mortar joint. The loaded beam-column joint was where the longitudinal reinforcement started the failure mode. The column's longitudinal support at that point started to fail and damaged severely.

4.6.1. Strength and Displacement Ductility Ratio

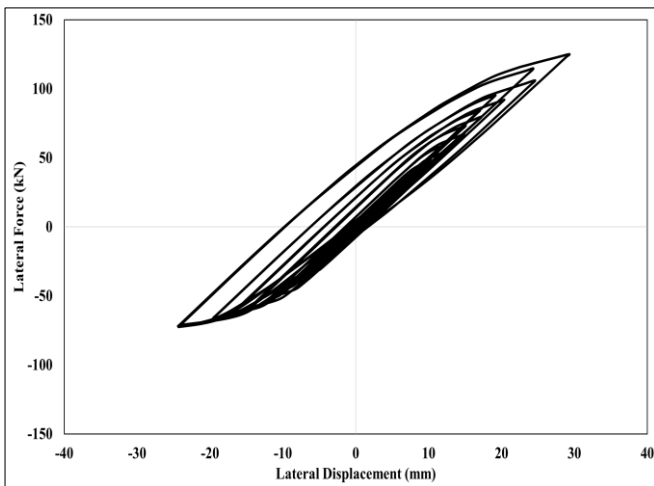


Figure 4.17. Hysteresis curve - Experimental

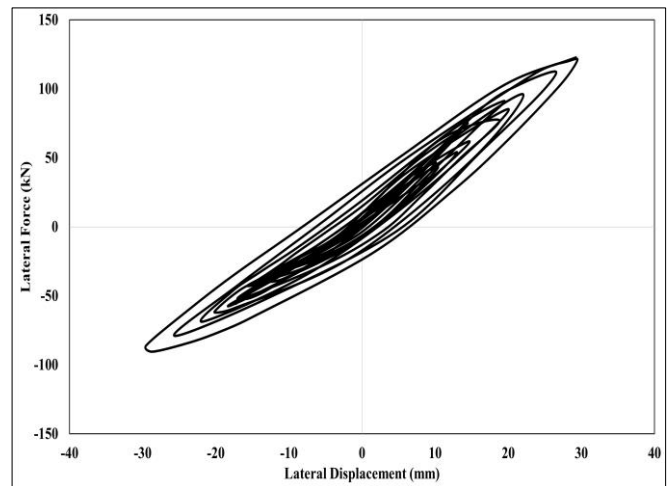


Figure 4.18. Hysteresis curve - Numerical

Figures 4.17 and 4.18 show the specimens' lateral load-displacement hysteretic curves of both the experiment and the validation model, respectively. The initial cracks were noticed during the first cycle in the positive direction of loading, at a top displacement of around 6 mm; only the infill experienced the bottom toe crushing cracks. The loaded beam-column joint had joint failure mode during the pushing direction, with the concrete failure and the reinforcement deformation. The second cycle of stress caused already cracked portions to widen and spread throughout the infill's body, significantly reducing the frame's total lateral rigidity. As the load increased, the frame separated from the wall and deflected, having a significant space between

the two elements. In addition, throughout that cycle, the little shear cracks that had begun at the tops of both columns became wider, notably at the top of the column on the right.

The specimen's post-peak behaviour was asymmetrical. In contrast to negative loading, the descending branch of the hypothetical curve is substantially softer when positive loading is present. According to the post-peak behaviour for the positive direction of loading, the beam column joint gradually failed at the corners due to excessive compressive stresses. The post-peak behaviour, however, for the opposite direction of loading, illustrates the shear failure at the top of the right column at a drift ratio as low as 0.7%. The test was purposefully stopped after the fifth cycle.

Regarding the numerical analysis conducted, the infill wall, the top portion of the masonry system displayed some stress formation, and minor cracks have formed in the wall's bottom corner near the frame, as shown in Figure 4.11. Figure 4.18 shows the corresponding numerical hysteresis curve obtained in the ABAQUS for infill wall. The load recorded on the compression (push) direction is comparatively more than the tension (pull) direction. This is because the specimen deflected more in the push direction whereas in the pull direction, both the deflection and the load are lesser. The maximum load-carrying capacity and the maximum deformation values are almost congruent.

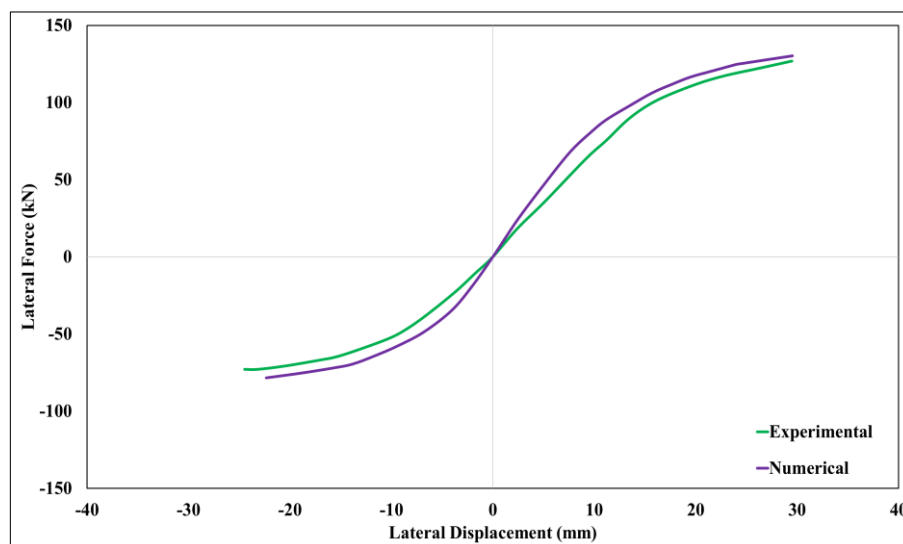


Figure 4.19. Envelope curve

However, regarding the importance of the maximum lateral displacement, the numerical analysis values are always more significant than those obtained in the experimental results. Figure 4.19 shows the maximum envelope curves of both experimental and numerical

results. Compared to the experimental results, Abaqus generally over-predicts the specimens' maximum lateral displacement and loading bearing capacity by a full range of 5%. Overall, Abaqus simulated results are in good comparison with experimental ones. For both loading directions, the maximum force and corresponding displacements are shown in Table 4.2.

Table 4.2. Experimental and numerical results

Specimen	Results	u (mm)		P (kN)		Mode of Failure
	Δ (%)	Push (+ve)	Pull (-ve)	Push (+ve)	Pull (-ve)	
Experimental Analysis	2.23	29.49	-24.45	126.86	-72.85	Frame-infill separation, joint cracking
Numerical Analysis	2.24	29.53	-28.53	130.27	-78.38	Frame-infill separation, joint cracking

Where P = maximum lateral load, u = maximum lateral displacement, Δ = maximum drift (%)

4.7. SUMMARY

The obtained results have prompted us to divide the experimental work into two chapters, as the observed failure pattern of the specimen should not be the governing mode of failure. The two prerequisites for converting masonry infills to a load bearing (structural) element are: (i) enhancing the strength and deformation capacity of the masonry infill walls themselves, and (ii) eliminating any adverse local effects in the frame members that might cause their premature failure. Textile reinforced mortar (TRM), which increases the panel's shear strength and deformation capacity, is better to achieve the first goal. RC frames must be strengthened against shear failure brought on by insufficient transverse reinforcement to prevent early loss of the RC frame components (the strategy's second criterion). Moreover, as the degree of "monolithic" of the infill-frame interface influences the objective of changing the role of the infilling towards that of an essential structural element, extra attention is required to the methods of attaining such connection. Therefore, the bonding between the masonry wall and the surrounding RC frame should be resilient. The presence of an opening in an infill wall modifies the behaviour of the whole structure under lateral loads that should be given importance.

Based on the observations from this Chapter, improvisations were made to the specimen in the following Chapter (Chapter 5) considering the ductile reinforcement of the RC frame, reduction of the compressive strength of the brick, thickness of the infill wall is decreased for the overall behaviour of the masonry structure under lateral loading conditions. Regarding the strengthening of the infills in the focus of the following experimental campaign, the correct installation of the TRM and distinctive anchoring features are also taken into consideration.

CHAPTER 5

EXPERIMENTAL INVESTIGATION OF DUCTILE REINFORCED CONCRETE (RC) FRAMES WITH MASONRY INFILL WALL (MIW) WITH OPENING

5.1. INTRODUCTION

This chapter illustrates the experimental study in which a set of two 2/5th scale ductile reinforced concrete (RC) frames with masonry infill wall (MIW) with opening were subjected to quasi-static reversed cyclic lateral loading that was controlled by sinusoidal displacement. The specimen was rigidly anchored to the ground at the foundation level and was provided customized out-of-plane resistance. Parameters considered for the test included the presence of a door opening in the wall, the number of textile reinforced mortar (TRM) layers, and the location of application of the fiber on the specimen. The wall panel configurations are described in greater detail in the following sections.

5.1.1. Objectives

The objectives of this framework are

- a. To record the cyclic load-displacement (P- Δ) behaviour of the walls, for:
- b. To study the wall cracking patterns, measure their deformation profiles, and assess the accuracy of idealized failure mechanisms used in the various numerical methods.
- c. To contribute to the available pool of experimental data of reduced scale MIW with openings and strengthening using TRM, which is surprisingly lacking in the available literature.

The test study undertaken is believed to provide a significant contribution to the existing pool of experimental work, by filling several research gaps identified through a review of literature (specified in Chapter 2). In addition, from the observations in the previous Chapter (Chapter 4), the ductility of the RC frame is implemented; thickness of the wall and the compressive strength of the brick is reduced. Among the unique aspects of this study are the opening in the wall along with the fibers as a strengthening material and also the location and number of TRM layers on the MIW. In this study, vertical edges of the MIW system were not

restrained against translation or rotation and therefore were considered as a vertical cantilever. By contrast, the bottom of the specimen i.e. the foundation beam was made rigid and anchored to the ground to avoid any translation and rotation that is commonly implemented in the experimental procedure conducted in laboratories. Another significant aspect of the tests was subjecting the test specimens to pre-compression, in order to simulate loads that are transferred from the top stories. In addition, both the primary parameters considered in this study contained a door opening in the wall, and furthermore, as most of the experimental studies encountered in literature focused on the opening and strengthening of MIW using TRM separately, this study combined these both factors centrally positioned opening with two layers of glass fiber TRM layers on either surface of the wall.

The outline of this chapter is as follows: Section 5.2 elaborates the test program and methodology including the material properties, wall configurations. The strengthening material TRM is introduced in the Section 5.3 and its configuration, application procedure is discussed in the Sections 5.4. The test setup and loading regime are explained in Sections 5.5 and 5.6, respectively. Results of the experimental study are then presented in terms of the specimen's load-displacement behaviour, the observed damage and crack patterns, and a study of the stiffness degradation and energy dissipation profiles is presented in Section 5.7. The chapter concludes by summarizing the key observations and lessons derived from the experimental program. Section 5.8 summarizes the key observations from this Chapter.

Supporting appendices are also provided about the work at the end of the thesis. Appendix A reports details of the design of the loading frame to mount the actuator in the laboratory to carry out the experimental test.

5.2. TEST PROGRAM AND METHODOLOGY

5.2.1. Materials

All brickwork used in this study, including the masonry panels and the small-scale material test specimens, were constructed by qualified bricklayers under controlled laboratory conditions at an ambient temperature between 30°C - 35°C to ensure the best possible quality control. The burnt clay red masonry units were 230 x 110 x 78 mm³ (L x B x H) in dimension and had a nominal specified compressive strength of 6.83 MPa. To minimize variability in the material properties, all masonry was constructed using brick units originating from the same

batch at manufacture. The compressive strength of three brick units that were randomly selected from the batch was examined.

In both the bed and head joints, mortar layer was maintained at a standard thickness of 12 mm using 1:3 mortar (Portland cement and sand). Each batch of masonry mortar produced three identical 50 mm³ cubes, which were then tested for compression strength. The clay content of the sand was determined to be 8.2%. Quality control measures were undertaken during the mixing of the mortar to ensure consistency. This included bucket batching of the ingredients and ensuring that all sand was air-dried before mixing. Water was added to the mix of cement and sand inside the mortar mixer to provide the desired workability based on the bricklayers' experience. All water additions were recorded. The average volumetric water content of the mortar was 19.9%, with a coefficient of variation (CoV) of 0.13. Tests on small masonry specimens were conducted following the guidelines given in the (ASTM, 2009), to determine values of key material properties for use in subsequent numerical studies. Similarly, each batch of provided concrete mixture was used to create a set of three identical concrete cubes (150 x 150 x 150 mm³) and cylinders, each measuring 150 mm in diameter and 300 mm in height. Following 28 days, the compression strength of each concrete cube and cylinder was evaluated.

Table 5.1. Experimentally determined material properties of steel rebars

Diameter	Yield Stress (MPa)	Tensile Strength (MPa)	Ultimate strain (%)
8 mm	468.32	565.77	9.0
10 mm	510.36	623	9.33
12 mm	510.42	598.36	10.83
16 mm	551	653	23

Tensile strength tests were done on the steel bars utilized and the values are given in Table 5.1. The 8 mm diameter deformed longitudinal bars had yield stress, tensile strength, and ultimate strain values of 468.32 MPa, 565.77 MPa, and 9.0%, respectively. The comparable results for the 10-mm diameter deformed bars were 510.364 MPa, 623 MPa, and 8.33% (three specimens' average values). For the 12 mm diameter deformed bars, the equivalent findings (average values from three specimens) were 10.83%, 598.36 MPa, and 510.42 MPa. The

equivalent results (average values from three specimens) were 551 MPa, 653 MPa, and 23% for the 16-mm diameter deformed bars.

5.2.2. Test Specimen Preparation

Two 1:2.5 scale, one-story one-bay RC portal moment resisting frames were utilized as a prototype building to replicate the characteristics seen in the ground floor walls of typical existing two-story Indian houses. One specimen served as a conventional specimen (denoted as URS, hereafter), and the other had an AR-resistant glass fiber TRM grid retrofitted into the wall (denoted as DRS, hereafter). Test frames were assigned the URS and DRS codes, where UR denotes an unretrofitted infill wall, S represents a specimen, and DR suggests an infill wall with TRM reinforcement applied to both sides.

5.2.3. Frame Configurations

The surrounding RC frame was constructed with M20 grade concrete and Fe500D grade steel bars implementing the ductile detailing and design according to the (BUREAU OF INDIAN STANDARD, 2016). As a prototype construction, a typical moment-resisting single-bay reinforced concrete portal frame was used to mimic the features present in current MIW structures. Figure 5.4(a) depicts the geometry of the tested frames. The distance between the peripheral faces of the columns was 2260 mm, while the overall story height was 1440 mm. Customized moulds were prepared before initiating the construction of the beam, columns, and foundation beam.

The reinforcement details adopted for the construction of the test specimen are shown in Figure 5.1. The columns had a 185 x 210 mm rectangular cross-section (Figure 5.2(b)), with the longer side parallel to the length of the wall specimen. In contrast, the beam had a width that was 185 mm and a depth of 240 mm (Figure 5.2(a)). The beam and column cross-sections are shown in Figs. 5.2(a) and 5.2(b), respectively. The beam is designed as a doubly reinforced section, with a total of 3 bars with a 12 mm diameter in the bottom portion of the beam. The compression zone comprises 2 bars of 12 mm diameter provided at the top with a clear cover of 10 mm on all sides. Two-legged stirrups with 8 mm diameter bars and a 50 mm center-to-center spacing are offered to withstand shear. 450 mm of the beam's top reinforcement bars are embedded into columns on both sides, and 172 mm of the bottom reinforcement bars are bent upward in the beam-column connection to provide development length.

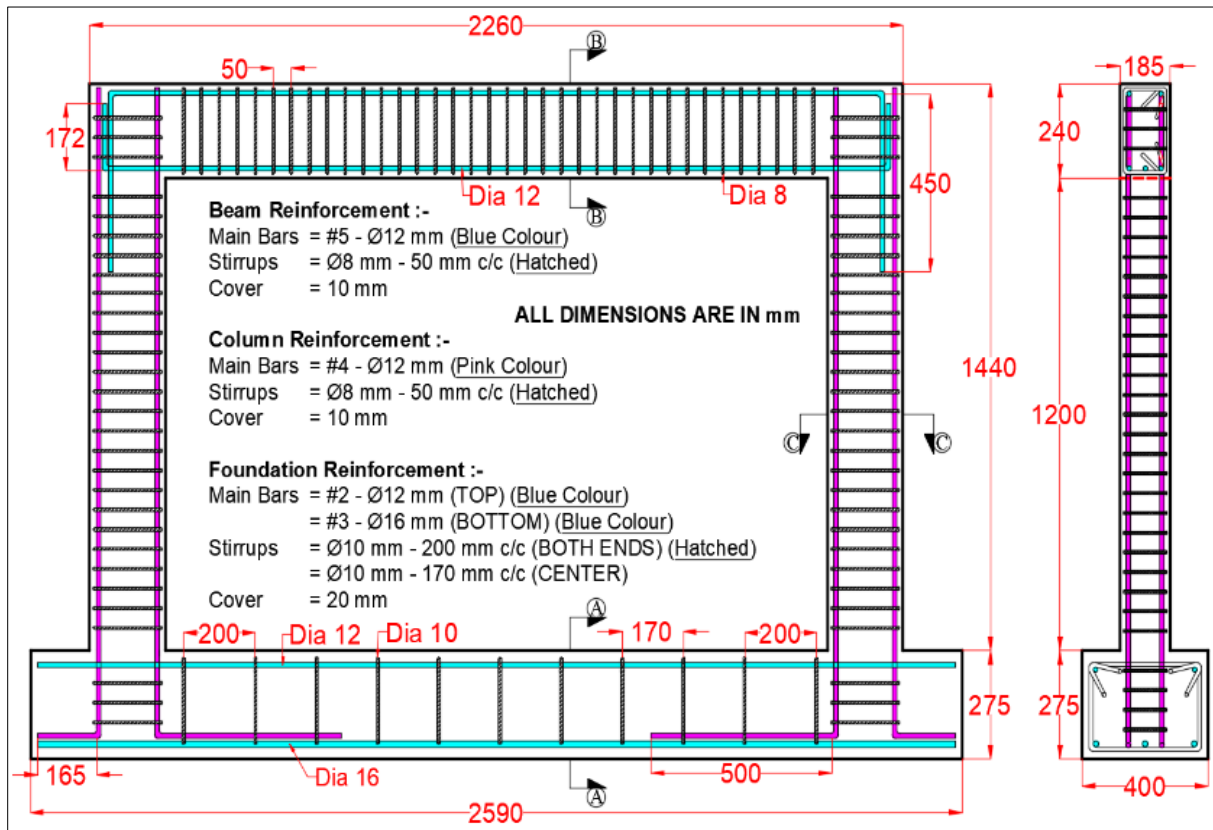


Figure 5.1. Reinforcement details (all dimensions in mm)

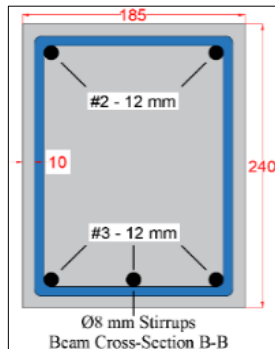


Figure 5.2(a) Beam cross-section

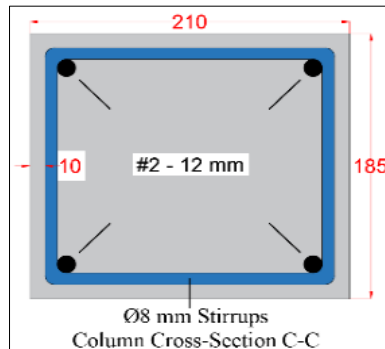


Figure 5.2(b) Column cross-section

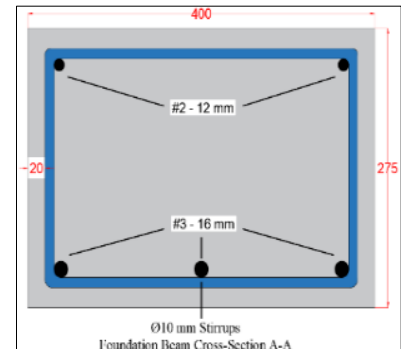


Figure 5.2(c) Foundation cross-section

There is a 1200 mm clear spacing between the columns. Two-legged stirrups with 8 mm diameter bars spaced 50 mm from center-to-center are linked to four bars with a 12 mm diameter reinforcement and a 10 mm clear cover on either side of the column. To meet the requirements for development length, the column's inner face reinforcement and peripheral face reinforcement are each inserted into the foundation to a depth of 500 mm and 165 mm on the inner and outer sides, respectively. The foundation plinth beam has two bars of 12 mm diameter in the compression zone and three bars of 16 mm diameter in the tension zone, with

a 20 mm clear cover on both sides. It is intended as a doubly reinforced section and purposefully made robust. Stirrups with a diameter of 10 mm and center spacings of 200 mm on both ends and 170 mm in the midspan are tied around the bars. To avoid damage, the 275 x 400 mm² foundation beam was purposely over-reinforced (Figure 5.2(c)).

5.2.4. Brick Panel Configurations and Construction

The walls had dimensions of 1840 x 1200 mm (L x H) with an aspect ratio (wall length/wall height) of 1.56 and each contained a centrally positioned door opening with a dimension of 460 x 840 mm. The thickness of the wall was 78 mm. A lintel beam (700 x 115 x 78 mm) was placed exactly above the opening in the wall to replicate the practical scenario whose thickness was maintained equal to the wall's thickness. All walls were constructed entirely using half-overlap stretcher-bonded masonry. Brick masonry walls were built up against side columns to fill both test frames.

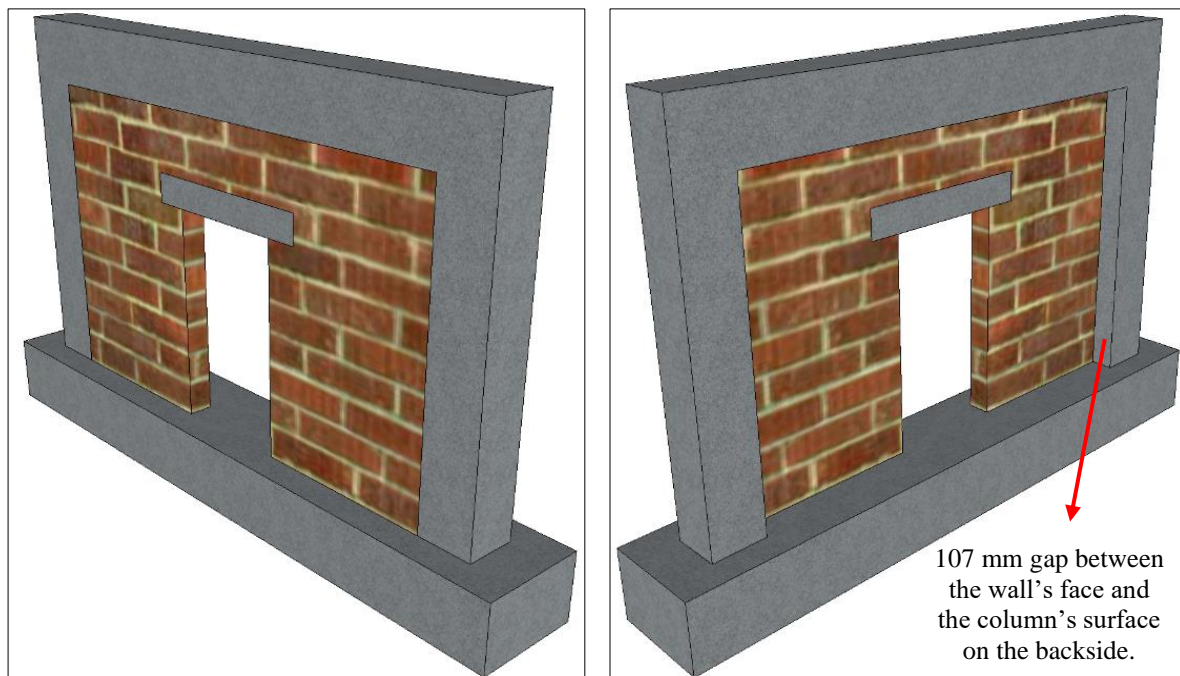


Figure 5.3(a) Front face (F.F.) of the test specimen

Figure 5.3(b) Back face (B.F.) of the test specimen

The minor gaps between the masonry infill and the beam were filled with the same masonry mortar after the infill construction. There were 13 brick layers total along the height of the wall, while there were 7.5 brick layers along the length of the wall. The half brick was prepared in such a way that it was cut exactly at the midspan and one of its ends was placed

exactly above the midpoint of the full-length brick. The inner portion of both the columns present in the surrounding frame was pricked and made rough with the trowel throughout the height to provide a grip between the concrete and the bricks. The brick wall was placed in such a way that the face of the wall is in alignment with the surface of the column on one side (front face (F.F.)), as shown in Figure 5.3(a), while a gap of 107 mm occurs on the other side of the specimen (back face (B.F.)) as shown in Figure 5.3(b). The final test frames were exposed to ambient conditions for a further seven days after being wet cured for seven days using wet burlap cloth. The built-in masonry infills were subjected to curing for 21 days using a wet burlap cloth and the curing continued for another 7 days without any cloth.

5.3. APPLICATION OF TRM SYSTEM ON THE MASONRY WALL

The terms ‘fiber reinforced cementitious matrix (FRCM) or textile reinforced mortar (TRM)’ refer to textile-based composite materials that are composed of cementitious mortar and fabric meshes. Textile-reinforced composites are used in several industries, including aerospace, construction, automotive, medical, and sports, because of their unique advantages over traditional materials like metals and composites. Fiber-reinforced composite materials are light, stiff, and robust. They have strong impact and fatigue resistance (Drahansky et al., 2016). Fibre Reinforced Polymers (FRP), a conventional reinforcing material, did not fare well in alkaline conditions, high temperatures, or fire loads. Organic epoxy resins were used to attach it to a substrate. These shortcomings of FRP have been removed with the introduction of FRCM composites which are comprised of open-mesh, high-strength textiles (such as carbon, glass, or basalt) blended with cement- or lime-based inorganic mortars to create composite materials that have several benefits over fiber-reinforced polymers (FRP) systems, such as tolerance to high temperatures (Tetta & Bournas, 2016), (Raof & Bournas, 2017), a reduction in costs, suitability for use on saturated or wet surfaces, and compatibility with masonry or concrete substrates. Other strengthening methods that were popular earlier have disadvantages, such as the requirement of sophisticated methods for proper fixation with existing frames and corrosion, which can occur in the steel bracing method and welded wire mesh (WWM) techniques, respectively, which are made up of steel (Ratnesh Kumar, Yigendra Siingh, 2009). The structural repointing procedure includes limitations such as being time-consuming (Jeffs, n.d.). Considering all these limitations, TRM proved to be promising with its advantages and also by overcoming the limitations of the strengthening techniques as discussed. The most recent cutting-edge research indicates that TRM is useful for fortifying masonry and concrete constructions.

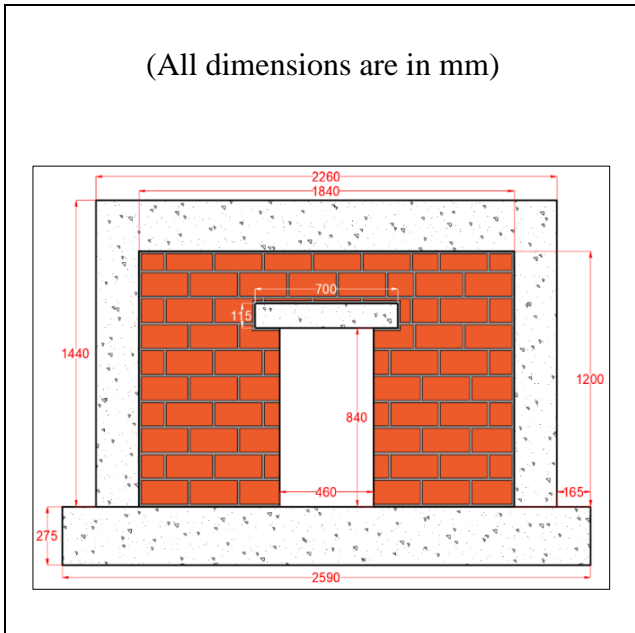


Figure 5.4(a) Schematic geometry of the MIW

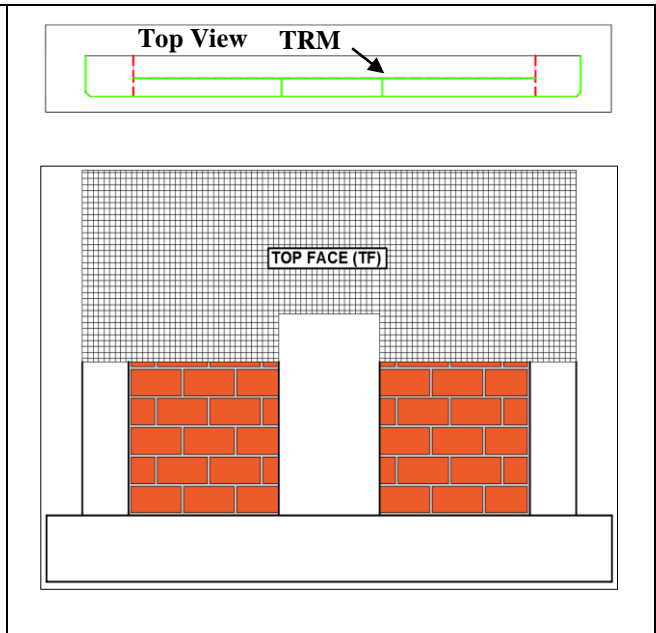


Figure 5.4(b) Application of TRM on the TF

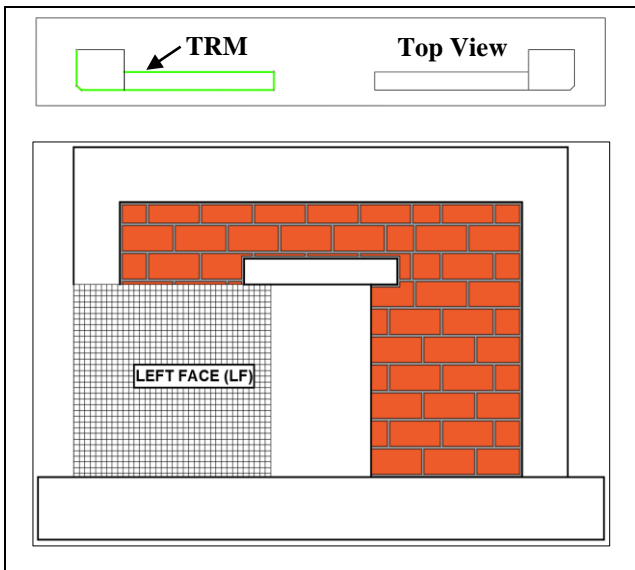


Figure 5.4(c) Application of TRM on the LF

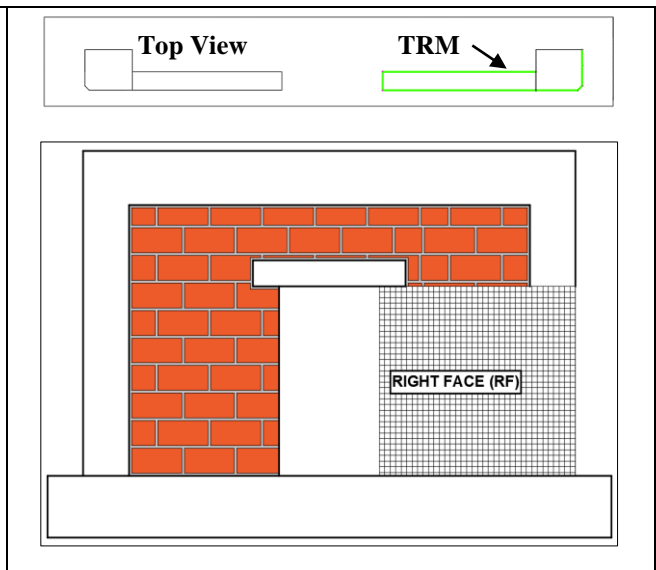


Figure 5.4(d) Application of TRM on the RF

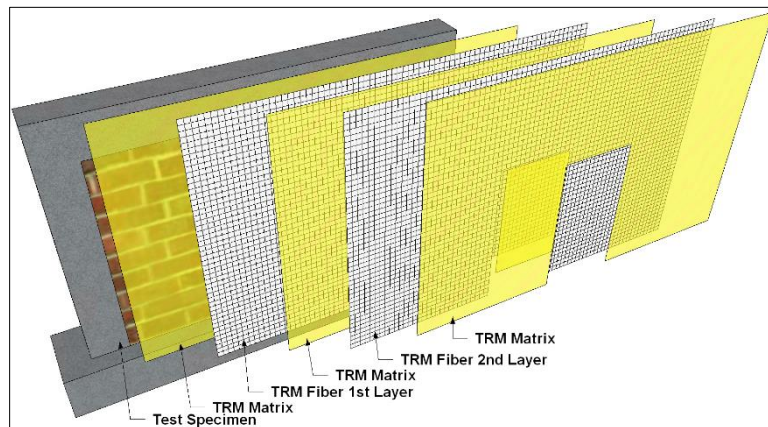


Figure 5.5. Graphical example of full-surface application of TRM in the experimental procedure

Five FRCM-enhanced RC frames with hollow-brick wall infill were investigated for their in-plane behaviour (F. Wang, 2023) to look at the improvement in earthquake resistance under cyclic loading. Ultimately, it was demonstrated that the mechanical and seismic performance of RC frames filled with masonry could be significantly improved by using this innovative integrated technique. (L. Koutas et al., 2014) concluded that the ultimate flexural or shear capacity, stiffness, and performance of concrete members could be increased by strengthening those with TRM.

Two crucial components of the TRM system are a moist fabric with a fiber-strand grid pattern and an inorganic cementitious matrix in which the fiber is applied to the substrate in layers of matrix and fabric reinforcement that are present in alternate layers, as seen in Figures 5.4 (b)-(d) and Figure 5.5. The green line indicates the TRM layer applied on the masonry wall's surface shown in every top view of the experimental setup. Figure 5.4(a) displays the elevation of the specimen along with the dimensions.

Figure 5.4(b) shows the application of the 1st layer of the fiber (green line colour) on the wall's top surface, i.e. above the opening (spandrel region). Figures 5.4(c) and 5.4(d) indicate the 2nd and 3rd layer of the fiber on the wall's left and right surface, respectively, i.e. to the left side of the opening and right side of the opening (pier region adjacent to the opening). Grids for FRCM applications are often constructed using carbon fibers, individually treated basalt fibers, and glass fibers that are resistant to alkalis. The application of TRM in concrete and masonry projects has been documented on several occasions (L. N. Koutas et al., 2019). These fabrics are warp-knitted fabrics, which are manufactured for applications in civil engineering, which have the inlay yarns are spread throughout the textile in two orthogonal directions, which are 0° straight yarns in the longitudinal direction and 90° straight yarns in the transverse direction. The inlay yarns are sometimes placed diagonally and are also consecutive yarns oriented at a 45° angle in the warp-knitted fabric (Gries et al., 2016).

5.4. STRENGTHENING OF SPECIMENS

5.4.1. Application of Fiber to the Specimen

Once the wall specimen is cured for 28 days, the application procedure of the textile fiber is initiated. The specimen surface was physically cleaned with a wire brush to remove any dust and mortar protrusions before the application of the TRM laminates. During this preparation, special care was paid to cleaning the joints and clearing the wall surface of excess

mortar and loose particles. The wall surface was then made wet by spraying a mild amount of water to ensure the matrix got in good bondage with the wall. First, polymer-modified cement-based mortar is taken into a container and made into a slurry with a predefined water-cement ratio. Before application on the walls, the dry fabrics were cut to length (according to specimen dimensions). The so-formed mixture was then applied to the cleaned and wet surface of the specimen, and immediately the pre-cut textile fiber was applied to the mortar layer on the surface of the masonry system. Before the application of the second TRM layer, another thin coat of the prepared matrix was applied between the first and the second layers to about 5 – 7 mm, leaving the system to dry until the initial setting time of the fiber layer. The second TRM layer was then placed on top of the first, and one more cementitious matrix was applied to achieve a finished aesthetic look of the wall. The roller was driven continuously on the wet textiles many times to reduce trapped air gaps. To guarantee that the TRM laminates had had time to cure, all reinforced specimens were held for a minimum of five days prior to testing, and all infilled frames were tested around 28 days following the completion of their corresponding walls.

5.4.2. Strengthening Procedure

The test specimens underwent TRM strengthening after a 28-day curing period for the infill masonry. The test panel surface was brought to a saturated surface dry state by intermittently spraying water after both faces of the test frames were cleaned to eliminate dust and wabby brickwork particles (see Figure 5.6a). The fabric reinforcement was bonded using a two-component (liquid and powder) pozzolanic reaction-based matrix that contained synthetic polymers, fine-grained aggregates, and unique admixtures. To create a homogenous matrix, paste, the dry component was put in a pan (see Figure 5.6c). Next, the paste was added gradually to the container while being stirred carefully. The test frame's surface was covered with a homogeneous matrix layer that was between 5 and 7 mm thick using a flat metal trowel (see Figure 5.6d). After being properly sized (refer to Figure 5.6b), the reinforcing fabric was gently pressed into the wet matrix layer that had been previously positioned. Before applying the second finishing layer of 5 – 7 mm thick matrix, the surface was trowel polished to obtain consistent thickness (see Figure 5.6e). The prepared TRM layer was kept between 10 and 14 mm thick overall. A 200 mm overlap splicing was used. The reinforced test frames (see Figure 5.6f) were allowed to cure under ambient conditions for 28 days before testing.



Figure 5.6(a) Preparing the surface of the specimen



Figure 5.6(b) Cutting of fiber



Figure 5.6(c) Mixing of plaster



Figure 5.6(d) Applying the plaster 1st layer



Figure 5.6(e) Placing the 1st layer of TRM fiber



Figure 5.6(f) Specimen after placing two layers of the TRM

The final test frames were covered with damp burlap cloth and allowed to cure for seven days before being left outside for a further seven days. The tiny gaps between the masonry infill and the beam were filled with the same masonry mortar after the infill was constructed. The built-in masonry infills were dried for seven days using a damp burlap cloth and then allowed to cure naturally for a further twenty-one days.

5.5. TEST SETUP AND INSTRUMENTATION

The ends of the foundation beam were fastened to the robust floor with the aid of high strength; 24 mm diameter threaded steel rods. Two specifically made steel safety frames were installed perpendicular to the loading direction to provide test frames with out-of-plane restraint. Two customized heavy-duty steel rollers (placed between the beam and the beam top) and a robust steel runner beam with stiffeners gave each column an axial force of 100 kN. A load cell and a hydraulic jack were used throughout the experiment to apply a constant vertical load.

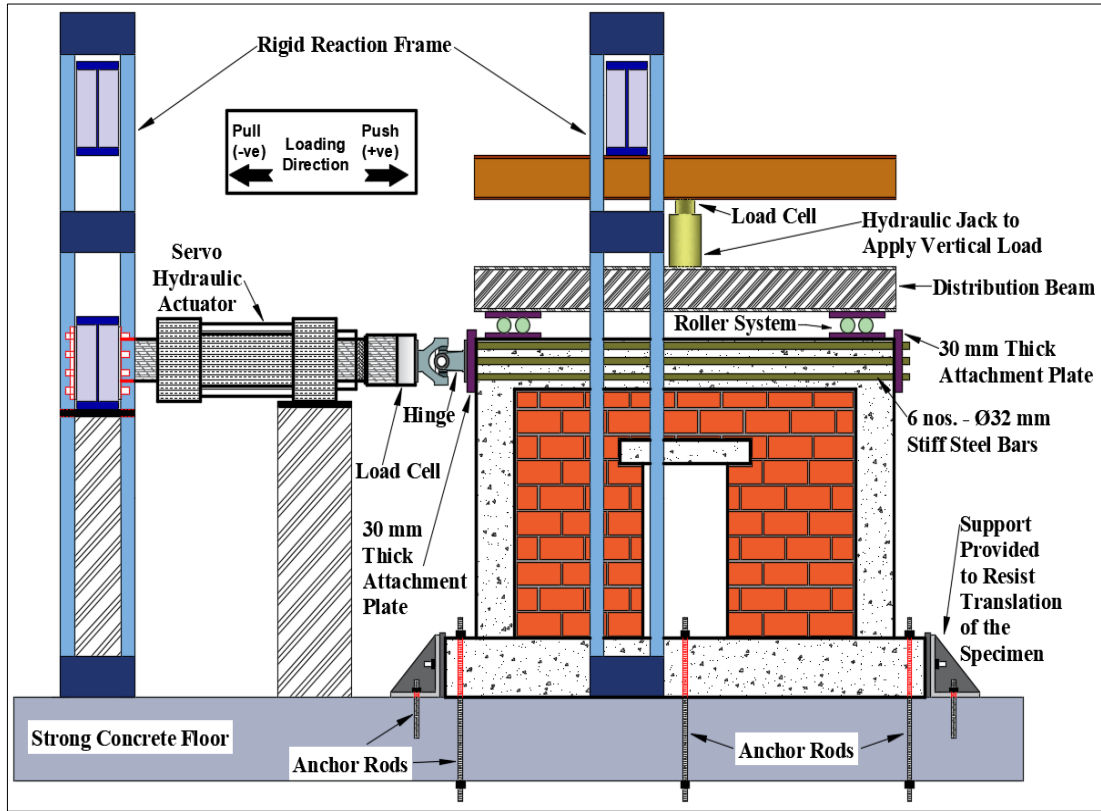


Figure 5.7. Test setup details

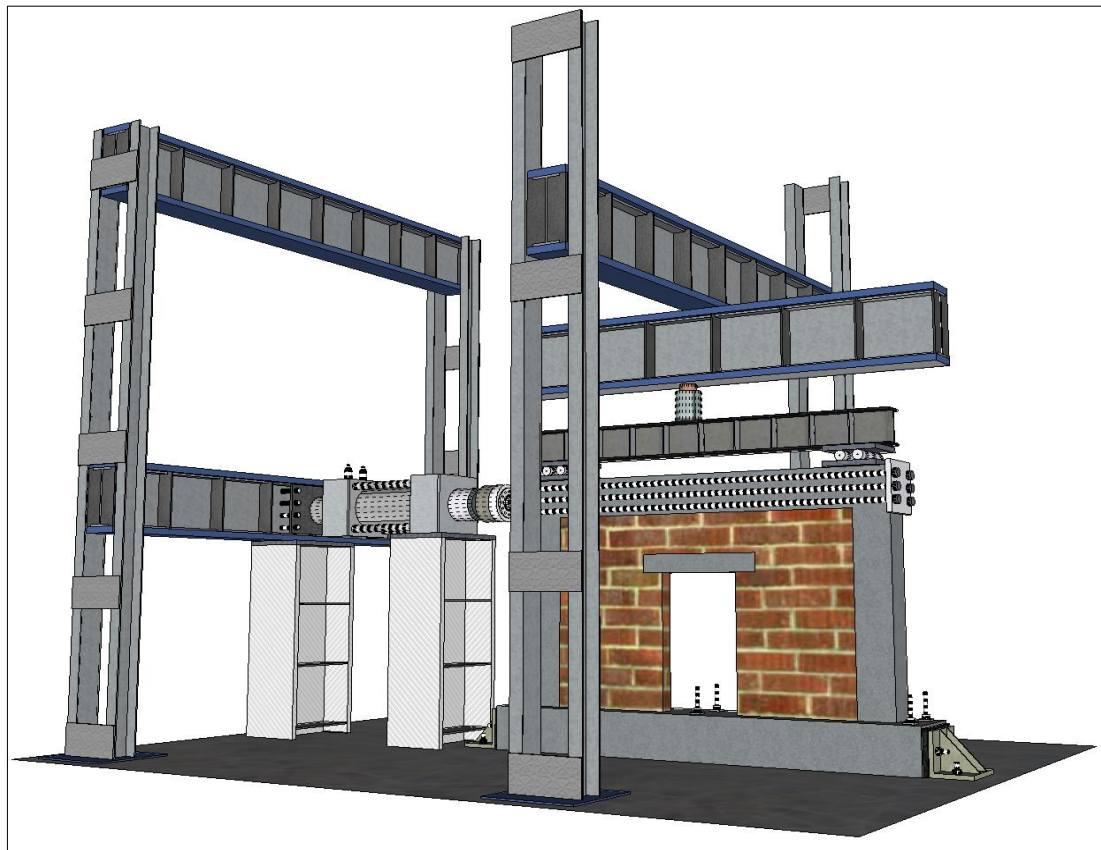


Figure 5.8. Isometric view of the test setup

Lateral loading was provided by a 250 kN servo-hydraulic actuator mounted horizontally on a 1000 kN strong steel reaction frame. The experimental setup is shown in Figure 5.7, which displays the loading directions [compression = push (+ve) & tension = pull (-ve)], applied by the servo-hydraulic actuator of 200 kN capacity to the masonry specimen.

The vertical (pre-compression) load of 100 kN was applied to the masonry system using a hydraulic jack; specially designed structures suitably supported the system. The jack was positioned on top of a steel beam, which transfers the load to the masonry system—precisely placed above both columns through the roller support system. The actuator load is applied to the specimen using an attachment system consisting of two 30 mm attachment plates on either side of the beam attached with six 32 mm diameter threaded bars secured with nuts. A biaxial hinge system connects the attachment system to the actuator load cell. Customized plate supports are attached to both sides of the whole testing unit to prevent horizontal translation when applying cyclic loading.

The actuator's integrated load cell recorded the applied lateral force, and the resulting lateral displacement was measured by a linear variable differential transformer (LVDT) connected to the top end of the test frame. The diagonal placement of the second and third LVDTs allowed for the measurement of the wall's diagonal tension and compression, respectively. Fourth LVDT was positioned near the opening in order to gauge its deflection. Every LVDT was calibrated and linked to the data acquisition system using the appropriate connection system. The isometric view of the test setup is shown in Figure 5.8, and the instrumentation configuration utilized to test both test frames is shown in Figure 5.9. Tensile strain in longitudinal steel bars was measured at potential hinge points using eight numbers of 5 mm long steel strain gauges. The notation SG-X for strain gauges represents the steel strain gauge (SG) and the gauge number (X). Eight strain gauges were installed on the column's primary reinforcement, four of which were positioned just below the beam and the other four directly above the foundation beam.

The vertical load was applied to the masonry system using a hydraulic jack; specially designed structures suitably supported the system. The jack was positioned on top of a steel beam, which transfers the load to the masonry system—precisely placed above both columns through the roller support system. The actuator load is applied to the specimen using an attachment system consisting of two 30 mm attachment plates on either side of the beam attached with six 32 mm diameter threaded bars secured with nuts. A biaxial hinge system

connects the attachment system to the actuator load cell. Customized plate supports are attached to both sides of the whole testing unit to prevent horizontal translation when applying cyclic loading.

5.6. LOADING REGIME

A range of loading techniques, including those in (Comartin & Rojahn, 1996; Security & Agency, 2005; STANDARD, 2003), have been used by researchers to evaluate the behaviour of the infilled RC frame. The loading pattern created by ATC 24 (ATC 24, 1992) is one of the most often used loading strategies for seismic testing of large structural systems in this study. The load was applied to each specimen at a rate of 0.1 mm/s in a quasi-static loading pattern of regulated displacements. The loading sequence comprised cycles in both the push and pull directions with progressively greater displacement amplitudes. For each amplitude level, a single loading cycle was used, and there was a 1 mm rise in displacement amplitude. The whole test procedure was computerized and ended manually by pushing the piston back to zero when the wall's maximum capacity was achieved. A significant load drop was seen in either direction (push or pull). A total of twelve drift levels were applied to the test specimen; each level was repeated only once. The lateral displacement-controlled loading that was put on the frame is shown in Figure 5.10.

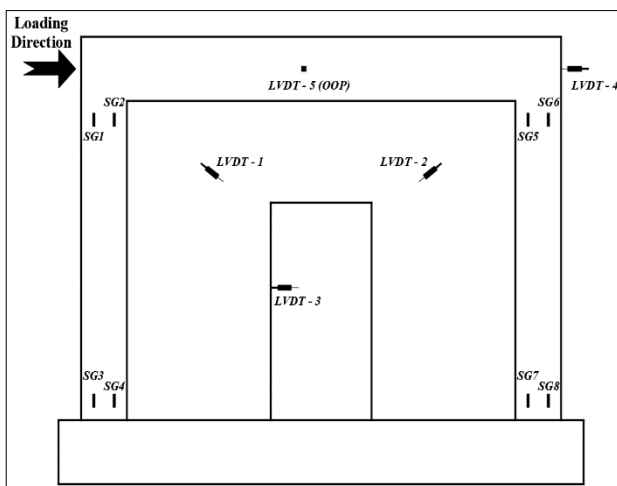


Figure 5.9. Instrumentation details

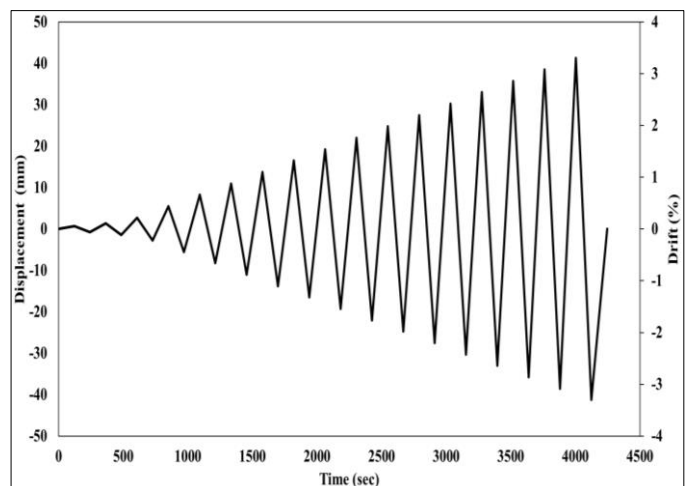


Figure 5.10. Applied loading protocol

5.7. EXPERIMENTAL RESULTS

5.7.1. Experimental Phenomena and Load-Deformation Curves

The observed force-drift hysteretic data for both tests in Figures. 5.11 (a)-(b) show that all specimens reacted elastically before breaking when the horizontal loading magnitude was less than 50% of the ultimate load. The hysteretic loops on these specimens were thin and contained a tiny region. An elastic-plastic force-drift reaction was commonly triggered, and cracking began on the wall when the horizontal load approached approximately 60% of the ultimate load. This cracking gradually worsened, generating a network of horizontal and inclined cracks with incrementally increasing width as the load reached 80% - 90% of the ultimate load. The reaction in the two loading directions was often symmetrical. Hence, the force and associated displacements displayed in Table 5.2 represent the maximum for the two loading directions. Cracking happened along the mortar bed and head joints rather than through the masonry units, as would be expected when the mortar strength is much lower than the strength of the brick units.

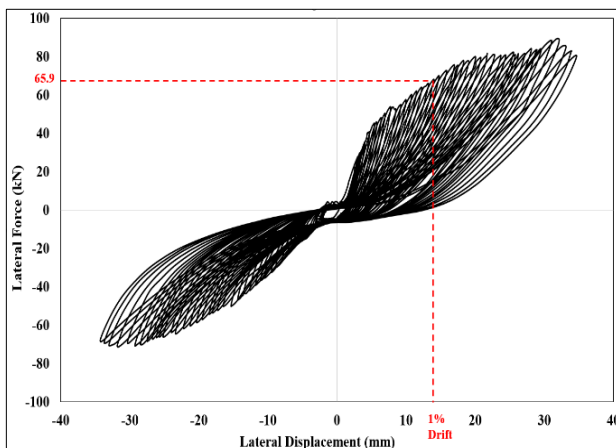


Figure 5.11(a) Hysteresis curve for URS specimen

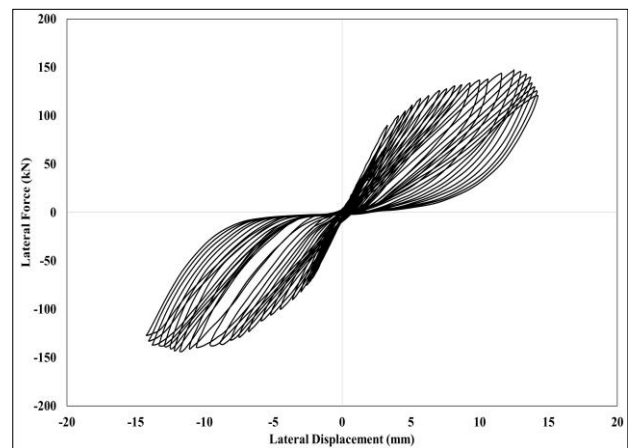


Figure 5.11(b) Hysteresis curve for DRS specimen

Figure 5.12 (a)-(b) and 5.13 (a)-(b) display the failure condition of URS and DRS specimens, respectively, at the end of testing. The primary wall cracks were generally aligned diagonally for both loading orientations; however, because the boundary components offered more integrity, the wall without TRM had more cracks dispersed across a more significant portion of the wall surface. There was a more intricate damage pattern, with diagonal cracking usually seen on every pier.



Figure 5.12(a) Initial cracks in URS specimen Figure 5.12(b) Initial cracks in DRS specimen



Figure 5.13(a) Final cracks in URS specimen Figure 5.13(b) Final cracks in DRS specimen

The first crack was usually seen to appear at the mortar joint at the corner of the lintel beam on both sides in the case of the strengthened specimen. Previous investigations (Cavaleri & Di, 2019) and (Doudoumis, 2007) have shown similar effects, which have been primarily attributed to the poor strength of mortar and the stress concentration that occurs at the specimen's corner. The initial fracture in the pier region partially caused the masonry infill to weaken next to the opening; it only continued to be in touch with the spandrel region above the lintel beam. Because the wall's brick units were built by altering their orientation, which ultimately decreased the wall's overall thickness, the bottom masonry unit next to the opening usually failed in diagonal cracking as the amount of the wall's cracking increased. During the drift cycle of 0.3%, the masonry infill's loaded corners experienced mortar crushing, resulting in the initial fracture in the conventional built-tested infilled frame (URS). A lateral load of 48.4 kN was observed at this limit situation. A step-type shear crack developed through the

mortar bed and head joints alongside the infill diagonal close to the entry after a 0.5% lateral drift on the otherwise intact masonry infill.

Along with micro-tension cracks and shear cracks initiated in the top region of the columns, further diagonal fractures were seen to be progressing at a drift of 1.0%. The masonry infill showed increased mortar crushing and cracking in the head and bed joints over 1.25 – 1.75% drift cycles. A shear slide was also seen at a bed joint in the spandrel section, one course above the opening, with a lateral drift of 1.75 percent. A maximum fracture opening of 1.47 mm was observed in filled RC frames. The initial fracture in the DRS specimen occurred at the 0.5% lateral drift masonry and frame interfaces on the bottom left and right. The strengthening portion did not appear to have any defects.

5.7.2. Energy Dissipation

Graphs of the hysteresis response with varying pinching extents that correlate to varying energy dissipation levels are shown in Figure 5.16. The hysteresis loop pinching, which indicates a decrease in energy dissipation was caused by horizontal deformations that happened in tandem with the opening and closing of cracks in the infill. Shear friction from bed joint sliding and reinforcement yielding consumed little energy (Demetrios, Kakaletsis & Karayannis, 2009), (Murty & Jain, 2000). Specifically, the hysteresis loops of the URS and DRS walls showed precise pinched forms. Reduced vertical compressive load, as is well known, reduces the frictional resistance caused by shear sliding on mortar bed joints, which lowers energy dissipation and narrows hysteresis loops. Previous research (Panagiotis G. Asteris, 2023; Mondal & Jain, 2008) indicates that the RC frame contributes around 11% to the lateral stiffness of infilled masonry without openings. The lateral stiffness of MIW diminishes with more openings.

5.7.3. Hysteresis Behaviour

The corresponding lateral drift was obtained by dividing the lateral displacement by the test frame height. The distance between the foundation beam's top and beam centerline was measured to provide the test frame height for the drift calculation. The lateral drift and comparable overturning moments around the column base are displayed on the secondary vertical axis. The walls URS and DRS exhibited similar hysteresis loop geometries with minor pinching due to the greater amplitude of vertical overburden loads and the enhanced lateral

stiffness associated with the wall shape. As seen in Figure 5.15, envelope curves were created for each test by converging the highest excursion points of each cycle.

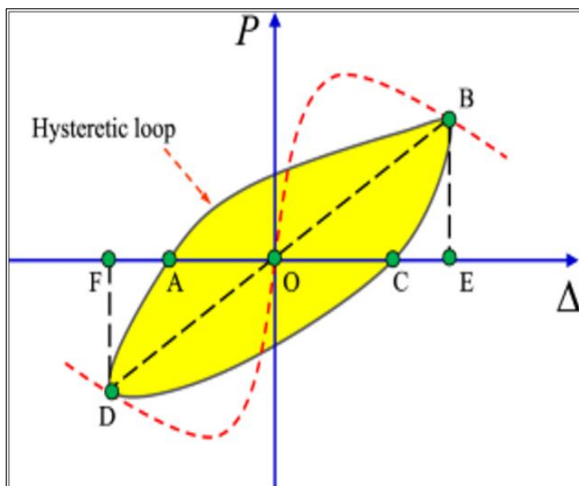


Figure 5.14. Dissipation capacity area
(Z. Chen et al., 2020)

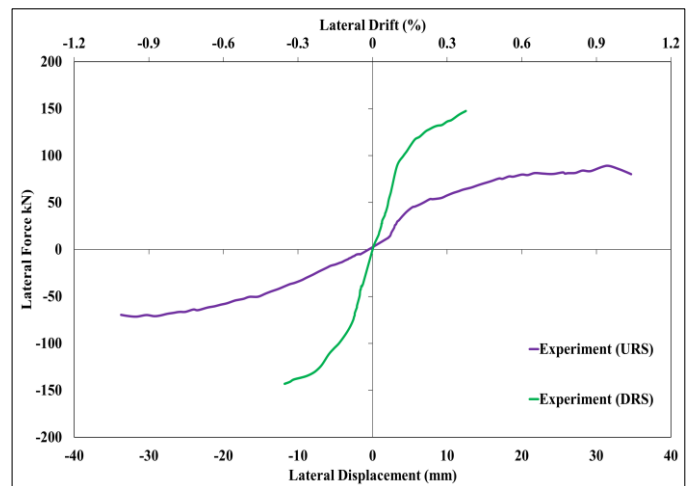


Figure 5.15. Maximum excursion curve

In recent years, (Lutman et al., 2006; Magenes et al., 2008; T. Zimmermann, 2011) have examined the reaction of masonry buildings using the equivalent viscous damping coefficient (EVDC). The following equation (1) is used to compute the EVDC, which is denoted by the symbol ζ_{eq} :

$$\zeta_{eq} = \frac{1}{2\pi} \frac{S(ABC+CDA)}{S(OBE+ODF)} \quad (1)$$

As seen in Figure 5.14, where $S(OBE+ODF)$ is the total of the areas of the two triangles OBE and ODF, which is the strain energy calculated using the equation (2), on the other hand, $S(ABC+CDA)$ is the area encircled by the hysteresis curve which denotes the energy dissipation capacity derived from the hysteresis loops generated real-time during the experiment. The elastic input energy effectively dissipates when EVDC (ζ_{eq}) is high. This suggests that energy dissipation benefits from high EVDC values.

$$S(OBE+ODF) = 0.5 * (P_x \cdot u_x) \quad (2)$$

where P_x and u_x indicate the maximum load and displacement during the i^{th} loading cycle when the displacement equals x . The DRS specimen's ultimate lateral strength was 49.47% greater than the URS specimen's strength. It is evident that the retrofitted frame has narrow loops in the initial cycles, which enlarge in the following cycles due to separation

starting at the bottom corner interfaces of the masonry infill and a few minute fractures in the masonry and frame portions. Plots were created by deducting any slide recorded from the applied displacement. The DRS specimen's hysteresis curves are displayed or acquired up to a lateral drift of 0.80% to 1.05% to maintain the health and safety concerns due to the limited capacity of the hydraulic actuator used to conduct the experiment.

When the residual strength decreased to around 60% of the peak strength, the infilled RC frame without retrofit (URS) displayed a slightly brittle bi-linear behaviour, with the ascending limb drifting up to 0.8% and the descending limb drifting up to 2.0%. As a result of substantial energy loss and damage accumulation, the hysteretic loops (Figure 5.11(a)) were much more comprehensive. The peak lateral force recorded for the URS and DRS specimens were 89 kN and 148 kN, respectively. The lateral load-displacement hysteresis curves for the TRM-reinforced test frames (DRS) are displayed in Figure 5.11(b).

5.7.4. Stiffness Degradation

Figure 5.17 depicts the stiffness degradation factor of specimen vs displacement to show how stiffness deteriorates. The following equation (3) is the stiffness degradation coefficient (K_s):

$$K_s = \frac{\sum_{i=1}^{i=n} P_x}{\sum_{i=1}^{i=n} u_x} \quad (3)$$

where P_x and u_x denote the maximum load and displacement during the i^{th} loading cycle when the displacement equals x . The number of loading cycles in each loading cycle is defined by n .

The stiffness degrades with the increase in displacement. Each specimen's hysteretic loops were used to calculate the stiffness values from peak to peak. Peak-to-peak stiffness at each displacement level was calculated by squaring the slope of the line joining the maximum load points in the load-displacement curve attained at each displacement level. As anticipated, URS stiffness decreases noticeably with increasing lateral displacement. The URS specimen's rigidity has been shown to grow initially and steadily decrease from 5 mm to 10 mm. The URS specimen's rigidity progressively reduced from 10 mm until the test's conclusion. Similar to this, the DRS specimen's stiffness increased abruptly and then progressively reduced up to a displacement of 15 mm.

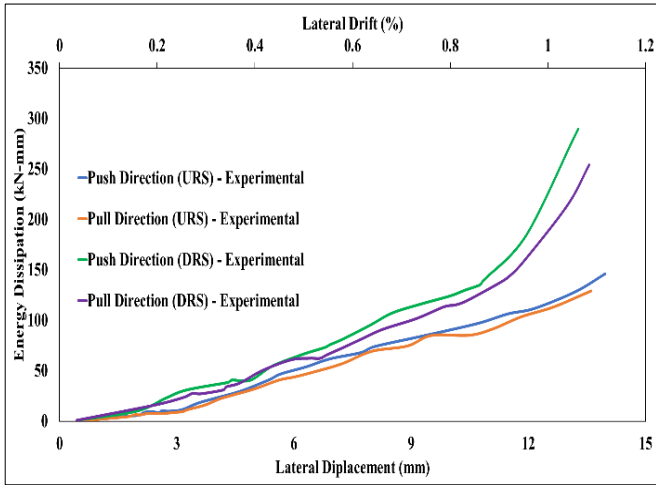


Figure 5.16. Energy dissipation – Experiment

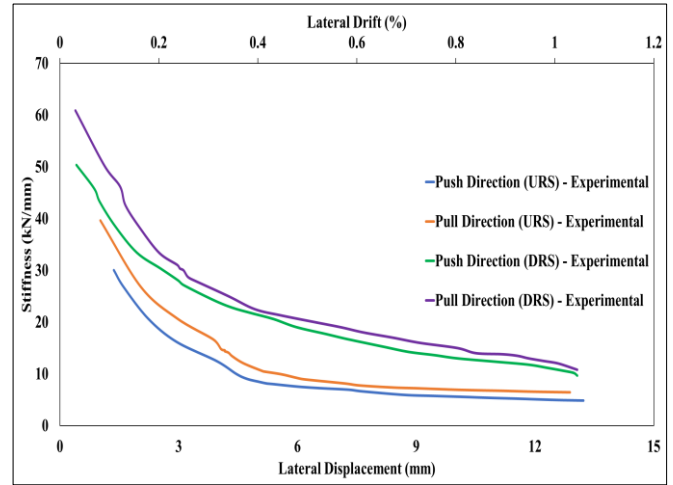


Figure 5.17. Stiffness degradation – Experiment

Because testing on strengthened test frames terminated at drifts of 0.75 to 1.10%, the stiffness diminution was inconsequential in contrast to the conventional structure. The test results are summarized in Table 6.2 (Chapter 6) concerning energy dissipation, stiffness deterioration, peak load, displacement at maximum load, and strengthening efficacy. The strengthening efficiency of a strengthening material is defined as the ratio of the retrofitted specimen's maximum load to the control specimen's capacity. The stiffness degradation calculation involves dividing the peak load points of each loop by the relevant displacement values. The hysteresis loops are also used to measure the specimen's energy dissipation. The area contained by each loop is determined, and each specimen's energy dissipation capacity is plotted against the associated displacements. The displacement recorded at the upper corner of the masonry unit serves as the in-plane displacement that characterizes the behaviour of both specimens.

Table 5.2. Experimental results of URS and DRS

Specimen	Results	Δ (%)	u_{max} (mm)		P_{max} (kN)		P/P_o	K_{si} kN/ mm	K/K_1 -	K_{sf} kN/ mm	E kNm	E/E_1 -	EDR %	Mode of Failure
			Push (+ve)	Pull (-ve)	Push (+ve)	Pull (-ve)								
Experi.	URS	2.6	34.34	-31.13	89	-81.5	-	30.06	-	4.31	2.52	-	4.81	SCM
Analysis	DRS	1.08	14.25	-13.24	147.5	-144	1.66	50.36	1.66	8.45	3.29	1.30	8.38	DC

P_{\max} = maximum lateral load, u_{\max} = maximum lateral displacement, Δ = maximum drift (%), K_{si} = initial stiffness, K_{sf} = final stiffness, E = energy dissipation, EDR = equivalent damping ratio, SCM = step cracking/diagonal failure mode of masonry wall, DC = distributed cracking on the surface of the TRM matrix.

5.8. SUMMARY

A comprehensive experimental investigation was conducted to study the response of ductile RC frames including MIW consisting of central door openings strengthened with TRM was subjected to in-plane cyclic load. This study evaluated the effectiveness of TRM as a strengthening material in contributing to the maximum load-carrying capacity and deflection-resisting phenomena of the MIW. For this purpose, two separate specimens were constructed: (1) RC frame with an infill wall with an opening without retrofitting (URS) and (2) RC frame with an infill wall with an opening with retrofitting (DRS) on both sides of the wall. It was found that significant differences in the damage patterns, resisting the deformation capacity, lateral stiffness and strength, and energy dissipation capacity were observed in these two specimens. The results showed that the URS produced 65.73% less lateral strength and stiffness and a 58.88% increase in the maximum deflection compared to the DRS specimen. This indicates that the presence of TRM significantly increased the infill wall system's lateral stiffness and strength and decreased the frame's deflection when subjected to lateral forces. The double layer of TRM is considered on both sides of the specimen after carrying out a parametric study which is detailed in the following Chapter (Chapter 6). The parametric study carried out using ABAQUS considers various TRM application patterns including the location and number of TRM layers on the MIW.

CHAPTER 6

NUMERICAL VALIDATION AND PARAMETRIC STUDY OF TEXTILE REINFORCED MORTAR (TRM) STRENGTHENED MASONRY INFILL WALL (MIW) WITH OPENINGS

6.1. OVERVIEW

In this chapter, the results of the finite element analysis (FEA) of the strengthened masonry infill wall (MIW) models described in Chapter 5 are presented and discussed including the cracking pattern and failure mechanism of the MIW, load-displacement response, stiffness, and energy dissipation capacity of the MIW frames. Of particular interest is to find out how effectively the method can deal with the specific aspects of the tested walls, such as the behaviour of MIW with an opening, application of textile reinforced mortar (TRM) layers, and to suggest improvements and refinements to the methods, if necessary.

This chapter is structured as follows: Section 6.2 provides the details of suitable numerical models; and suitable constitutive models based on the concrete damage plasticity (CDP) approach to characterize the nonlinear response of TRM, MIW, and reinforced concrete (RC) frames. Section 6.3 provides the validation study of the experimental investigation discussed in the previous Chapter (Chapter 5). Section 6.4 discusses the parametric study conducted to determine the significance of the full-bond scenario between the RC frame infilled with masonry and the TRM. Section 6.5 presents the results and discussion. Section 6.6 proposes empirical equations to determine the load-carrying capacity of the specimen. Finally, Section 6.7 reports the cost analysis required to construct a test specimen for an experiment.

6.1.1. Objectives

The objectives of this framework are

- a. Comparing the walls' strength obtained in the experiments to the numerical predictions carried out and validating the values of key hysteretic properties including stiffness and energy dissipation capacities.

- b. To carry out a parametric study considering various factors that affect the performance of MIW when subjected to lateral loads.
- c. To prepare and report cost analysis and predictions which displays the cost required to construct a test specimen (reduced scale and full scale) for an experiment that includes the construction cost, transportation costs, workmanship, and miscellaneous costs.

6.2. NUMERICAL ANALYSIS

Experimental research provides accurate results but on the other side also has a few disadvantages in the form of the economic aspect, space occupation to conduct tests, and time-consuming setup of the test such as mounting the types of equipment like actuators, sensing meters like strain gauges, linear variable differential transformer (LVDT), data acquisition system, slow motion cameras to capture the crack propagation. Hence, to overcome these limitations involved in conducting the experimental tests, the best-suited alternative is numerical simulation or modeling, which becomes crucial for evaluating seismic behavior and undertaking parametric studies. Numerical modeling encoded in computer programs has become increasingly employed to predict the behavior of masonry-infilled frames as computing capability has advanced over the previous two decades. A three-dimensional numerical model was developed in order to replicate the nonlinear behaviour of the TRM-retrofitted masonry-infilled RC frame that was discussed in the preceding sections. The ABAQUS finite element (FE) software version 2022 was used for this investigation.

6.2.1. Numerical Simulation Approach

This section presents specifics on the implemented finite element (FE) model, such as the model geometry, modeling strategy, and validation findings. This modeling approach was used to carry out a parametric investigation of the behavior of RC frames with solid masonry infill walls after the numerical model's accuracy was confirmed. This study used popular FEA software ABAQUS to model the masonry-infilled RC frame strengthened with TRM. Solid components were used to simulate the brick units and RC frame members. As mentioned earlier, the detailed micro-modeling approach is too difficult to use, whereas the macro model is unable to simulate the cracks occurring in the mortar joints. As a result, this research adopts a comparatively homogenized model i.e., simplified micro-modeling in which the brick unit is expanded on all the sides (known as an expanded brick unit or combination block) with half of the mortar thickness on the side as shown in Fig 2.2 (Chapter 2) (Kouris et al., 2020). In other

words, to connect the discrete masonry blocks and allow them to interact with one another, their dimensions were raised by the mortar joint's half thickness in both the horizontal and vertical directions.

6.2.2. Constitutive Model

The constitutive softening model concrete damage plasticity (CDP) previously developed and available in the FEM application ABAQUS is utilized in the model. Since the CDP can handle brittle and quasi-brittle materials, it is advantageous for masonry as well and was also adopted to replicate concrete. Elasto-plastic trusses are then used to model the TRM on the homogenized model to imitate the fiber mesh present in the cementitious matrix. It should be noted that although ABAQUS offers general material constitutive and interfacial behaviour models for a variety of structural applications, the contribution of this study lies in the selection of appropriate models and important material parameters, and executing the accurate and efficient computational simulation of masonry infills surrounded by RC frame members with TRM as a strengthening material. By specifying the stress-strain relationship of the material under the compression and tensile behaviour, the CDP model simulates the nonlinear response of the entire structure during earthquake activity. (Documentation, 2010) describes the concrete's constitutive relationship. The primary purpose of the concrete damaged plasticity model is to offer a general capacity for the evaluation of concrete structures subjected to cyclic and/or dynamic loads. Concrete has brittle behaviour at low confining pressures; the major modes of failure are tension cracking and compression crushing. When the confining pressure is sufficient to prevent fracture propagation, concrete loses its brittle nature. The plastic-damage model in Abaqus is based on the models proposed by (Lubliner J, Oliver J, 1988) and detailed by (Lee & Fenves, 1998) The major features of the governing equations for the concrete-damaged plasticity model are given in this section.

6.2.3. Concrete Damage Plasticity (CDP) Model

Before the concrete supporting external loads, the concrete had some "damage" in the form of microscopic cracks and splits. Specifically, the emergence and evolution of cumulative damages (micro-cracks, holes, and so forth) at different scales is what causes the failure process. Consequently, the micro-cracks are primarily responsible for the nonlinear features of stress-strain (Stauffer et al., 2006). Concrete stiffness deterioration is frequently linked to plastic deformation, which exhibits slipping and deformation connected to the material flow

mechanism in addition to the allowance of micro cracks and faults in the microscopical mechanism. Consequently, the elastic-plastic damage constitutive model, which reflects two different mechanisms, such as plastic deformation and elastic damage – should be the appropriate constitutive relation (Nguyen & Korsunsky, 2008). It is usually believed that concrete is a macroscopic and isotropic material such that its process of distortion and failure pattern may be investigated, eliminating the inconvenience of analyzing the material's microstructure. Concrete's CDP model in FE software (Jian Ying Wu, Jie Li, 2006) is determined using the model as a basis by (Lubliner J, Oliver J, 1988). Using the isotropic elastic-damage model in combination with the isotropic tensile or compressive plasticity model, this model simulates the inelastic behaviour of concrete (Nguyen & Korsunsky, 2008). It was predicated on the notion that there was identical damage in all directions, which holds true for concrete subjected to whimsical loading pressures, such as cyclic loading. In addition, the regaining of elastic stiffness during loading cyclically is taken into consideration, as well as the deterioration of elastic stiffness brought on by compressive and tensile plastic strain.

In the elastic stage, the CDP model using the elastic model describes the mechanical characteristics of materials. The relation between the CDP model's elastic modulus may be explained as follows after reaching the damage stage:

$$E = (1 - d) E_0 \quad (1)$$

where the initial elastic modulus is represented by E_0 , the plastic-damage factor is represented by d with d_c or d_t in compression or tension and ranging from 0 to 1, where 0 denotes the model is undamaged and 1 denotes the strength of the solid material is vanished.

6.2.3.1. CDP Model under Uniaxial Cyclic Loading

The model employs w_t and w_c to manage the material's ability to regain rigidity during the reverse loading action of uniaxial reciprocating loading (Lee & Fenves, 1998; O Omid & Lotfi, 2010; Omid Omid & Lot, 2012). Figure 6.1 depicts the graphical representation of concrete elastic modulus recovery shown under tension-compression stress transition. During uniaxial cyclic loading (tension to compression, then back to tension), the elastic modulus recovery in the CDP model is as follows: the loading factors for tension and compression are described as $w_t = 0$ (compression till tension) and $w_c = 1$ (tension back to compression). The tensile stress of concrete rises with axial tension. Concrete will fracture if stress reaches the peak value (point A), and tensile stiffness will decrease if loading is applied to point B, where

the stiffness reduction factor d_t may be written as shown in Equation (1). The effective stiffness $[(1 - d) E_0]$ slope, particularly, the trail BC will cause the curve to decrease if it is unloaded at that point. If the loading component is present $w_c = 0$ (that the compression stiffness will not recover with tension reparations), The concrete will be loaded on the CD path, subjected to inverse axial pressure, and placed on the CMF path if the weighting factor (w_c) is equal to 1. It is dropped off and subjected to reverse tension at point F. If the stiffness recovery factor is 1, it will be loaded on path GJ and trail GH if it is zero.

In Figure 6.2, σ_{un} and ϵ_{un} , respectively, designate the stress and strain of the unloading point; ϵ_t^{el} , ϵ_{ot}^{el} respectively, show the concrete's tensile plastic strain which is damaged and undamaged; and ϵ_t^{ck} , ϵ_t^{el} respectively, denote the cracking strain and tensile plastic of the concrete.

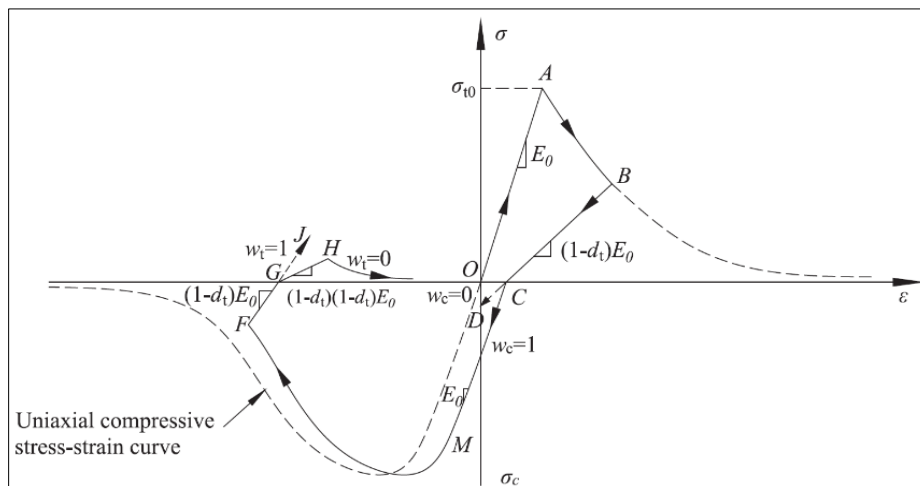


Figure 6.1. Concrete elastic modulus recovery shown under tension-compression stress transition (Xiao et. al., 2017)

The finite element program will be given the tensile damage data in the format $d_t - \epsilon_t^{ck}$. Using the following formula, the program will convert the cracking strain into plastic strain automatically.

$$\epsilon_t^{pl} = \epsilon_t^{ck} - \frac{d_t}{1 - d_c} \frac{\sigma_t}{E_0} \quad (2)$$

When the tensile unloading path traverses, as indicated by a negative plastic strain value ϵ_t^{pl} or a minor cracking strain ϵ_t^{ck} , the finite element program signals errors that tensile damage $\epsilon_t^{pl} = \epsilon_t^{ck}$ won't arise. Regarding the compressive stress-strain curve, data that surpasses the elastic part's range will be input into the finite element software in the format of $\sigma_c - \epsilon_c^{in}$. As

seen in Figure 6.3, the compressive cracking strain is calculated as the total strain minus the elastic strain of the undamaged material.

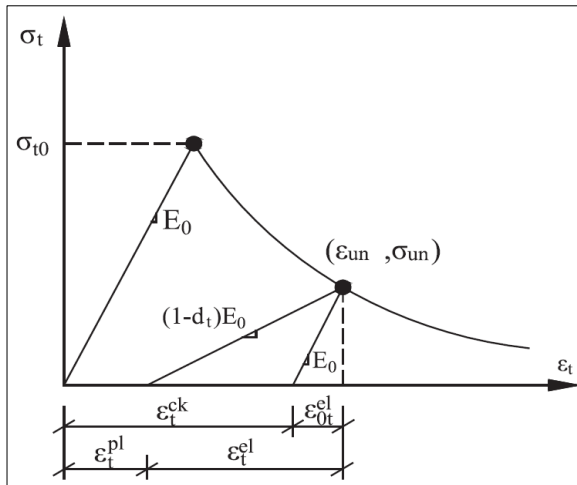


Figure 6.2. CDP model's tensile stress-strain curve (Xiao et. al., 2017)

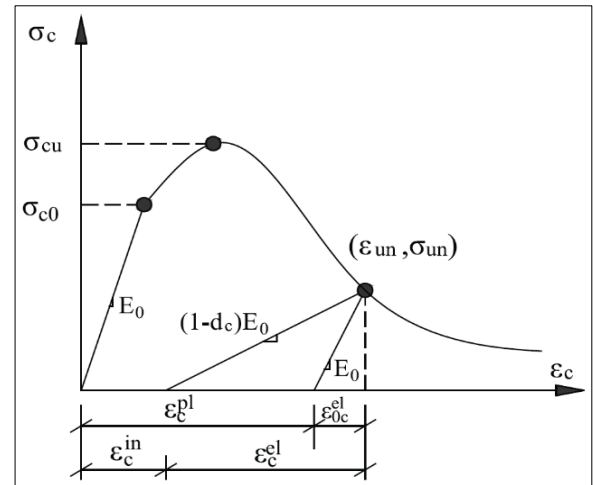


Figure 6.3. CDP model's compressive stress-strain curve (Xiao et. al., 2017)

In Figure 6.3, σ_{un} and ϵ_{un} , respectively, denote the stress and strain of the unloading point; ϵ_c^{el} , ϵ_{oc}^{el} respectively, show the concrete's compressive plastic strain which is damaged and undamaged; ϵ_c^{in} , ϵ_c^{pl} , respectively, indicate the cracking strain and plastic compression of concrete.

The compression damage data will be input into the finite element program in a given form of $d_c - \epsilon_c^{in}$. Next, using the following formula, the program will convert the cracking strain into plastic strain automatically.

$$\epsilon_c^{pl} = \epsilon_c^{in} - \frac{d_c}{1-d_c} \frac{\sigma_c}{E_0} \quad (3)$$

The finite element program will alert errors that compressive damage won't occur in the event that the plastic strain value ϵ_c^{pl} is negative or the cracking strain ϵ_c^{in} is small, indicating that the compressive unloading pathway merges $\epsilon_c^{pl} = \epsilon_c^{in}$.

6.3. VALIDATION OF THE EXPERIMENTAL STUDY

6.3.1. Material Properties

The numerical analysis, simulation approach, meshing of the solid parts, and the interaction properties are directly used from the previous section. The majority of the material

properties and other parameters that are employed in this study are derived from the above-described experimental examination. Table 6.1 displays the material parameters utilized for the TRM, infill, steel, and concrete.

Table 6.1. Mechanical properties of all elements

Concrete		Steel	
Young's Modulus	25000 MPa	Young's Modulus	210000 MPa
Poisson's ratio	0.17	Poisson's ratio	0.33
Compression strength	20 MPa	Grade	Fe 500
Infills		TRM	
Young's modulus	14800 MPa	Tensile Strength (kN/m) [MD x CMD]	25 x 25
Poisson's ratio	0.15	Tensile Elongation (%)	3
Dilation Angle	10	Aperture Size (mm)	5 x 5
Eccentricity	0.1	Fabric density (g/m ²)	420
f _{bo} /f _{co}	1.16	Cross-sectional area of fibers (mm ² /m)	45.3
Stiffness	0.66	Tensile elastic modulus (GPa)	32
Viscosity Parameter	0.015		

6.3.2. Interface Simulation between Expanded Bricks

The surface-based cohesive contact model has been chosen as the interaction model between various blocks. The specification of the tensile strength and the softening behavior may be used to simulate the fracture between blocks. The compression between blocks is specified by the hard contact concept. Cohesive and friction models are the two types of shear models. Three components make up the surfaced-based cohesive contact model: formula 3 defines the relation between the elastic stiffness matrix K , nominal traction vector t , and corresponding separation vector d , of the joint interfaces; formula 4 defines the damage start criterion; and formula 5 decrypts the damage evolution criterion (Abdulla et al., 2017).

$$t = \begin{Bmatrix} t_n \\ t_s \\ t_t \end{Bmatrix} = \begin{bmatrix} K_{nn} & K_{ns} & K_{nt} \\ K_{sn} & K_{ss} & K_{st} \\ K_{tn} & K_{ts} & K_{tt} \end{bmatrix} \quad (4)$$

$$\left\{ \frac{t_n}{t_n^0} \right\}^2 + \left\{ \frac{t_s}{t_s^0} \right\} + \left\{ \frac{t_t}{t_t^0} \right\} = 1 \quad (5)$$

$$t_n = \begin{cases} (1-D)\bar{t}_n, & \bar{t}_n \geq 0 \\ \bar{t}_n, & \text{Otherwise} \end{cases} \quad t_s = (1-D)\bar{t}_s \quad t_t = (1-D)\bar{t}_t \quad (6)$$

The symbols t_n , t_s , t_t show both the shear and normal tractions. The letters n, s, and t represent the pertinent separations. Peak values are indicated by the 'o' superscript. Pure normal slip or pure shear separation with zero normal parting does not produce cohesive forces in the normal direction because the traction-separation behaviour is decoupled in this scenario. The Macaulay bracket in Eq. (7) shows that the compressive stresses are not considered for the joints' typical direction fracture behaviour. Under the same boundary conditions, the stiffness matrix K components for joint interfaces in a meso micromodel (interface between enlarged masonry bricks) ought to be identical to the original brick-and-mortar masonry joint interface stiffness. The elasticity moduli of the mortar and unit and the thickness of the mortar, equations (7) and (8) are used to define the joint interfaces of the equivalent stiffness.

$$k_n = \frac{E_u E_m}{h_m(E_u - E_m)}, \quad k_s = \frac{G_u G_m}{h_m(G_u - G_m)} \quad (7)$$

The concrete-rebar interaction was simulated using the embedded area. In this numerical model, the surface of the strengthening material was efficiently attached to the MIW since the debonding of the TRM surface from the RC frame and the masonry was not taken into consideration. As a result, tie constraints were used to control the surface interactions between the fibers and the concrete, with the wall surface acting as the master surface and the TRM fiber as the slave surface. In addition, the thickness of the mortar is included in the set 15 mm thickness of TRM. The RC frame and the brick were both seen as solid parts, and their relationship was represented by a tie element in which the brick served as a slave surface and the concrete as the master. Additionally, in order to replicate the strong foundation RC-beam plate that was used at the bottom of the frame in the experiment, all of the nodes at the base of both columns were restricted using coupling constraints to prevent any translation and represented as fixed connections. Either load control or displacement control is the foundation for the actions (load or displacement) that the numerical analysis techniques imposed on the model. Both circumstances involve a progressive application of the actions.

The dimensions of the bare frame, modeling of the TRM fiber, assembly of the whole masonry wall system, and the generated mesh in ABAQUS of the RC frame including the infill wall are shown in Figure 6.4 to 6.7 respectively. As masonry joints soften and their stiffness

deteriorates, viscous regularization is required as a damage stabilizer in the surface-based cohesive behaviour model in order to simulate the complete failure of masonry joints without encountering numerical convergence issues.

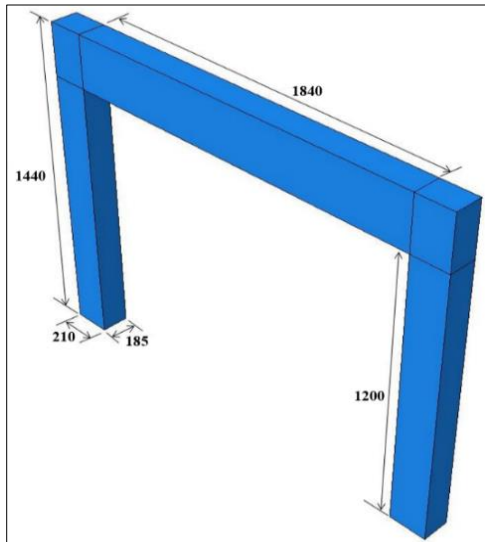


Figure 6.4. RC frame dimensions

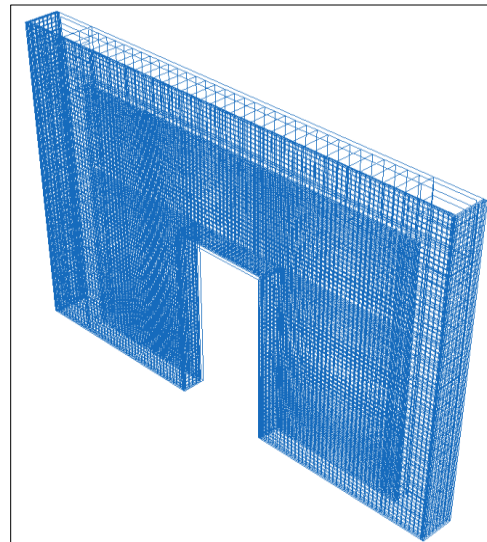


Figure 6.5. Modelling of TRM

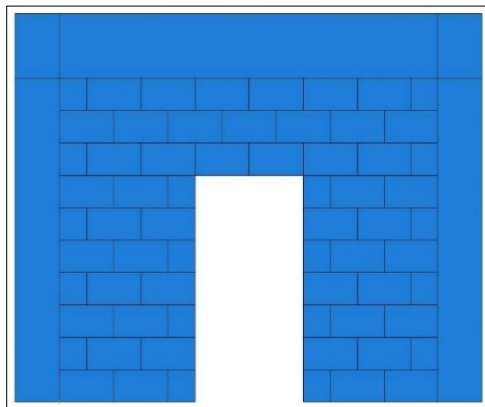


Figure 6.6. Infill frame

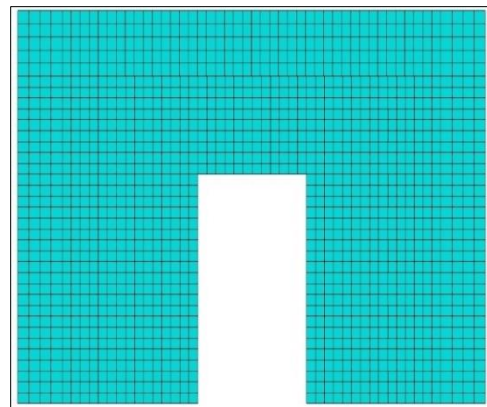


Figure 6.7. Meshing of the model

The effect of large displacement non-linear geometry was considered in all models. A broad non-linear static process came after the Newton-Raphson algorithm solution, which iteratively solves equilibrium in each increment. The numerical analysis was performed in two stages: the horizontal cyclic force and the vertical compression. In order to reflect the system's dead load, a vertical pre-compressive load of 100 kN was applied at the top of each column in the first phase of the vertical compression process. Rigidity was added to both beam-column connections to avoid stress concentration. A prescribed deformation load was also applied for the horizontal cyclic loading at the top of each level in order to accurately duplicate the experimental loading. The top beam-column joint level of the structure undergoes cyclic

loading from the lateral forces applied in an in-plane direction. The second step involved holding the imposed vertical compression load constant while gradually applying the horizontal in-plane cyclic load under displacement control. This was done while restricting the vertical and out-of-plane horizontal displacements and rotations about all axes at the top of the wall to maintain the same boundary conditions as in the experiment. ABAQUS/Explicit was used to do the FEM analysis, and the analysis type was set to dynamic explicit (Dassault Systemes, 2014a). The loading approach is a displacement-control technique that is used consistently on every specimen. The loading technique utilized in the experimental campaign, as shown in Figure 4.10 (Chapter 4), is the same as the one employed for numerical analysis.

6.3.3. Model Development in ABAQUS

In this numerical model, the surface of the strengthening material was efficiently attached to the MIW since debonding of the TRM surface from the RC frame and the masonry was not taken into consideration. As a result, tie constraints were used to control the surface interactions between the fibers and the concrete, with the wall surface acting as the master surface and the TRM fiber as the slave surface. In addition, the thickness of the mortar is included in the set 15 mm thickness of TRM. The RC frame and the brick were both seen as solid parts, and their relationship was represented by a tie element in which the brick served as a slave surface and the concrete as the master. Additionally, in order to replicate the strong foundation RC-beam plate that was used at the bottom of the frame in the experiment, all of the nodes at the base of both columns were restricted using coupling constraints to prevent any translation and represented as fixed connections. Either load control or displacement control is the foundation for the actions (load or displacement) that the numerical analysis techniques imposed on the model. Both circumstances involve a progressive application of the actions.

All models considered the impact of large displacement non-linear geometry. The solution of the Newton-Raphson method, which solves equilibrium repeatedly with each increment, was followed by a broad non-linear static process. The numerical analysis was conducted in two phases: the vertical compression and the horizontal cyclic force. During the first stage of the vertical compression process, a vertical pre-compressive load of 100 kN was applied at the top of each column to represent the dead load of the system. In order to prevent stress concentration, rigidity was provided to both beam-column connections. To precisely replicate the experimental loading, a specified deformation load was also applied for the horizontal cyclic loading at the top of each level. The lateral loads applied in the in-plane

direction cause cyclic loading at the top beam-column joint level of the structure. In the second stage, the horizontal in-plane cyclic load was gradually applied under displacement control, while the imposed vertical compression load remained constant. To preserve the same boundary conditions as in the experiment, this was accomplished while limiting the rotations around all axes and vertical and out-of-plane horizontal displacements at the top of the wall. The FEM analysis was performed using ABAQUS/Explicit, with the analysis type set to dynamic explicit (Dassault Systemes, 2014b). A displacement-control method that is consistently applied to each specimen is the loading strategy.

According to Table 6.1, some of the properties of the masonry infill model in ABAQUS have different dimensions compared to the experimental specimen. For example, as mentioned earlier, masonry units modelled in ABAQUS are expanded brick units, which have the dimensions increased to half the thickness of the mortar on all the sides, whereas in the experimental procedure, the process of construction of the infill wall is same as the typical house construction procedure followed in India. The purpose of the foundation beam in the experimental campaign is to fix the test specimen to the rigid floor in the laboratory using anchor rods as shown in Figure 5.7. During simulation process, since we are conducting finite element analysis, due to the limitation of the number of nodes in ABAQUS software, the foundation beam is not created, instead, the base of the superstructure is provided with encastre support.

A regular squared mesh (Ho-Le, 1988) with the discretization was used. The mesh size was established by a mesh sensitivity study. A 50 x 50 x 50 mm three-dimensional element was used to represent the RC frame, which consists of two columns and one beam. In the half brick unit width scenario, each unit had a model with 3 x 2 x 3 parts for the analysis, whereas a complete masonry unit (230 mm long, 110 mm high, and 78 mm thick) was modelled with 7 x 2 x 3 elements for analysis. For the TRM meshing, a regular tetrahedron with a dimension of 50 mm was used. The dimensions of the bare frame, modelling of the TRM fiber, assembly of the whole masonry wall system, and the generated mesh in ABAQUS of the RC frame including infill wall are shown in Figure 6.4 to 6.7 respectively. As masonry joints soften and their stiffness deteriorates, viscous regularization is required as a damage stabilizer in the surface-based cohesive behaviour model in order to simulate the complete failure of masonry joints without encountering numerical convergence issues.

Table 6.2. Calibration of model parameters

Structural Element	Parameters		Experimental Campaign	Numerical Analysis
Beam	Cross-section		240 x 185 mm	240 x 185 mm
	Reinforcement	Main bars	12 mm diameter	Modelled as wire element with same diameter as in experiment
		Stirrups	8 mm diameter	
Column	Cross-section		210 x 185 mm	Modelled as wire element with same diameter as in experiment
	Reinforcement	Main bars	12 mm diameter	
		Stirrups	8 mm diameter	
Foundation Beam	Cross-section		400 x 275 mm	Instead of modelling the beam in ABAQUS base of the specimen is provided with fixed support
	Reinforcement	Main bars	Top – 12 mm & Bottom – 16 mm	
		Stirrups	10 mm	
Infill Wall	Brick dimensions		230 x 110 x 78 mm ³	242 x 122 x 78 mm ³ (Expanded brick unit, Section 2.4)
	Mortar thickness		12 mm	-
Strengthening Material	TRM matrix thickness		15 mm	15 mm
	TRM Fabric		Grid size 10 x 10 mm	Grid size 10 x 10 mm
Loading	Vertical loading		100 kN applied using hydraulic jack at the midspan of the beam	50 kN applied on top of each column

6.4. PARAMETRIC STUDY

This section elaborates the parameters considered in the study and their modelling procedures as shown in Figure 6.8. The first specimen (excluding the bare frame (BF)) was used as the unretrofitted (URS), without TRM. The parametric study was conducted to determine the significance of the full-bond scenario between the RC frame infilled with

masonry and the TRM considering: (1) the location of the strengthening fiber material on the specimen and (2) the number of layers of the strengthening material.

- a. **BF** Specimen with only the surrounding RC frame having neither MIW nor TRM
- b. **URS** Specimen without any layers of strengthening material (TRM retrofitting)
- c. **SRS-F1** Specimen with only one layer of strengthening material (TRM retrofitting) on the front face of MIW
- d. **SRS-B1** Specimen with only one layer of strengthening material (TRM retrofitting) on the back face of MIW
- e. **SRS-F2** Specimen with two layers of strengthening material (TRM retrofitting) on the front face of MIW
- f. **SRS-B2** Specimen with two layers of strengthening material (TRM retrofitting) on the back face of MIW
- g. **SRS-F1B1** Specimen with only one layer of strengthening material (TRM retrofitting) each on both the back face and front face of MIW
- h. **DRS** Specimen with two layers of strengthening material (TRM retrofitting) on both the back face and front face of MIW

Specimen URS and DRS are given different notations compared to the other specimen names because experiment was conducted on these two specimens and the numerical modelling was carried out which paving the way to the parametric study with different layers of TRM implemented on different locations on the surface of MIW as discussed in this section.

A total of eight specimens were modelled in ABAQUS software. The notation of specimens comprises a series of numbers and letters. The Letter U, S, or D, at the beginning of the specimens' notation denotes unretrofitted, single retrofitted and double retrofitted, respectively; the numbers (1 or 2) indicate the number of layers of the textile fiber. The letter UR denotes an unretrofitted infill wall, S represents a specimen, SR suggests an infill wall with TRM reinforcement applied on single face of the specimen (either front face (F.F.) or back face (B.F.)) and DR suggests an infill wall with TRM reinforcement applied to both faces of the specimen. Moreover, the blue line represents the numeral of strengthening fiber layers (one or two) and location (front side or back side) TRM layer. The coverage of surface area of TRM fiber material on the masonry wall's back face is lesser than that on the front face. This disparity

is due to the alignment of the brick wall along the plane of the column's face, in contrast to the back side where a 107 mm gap bridges between the surfaces of the column and brick wall.

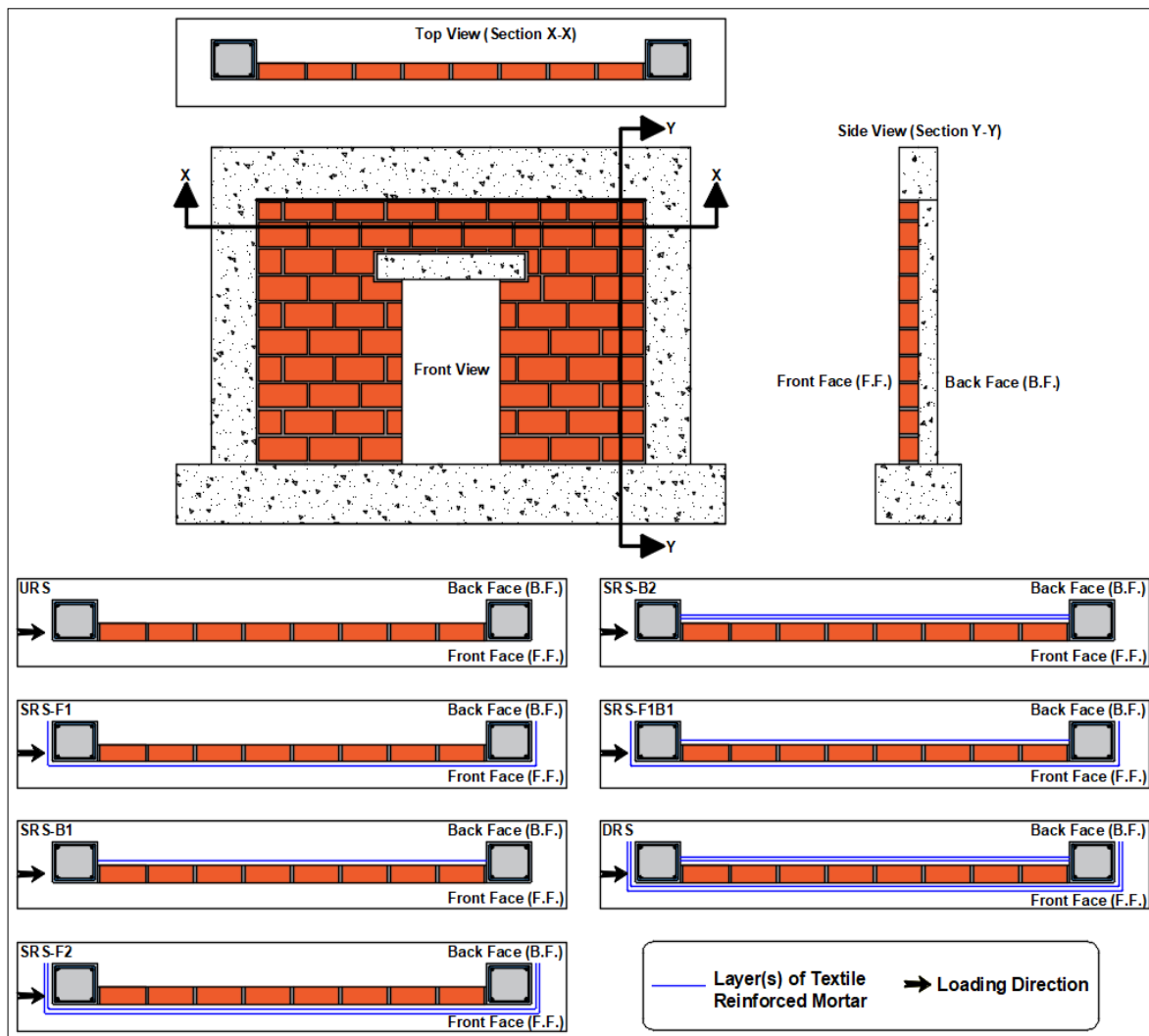


Figure 6.8. Configurations of the strengthened specimens to summarize the various parameters considered

In the case of SRS-F1, as can be seen in Figure 6.8, the TRM fiber layer is present on the front face of the MIW which covers the front face of the beam and the adjacent columns of the surrounding frame including their side faces. Whereas in the case of SRS-B1, the TRM layer is present only on the back side of the MIW, which covers neither the beam nor the column. SRS-F2 and SRS-B2 follow the same procedure of application and location of the fiber as in SRS-F1 and SRS-B2 except with the increase in the number of layers of TRM, respectively. As the number in the name of the configuration represents the number of layers of TRM fibers, SRS-F2 and SRS-B2 contains two layers of fiber on the front and back faces of the infill wall, respectively. With regard to SRS-F1B1, one layer of the TRM fibers is applied

both on the front and back faces of MIW. Instead of one layer of TRM fiber as in the case of SRS-F1B1, DRS specimen has two layers of TRM on both the faces of the MIW.

In order to understand the contribution of the TRM strengthened walls under in-plane forces, a non-linear finite element (FE) model was adopted, obtained starting from the geometry of the real specimens. A parametric study was performed in order to further understand the efficiency of applied strengthening method on varying location and the number of TRM layers on the MIW. The numerical models of 1:2.5 scaled frames having various TRM layers were generated for this purpose. The generated models had identical properties except for their varying number of fiber layers and the location on the surface of the infill walls. The location of the fiber layers was decided based on the face of the infill walls, i.e., front face and back face. All of the analyzed frame models had one-bay and one-storey. The same column/beam cross-sectional dimensions and reinforcement layout were used as in the test specimens in the experimental procedure. During the numerical procedure, the fibers were modelled separately related to the faces of the application of the fiber as shown in Figures 6.8.

6.5. RESULTS & COMPARISON

This part of the thesis explains the numerical findings obtained from the current investigation, followed by a comparison between the outcomes of both numerical and experimental non-linear cyclic analysis.

The failure patterns of all the numerical models are shown in Figures. 6.11 - 6.18. The load-bearing capacity values derived from the numerical outcomes are marginally more significant than the experimental results. Nonetheless, the numerical analysis values are consistently higher than those found in the experimental data regarding the values of the maximum lateral displacement. Generally, ABAQUS over-predicts the specimens' maximum lateral displacement and maximum loading bearing capacity by a maximum of 10% allowance compared to the actual experimental data. (This may be the result of idealizations created in ABAQUS, such as the surface smoothness, the materials' lack of flaws, and the mortar material's total absence to simulate the performance of the infill wall). Overall, ABAQUS simulated findings compare favorably with experimental data, as shown by the maximum excursion curves.

The hysteresis curves for strengthened specimens considered both in the numerical and parametric study are plotted/obtained up to the maximum lateral displacement exhibited by the

specimens shown in Figs. 6.19 - 6.26. As seen in Figures 6.9-6.10, envelope curves were constructed for both experimental tests and for each model by converging the highest excursion points of each cycle.

According to the obtained hysteresis graphs for all the numerical models, it can be observed that the maximum load-bearing capacity of the URS specimen is 95.17 kN whereas the maximum displacement is 31.98 mm. The maximum load-bearing capacity of the DRS specimen is 155.77 kN and the maximum displacement is 13.34 mm. It is obvious from these values that the URS specimen outperformed the experimental values by 6.70% in terms of load-carrying capacity whereas the DRS specimen showed a 3.59% increase in the same aspect.

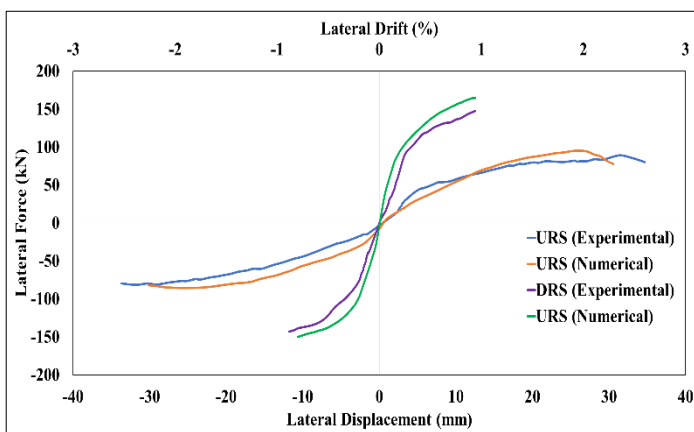


Figure 6.9. Envelope curves of URS and DRS

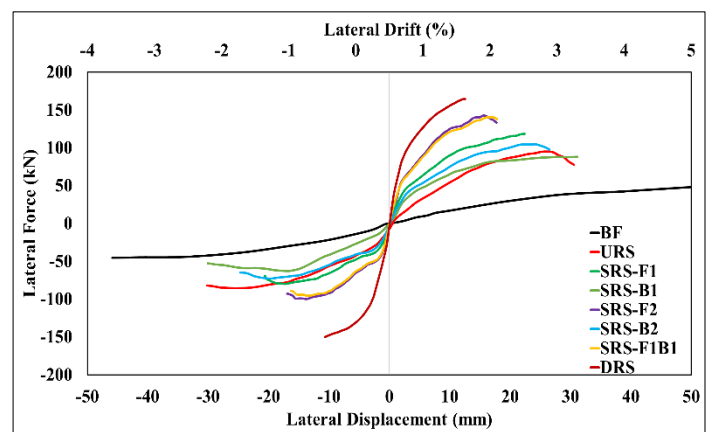


Figure 6.10. Envelope curves of all numerical models

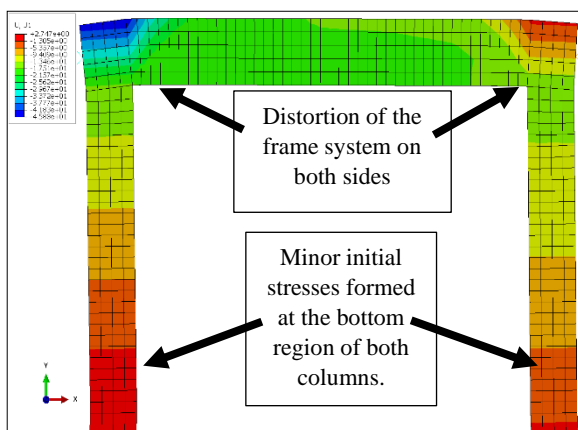


Figure 6.11. Failure patterns of the BF

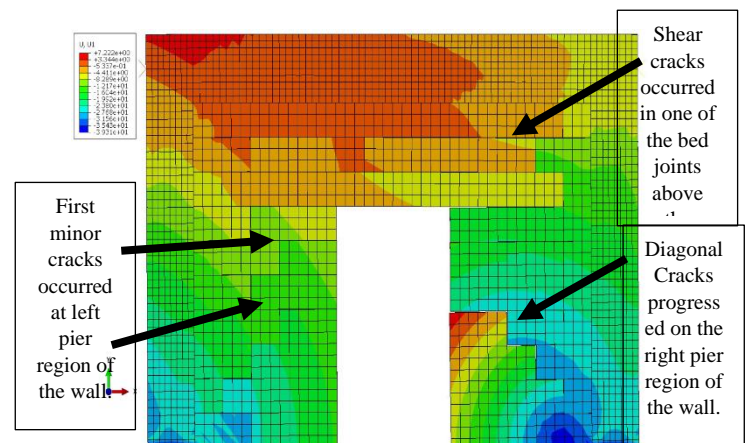


Figure 6.12. Failure patterns of the URS

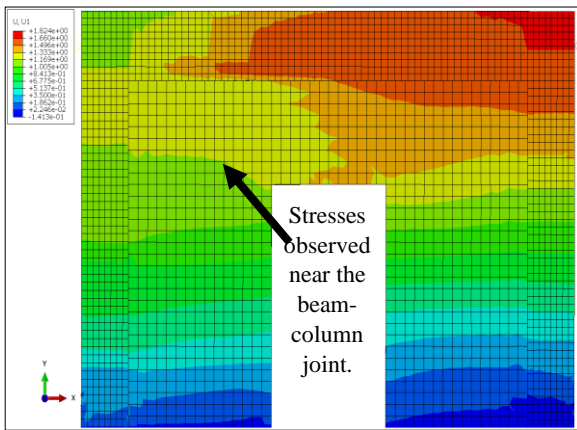


Figure 6.13. Failure patterns of SRS-F1

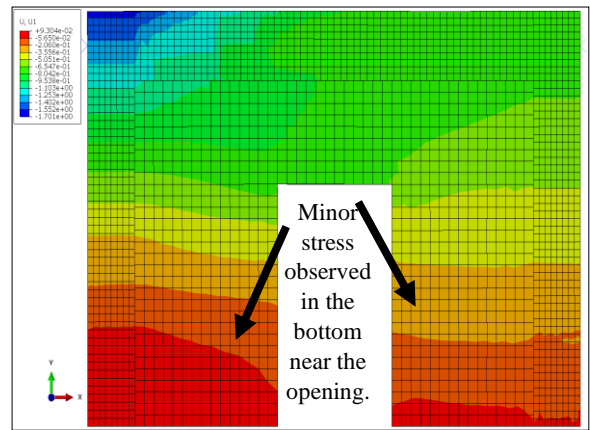


Figure 6.14. Failure patterns of SRS-B1

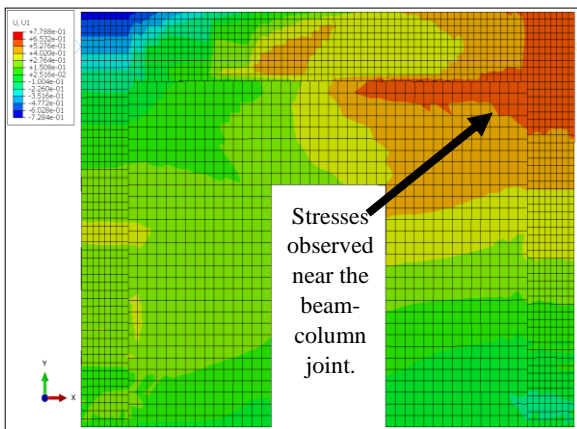


Figure 6.15. Failure patterns of SRS-F2

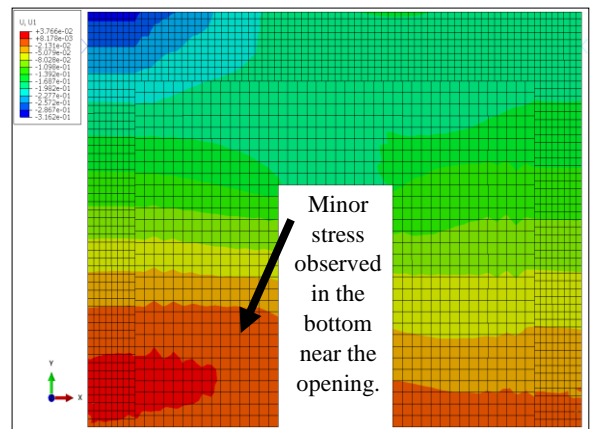


Figure 6.16. Failure patterns of SRS-B2

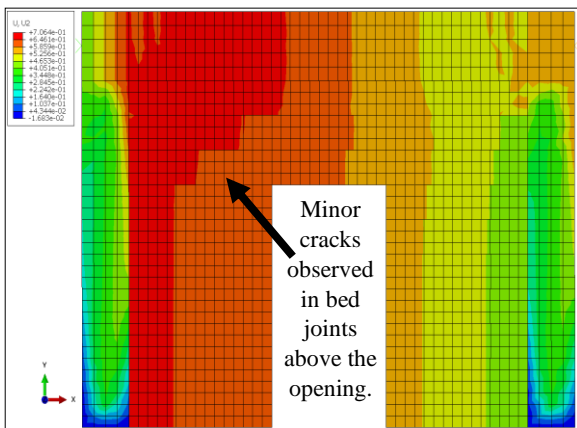


Figure 6.17. Failure patterns of SRS-F1B1

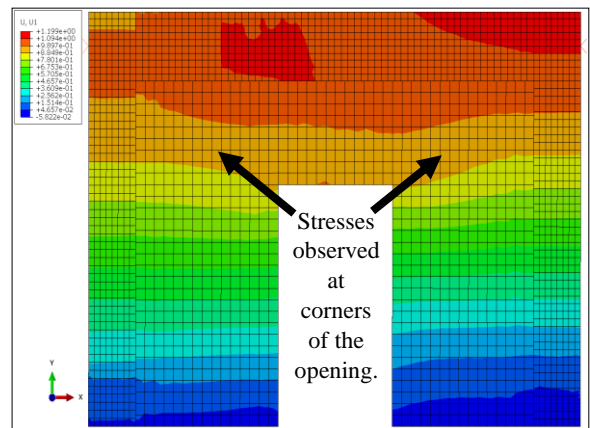


Figure 6.18. Failure patterns of DRS

The URS specimen reduced the maximum deflection by 7.12% compared to the experimental values while the DRS specimen showed a small spike of 6.59%. As can be seen, according to the parametric study conducted, there was not much significant difference between SRS-F2 (133.14 kN) and SRS-F1B1 (138.03 kN) in terms of load-carrying capacity.

The load-carrying capacity of SRS-F1 (118.57 kN) is 28.97% more compared to SRS-B1 (88.56 kN). Regarding strengthening with two layers, SRS-F2 has produced a 30.67% increase in the load-carrying capacity compared to SRS-B2. However, by comparing SRS-F1 (118.57 kN) and SRS-F2 (133.14 kN), the difference in the load-carrying capacity is 11.58%. With regard to SRS-B1 and SRS-B2, the former displayed inferior results around 9.84% compared to the latter in terms of load-carrying capacity while in terms of deflection, 15.91% more was observed. Hence, from the parametric study conducted, it can be observed that strengthening on the front face of the masonry wall proved to be more effective compared to the strengthening on the back face because of the less surface area covered with the TRM fibers. Less surface area of the masonry wall was covered on the backside because the alignment of the surface of the surrounding RC column was not along with the surface of the infill wall with a difference of 107 mm. whereas, on the front side, the wall's surface was constructed in alignment with that of the RC frame.

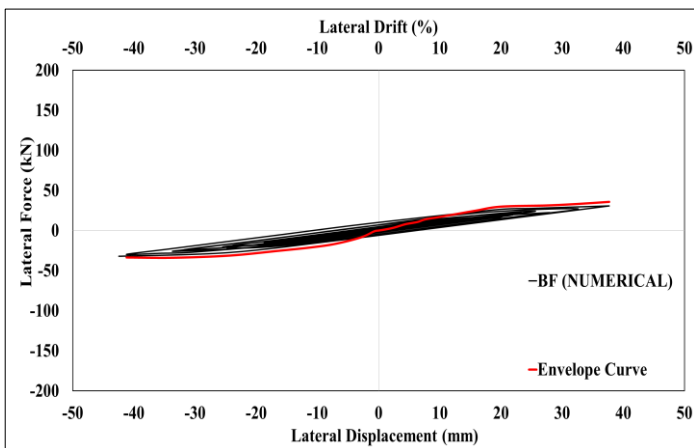


Figure 6.19. Hysteresis Curve of the BF

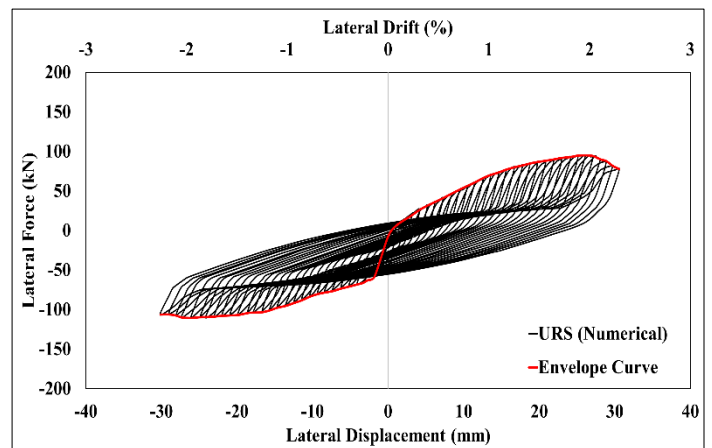


Figure 6.20. Hysteresis Curve of URS

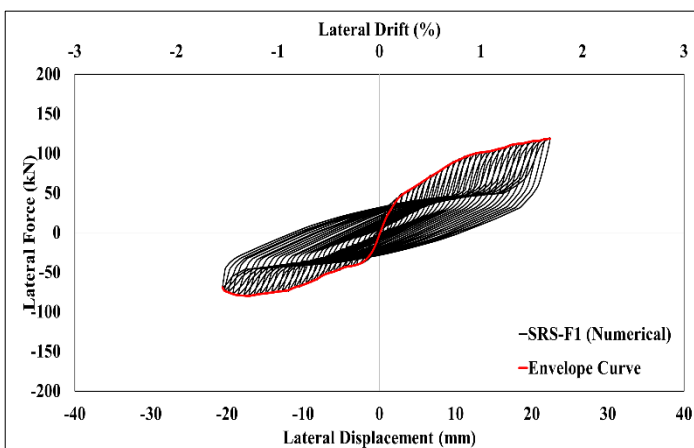


Figure 6.21. Hysteresis Curve of SRS-F1

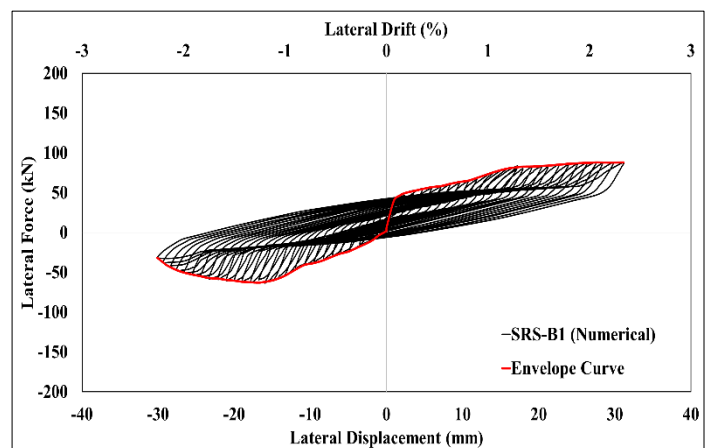


Figure 6.22. Hysteresis Curve of SRS-B1

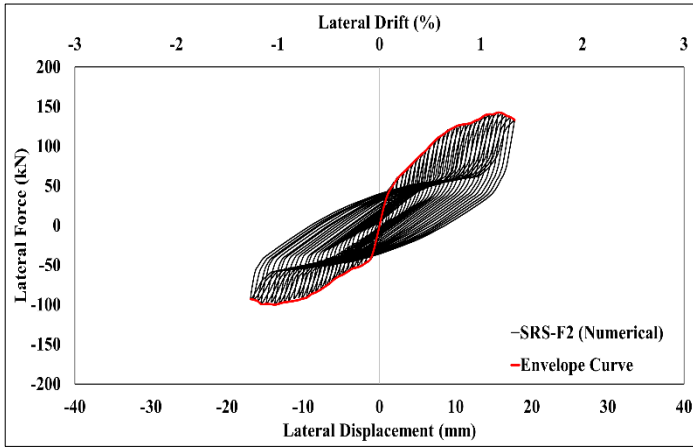


Figure 6.23. Hysteresis Curve of SRS-F2

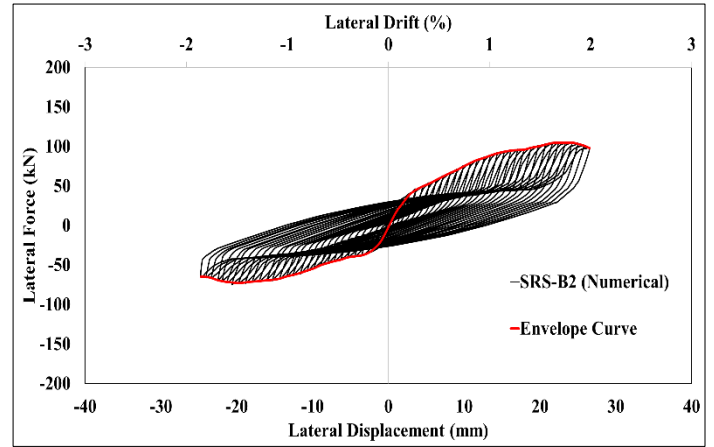


Figure 6.24. Hysteresis Curve of SRS-B2

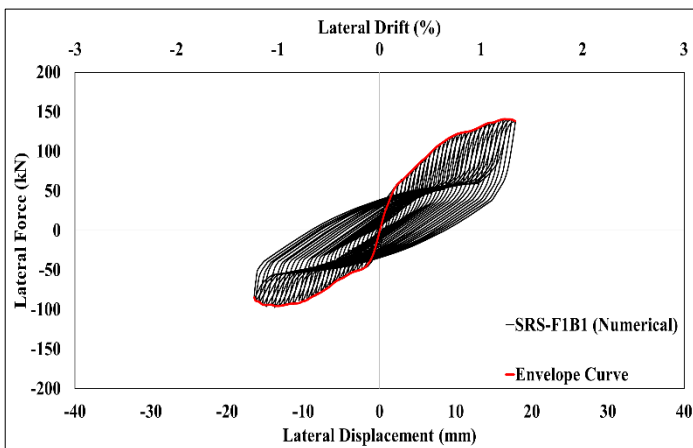


Figure 6.25. Hysteresis Curve of SRS-F1B1

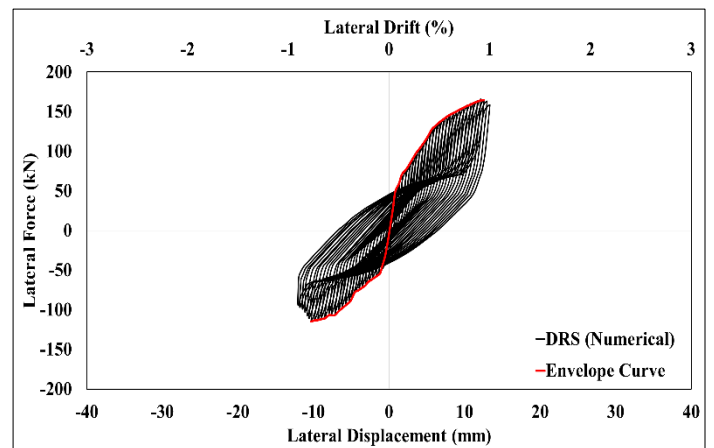


Figure 6.26. Hysteresis Curve of DRS

6.5.1. Stiffness and Energy Dissipation

The first hysteretic loop's slope of the first linear loading limb (the displacement equivalent to 1 mm displacement) was used to compute the initial stiffness (K_i) of the tested frames. The URS specimen's rigidity has been shown to grow initially and steadily decrease from 5 mm to 10 mm. The URS specimen's rigidity progressively reduced from 10 mm until the test's conclusion. Similar to this, the DRS specimen's stiffness increased abruptly and then progressively reduced up to a displacement of 15 mm. Because testing on strengthened test frames terminated at drifts of 0.75 to 1.10%, the stiffness diminution was inconsequential in contrast to the conventional structure. The bracing action and the infill-frame composite behaviour were identified as the causes of the higher initial stiffness of the infilled RC frame (URS) and retrofitted frames.

Abaqus typically over-predicts the maximum lateral displacement and the maximum loading-bearing capacity of the specimens by a maximum of 5% when compared to the testing data. (This may result from idealizations created in ABAQUS, such as the bricks' smoothness, the materials' shortage of deficiencies, or the mortar material's total absence as a means of simulating the behaviour of the masonry wall).

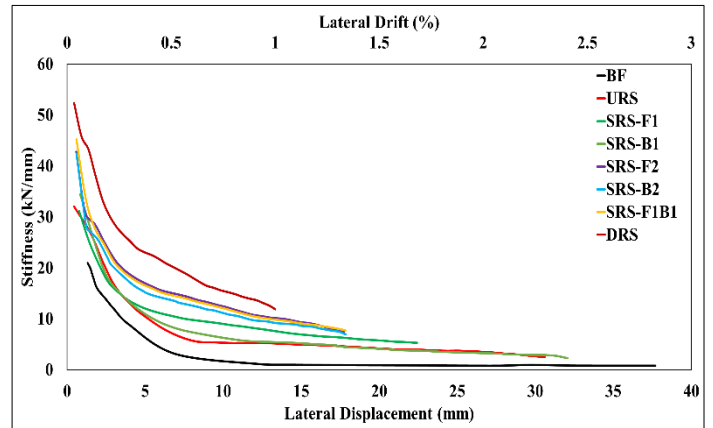
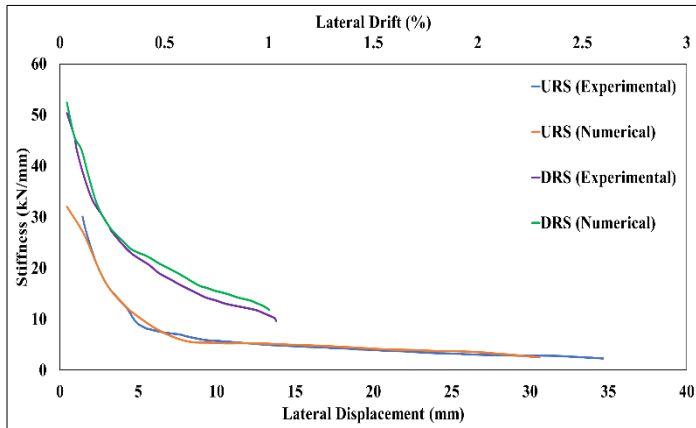


Figure 6.27. Stiffness degradation of URS and DRS

Figure 6.28. Stiffness degradation of all numerical models

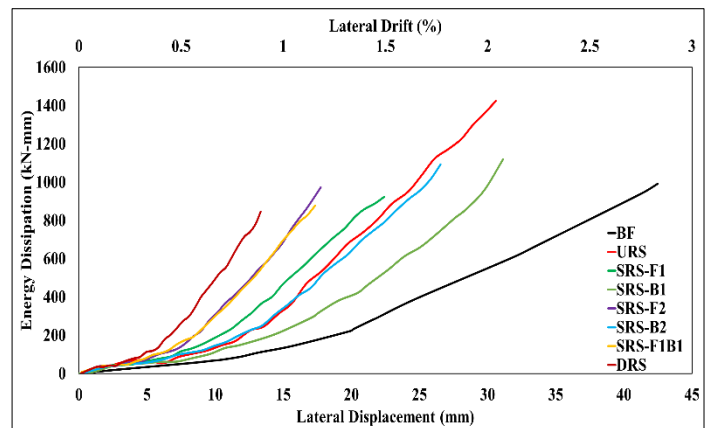
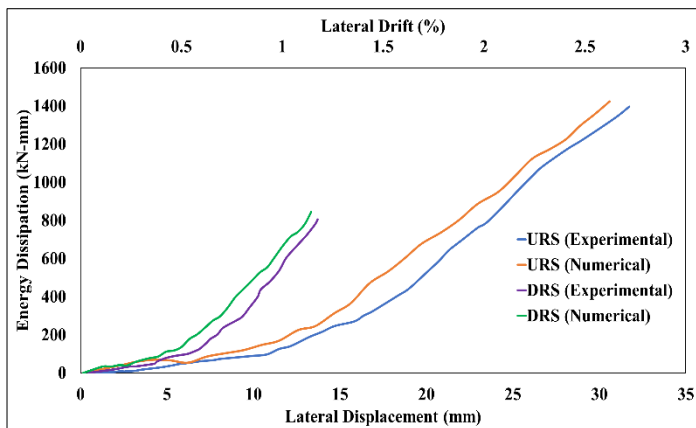


Figure 6.29. Energy dissipation of URS and DRS

Figure 6.30. Energy dissipation of all numerical models

Figures 6.27 – 6.30 display the stiffness degradation and energy dissipation curves obtained in the numerical analysis. The stiffness decreases with an increase in the displacement. The specimen's hysteretic loops were used to calculate the stiffness values from peak to peak. The load-displacement curve's maximum load points are connected at each displacement level by a line whose slope is determined, and the peak-to-peak stiffness at each displacement level is determined. The URS specimen's rigidity has been shown to grow initially, steadily decrease from 5 mm to 10 mm, and then progressively reduced from 10 mm until the test's conclusion.

Similarly, the DRS specimen's stiffness increased abruptly. It then progressively reduces up to a displacement of 15 mm.

The experimental results suggested strengthening technique significantly increased the infill walls' capacity by up to 66% to support in-plane loads. The main damage pattern observed in the TRM-enhanced test specimens was scattered cracking on the exterior of the TRM matrix, with no signs of fiber rupture or TRM deboning. Every test frame with TRM reinforcement exhibited this separation fracture. Altogether, it can be claimed that the seismic behaviour of RC bounding frames with burnt red clay masonry walls that were seismically vulnerable was successfully enhanced by greater than fifty percent in terms of carrying capacity by using TRM as a strengthening material. The eventual increase in the lateral strength, the initiation of cracking, and the final damage were significantly postponed due to the implementation of the TRM. Hence, the force and the associated displacements are displayed in Table 6.3. Reduced vertical compressive load, as is well known, reduces the resistance due to friction caused by shear slipping on mortar bed joints, which lowers energy dissipation and narrows hysteresis loops. Previous research (P G Asteris, 2003; Mondal & Jain, 2008) indicates that the RC surrounding frame contributes around 11% to the infilled masonry's lateral stiffness without openings. The lateral stiffness of infilled masonry diminishes with an increasing number of openings.

6.6. EXPRESSION TO DETERMINE THE LOAD-CARRYING CAPACITY OF THE SPECIMEN

Empirical equations are proposed to determine the load-carrying capacity of the eight 1:2.5 scaled one-bay one-story RC masonry test specimens including the retrofitted specimen that had been modeled for the parametric study considering the location and number of layers of the TRM fiber. The factors employed in the formula represent the engineering/experimental constants derived with respect to the unretrofitted specimen (URS) which is constructed without any retrofitting. Hence, the engineering constants will be increased according to the number of layers applied on the surface area of the masonry wall specimen, which is also called the scaling factor.

The following expression determines the load-carrying capacity of the URS specimen:

$$\frac{(A_s - A_0) \times t_w \times \Delta \times f_{ck \text{ brick}}}{\pi \times (E_{conc} - E_{brick}) \times 3.4} \times 1.1 \quad (8)$$

The following expression determines the load-carrying capacity of the SRS-F1 specimen:

$$\frac{1}{2\pi} \times \frac{(A_s - A_o) \times t_w \times \Delta \times f_{ck \text{ brick}} \times A_f}{(E_{conc} - E_{brick}) \times E_f \times 3.4} \times 3.2 \quad (9)$$

The following expression determines the load-carrying capacity of the SRS-B1 specimen:

$$\frac{1}{2\pi} \times \frac{(A_s - A_o) \times t_w \times \Delta \times f_{ck \text{ brick}} \times A_f}{(E_{conc} - E_{brick}) \times E_f \times 3.4} \times 2.4 \quad (10)$$

The following expression determines the load-carrying capacity of the SRS-F2 specimen:

$$\frac{1}{2\pi} \times \frac{(A_s - A_o) \times t_w \times \Delta \times f_{ck \text{ brick}} \times A_f}{(E_{conc} - E_{brick}) \times E_f \times 3.4} \times 3.8 \quad (11)$$

The following expression determines the load-carrying capacity of the SRS-B2 specimen:

$$\frac{1}{2\pi} \times \frac{(A_s - A_o) \times t_w \times \Delta \times f_{ck \text{ brick}} \times A_f}{(E_{conc} - E_{brick}) \times E_f \times 3.4} \times 2.6 \quad (12)$$

The following expression determines the load-carrying capacity of the SRS-F1B1 specimen:

$$\frac{1}{2\pi} \times \frac{(A_s - A_o) \times t_w \times \Delta \times f_{ck \text{ brick}} \times A_f}{(E_{conc} - E_{brick}) \times E_f \times 3.4} \times 3.6 \quad (13)$$

The following expression determines the load-carrying capacity of the DRS specimen:

$$\frac{1}{2\pi} \times \frac{(A_s - A_o) \times t_w \times \Delta \times f_{ck \text{ brick}} \times A_f}{(E_{conc} - E_{brick}) \times E_f \times 3.4} \times 4.2 \quad (14)$$

Where, A_s = Area of specimen (area of RC frame and area of infill wall); A_o = Area of opening in infill wall; t_w = thickness of infill wall; Δ = maximum drift (%); E_{conc} = concrete elastic modulus, E_{brick} = infills elastic modulus, $f_{ck \text{ brick}}$ = infills compressive strength, A_f = cross-sectional area of fibers, E_f = tensile elastic modulus of fibers, values are given in Table 6.1.

According to the numerical data, the URS specimen outperformed the experimental values by 6.69% in the push direction and 4.76% in the pull direction. The numerical results for the DRS specimen showed a 3.59% increase in the pull direction and a 5.45% increase in lateral force in the push direction. The URS specimen reduced the maximum deflection in the push direction by 7.12% and the maximum deflection in the pull direction by 3.24% compared to the experimental values. The numerical results for the DRS specimen showed a maximum deflection in the push direction of 6.59% and an increase in the pull direction of 4.72%.

Table 6.3. Experimental, numerical, and analytical results of all the models

Results Specimen	Experimental		Analytical								
	P_{max} (kN)	u_{max} (mm)	P_{max} (kN)	K_{si} (kN/mm)	K/K_1	E (kN-mm)	E/E_1	F_s (kN)	F/F_1	R_s (kN)	R/R_1
BF	49.85	39.69	-	11.62	-	-	-	49.85	-	-	-
URS (Experimental)	89	34.34	98.48	30.06	-	2.52	-	89	-	270.37	-
URS	95.17	31.98		32.06	1	2.42	1	95.17	1	285.55	1
SRS-F1	118.57	22.42	119.28	34.14	1.06	3.38	1.39	118.57	1.25	321.71	1.13
SRS-B1	99.56	31.14	89.46	33.49	1.04	3.22	1.33	99.56	1.05	309.62	1.08
SRS-F2	138.03	17.75	141.65	45.24	1.41	3.62	1.49	138.03	1.45	345.47	1.21
SRS-B2	104.73	26.55	96.91	42.46	1.32	3.43	1.42	104.73	1.10	334.26	1.17
SRS-F1B1	133.14	17.84	134.19	44.77	1.39	3.51	1.45	133.14	1.39	362.98	1.27
DRS (Experimental)	147.50	14.25	156.56	50.36	-	3.29	-	147.50	-	373.04	-
DRS	155.77	13.34		52.36	1.63	3.84	1.59	155.77	1.64	378.48	1.33

P_{max} = maximum lateral load, u_{max} = maximum lateral displacement, K_{si} = initial stiffness, E = energy dissipation capacity, F_s = Shear Force, R_s = Shear Resistance

Nonetheless, the numerical analysis values are significantly higher than the values found in the experimental data when it comes to the values of both maximum load and the maximum lateral displacement. Analytically, it can be observed that the conventional specimen (URS) was noted to be 10% more compared to experimental values in terms of load-carrying capacity. In the case of the DRS specimen, a 6% difference was observed in terms of load-carrying capacity. With regard to the shear force, the values are same as the maximum load carrying capacity of the specimen, because the shear force is considered as the component of the compression diagonal of the infill wall considering the push direction during applying the cyclic load. In other words, the horizontal component of the force (resultant) in the compression diagonal is considered as the shear force of the infill wall which is the counterforce, or the reaction force of the lateral load applied on the test specimen. Hence, both the factors contain the same values. Masonry shear strength (v_{me}) can be calculated from (ASCE, 2000) which is as follows.

$$\text{For URM components, } v_{me} = \frac{0.75 (0.75v_{te} + \frac{P_{CE}}{A_n})}{1.5}$$

Where,

v_{te} = standard in-situ bed joint shear tests can be used to establish the average bed joint shear strength (Shapiro et al., 2000),

P_{CE} = applied compressive force of gravity that is anticipated for a wall panel,

A_n = area of the wall panel's cross-section

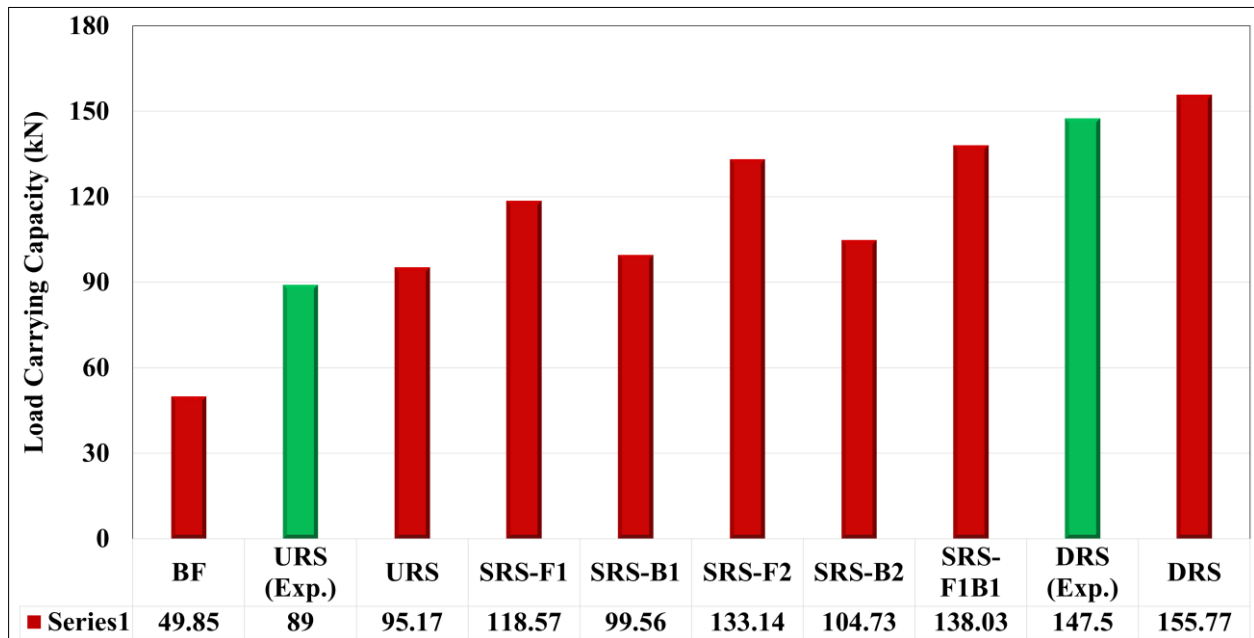


Figure 6.31. Load carrying capacity of the models determined using numerical models

According to the hysteresis graphs acquired from the linear regression analysis conducted, the average value of the coefficient of determination (R^2) is determined to be 0.965, which evaluates how well the numerical model predicts the results. Figure 6.31 plots the load carrying capacity of the MIW strengthened with TRM considering different parameters as discussed earlier. The y-axis of the bar chart shows the value of the load-carrying capacity of the particular specimen whereas the x-axis of the bar chart shows the name of the model along with the legend attached to it. The values for the graph are taken from Table 6.3.

6.7. COST ANALYSIS

The major goal of this section is to evaluate the costs and benefits associated with using TRM to strengthen the MIW for reducing the infill walls damage and prevention of the IP failure. For this, it was assessed the effectiveness of the TRM to strengthening three 2/5th scale masonry infill walls was assessed and explained in the previous Chapters. Based on the testing campaigns and the specimens' strengthening techniques, the results in terms of strength,

deformation and energy dissipation capacity are already discussed in the preceding Chapters. Based on these factors, the cost to conduct an experiment of these specimens is deeply analyzed, estimation of the percentage of each component is computed.

6.7.1. Quantification of the Test Specimen

This section aims to quantify the costs of the MIW specimen adopted in the experimental campaigns carried out. The global cost of each solution comprises the cost of the material used, workmanship and the cost of the equipments used. Table 6.3 summarizes costs of each construction material used for the construction of the specimen before first wave of Covid-19 (February 2020) and after the second wave of Covid-19 (October 2021). This cost considers all the materials used such as cement, sand, aggregates, steel rebars of different diameters and brick units. The areas and volumes of each structural and non-structural component are calculated and tabulated. The TRM was bought for once; hence, its cost is independent of the Covid-19 timeline.

Table 6.4. Cost of construction materials before and after Covid-19

Items	Size/Grade/Type	UNIT	Market Amount (₹)	
			February 2020	October 2021
Cement	43 OPC (kg)	Per bag (50 kg)	360	400
Sand	Crusher (kg)	Per tractor	4200	4600
Aggregate	20 mm (kg)	Per tractor	6700	7500
Bricks	Class II	Per brick	6	7
Steel	16 mm (m)	Per kg	43.5	59.75
Rebars	12 mm (m)	Per kg	43	58.5
Steel	10 mm (m)	Per kg	45	561
Links	8 mm (m)	Per kg	46	62
	6 mm (m)	Per kg	48	62

The relative component costs were computed by performing the ratio between each component cost with the global cost helping to understand the relevance of each one, which are plotted in Figure 6.32. From this analysis, it is possible to observe that the cost of construction materials used for a single specimen is approximately Rs. 24,000 excluding the transportation costs, workmanship, and the miscellaneous costs (Table 6.5).

Table 6.5. Cost estimation for construction materials

Scale	Components	Cross-Section		Length (m)	Clear Cover (mm)	Main Rein (mm)	Stirrups (mm)
		Width (m)	Depth (m)				
1:2.5	Beam	0.185	0.24	1.84	10	12	Ø 8 - 50 c/c
	Column	0.185	0.21	1.2	10	12	Ø 8 - 50 c/c
	Plinth	0.275	0.4	2.6	20	12 - top 16 - bot	Ø 10 - 170 c/c - midspan Ø 10 - 200 c/c – both ends
1:1	Beam	0.25	0.45	4.6	20	12	Ø 8 - 50 c/c
	Column	0.25	0.4	3	20	12	Ø 8 - 50 c/c
	Plinth	0.55	0.45	6.5	25	12 - top 16 - bot	Ø 10 - 170 c/c - midspan Ø 10 - 200 c/c – both ends
QUANTITY (kg) or (m)							
Items	Size/ Grade/ Type	QUANTITY (kg) or (m)		TOTAL QUANTITY		Amount (₹)	
		Reduced Scale (1:2.5)	Full Scale (1:1)	Reduced Scale (1:2.5)	Full Scale (1:1)	Reduced Scale (1:2.5)	Full Scale (1:1)
Cement	OPC 43	205 kg	1200 kg	5 Bags	24 Bags	2000	9600
Fine Aggregate	Crusher	341 kg	2000 kg	4 quintal	20 quintal	4600	9200
Coarse Aggregate	20 mm	618 kg	3620 kg	7 quintal	37 quintal	7500	15000
Bricks	Class II	100 nos.	625 nos.	500 nos.	1000 nos.	3500	7000
Steel	16 mm	12 m	30 m	12 m (or) 19 kg	30 m (or) 48 kg	1135.25	2868
Rebars	12 mm	50 m	90 m	50 m (or) 45 kg	90 m (or) 81 kg	2632.5	4738.5
Steel	10 mm	24 m	58 m	24 m (or) 15 kg	58 m (or) 36 kg	915	2196
Links	8 mm	46 m	96 m	46 m (or) 19 kg	96 m (or) 39 kg	1178	2418
TOTAL						23,462	50,327

The costs are calculated based on the volumes of the beam, columns, and the foundation beam. The dimensions are given in Table 6.4 based on which the cost per specimen is evaluated and the total amount for all the materials is summed up and displayed at the end of the table. Additional costs that include transportation, workmanship, and other costs, are given in Table 6.5, which vary depending on the region, distance, and load per trip.

Table 6.6. Transportation, workmanship, and other costs

Transportation (depends on distance, location, and load)			
Cement	No. of bags	Per load	100
Sand	Quintal/cubic feet	Per tractor	150
Aggregate	Quintal/cubic feet	Per tractor	150
Bricks	No. of bricks	Per tractor	200
Steel bars	Distance	Per tractor	200
TRM	Distance	Per km	720
Workmanship			
Steel Tier	Bar bending	Per day	650
Mason	Concrete Work	Per day	650
Helper	Concrete Work	Per day	500
Drilling Work			
Rent		Per hour	50
Worker		Per day	150

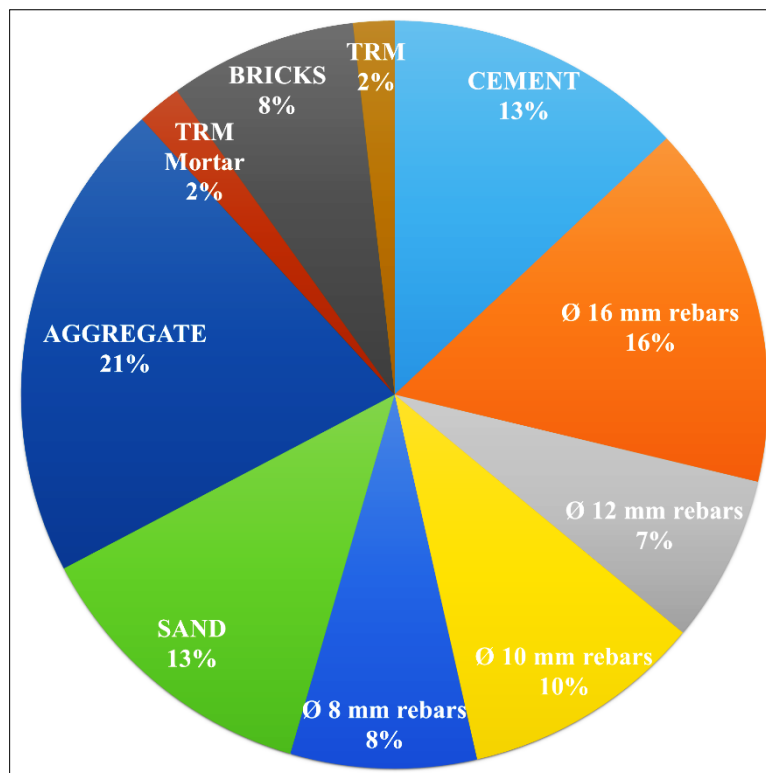


Figure 6.32. Relative component costs

6.7.2. Costs Quantification of MIW Strengthening Using TRM

This section aims quantifying the costs of the TRM solutions adopted for the two experiments and the parametric study elaborated in Chapter 5 and Section 6.4, respectively. Cost-benefit analysis is of full importance to understand if expensive strengthening TRM solutions means better performance of the MIW under IP loadings. For this, the cost of each strengthening solution was compared with respect to the factors considered in the parametric study i.e., number of layers and location of the TRM strengthening fibers which are tabulated in Table 6.5. Figure 6.33 plots the cost comparison of the MIW strengthened with TRM considering cost of the construction materials, TRM, the mortar used for TRM and the calculated total cost.

Table 6.7. Costs of Reduced Scale and Full-Scale Specimen Strengthened with TRM

Items	Size/ Grade/ Type	QUANTITY (kg) or (m)		TOTAL QUANTITY		Amount (₹)				
		Reduced Scale (1:2.5)	Full Scale (1:1)	Reduced Scale (1:2.5)	Full Scale (1:1)	Reduced Scale (1:2.5)	Full Scale (1:1)			
TRM	50 m x 1 m (L x B)	7 m ²	21 m ²	770	2310	1 roll = 50 m ²	5500			
TRM mortar (DRS)	Per bag (30 kg)	120 kg	600	4 Bags	36 Bags	3,300	30,341			
Specimen	AREA OF TRM ON THE SPECIMEN (m ²)		COST OF MATERIALS (₹)		Cost of TRM (₹)		Cost of TRM mortar (₹)		Total Cost (₹)	
	Reduced Scale (1:2.5)	Full Scale (1:1)	Reduced Scale (1:2.5)	Full Scale (1:1)	Reduced Scale (1:2.5)	Full Scale (1:1)	Reduced Scale (1:2.5)	Full Scale (1:1)	Reduced Scale (1:2.5)	Full Scale (1:1)
BF	-	-	19,962	43,327	-	-	-	-	19,962	43,327
URS	-	-	23,462	50,327	-	-	-	-	23,462	50,327
SRS-F1	3.6	16.9			5500	5500	1682	7939	80,971	87,228
SRS-B1	2	15.4			937	7232	80,226	86,521		
SRS-F2	7.2	33.7			3364	15878	82,653	95,167		
SRS-B2	4	30.7			1875	14463	81,164	93,752		
SRS-F1B1	5.6	32.2			2619	15171	81,908	94,460		
DRS	11.2	64.36			5239	30341	84,528	1,09,630		

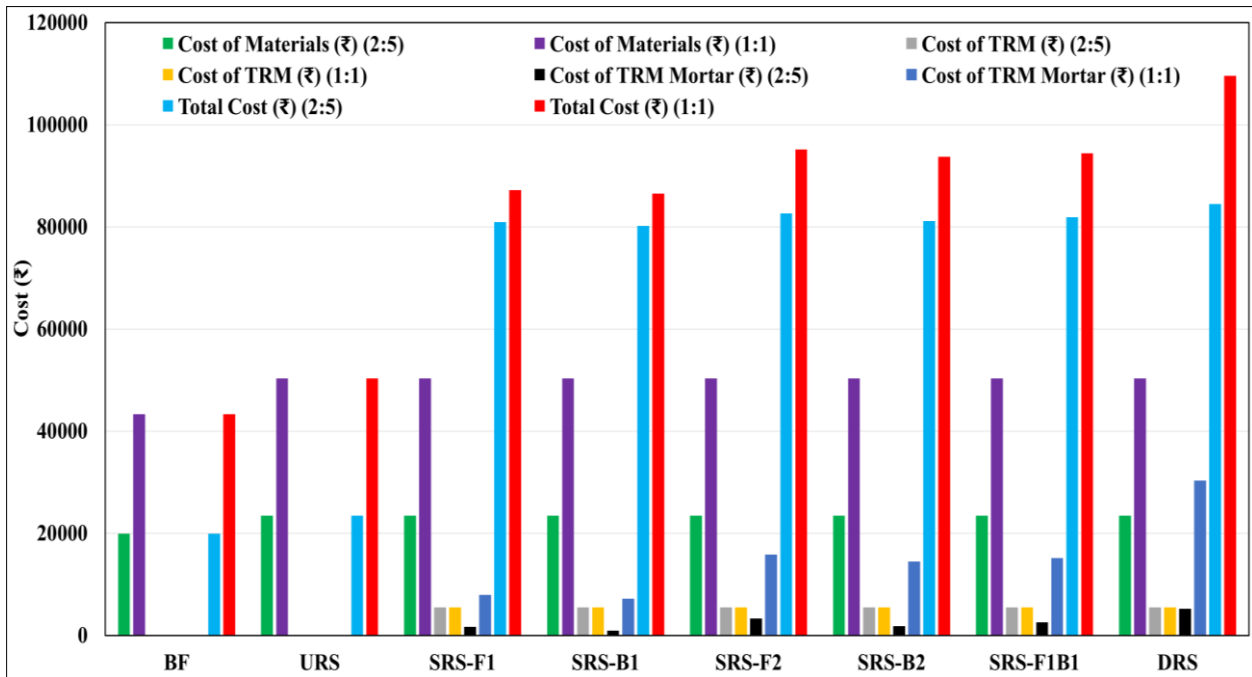


Figure 6.33. Cost comparison of MIW strengthened with TRM considering different parameters

6.8. SUMMARY

A numerical study was carried out to simulate the in-plane behaviour of eight 1:2.5 scaled one-storey one-bay masonry-infilled reinforced concrete (RC) frames retrofitted with textile-reinforced mortar (TRM). The study used ABAQUS finite element analysis (FEA) software and a three-dimensional (3-D) finite element method. Employing a ductile design and details, the TRM-retrofitted structure encountered in-plane displacement-control cyclic loads during the test. This study assesses how accurately a representative numerical model can replicate the results of an experimental test. Parametric research was conducted following the numerical model's validation. To develop a suitable numerical model, suitable constitutive models based on the concrete damage plasticity (CDP) approach were used to characterize the nonlinear response of TRM, masonry infill, steel, and concrete. The numerical model demonstrated accurately the ability to simulate the in-plane (IP) behaviour of the modified RC frame with infill walls, including its initial stiffness, deterioration, deformation-resisting ability, and failure patterns. Furthermore, a parametric study was conducted to determine the significance of the full-bond scenario between the RC frame infilled with masonry and the TRM considering: (1) the location of the strengthening material on the specimen and (2) the number of layers of the strengthening material. All retrofitted wall specimens showed a

considerable improvement in the in-plane performance; some features of the wall's behaviour were found to be strongly influenced by the parameters under examination. It can be observed that the specimen with two layers of TRM on both sides of the infill wall (DRS) exhibit the maximum lateral load carrying capacity and maximum deflection resisting characteristics while the other retrofitted specimens controlled the deflection to some extent and significantly enhancing the load carrying capacities of the masonry system. Finally, cost analysis and predictions were reported which display the cost required to construct a test specimen for an experiment with different scales of the specimen (reduced scale and full-scale) that includes the construction cost, transportation costs, workmanship, and miscellaneous costs.

CHAPTER 7

CONCLUSIONS AND FUTURE STUDY

7.1. CONCLUSIONS

Masonry infill walls (MIW) are important non-structural elements of modern multi-storey frame buildings. The in-plane seismic vulnerability of such infill wall remains also in the modern structures complying with the recent seismic codes, which can result in huge economic losses besides safety threats to the people. The in-plane behaviour of infills during the earthquake is still difficult to predict. Therefore, in this study, attention was given to understanding the response of infill walls to earthquake-induced in-plane seismic forces.

Initially, this Chapter discusses the numerical simulation outcomes of the wall panel model with the experimental results given by [N. Ismail et. al. 2018], followed by the results of the experimental investigation discussed in the Chapter 4 and finally, the conclusions of the parametric study conducted to determine the significance of the full-bond scenario between the RC frame infilled with masonry and the textile reinforced mortar (TRM) are presented. Furthermore, recommendations are also provided for the future scope of the study.

In this work, the IP performance of non-ductile RC frames with strengthened masonry infills is demonstrated via a simulation of a numerical model that was employed in the ABAQUS finite element analysis (FEA) program. This study explored the numerical simulation of the wall panel model with the experimental data to create a straightforward strut model for a complete structure and predict structural performance, including maximum deflection and ultimate strength using the proposed empirical equations (section 4.7) for evaluating the structural integrity of infilled frames. As mentioned in Table 3.5, the maximum load-carrying capacity of the MIW frame systems is validated with both the numerical simulation and the proposed analytical empirical equations.

Based on the results of the experimental analysis as mentioned in Section 4, analysis, eight models—the bare frame (BF-1), the infill frame (IF-2), and the masonry infill frame reinforced with carbon, basalt, and glass fiber FRCM bands spaced 1/3 and 1/6 the diagonal length apart were employed for the numerical validation study. To simulate reinforced concrete

(RC) frames reinforced with fiber reinforced cementitious matrix (FRCM) and filled with masonry under in-plane (IP) cyclic loads, this work focuses on the constitutive model for numerical modeling of all the structural system's components. Numerous constitutive models that are based on continuum damage mechanics, elasticity, and plasticity theories may be found in the literature. The obtained numerical results were then compared with the analytical formulae and were convinced with the experimental data, for which numerous input parameters were adjusted as necessary to provide an acceptable output. For each test, backbone curves were plotted by interconnecting the highest excursion points of each cycle, as illustrated in Figure 3.31.

- It is possible to estimate how infilled frame models would behave under hysteresis using cyclic displacement control analysis.
- To evaluate the impact of each feature on the frame's IP response, numerical models are created for the bare frame, the frame with a fully solid infill wall, and the frame with an infill wall reinforced with FRCM.
- The experimental geometry was as closely matched as feasible in the FRCM-retrofitted masonry infill RC frame models utilized in this investigation.
- In terms of load-displacement relationships, the computational calculations and analytical results are quite close to the actual data (Table 5).
- The results of the trials were consistent with the failure patterns anticipated by the numerical models. ABAQUS' predictions for the specimens' maximum load-bearing capacity and maximum lateral displacement are slightly inflated, but they may still be used moving forward because they are roughly in a tie with the experimental outcomes.
- In terms of the crucial characteristics, such as load-carrying capacity, deformation capacity, and cracking patterns, the results of the calculations and experiments of the FRCM-strengthened masonry-infilled RC frame show outstanding consistency.
- Regarding the landmark and trajectory of the cracks, the fracture patterns of the FRCM specimen exhibit satisfactory concurrence with the results of the experiment.

The creation of a multi-crack pattern and the inclusion of an effective load transmitting mechanism at the bottom level in FRCM jacketing have shown beneficial in large shear deformations through experimental and computational research.

An experimental program examined the in-plane behaviour of ductile reinforced concrete frames with fabric-reinforced cementitious matrix and adhering burnt clay red brick

infill. Two one-story, one-bay test frames were exposed to a constant vertical axial load of 100 kN and subjected to a quasi-static, cyclic in-plane loading history. Glass fiber was integrated into the test frame. Among the significant discoveries are the following:

- The suggested strengthening technique significantly increased the infill walls' capacity by up to 66% to support in-plane loads.
- The failure that began at the bottom masonry-frame contact in the TRM-reinforced test frames indicated the early separation of the masonry from the surrounding frame.
- The main damage pattern observed in the TRM-enhanced test frames was distributed cracking on the surface of the TRM matrix, with no signs of fiber slippage rupture or TRM deboning. Every test frame with TRM reinforcement exhibited this separation fracture, with a lateral drift of approximately 0.4 - 0.6%.
- TRM has generally been successful in improving the seismic performance of RC frames with burnt clay red brick masonry infills that are seismically vulnerable. There was a noticeable delay in the onset of cracking and damage, and the ultimate gain in lateral strength was between 50 and 70 percent.

Altogether, it can be claimed that the seismic performance of RC frames with burnt red clay masonry infills that were seismically vulnerable was successfully enhanced by more than 50% in terms of load-carrying capacity by using TRM as a strengthening material. The eventual increase in the lateral strength, the initiation of cracking and the final damage were significantly postponed due to the implementation of the TRM.

Using a finite element framework and the simplified micro-modelling technique, the masonry structure is simulated at the infill component level. The numerical model demonstrated accurately the ability to simulate the in-plane behaviour of the RC frame with infill walls, including its initial stiffness, deterioration, deformation-resisting ability, and failure patterns. Additionally, a parametric study was conducted to determine the significance of the RC frame infilled with masonry and the TRM considering: (1) the location of the strengthening fiber material on the specimen and (2) the number of layers of the strengthening material. All modified walls showed a considerable improvement in in-plane performance, with the parameters under examination having a major impact on certain elements of the wall's behaviour. Empirical equations were developed analytically to assess the specimen's load-carrying capability with opening which let the users/customers select the configuration of the TRM according to on their requirement and also depending on the seismic hazard of the

particular area. It can be observed that the specimen with two layers of the TRM fiber on both sides of the infill wall exhibit the maximum lateral load carrying capacity and maximum deflection resisting characteristics while the other retrofitted specimens controlled the deflection to some extent and significantly enhancing the load carrying capacities of the masonry system. It can be observed that DRS strengthening pattern was the best retrofit option in terms of boosting strength in contrast to singly retrofitting scheme. With regard to the single retrofitting scheme, the strengthening of the front face of the specimen offered relatively best results when compared to the retrofitting on the backside of the masonry wall. Among the significant discoveries are the following:

- The suggested strengthening technique significantly increased the infill walls' capacity by up to 66% to support in-plane loads.
- The parametric study suggests that the strengthening on the front face of the specimen by applying one layer of TRM (SRS-F1) is contributing 28.97% more compared to the strengthening on the back face of the masonry specimen (SRS-B1) which was less effective about 32.56% increase in terms of the deflection resisting capacity.
- The parametric study suggests that the strengthening on the front face of the specimen by applying two layers of TRM (SRS-F2) is contributing 33.26% more compared to the strengthening on the back face of the masonry specimen (SRS-B2) which was less effective about 39.73% in terms of the deflection resisting capacity.
- The parametric study suggests that the strengthening on the front face and back face of the specimen by applying one layer of TRM (SRS-F1B1) is contributing 12.03% more compared to the strengthening with two layers on both front face and back face of the masonry specimen (DRS) which was less effective about 28.86% in terms of the deflection resisting capacity
- TRM has generally been successful in improving the seismic performance of RC frames with burnt clay red brick masonry infills that are seismically vulnerable. There was a noticeable delay in the onset of cracking and damage, and the ultimate gain in lateral strength was between 50 and 70 percent.
- The validation model displayed that the numerical model can precisely simulate the behaviour and predict the capacity of retrofitted masonry-infilled RC frames.

- The difference in the experiment and numerical values was below 10% in terms of maximum lateral load carrying capacity and maximum displacement values, proving that the results of the simulated models agreed with the experimental results.

Altogether, it might be argued that RC frames' seismic performance with burnt red clay masonry infills that were seismically vulnerable was successfully enhanced by greater than fifty percent in terms of carrying capacity by using TRM as a strengthening material. The eventual increase in the lateral strength, the initiation of cracking and the final damage were significantly postponed due to the implementation of the TRM.

7.2. CONTRIBUTIONS OF RESEARCH CONDUCTED

- This thesis contributes to three categories of the research and development of masonry infilled RC frames, i.e., experimental work, numerical work, and analytical work.
- The experiment is conducted on two 1:2.5 scale specimens to understand the cyclic performance of MIW under lateral loading conditions.
- Numerical simulation provides the validation of the experimental hysteresis behaviour.
- Finally, cost analysis for reduced scale and full-scale models is provided to compare the rates, which lets the users/customers select the configuration of the TRM according to their requirements and also depending on the seismic hazard of the particular area.

7.3. LIMITATIONS OF RESEARCH CONDUCTED

- Reduced scale specimens were taken into consideration in the research because of the laboratory's space limitations and the servo-hydraulic actuator's (250 kN) restricted capability.
- In the numerical analysis, a simplified micro-model method was used because there were only a few nodes accessible in the student edition of ABAQUS.
- With respect to the analytical analysis, the suggested equations are empirical equations as they are currently in the research and development stage and will eventually become generalized equations through more study.

7.4. SCOPE OF FUTURE WORK

- Combined in-plane (IP)/out-of-plane (OOP) loads can be taken into consideration for testing MIW, with/without openings and with/without strengthening.
- Investigation into different types of openings, such as both door and window in an MIW can be considered for future research.
- The behavior of MIW on slope surfaces has a lot of scope to be explored for future research.
- Since the empirical equations proposed are limited to the current research, further research will be carried out to propose generalized equations to determine the load carrying capacity of the MIW specimen which can be applied in practical scenarios.

REFERENCES

- Abdel-hafez, L. M., Abouelezz, A. E. Y., & Elzefeary, F. F. (2015). Behavior of masonry strengthened infilled reinforced concrete frames under in-plane load. *HBRC Journal*, *11*(2), 213–223. <https://doi.org/10.1016/j.hbrcj.2014.06.005>
- Abdulla, K. F., Cunningham, L. S., & Gillie, M. (2017). Simulating masonry wall behaviour using a simplified micro-model approach. *Engineering Structures*, *151*, 349–365. <https://doi.org/10.1016/j.engstruct.2017.08.021>
- Adem Doğangün, Ali Ural, Halil Sezen, Y. G. and F. K. F. (2013). The 2011 Earthquake in Simav, Turkey and Seismic Damage to Reinforced Concrete Buildings. *Buildings MDPI*, *3*, 173–190. <https://doi.org/10.3390/buildings3010173>
- Ademovi, N., Hadzima-nyarko, M., Zagora, N., & Stojnovi, V. (2023). Various numerical modeling procedures of XIX-century masonry building. *Engineering Structures*, *301*, 1–19. <https://doi.org/10.1016/j.engstruct.2023.117361>
- Akhoundi, F., Vasconcelos, G., Lourenço, P., Silva, L. M., Cunha, F., & Figueiro, R. (2018). In-plane behavior of cavity masonry infills and strengthening with textile reinforced mortar. *Engineering Structures*, *156*(December 2017), 145–160. <https://doi.org/10.1016/j.engstruct.2017.11.002>
- Al-Chaar, G. (2008). Finite element interface modeling and experimental verification of masonry-infilled R/C frames. *TMS Journal*, 9–29. <https://www.researchgate.net/publication/284415010>
- Ali . Laftah. Abbas and Maan. H. Saeed. (2017). Representation of The Masonry Walls Techniques By Using FEM. *AUSTRALIAN JOURNAL OF BASIC AND APPLIED SCIENCES*, *11*(13), 39–48. <https://doi.org/10.22587/ajbas.2017.11.13.5>
- AlKhaldi, K. H. (2024). 96 - Earthquakes. *Ciottono's Disaster Medicine (Third Edition)*, Elsevier, 601–604. <https://doi.org/https://doi.org/10.1016/B978-0-323-80932-0.00096-3>
- Almusallam, T. H., & Al-salloum, Y. A. (2007). Behavior of FRP Strengthened Infill Walls under In-Plane Seismic Loading. *Journal of Composites for Construction*, *11*(3), 308–318. [https://doi.org/10.1061/\(ASCE\)1090-0268\(2007\)11](https://doi.org/10.1061/(ASCE)1090-0268(2007)11)
- Altin, S., Anil, Ö., Koprman, Y., & Belgin, Ç. (2010). Strengthening masonry infill walls with reinforced plaster. *Proceedings of the Institution of Civil Engineers: Structures and Buildings*, *163*(5), 331–342. <https://doi.org/10.1680/stbu.2010.163.5.331>

- Alwathaf, A. H., Thanoon, W., Alwathaf, A. H., Thanoon, W. A. M., Noorzaei, J., Saleh Jaafar, M., Razali Abdulkadir, M., & Student, P. D. (2003). *ANALYTICAL MODELS FOR DIFFERENT MASONRY SYSTEMS: CRITICAL REVIEW*. 1–12. <https://www.researchgate.net/publication/315381242>
- Amato, G., Cavaleri, L., Fossetti, M., & Papia, M. (2008). Infilled Frames: Influence of Vertical Load On The Equivalent Diagonal Strut Model. *Proceedings of 14th WCEE, Beijing, China. CD-ROM, Paper, 05–01*.
- Amir Saedi Daryan, Masood Ziaei, Ali Golafshar, A. P. and M. A. A. (2009). A Study of the Effect of Infilled Brick Walls on Behavior of Eccentrically Braced Frames Using Explicit Finite Elements Method. *American J. of Engineering and Applied Sciences*, 2(1), 96–104.
- Andonov, A., Baballëku, M., Baltzopoulos, G., Blagojević, N., Brûlé, S., Brzev, S., Carydis, P., Duni, L., Dushi, E., Freddi, F., Gentile, R., Giarlelis, C., Greco, F., Guri, M., Isufi, B., Koçi, R., Lekkas, E., Marinković, M., Markogiannaki, O., ... Wald, D. (2022). *EERI Earthquake Reconnaissance Report : M6 . 4 Albania Earthquake on November*.
- Anić, F., Penava, D., Guljaš, I., Sarhosis, V., & Abrahamczyk, L. (2021). Out-of-plane cyclic response of masonry infilled RC frames: An experimental study. *Engineering Structures*, 238. <https://doi.org/10.1016/j.engstruct.2021.112258>
- Anil, Ö., & Altin, S. (2007). An experimental study on reinforced concrete partially infilled frames. *Engineering Structures*, 29(3), 449–460. <https://doi.org/10.1016/j.engstruct.2006.05.011>
- Arede, H. V. A. F. H. R. J. D.-O. N. V.-P. A. (2017). Seismic performance of the infill masonry walls and ambient vibration tests after the Ghorka 2015 ., *Bull Etin of Earthquake Engineering*, 15, 1185–1212. <https://doi.org/10.1007/s10518-016-9999-z>
- Armin B. Mehrabi, P. Benson Shing, Michael P. Schuller, J. L. N. (1996). EXPERIMENTAL EVALUATION OF MASONRY-INFILLED RC FRAMES. *JOURNAL OF STRUCTURAL ENGINEERING*, 89(3), 228–237.
- Armin Mehrabi, B. B., Member, S., Benson Shing, P., Schuller, M. P., Member, A., & Noland, J. L. (1996). EXPERIMENTAL EVALUATION OF MASONRY-INFILLED RC FRAMES. *JOURNAL OF STRUCTURAL ENGINEERING*, 122, 228–237.
- ASCE. (2000). Fema 356 - Prestandard and Commentary for the Seismic Rehabilitation of Building. *FEDERAL EMERGENCY MANAGEMENT AGENCY, November*, 1–518.
- Asteris, P. G. and C. Z. C. (2011). Failure Modes of In-filled Frames. *Electronic Journal of*

- Structural Engineering*, 11(1), 11–20.
- Asteris, P G. (2003). Lateral Stiffness of Brick Masonry Infilled Plane Frames. *Journal of Structural Engineering (United States)*, 129, 1071–1079. [https://doi.org/10.1061/ASCE0733-9445\(2003\)129:8\(1071\)CE](https://doi.org/10.1061/ASCE0733-9445(2003)129:8(1071)CE)
- Asteris, P G, Cotsovos, D. M., Chrysostomou, C. Z., Mohebkah, A., & Al-chaar, G. K. (2013). Mathematical micromodeling of infilled frames : State of the art. *Engineering Structures*, 56, 1905–1921. <https://doi.org/10.1016/j.engstruct.2013.08.010>
- Asteris, Panagiotis G. (2023). Lateral Stiffness of Brick Masonry Infilled Plane Frames. *Journal of Structural Engineering*, 1071–1081. [https://doi.org/10.1061/\(ASCE\)0733-9445\(2003\)129:8\(1071\)](https://doi.org/10.1061/(ASCE)0733-9445(2003)129:8(1071))
- ASTM. (2009). *Standard Test Method for Compressive Strength of Masonry Prisms*.
- ATC 24. (1992). Guidelines for Cyclic Seismic Testing of Components of Steel Structures for Buildings, Report No. ATC-24. In *Applied Technology Council* (Vol. 24). https://store.atcouncil.org/index.php?dispatch=products.view&product_id=42
- Augenti, N., Parisi, F., Prota, A., & Manfredi, G. (2011). In-Plane Lateral Response of a Full-Scale Masonry Subassemblage with and without an Inorganic Matrix-Grid Strengthening System. *Journal of Composites for Construction*, 15(4), 578–590. [https://doi.org/10.1061/\(asce\)cc.1943-5614.0000193](https://doi.org/10.1061/(asce)cc.1943-5614.0000193)
- Azmat, S., Shah, A., Shahzada, K., Gencturk, B., Ullah, Q. S., Hussain, Z., & Javed, M. (2022). In-plane Quasi-static Cyclic Load Tests on Reinforced Concrete Frame Panels with and without Brick Masonry Infill Walls. *Journal of Earthquake Engineering*, 26(11), 5592–5616. <https://doi.org/10.1080/13632469.2021.1884147>
- B. P. Sinha, M. D. Loftus, R. T. (1979). Lateral strength of model brickwork panels. *Proceedings of the Institution of Civil Engineers*, 67, 191–197.
- Babaeidarabad, S., Caso, F. De, & Nanni, A. (2014). Out-of-plane behavior of URM walls strengthened with fabric-reinforced cementitious matrix composite. *Journal of Composites for Construction*, 18(4), 1–11. [https://doi.org/10.1061/\(ASCE\)CC.1943-5614.0000457](https://doi.org/10.1061/(ASCE)CC.1943-5614.0000457)
- Baek, E. R., Pohoryles, D. A., & Bournas, D. (2024). Seismic assessment of the in-plane/out-of-plane interaction of masonry infills in a two-storey RC building subjected to bi-directional shaking table tests. *Earthquake Engineering and Structural Dynamics*, 1–22.

<https://doi.org/10.1002/eqe.4109>

- Baghi, H., Oliveira, A., Valença, J., Cavaco, E., Neves, L., & Júlio, E. (2018). Behavior of reinforced concrete frame with masonry infill wall subjected to vertical load. *Engineering Structures*, *171*, 476–487. <https://doi.org/10.1016/j.engstruct.2018.06.001>
- Basili, M., Marcari, G., & Vestroni, F. (2016). Nonlinear analysis of masonry panels strengthened with textile reinforced mortar. *Engineering Structures*, *113*, 245–258. <https://doi.org/10.1016/j.engstruct.2015.12.021>
- Bertolesi, E., Milani, G., & Poggi, C. (2016). Simple holonomic homogenization model for the non-linear static analysis of in-plane loaded masonry walls strengthened with FRCM composites. *Composite Structures*, *158*, 291–307. <https://doi.org/10.1016/j.compstruct.2016.09.027>
- Bilotta, A., Ceroni, F., Lignola, G. P., & Prota, A. (2017). Use of DIC technique for investigating the behaviour of FRCM materials for strengthening masonry elements. *Composites Part B: Engineering*, *129*, 251–270. <https://doi.org/10.1016/j.compositesb.2017.05.075>
- Block, B., & Block, M. (2023). DESIGN OF CONCRETE MASONRY INFILL. In *NATIONAL CONCRETE MASONRY ASSOCIATION*. <https://ncma.org/resource/design-of-concrete-masonry-infill/>
- Bournas, D., & Triantafyllou, T. (2008). Innovative seismic retrofitting of old-type RC columns through jacketing: Textile-Reinforced Mortars (TRM) versus Fiber-Reinforced Polymers (FRP). *Proceeding of the 14 World Conference on Earthquake Engineering*, 1–8.
- Breiholz, D. C. (1993). Centercore strengthening system for seismic hazard reduction of unreinforced masonry bearing wall buildings. *12th World Conference of Earthquake Engineering (12WCEE 2000)*, 319–324.
- Brick, R. T. (2023). *Skyscrappers - bricks or terracota*. <https://www.realthinbrick.com/post/history-of-bricks-as-building-materials-in-the-us>.
- Brzev, S. (2007). *EARTHQUAKE-RESISTANT CONFINED MASONRY CONSTRUCTION*.
- BS EN 1998-1:2004 EN 1998-1:2004 (E). (2011). *Eurocode 8: Design of structures for earthquake resistance - Part 1: General rules, seismic actions and rules for buildings Eurocode* (Vol. 1, Issue 2004).

- BUREAU OF INDIAN STANDARD. (2016). *Ductile Design and Detailing of Reinforced Concrete Structures Subjected to Seismic Forces - Code of Practice IS 13920 : 2016* (Issue July).
- Caliò, I., & Pantò, B. (2014). A macro-element modelling approach of Infilled Frame Structures. *Computers and Structures*, *143*, 91–107. <https://doi.org/10.1016/j.compstruc.2014.07.008>
- Cardone, D., & Perrone, G. (2015). Developing fragility curves and loss functions for masonry infill walls. *Earthquake and Structures*, *9*(1), 257–279. <https://doi.org/10.12989/eas.2015.9.1.257>
- Carlo Del Gaudio, Maria Teresa De Risi, Paolo Ricci, G. M. V. (2019). Empirical drift-fragility functions and loss estimation for infills in reinforced concrete frames under seismic loading. *Bulletin of Earthquake Engineering*, *17*, 1285–1330. <https://doi.org/https://doi.org/10.1007/s10518-018-0501-y>
- Carlo Del Gaudioa, Maria Teresa De Risia, Paolo Riccia, G. M. V. (2017). Drift-based fragility functions for hollow clay masonry infills in RC buildings under in-plane seismic actions. *ANIDIS 2017 - XVII Conference, Pistoia and the Pistoia*, 126–138.
- Carozzi, F. G., D'Antino, T., & Poggi, C. (2018). In-situ experimental tests on masonry panels strengthened with Textile Reinforced Mortar composites. *Procedia Structural Integrity*, *11*, 355–362. <https://doi.org/10.1016/j.prostr.2018.11.046>
- Carozzi, F. G., & Poggi, C. (2015). Mechanical properties and debonding strength of Fabric Reinforced Cementitious Matrix (FRCM) systems for masonry strengthening. *Composites Part B: Engineering*, *70*, 215–230. <https://doi.org/10.1016/j.compositesb.2014.10.056>
- Cavaleri, L., & Di, F. (2019). Prediction of the additional shear action on frame members due to infills. *Bulletin of Earthquake Engineering*, *August 2014*, 1–31. <https://doi.org/10.1007/s10518-014-9668-z>
- Chen, X., & Liu, Y. (2015). Numerical study of in-plane behaviour and strength of concrete masonry infills with openings. *Engineering Structures*, *82*, 226–235. <https://doi.org/10.1016/j.engstruct.2014.10.042>
- Chen, Z., Zhou, J., Li, Z., Wang, X., & Zhou, X. (2020). Seismic Behavior of Concrete-Filled Circular Steel Tubular Column – Reinforced Concrete Beam Frames with Recycled Aggregate Concrete. *Applied Sciences (Switzerland)*, *10*(2609), 1–15. <https://doi.org/10.3390/app10072609>

- Chiozzi, A., & Miranda, E. (2017). Fragility functions for masonry infill walls with in-plane loading. *Earthquake Engineering and Structural Dynamics*, 46(15), 2831–2850. <https://doi.org/10.1002/eqe.2934>
- Choudhury, T., & Kaushik, H. B. (2019). Treatment of uncertainties in seismic fragility assessment of RC frames with masonry infill walls. *Soil Dynamics and Earthquake Engineering*, 126(April), 105771. <https://doi.org/10.1016/j.soildyn.2019.105771>
- Chuang, S. W., & Zhuge, Y. (2005). Seismic Retrofitting of Unreinforced Masonry Buildings – A Literature Review. *Australian Journal of Structural Engineering*, 6(1), 25–36. <https://doi.org/10.1080/13287982.2005.11464942>
- Chungman, K., Eunjong, Y., & Minjae, K. (2016). Finite Element Analysis of Reinforced Concrete Masonry Infilled Frames with Different Masonry Wall Thickness Subjected to In-plane Loading. *Journal of the Computational Structural Engineering Institute of Korea*, 29(1), 177–185. <https://doi.org/10.7734/coseik.2016.29.1.85>
- Comartin, C. D., & Rojahn, C. (1996). *ATC-40 Seismic Evaluation and Retrofit of Concrete Buildings* (Vol. 1). APPLIED TECHNOLOGY COUNCIL.
- Crisafulli, F. J., Carr, A. J., & Park, R. (2000). ANALYTICAL MODELLING OF INFILLED FRAME STRUCTURES - A GENERAL REVIEW. *BULLETIN OF THE NEW ZEALAND SOCIETY FOR EARTHQUAKE ENGINEERING*, 33(1), 30–47.
- Curbach, M., & Jesse, F. (n.d.). *High-Performance Textile-Reinforced Concrete*.
- Cyclic, R., Tanjung, J., Hayati, Y., & Medriosa, H. (2019). *Behaviour of Reinforced Concrete Frames with Central Opening Masonry Infill Behaviour of Reinforced Concrete Frames with Central Opening Masonry Infill under Lateral Reversed Cyclic Loading* . January. <https://doi.org/10.1051/mateconf/201925805009>
- D'Ambra, C., Lignola, G. P., Prota, A., Sacco, E., & Fabbrocino, F. (2018). Experimental performance of FRCM retrofit on out-of-plane behaviour of clay brick walls. *Composites Part B: Engineering*, 148(April), 198–206. <https://doi.org/10.1016/j.compositesb.2018.04.062>
- da Porto, F., Donà, M., Verlato, N., & Guidi, G. (2020). Experimental Testing and Numerical Modeling of Robust Unreinforced and Reinforced Clay Masonry Infill Walls, With and Without Openings. *Frontiers in Built Environment*, 6. <https://doi.org/10.3389/fbuil.2020.591985>
- Daniel Abrams. (1996). Effects of Scale and Loading Rate with Tests of Concrete and Masonry

- Structures. *Earthquake Spectra*, 12(1), 13–29.
- Dassault Systemes, 2014. (2014a). *ABAQUS Simulia Abaqus 6.14*.
<http://130.149.89.49:2080/v6.14/books/stm/default.htm?startat=ch04s05ath119.html>
- Dassault Systemes, 2014. (2014b). *ABAQUS Simulia Abaqus 6.14*.
- Dautaj, A. D., & Kabashi, N. (2018). *Proposed analysis model for infilled reinforced concrete frames*.
- Dautaj, A. D., Muriqi, A., Krasniqi, C., & Shatri, B. (2019). Shear resistance of masonry panel in infilled RC frames. *International Journal of Advanced Structural Engineering*, 11(2), 165–177. <https://doi.org/10.1007/s40091-019-0223-7>
- Dawe, J. L., & Seah, C. K. (n.d.). *Behaviour of masonry infilled steel frames*.
www.nrcresearchpress.com
- De Angelis, A., & Pecce, M. R. (2018). Out-of-plane structural identification of a masonry infill wall inside beam-column RC frames. *Engineering Structures*, 173, 546–558. <https://doi.org/10.1016/j.engstruct.2018.06.072>
- De Risi, M. T., Del Gaudio, C., Ricci, P., & Verderame, G. M. (2018). In-plane behaviour and damage assessment of masonry infills with hollow clay bricks in RC frames. *Engineering Structures*, 168(March), 257–275. <https://doi.org/10.1016/j.engstruct.2018.04.065>
- De Risi, M. T., Gaudio, C. Del, Ricci, P., Verderame, G. M., & Verderame, G. M. (2017). *Simplified numerical modelling for hollow clay-masonry infills in RC frames under in-plane seismic loads*. <https://www.researchgate.net/publication/319963262>
- Del Gaudio, C., De Martino, G., Di Ludovico, M., Manfredi, G., Prota, A., Ricci, P., & Verderame, G. M. (2019). Empirical fragility curves for masonry buildings after the 2009 L'Aquila, Italy, earthquake. *Bulletin of Earthquake Engineering*, 17(11), 6301–6330. <https://doi.org/10.1007/s10518-019-00683-4>
- Demetrios, Kakaletsis & Karayannis, C. . (2009). *Experimental Investigation of Infilled Reinforced Concrete Frames with Openings*. *Aci Structural Journal*. Vol. 106. (pp. 132–141).
- Deng, H., & Sun, B. (2016). Finite Element Modeling and Mechanical Behavior of Masonry-Infilled RC Frame. *The Open Civil Engineering Journal*, 10(1), 76–92. <https://doi.org/10.2174/1874149501610010076>
- Deng, M., Zhang, W., & Li, N. (2020). In-plane cyclic loading tests of concrete hollow block

- masonry walls retrofitted with high ductile fiber-reinforced concrete. *Construction and Building Materials*, 238, 117758. <https://doi.org/10.1016/j.conbuildmat.2019.117758>
- Di Domenico, M., De Risi, M. T., Ricci, P., Verderame, G. M., & Manfredi, G. (2021). Empirical prediction of the in-plane/out-of-plane interaction effects in clay brick unreinforced masonry infill walls. *Engineering Structures*, 227, 1–16. <https://doi.org/10.1016/j.engstruct.2020.111438>
- Do, A., Livao, R., Uluda, C. E., Faculty, C. E., Do, A., Livao, R., Do, A., Uluda, C. E., Faculty, C. E., Do, A., Livao, R., Livao, R., Uluda, C. E., & Engineering, C. (2019). *Comparison and assessment of material models for simulation of infilled RC frames under lateral loads*. 71, 45–56.
- Documentation. (2010). *Documentation A. ABAQUS Analysis User's Manual. Materials Other plasticity models Concrete*. 2010;113. ABAQUS Analysis User's Manual.
- Doherty, K., Griffith, M. C., Lam, N., & Wilson, J. (2002). Displacement-based seismic analysis for out-of-plane bending of unreinforced masonry walls. *Earthquake Engineering and Structural Dynamics*, 31(4), 833–850. <https://doi.org/10.1002/eqe.126>
- Dolatshahi, K. M., & Aref, A. J. (2015). *Computational, Analytical, and Experimental Modeling of Masonry Structures*. <http://mceer.buffalo.edu>
- Dolatshahi, K. M., Aref, A. J., Whittaker, A. S., Dolatshahi, K. M., Aref, A. J., & Interaction, A. S. W. (2015). Interaction Curves for In-Plane and Out-of-Plane Behaviors of Unreinforced Masonry Walls. *Journal of Earthquake Engineering*, 19(1), 60–84. <https://doi.org/10.1080/13632469.2014.946571>
- Doudoumis, I. N. (2007). Finite element modelling and investigation of the behaviour of elastic infilled frames under monotonic loading. *Engineering Structures* 29, 29, 1004–1024. <https://doi.org/10.1016/j.engstruct.2006.07.011>
- Dr. Sudhir K Jain, D. C. V. R. M. (n.d.). *EQ05 - IS 1893 commentary part 1: Vol. IITK-GSDMA*.
- Drahansky, M., Paridah, M. ., Moradbak, A., Mohamed, A. ., Owolabi, F. abdulwahab taiwo, Asniza, M., & Abdul Khalid, S. H. . (2016). Textile Reinforced Structural Composites for Advanced Applications. In *Intech* (p. 49). <https://doi.org/http://dx.doi.org/10.5772/57353>
- Drysdale, R. G., & Essawy, A. S. (1988). OUT-OF-PLANE BENDING OF CONCRETE BLOCK WALLS. *Journal of Structural Engineering*, 114, 121–134.

- Dutu, A., Sakata, H., Asce, A. M., Yamazaki, Y., & Shindo, T. (2016). *In-Plane Behavior of Timber Frames with Masonry Infills under Static Cyclic Loading*. *04015140*(18), 1–18. [https://doi.org/10.1061/\(ASCE\)ST.1943-541X.0001405](https://doi.org/10.1061/(ASCE)ST.1943-541X.0001405).
- Edri, I. E., & Yankelevsky, D. Z. (2017). An analytical model for the out-of-plane response of URM walls to different lateral static loads. *Engineering Structures*, *136*, 194–209. <https://doi.org/10.1016/j.engstruct.2017.01.001>
- Eduardo Charters Morais, L. G. V. and J. K. (2016). Fragility Estimation and Comparison Using IDA and Simplified Macro-Modeling of In-Plane Shear in Old Masonry Walls. In *Dynamical Systems: Modelling, Springer Proceedings in Mathematics & Statistics* (pp. 277–292). https://doi.org/10.1007/978-3-319-42402-6_23
- El-Dakhakhni, W. W., Elgaaly, M., & Hamid, A. A. (2003). Three-Strut Model for Concrete Masonry-Infilled Steel Frames. *Journal of Structural Engineering*, *129*(2), 177–185. [https://doi.org/10.1061/\(asce\)0733-9445\(2003\)129:2\(177\)](https://doi.org/10.1061/(asce)0733-9445(2003)129:2(177))
- ELOUALI, T. (2008). Effect Of Infill Masonry Panels On The Seismic Response Of Frame Buildings. *14th World Conference on Earthquake Engineering (14WCEE)*, 1–8.
- Elsanadedy, H. M., Al-Salloum, Y. A., Al-Zaheri, Z. M., Alsayed, S. H., & Abbas, H. (2016). Behavior and Design Aspects of FRP-Strengthened URM Walls under Out-of-Plane Loading. *Journal of Composites for Construction*, *20*(6), 04016048. [https://doi.org/10.1061/\(asce\)cc.1943-5614.0000695](https://doi.org/10.1061/(asce)cc.1943-5614.0000695)
- Erdem, I., Akyuz, U., Ersoy, U., & Ozcebe, G. (2006). An experimental study on two different strengthening techniques for RC frames. *Engineering Structures*, *28*(13), 1843–1851. <https://doi.org/10.1016/j.engstruct.2006.03.010>
- Esposito, F. M. R., & Rots, G. J. P. R. J. G. (2020). Experimental investigation of the in - plane cyclic behaviour of calcium silicate brick masonry walls. In *Bulletin of Earthquake Engineering* (Vol. 18, Issue 8). Springer Netherlands. <https://doi.org/10.1007/s10518-020-00835-x>
- F. Di Trapani, M. Malavisi, P.B. Shing, L. C. (2020). *Definition of out-of-plane fragility curves for masonry infills subject to combined IP and OOP damage* (pp. 1–9). <https://doi.org/10.1201/9781003098508-134>
- Fagone, M., & Ranocchiai, G. (2018). Experimental investigation on out-of-plane behavior of masonry panels strengthened with CFRP sheets. *Composites Part B: Engineering*, *150*(March), 14–26. <https://doi.org/10.1016/j.compositesb.2018.05.031>

- Fallahi, M., Roudsari, S. S., Haghhighifar, M., & Madandoost, R. (2018). Modeling of Reinforced Concrete Frames with Infill Walls Under Cyclic Loading Strengthening with CFRP. *American Journal of Engineering and Applied Sciences*, 11(3), 1086–1099. <https://doi.org/10.3844/ajeassp.2018.1086.1099>
- Fardis, M. N., & Panagiotakos, T. B. (2007). SEISMIC DESIGN AND RESPONSE OF BARE AND MASONRY-INFILLED REINFORCED CONCRETE BUILDINGS . PART II : INFILLED STRUCTURES RESPONSE OF BARE AND MASONRY-INFILLED REINFORCED CONCRETE BUILDINGS . PART. *Journal of Earthquake Engineering*, 3, 475–503. <https://doi.org/10.1080/13632469708962375>
- Filippou, C. A., Kyriakides, N. C., & Chrysostomou, C. Z. (2020). Numerical Modelling and Simulation of the In-Plane Response of a Three-Storey Masonry-Infilled RC Frame Retrofitted with TRM. *Advances in Civil Engineering*, 2020. <https://doi.org/10.1155/2020/6279049>
- Filippou, C., Furtado, A., De Risi, M. T., Kyriakides, N., & Chrysostomou, C. Z. (2022). Behaviour of Masonry-Infilled RC Frames Strengthened Using Textile Reinforced Mortar: An Experimental and Numerical Studies Overview. *Journal of Earthquake Engineering*, 00(00), 1–25. <https://doi.org/10.1080/13632469.2021.1988763>
- Finite Element Micro-Modeling of Infilled Frames. (2008). *Electronic Journal of Structural Engineering*, 8, 1–11.
- Furtado, A., Rodrigues, H., & Arêde, A. (2021). Experimental and numerical assessment of confined infill walls with openings and textile-reinforced mortar. *Soil Dynamics and Earthquake Engineering*, 151(May 2020). <https://doi.org/10.1016/j.soildyn.2021.106960>
- Furtado, A., Rodrigues, H., Arêde, A., & Varum, H. (2018). Out-of-plane behavior of masonry infilled RC frames based on the experimental tests available: A systematic review. In *Construction and Building Materials* (Vol. 168, pp. 831–848). Elsevier Ltd. <https://doi.org/10.1016/j.conbuildmat.2018.02.129>
- Furtado, A., Rodrigues, H., Arêde, A., & Varum, H. (2020). Effect of the Panel Width Support and Columns Axial Load on the Infill Masonry Walls Out-Of- Plane Behavior Effect of the Panel Width Support and Columns Axial Load on. *Journal of Earthquake Engineering*, 24(4), 653–681. <https://doi.org/10.1080/13632469.2018.1453400>
- G. Michele Calvi, Gregory R. Kingsley, G. M. (1996). Testing of Masonry Structures for Seismic Assessment. *Earthquake Spectra*, 12(1), 145–162.

- Gattesco, N., & Boem, I. (2015). Experimental and analytical study to evaluate the effectiveness of an in-plane reinforcement for masonry walls using GFRP meshes. *Construction and Building Materials*, 88, 94–104. <https://doi.org/10.1016/j.conbuildmat.2015.04.014>
- Gattesco, N., & Boem, I. (2017). Out-of-plane behavior of reinforced masonry walls: Experimental and numerical study. *Composites Part B: Engineering*, 128, 39–52. <https://doi.org/10.1016/j.compositesb.2017.07.006>
- Gautam, D. (2018). Observational fragility functions for residential stone masonry buildings in Nepal. *Bulletin of Earthquake Engineering*, 16(10), 4661–4673. <https://doi.org/10.1007/s10518-018-0372-2>
- Gautam, D., Adhikari, R., & Rupakhety, R. (2021). Seismic fragility of structural and non-structural elements of Nepali RC buildings. *Engineering Structures*, 232(May 2020), 111879. <https://doi.org/10.1016/j.engstruct.2021.111879>
- Gerson Moacyr Sisniegas Alva, Alessandro Onofre Rigão, João Kaminski Junior, M. A. S. P. (2021). Seismic analysis of reinforced concrete buildings with participating masonry infills. *IBRACON Structures and Materials Journal*, 14(3), 1–20. <https://doi.org/https://doi.org/10.1590/S1983-41952021000300015>
- Gianni Blasi, Daniele Perrone, M. A. A. (2018). Fragility functions and floor spectra of RC masonry infilled frames - influence of mechanical properties of masonry infills. *Bulletin of Earthquake Engineering*, 16, 6105–6130. <https://doi.org/https://doi.org/10.1007/s10518-018-0435-4>
- Gkournelos, P. D., Ph, D., Triantafillou, T. C., & Asce, M. (2023). Out-of-Plane Behavior of In-Plane Damaged Masonry Infills Retrofitted with TRM and Thermal Insulation. *Journal of Composites for Construction*, 27(6), 1–14. <https://doi.org/10.1061/JCCOF2.CCENG-4324>
- Gries, T., Raina, M., Quadflieg, T., & Stolyarov, O. (2016). Manufacturing of Textiles for Civil Engineering Applications. In *Textile Fibre Composites in Civil Engineering*. Elsevier Ltd. <https://doi.org/10.1016/B978-1-78242-446-8.00002-1>
- Grubišić, M., Kalman Šipoš, T., & Sigmund, V. (2013). Seismic Fragility Assessment of Masonry Infilled Reinforced Concrete Frames. *50 Years of European Earthquake Engineering (SE-50EEE)*, January 2013, 8.
- Haach, V. G., Ramalho, M. A., & Corrêa, M. R. S. (2013). Parametrical study of unreinforced

- flanged masonry walls subjected to horizontal loading through numerical modeling. *Engineering Structures*, 56, 207–217. <https://doi.org/10.1016/j.engstruct.2013.05.009>
- Hassanli, R., Asce, S. M., Elgawady, M. A., Asce, M., & Mills, J. E. (2016). *Experimental Investigation of In-Plane Cyclic Response of Unbonded Posttensioned Masonry Walls*. 142(5), 1–15. [https://doi.org/10.1061/\(ASCE\)ST.1943-541X](https://doi.org/10.1061/(ASCE)ST.1943-541X)
- Ho-Le, K. (1988). Finite element mesh generation methods: a review and classification. *Computer-Aided Design*, 20(1), 27–38. [https://doi.org/https://doi.org/10.1016/0010-4485\(88\)90138-8](https://doi.org/https://doi.org/10.1016/0010-4485(88)90138-8)
- HUGO RODRIGUES, HUMBERTO VARUM, and A. C. (2010). Simplified Macro-Model for Infill Masonry Panels. *Journal of Earthquake Engineering*, 14(3), 390–416. <https://doi.org/10.1080/13632460903086044>
- Hwang, S. H., Kim, S., Choi, Y. S., Yang, K. H., Kim, S., Choi, Y. S., & Out-of-plane, K. H. Y. (2022). Out-of-Plane lateral load capacity of unreinforced masonry walls. *Journal of Structural Integrity and Maintenance*, 7(4), 217–225. <https://doi.org/10.1080/24705314.2022.2088057>
- Hwee Tan, K., & H Patoary, M. K. (2004). Strengthening of Masonry Walls against Out-of-Plane Loads Using Fiber-Reinforced Polymer Reinforcement. *Journal of Composites for Construction*, 8, 79–87. <https://doi.org/10.1061/ASCE1090-026820048:179>
- IS 1077 : 1992 (Reaffirmed 2002). (2007). *COMMON BURNT CLAY BUILDING BRICKS - SPECIFICATION*.
- Ismail, N., El-Maaddawy, T., & Khattak, N. (2018a). Quasi-static in-plane testing of FRCM strengthened non-ductile reinforced concrete frames with masonry infills. *Construction and Building Materials*, 186, 1286–1298. <https://doi.org/10.1016/j.conbuildmat.2018.07.230>
- Ismail, N., El-Maaddawy, T., & Khattak, N. (2018b). Quasi-static in-plane testing of FRCM strengthened non-ductile reinforced concrete frames with masonry infills. *Construction and Building Materials*, 186, 1286–1298. <https://doi.org/10.1016/j.conbuildmat.2018.07.230>
- Ismail, Najif, & Ingham, J. M. (2016). In-plane and out-of-plane testing of unreinforced masonry walls strengthened using polymer textile reinforced mortar. *Engineering Structures*, 118, 167–177. <https://doi.org/10.1016/j.engstruct.2016.03.041>
- Jack P. Moehle. (1996). Displacement based seismic design criteria. *Eleventh World*

Conference on Earthquake Engineering, 1–8.

- Jaime, G. L., Tommaso, D., Francesco, F., Christian, C., & Carlo, P. (2019). Structural repointing of masonry structures. *Key Engineering Materials*, 817 KEM, 412–420. <https://doi.org/10.4028/www.scientific.net/KEM.817.412>
- Jalaeefar, A., & Zargar, A. (2020). Effect of infill walls on behavior of reinforced concrete special moment frames under seismic sequences. *Structures*, 28, 766–773. <https://doi.org/10.1016/j.istruc.2020.09.029>
- Jefferies, P. (n.d.). *Conservation of Heritage Structures & Older Buildings - Repointing Masonry Walls – Matching the Techniques for Success or Failure*. PJ Materials Consultants Limited.
- Jian Ying Wu, Jie Li, R. F. (2006). An energy release rate-based plastic-damage model for concrete. *International Journal of Solids and Structures*, 43, 583–612. <https://doi.org/10.1016/j.ijsolstr.2005.05.038>
- Jiang, H., Liu, X., & Mao, J. (2015). Full-scale experimental study on masonry infilled RC moment-resisting frames under cyclic loads. *Engineering Structures*, 91, 70–84. <https://doi.org/10.1016/j.engstruct.2015.02.008>
- Jong-Su Jeon, Ji-Hun Park, and R. D. (2015). Seismic fragility of lightly reinforced concrete frames with masonry infills. *EARTHQUAKE ENGINEERING & STRUCTURAL DYNAMICS*, 44, 1783–1803. <https://doi.org/10.1002/eqe>
- K. S. Sreekechava, Hugo Rodrigues, A. S. A. (2023). Response of Masonry-Infilled Reinforced Concrete Frames Strengthened at Interfaces with Geo-Fabric under In-Plane Loads. *Buildings MDPI*, 13(1495), 1–21. <https://doi.org/doi.org/10.3390/buildings13061495>
- Kabas, H. T., & Kusain, F. E. (2023). Experimental behavior of masonry infilled RC frames with openings strengthened by using CFRP strip. *Composite Structures*, 312(September 2021), 1–18. <https://doi.org/10.1016/j.compstruct.2023.116873>
- Kai, R., Su, L., & Lee, C. (2013). Development of seismic fragility curves for low-rise masonry infilled reinforced concrete buildings by a coefficient-based method. *Earthquake Engineering and Engineering Vibration*, 12(2), 319–332.
- Kakaletsis, D. J., & Karayannis, C. G. (2008). Influence of Masonry Strength and Openings on Infilled R/C Frames Under Cycling Loading. *Journal of Earthquake Engineering*, 2469, 197–221. <https://doi.org/10.1080/13632460701299138>

- Kareem, K. M., Abdulla, K. F., Panto, B., & Cunningham, L. S. (2022). Numerical simulation of the in-plane lateral response of RC infill frames using a FEM-DMEM modelling approach. *Journal of Building Engineering*, 51(February), 104305. <https://doi.org/10.1016/j.jobe.2022.104305>
- Karimi, A. H., Karimi, M. S., Kheyroddin, A., & Shahkarami, A. A. (2016). Experimental and Numerical Study on Seismic Behavior of An Infilled Masonry Wall Compared to An Arched Masonry Wall. *Structures*, 8, 144–153. <https://doi.org/10.1016/j.istruc.2016.09.012>
- Kariou, F. A., Triantafyllou, S. P., Bournas, D. A., & Koutas, L. N. (2018a). Out-of-plane response of masonry walls strengthened using textile-mortar system. *Construction and Building Materials*, 165, 769–781. <https://doi.org/10.1016/j.conbuildmat.2018.01.026>
- Kariou, F. A., Triantafyllou, S. P., Bournas, D. A., & Koutas, L. N. (2018b). Out-of-plane response of masonry walls strengthened using textile-mortar system. *Construction and Building Materials*, 165, 769–781. <https://doi.org/10.1016/j.conbuildmat.2018.01.026>
- Kaushik, H. B., Durgesh, ;, Rai, C., Jain, S. K., & Asce, M. (2007). Stress-Strain Characteristics of Clay Brick Masonry under Uniaxial Compression. *JOURNAL OF MATERIALS IN CIVIL ENGINEERING*, 19(9), 728–740. <https://doi.org/10.1061/ASCE0899-1561200719:9728>
- Kaushik, H. B., Rai, D. C., & Jain, S. K. (2008). A RATIONAL APPROACH TO ANALYTICAL MODELING OF MASONRY INFILLS IN REINFORCED CONCRETE FRAME BUILDINGS. *The 14 World Conference on Earthquake Engineering*, 1–10.
- Khalilzadeh Vahidi, E., & Moradi, R. (2019). Numerical Study of the Force Transfer Mechanism and Seismic Behavior of Masonry Infilled RC Frames with Windows Opening. *Civil Engineering Journal*, 5(1), 61. <https://doi.org/10.28991/cej-2019-03091225>
- Khan, M. W., Usman, M., Farooq, S. H., Zain, M., & Saleem, S. (2021). Effect of masonry infill on analytical fragility response of RC frame school buildings in high seismic zone. In *Journal of Structural Integrity and Maintenance* (Vol. 6, Issue 2, pp. 110–122). <https://doi.org/10.1080/24705314.2020.1865624>
- Khatiwada, A., & Jiang, H. (2017). Numerical Modeling of Masonry Infilled Reinforced Concrete Moment- Resisting Frame. *The Thirtieth KKHTCNN Symposium on Civil*

- Engineering*, 1–5. <https://www.researchgate.net/publication/320894057>
- Kostinakis, K., & Athanatopoulou, A. (2020). Effects of in-plan irregularities caused by masonry infills on the seismic behavior of R/C buildings. *Soil Dynamics and Earthquake Engineering*, 129. <https://doi.org/10.1016/j.soildyn.2019.03.012>
- Kouris, L. A. S., Bournas, D. A., Akintayo, O. T., Konstantinidis, A. A., & Aifantis, E. C. (2020). A gradient elastic homogenisation model for brick masonry. *Engineering Structures*, 208(110311), 1–20. <https://doi.org/10.1016/j.engstruct.2020.110311>
- Koutas, L., Bousias, S. N., & Triantafillou, T. C. (2015). Seismic strengthening of masonry-infilled RC frames with TRM: Experimental study. *Journal of Composites for Construction*, 19(2), 1–12. [https://doi.org/10.1061/\(ASCE\)CC.1943-5614.0000507](https://doi.org/10.1061/(ASCE)CC.1943-5614.0000507)
- Koutas, L. N., & Bournas, D. A. (2019). Out-of-Plane Strengthening of Masonry-Infilled RC Frames with Textile-Reinforced Mortar Jackets. *Journal of Composites for Construction*, 23(1), 1–13. [https://doi.org/10.1061/\(ASCE\)CC.1943-5614.0000911](https://doi.org/10.1061/(ASCE)CC.1943-5614.0000911)
- Koutas, L. N., Tetta, Z., Bournas, D. A., & Triantafillou, T. C. (2019). Strengthening of Concrete Structures with Textile Reinforced Mortars: State-of-the-Art Review. *Journal of Composites for Construction*, 23(1), 1–20. [https://doi.org/10.1061/\(ASCE\)CC.1943-5614.0000882](https://doi.org/10.1061/(ASCE)CC.1943-5614.0000882)
- Koutas, L., Pitytzogia, A., Triantafillou, T. C., & Bousias, S. N. (2014). Strengthening of infilled reinforced concrete frames with TRM: Study on the development and testing of textile-based anchors. *Journal of Composites for Construction*, 18(3), 1–12. [https://doi.org/10.1061/\(ASCE\)CC.1943-5614.0000390](https://doi.org/10.1061/(ASCE)CC.1943-5614.0000390)
- Koutromanos, I., Stavridis, A., Shing, P. B., & Willam, K. (2011). Numerical modeling of masonry-infilled RC frames subjected to seismic loads. *Computers and Structures*, 89(11–12), 1026–1037. <https://doi.org/10.1016/j.compstruc.2011.01.006>
- Krueger, R., Paris, I. L., Brien, T. K. O., & Minguet, P. J. (2002). Comparison of 2D finite element modeling assumptions with results from 3D analysis for composite skin-stiffener debonding. *Composite Structures*, 57, 161–168.
- Kumar, N., Amirtham, R., & Pandey, M. (2014). Plasticity based approach for failure modelling of unreinforced masonry. *Engineering Structures*, 80, 40–52. <https://doi.org/10.1016/j.engstruct.2014.08.021>
- Kuzik, M. D., Elwi, A. E., & Cheng, J. J. R. (2003). Cyclic Flexure Tests of Masonry Walls Reinforced with Glass Fiber Reinforced Polymer Sheets. *Journal of Composites for*

- Construction*, 7, 20–30. <https://doi.org/10.1061/ASCE1090-026820037:120>
- Leal G., J. M., Pérez Gavilán, J. J., Castorena G., J. H., & Velázquez D., J. I. (2017). Infill walls with confining elements and horizontal reinforcement: An experimental study. *Engineering Structures*, 150, 153–165. <https://doi.org/10.1016/j.engstruct.2017.07.042>
- Lee, J., & Fenves, G. L. (1998). Plastic-Damage Model for Cyclic Loading of Concrete Structures. *Journal of Engineering Mechanics*, 124(8), 892–900. [https://doi.org/10.1061/\(asce\)0733-9399\(1998\)124:8\(892\)](https://doi.org/10.1061/(asce)0733-9399(1998)124:8(892))
- Liberatore, L., & AlShawa, O. (2021). On the application of the yield-line method to masonry infills subjected to combined in-plane and out-of-plane loads. *Structures*, 32, 1287–1301. <https://doi.org/10.1016/j.istruc.2021.03.044>
- Liberatore, L., AlShawa, O., Marson, C., Pasca, M., & Sorrentino, L. (2020). Out-of-plane capacity equations for masonry infill walls accounting for openings and boundary conditions. *Engineering Structures*, 207, 1–15. <https://doi.org/10.1016/j.engstruct.2020.110198>
- Liberatore, L., Noto, F., Mollaioli, F., & Franchin, P. (2018). In-plane response of masonry infill walls: Comprehensive experimentally-based equivalent strut model for deterministic and probabilistic analysis. *Engineering Structures*, 167, 533–548. <https://doi.org/10.1016/j.engstruct.2018.04.057>
- Lin, K., Totoev, Y. Z., Liu, H., & Guo, T. (2016). *In-Plane Behaviour of a Reinforcement Concrete Frame with a Dry Stack Masonry Panel*. 1–17. <https://doi.org/10.3390/ma9020108>
- Liu, C., Nong, X., Zhang, F., Quan, Z., & Bai, G. (2019). Experimental study on the seismic performance of recycled concrete Hollow Block Masonry Walls. *Applied Sciences (Switzerland)*, 9(20). <https://doi.org/10.3390/app9204336>
- Lourenço, P. B. (1996). Computational strategies for masonry structures. In *PhD Thesis* (Vol. 70, Issue 08). <http://www.narcis.nl/publication/RecordID/oai:tudelft.nl:uuid:4f5a2c6c-d5b7-4043-9d06-8c0b7b9f1f6f>
- Lu, X., & Zha, S. (2021). Full-scale experimental investigation of the in-plane seismic performance of a novel resilient infill wall. *Engineering Structures*, 232. <https://doi.org/10.1016/j.engstruct.2020.111826>
- Lubliner J, Oliver J, O. S. and O. E. (1988). A Plastic-Damage Model For Concrete. *International Journal of Solids Structures*, 25(3), 299–326.

- Lutman, M., Bosiljkov, V., & Tomaz, M. (2006). Robustness of hollow clay masonry units and seismic behaviour of masonry walls. *Construction and Building Materials* 20, 20, 1028–1039. <https://doi.org/10.1016/j.conbuildmat.2005.05.001>
- Lyu, H., Deng, M., Han, Y., Ma, F., & Zhang, Y. (2022). In-plane cyclic testing of full-scale reinforced concrete frames with innovative isolated infill walls strengthened by highly ductile concrete. *Journal of Building Engineering*, 57(March), 104934. <https://doi.org/10.1016/j.job.2022.104934>
- Lyu, H., Deng, M., Ma, Y., Yang, S., & Cheng, Y. (2022). In-plane cyclic tests on strengthening of full-scale autoclaved aerated concrete blocks infilled RC frames using highly ductile concrete (HDC). *Journal of Building Engineering*, 49(November 2021), 104083. <https://doi.org/10.1016/j.job.2022.104083>
- Madan, A., Reinhorn, A. M., Mander, J. B., & Valles, R. E. (1997). Modeling of Masonry Infill Panels for Structural Analysis. *Journal of Structural Engineering*, 123(10), 1295–1302. [https://doi.org/10.1061/\(asce\)0733-9445\(1997\)123:10\(1295\)](https://doi.org/10.1061/(asce)0733-9445(1997)123:10(1295))
- Madan, B. A., Reinhorn, A. M., Mander, J. B., & Valles, R. E. (n.d.). *MODELING OF MASONRY INFILL PANELS FOR STRUCTURAL ANALYSIS*.
- Madan, B. A., Reinhorn, A. M., Mander, J. B., & Valles, R. E. (1997). MODELING OF MASONRY INFILL PANELS FOR STRUCTURAL ANALYSIS. *Journal of Structural Engineering*, 123, 1295–1302.
- Magenes, G., Morandi, P., & Penna, A. (2008). *In plane cyclic tests of calcium silicate masonry walls* (Issue February 2014, pp. 1–11).
- Maheri, M. R., Khajeheian, M. K., & Vatanpour, F. (2019). In-plane seismic retrofitting of hollow concrete block masonry walls with RC layers. *Structures*, 20, 425–436. <https://doi.org/10.1016/j.istruc.2019.05.008>
- Maidiawati, & Sanada, Y. (2017). R/C frame–infill interaction model and its application to Indonesian buildings. *Earthquake Engineering and Structural Dynamics*, 46(2), 221–241. <https://doi.org/10.1002/eqe.2787>
- MALLICK DV, & GARG RP. (1971). Effect of openings on the lateral stiffness of infilled frames. *Proc Inst Civ Eng*, 49, 193–209. <https://doi.org/10.1680/icep.1971.6263>
- Marco Nale, Fabio Minghini, Andrea Chiozzi, A. T. (2021). Fragility functions for local failure mechanisms in unreinforced masonry buildings - a typological study in Ferrara, Italy. *Bulletin of Earthquake Engineering*, 19, 6049–6079.

<https://doi.org/https://doi.org/10.1007/s10518-021-01199-6>

- Masuelli, M. A. (2013). *Introduction of Fibre-Reinforced Polymers – Polymers and Composites: Concepts, Properties and Processes*. IntechOpen. <https://doi.org/http://dx.doi.org/10.5772/54629>
- Matjaz Dolsek, P. F. (2008). The effect of masonry infills on the seismic response of a four-storey reinforced concrete frame — a deterministic assessment. *Engineering Structures*, 30, 1991–2001. <https://doi.org/10.1016/j.engstruct.2008.01.001>
- Mazza, F., & Donnici, A. (2018). Nonlinear modelling of the in-plane-out-of-plane interaction in the seismic analysis of masonry infills in r.c. framed buildings. *Procedia Structural Integrity*, 11, 218–225. <https://doi.org/10.1016/j.prostr.2018.11.029>
- Mbewe, P. B. K., & van Zijl, G. P. A. G. (2019). Characterization of Equivalent Struts for Macromodeling of Infilled Masonry RC Frames Subjected to Lateral Load. *Journal of Structural Engineering*, 145(5), 04019035. [https://doi.org/10.1061/\(asce\)st.1943-541x.0002316](https://doi.org/10.1061/(asce)st.1943-541x.0002316)
- Meharbi, A. B., & Benson, S. P. (2003). Seismic Analysis of Masonry-Infilled Reinforced Concrete Frames. *TMS Journal*, 81–95. [https://doi.org/10.1016/0045-7949\(88\)90278-7](https://doi.org/10.1016/0045-7949(88)90278-7)
- Mehrabi, A. B., & Benson Shing, P. (1997). FINITE ELEMENT MODELING OF MASONRY-INFILLED RC FRAMES. *Journal of Structural Engineering*, 604–614.
- Meillyta. (2012). Finite Element Modelling of Unreinforced Masonry (URM) Wall with Openings: Studies in Australia. *The Proceedings of 2nd Annual International Conference Syiah Kuala University 2012 & 8th IMT-GT Uninet Biosciences Conference*, 2(2), 236–241.
- Miglietta, P. C., Bentz, E. C., & Grasselli, G. (2017). Finite/discrete element modelling of reversed cyclic tests on unreinforced masonry structures. *Engineering Structures*, 138, 159–169. <https://doi.org/10.1016/j.engstruct.2017.02.019>
- Milanesi, R. R., Morandi, P., Hak, S., & Magenes, G. (2021). Experiment-based out-of-plane resistance of strong masonry infills for codified applications. *Engineering Structures*, 242(May), 112525. <https://doi.org/10.1016/j.engstruct.2021.112525>
- Milani, G., Lourenço, P., & Tralli, A. (2006). Homogenization Approach for the Limit Analysis of Out-of-Plane Loaded Masonry Walls. *Journal of Structural Engineering*, 132(10), 1650–1663. [https://doi.org/10.1061/\(asce\)0733-9445\(2006\)132:10\(1650\)](https://doi.org/10.1061/(asce)0733-9445(2006)132:10(1650))

- Misir, I. S. (2015). Potential Use of Locked Brick Infill Walls to Decrease Soft-Story Formation in Frame Buildings. *Journal of Performance of Constructed Facilities*, 29(5), 1–10. [https://doi.org/10.1061/\(ASCE\)CF.1943-5509.0000633](https://doi.org/10.1061/(ASCE)CF.1943-5509.0000633)
- Mohamed, H., & Rom, X. (2002). Seismic Fragility Analysis of Rc Frames With Masonry Infills. *16th European Conference on Earthquake Engineering*, 1–10.
- Mohammed Ashraf Nazief. (2014). *Finite Element Characterization of the Behaviour of Masonry Infill Shear Walls With and Without Openings* (Vol. 58, Issue 12) [University of Alberta]. <https://doi.org/10.1128/AAC.03728-14>
- Mohyeddin-kermani, A. (2011). *Modelling and Performance of RC Frames with Masonry Infill under In-Plane and Out-of-Plane Loading* (Issue July). The University of Melbourne.
- Mohyeddin, A., Goldsworthy, H. M., & Gad, E. F. (2013). FE modelling of RC frames with masonry infill panels under in-plane and out-of-plane loading. *Engineering Structures*, 51, 73–87. <https://doi.org/10.1016/j.engstruct.2013.01.012>
- Mondal, G., & Jain, S. K. (2008). Lateral Stiffness of Masonry Infilled Reinforced Concrete (RC) Frames with Central Opening. *Earthquake Spectra*, 24(3), 701–723. <https://doi.org/10.1193/1.2942376>
- Morandi, P., Hak, S., & Magenes, G. (2018). Performance-based interpretation of in-plane cyclic tests on RC frames with strong masonry infills. *Engineering Structures*, 156(March 2017), 503–521. <https://doi.org/10.1016/j.engstruct.2017.11.058>
- Moretti, M. L. (2015). Seismic design of masonry and reinforced concrete infilled frames: A comprehensive overview. *American Journal of Engineering and Applied Sciences*, 8(4), 748–766. <https://doi.org/10.3844/ajeassp.2015.748.766>
- Murty, C. V. R., & Jain, S. K. (2000). Beneficial Influence of Masonry Infill Walls on Seismic Performance of Rc Frame Buildings. *Twelfth World Conference on Earthquake Engineering (12WCEE)*, 1–6.
- Naaman, A. E. (2010). TEXTILE REINFORCED CEMENT COMPOSITES: COMPETITIVE STATUS AND RESEARCH DIRECTIONS. In *International RILEM Conference on Material Science-MATSCI: Vol. I* (Issue 3).
- Nadège, R., Zyed, M., Larbi, S., Emmanuel, F., Claude, U., Lyon, B., Lyon, I. U. T., & Bohr, N. (2018). *Experimental study of the in-plane cyclic behaviour of masonry walls strengthened by composite materials*. 164, 70–83. <https://doi.org/10.1016/j.conbuildmat.2017.12.215>

- Nasiri, E., & Liu, Y. (2017a). Development of a detailed 3D FE model for analysis of the in-plane behaviour of masonry infilled concrete frames. *Engineering Structures*, *143*, 603–616. <https://doi.org/10.1016/j.engstruct.2017.04.049>
- Nasiri, E., & Liu, Y. (2017b). Development of a detailed 3D FE model for analysis of the in-plane behaviour of masonry infilled concrete frames. *Engineering Structures*, *143*, 603–616. <https://doi.org/10.1016/j.engstruct.2017.04.049>
- Nasiri, E., & Liu, Y. (2019). The out-of-plane behaviour of concrete masonry infills bounded by reinforced concrete frames. *Engineering Structures*, *184*, 406–420. <https://doi.org/10.1016/j.engstruct.2019.01.098>
- Nassirpour, A., & D’Ayala, D. (2014). Fragility Analysis of Mid-Rise Masonry Infilled Steel Frame (MISF) Structures. *Second European Conference on Earthquake Engineering and Seismology, August*, 1–12.
- Nguyen, G. D., & Korsunsky, A. M. (2008). Development of an approach to constitutive modelling of concrete : Isotropic damage coupled with plasticity. *International Journal of Solids and Structures*, *45*, 5483–5501. <https://doi.org/10.1016/j.ijsolstr.2008.05.029>
- Niasar, A. N., Alaei, F. J., & Zamani, S. M. (2020). Experimental investigation on the performance of unreinforced masonry wall, retrofitted using engineered cementitious composites. *Construction and Building Materials*, *239*. <https://doi.org/10.1016/j.conbuildmat.2019.117788>
- Niu, L. H., Zheng, S. S., & Li, L. (2020). Experimental study on the seismic behavior of masonry walls under offshore environment. *Structures*, *28*, 433–445. <https://doi.org/10.1016/j.istruc.2020.08.064>
- Nyunn, S., Wang, F., Yang, J., Liu, Q. feng, Azim, I., & Bhatta, S. (2020). Numerical studies on the progressive collapse resistance of multi-story RC buildings with and without exterior masonry walls. *Structures*, *28*, 1050–1059. <https://doi.org/10.1016/j.istruc.2020.07.049>
- Omidi, O., & Lotfi, V. (2010). Numerical Analysis of Cyclically Loaded Concrete Under Large Tensile Strains by the Plastic-Damage Model. *Transaction A: Civil Engineering*, *17*(3), 194–208.
- Omidi, Omid, & Lot, V. (2012). Continuum large cracking in a rate-dependent plastic – damage model for cyclic-loaded concrete structures. *INTERNATIONAL JOURNAL FOR NUMERICAL AND ANALYTICAL METHODS IN GEOMECHANICS*, 1–28.

<https://doi.org/10.1002/nag>

- Padalu, P. K. V. R., Singh, Y., & Das, S. (2018a). Experimental investigation of out-of-plane behaviour of URM wallettes strengthened using welded wire mesh. *Construction and Building Materials*, *190*, 1133–1153. <https://doi.org/10.1016/j.conbuildmat.2018.09.176>
- Padalu, P. K. V. R., Singh, Y., & Das, S. (2018b). Experimental investigation of out-of-plane behaviour of URM wallettes strengthened using welded wire mesh. *Construction and Building Materials*, *190*, 1133–1153. <https://doi.org/10.1016/j.conbuildmat.2018.09.176>
- Panagiotis G. Asteris, Christis Z. Chrysostomou, Ioannis P. Giannopoulos, and E. S. (2011). MASONRY INFILLED REINFORCED CONCRETE FRAMES WITH OPENINGS. *Computational Methods in Structural Dynamics and Earthquake Engineering*, 1–15.
- Pantò, B., Silva, L., Vasconcelos, G., & Lourenço, P. B. (2019). Macro-modelling approach for assessment of out-of-plane behavior of brick masonry infill walls. *Engineering Structures*, *181*, 529–549. <https://doi.org/10.1016/j.engstruct.2018.12.019>
- Papanicolaou, C. G., Triantafillou, T. C., Papathanasiou, M., & Karlos, K. (2008). Textile reinforced mortar (TRM) versus FRP as strengthening material of URM walls: Out-of-plane cyclic loading. *Materials and Structures/Materiaux et Constructions*, *41*(1), 143–157. <https://doi.org/10.1617/s11527-007-9226-0>
- Parisi, F., Lignola, G. P., Augenti, N., Prota, A., & Manfredi, G. (2011). Nonlinear Behavior of a Masonry Subassemblage Before and After Strengthening with Inorganic Matrix-Grid Composites. *Journal of Composites for Construction*, *15*(5), 821–832. [https://doi.org/10.1061/\(asce\)cc.1943-5614.0000203](https://doi.org/10.1061/(asce)cc.1943-5614.0000203)
- Pasca, M., Liberatore, L., & Masiani, R. (2017). *Reliability of analytical models for the prediction of out-of-plane capacity of masonry infills*. *6*, 765–781.
- Pohoryles, D. A., & Bournas, D. A. (2020). Seismic retrofit of infilled RC frames with textile reinforced mortars : State-of-the-art review and analytical modelling. *Composites Part B*, *183*(November 2019), 107702. <https://doi.org/10.1016/j.compositesb.2019.107702>
- Pradhan, B. (2018). *Macro-element modelling of unreinforced masonry infill wall with openings under seismic action*. <https://doi.org/10.13140/RG.2.2.26776.01287>
- Pradhan, B., Cavaleri, L., Sarhosis, V., & Ferrotto, M. F. (2021). Generation of out-of-plane fragility functions for in-plane damaged unreinforced masonry infills. *COMPADYN Proceedings, 2021-June*(June). <https://doi.org/10.7712/120121.8536.19549>

- Pribadi, K. S., & Kusumastuti, Dyah, R. (2014). LEARNING FROM RECENT INDONESIAN EARTHQUAKES: AN OVERVIEW TO IMPROVE STRUCTURAL PERFORMANCE. *The 14 World Conference on Earthquake Engineering, October 12-17*, 1–9.
- R Ehsani, B. M., Saadatmanesh, H., & Velazquez-Dimas, J. I. (1999). BEHAVIOR OF RETROFITTED URM WALLS UNDER SIMULATED EARTHQUAKE LOADING. *JOURNAL OF COMPOSITES FOR CONSTRUCTION*, 3(3), 134–142.
- Rahgozar, A., & Hosseini, A. (2017). Experimental and numerical assessment of in-plane monotonic response of ancient mortar brick masonry. *Construction and Building Materials*, 155, 892–909. <https://doi.org/10.1016/j.conbuildmat.2017.08.079>
- Rai, N. K., Reddy, G. R., & Venkatraj, V. (2011). Effectiveness of multiple TSWDs for seismic response control of masonry-infilled RC framed structures. *ISET Journal of Earthquake Technology*, 48(2–4), 85–101.
- Raof, S. M., & Bournas, D. A. (2017). TRM versus FRP in flexural strengthening of RC beams : Behaviour at high temperatures. *Construction and Building Materials*, 154, 424–437. <https://doi.org/10.1016/j.conbuildmat.2017.07.195>
- Ratnesh Kumar, Yigendra Siingh, R. D. (2009). REVIEW OF RETROFITTING TECHNIQUES OF MASONRY INFILLED RC FRAMES. *Trends and Challenges in Structural Engineering and Construction Technologies*, 284–297.
- Redmond, L., Kahn, L., & Des Roches, R. (2016). Design and construction of hybrid concrete-masonry structures informed by cyclic tests. *Earthquake Spectra*, 32(4), 2337–2355. <https://doi.org/10.1193/051615EQS070M>
- Rodolico, B. (1985). *THE MODELLING OF EARTHQUAKE INDUCED COLLAPSE OF UNREINFORCED MASONRY WALLS COMBINING FORCE AND DISPLACEMENT PRINCIPALS*. 1–8.
- Rodrigues, H., Furtado, A., Vila, N., Humberto, P., & André, V. (2018). Seismic Assessment of a School Building in Nepal and Analysis of Retrofitting Solutions. *International Journal of Civil Engineering*, 0(0), 0. <https://doi.org/10.1007/s40999-018-0297-9>
- Roosta, S., & Liu, Y. (2021). Behavior of concrete masonry infills bounded by masonry frames subjected to in-plane lateral loading – Experimental study. *Engineering Structures*, 247(April), 113153. <https://doi.org/10.1016/j.engstruct.2021.113153>
- Sagar, S. L., Singhal, V., & Rai, D. C. (2019). In-Plane and Out-of-Plane Behavior of Masonry-Infilled RC Frames Strengthened with Fabric-Reinforced Cementitious Matrix. *Journal*

- of Composites for Construction*, 23(1), 1–14. [https://doi.org/10.1061/\(ASCE\)CC.1943-5614.0000905](https://doi.org/10.1061/(ASCE)CC.1943-5614.0000905)
- Salehi, R., & Nikghalb Rashti, A. A. (2018). Investigating the Effect of Heat on Reinforced Concrete Frame Using Finite Element Software. *American Journal of Engineering and Applied Sciences*, 11(2), 632–642. <https://doi.org/10.3844/ajeassp.2018.632.642>
- Saneinejad, A., & Hobbs, B. (1995). Inelastic Design of Infilled Frames. *Journal of Structural Engineering*, 121(4), 634–650. [https://doi.org/10.1061/\(asce\)0733-9445\(1995\)121:4\(634\)](https://doi.org/10.1061/(asce)0733-9445(1995)121:4(634))
- Sassun, K., Sullivan, T. J., Morandi, P., & Cardone, D. (2016). Characterising the in-plane seismic performance of infill masonry. *Bulletin of the New Zealand Society for Earthquake Engineering*, 49(1), 98–115. <https://doi.org/10.5459/bnzsee.49.1.98-115>
- Scacco, J., Ghiassi, B., Milani, G., & Lourenço, P. B. (2020). A fast modeling approach for numerical analysis of unreinforced and FRCM reinforced masonry walls under out-of-plane loading. *Composites Part B*, 180(October 2019), 107553. <https://doi.org/10.1016/j.compositesb.2019.107553>
- Schwarz, S., Hanaor, A., & Yankelevsky, D. Z. (2015). Experimental Response of Reinforced Concrete Frames With AAC Masonry In fill Walls to In-plane Cyclic Loading. *Structures*, 3, 306–319. <https://doi.org/10.1016/j.istruc.2015.06.005>
- Security, D. of H., & Agency, F. E. M. (2005). *FEMA 440 Improvement of Nonlinear Static Seismic Analysis Procedures* (Issue June).
- Shah, S. A. A., Ahmed, A., Shahzada, K., Ali, S. M., Khan, A. N., & Gul, A. (2021). Experimental and Numerical Assessment of Masonry Infill on Seismic Performance of RC Frame Structure. *Journal of Engineering and Applied Sciences*, 40(1). <https://doi.org/10.17582/journal.jeas/40.1.24.36>
- Shapiro, D., Rojahn, C., Reaveley, L. D., Smith, J. R., & Morelli, U. (2000). FEMA 273 - NEHRP Guidelines and Commentary for the Seismic Rehabilitation of Buildings. *FEDERAL EMERGENCY MANAGEMENT AGENCY*, 16(1), 1–435. <https://doi.org/10.1193/1.1586092>
- Shawkat, S. A., & Rahman, A. A. A. (2017). Influence of Adding Infill Walls on the Behavior of R.C. Frames during Earthquakes. In *International Journal of Applied Engineering Research* (Vol. 12). <http://www.ripublication.com>
- Shermi, C., & Dubey, R. N. (2017). Study on out-of-plane behaviour of unreinforced masonry

- strengthened with welded wire mesh and mortar. *Construction and Building Materials*, 143, 104–120. <https://doi.org/10.1016/j.conbuildmat.2017.03.002>
- Shrivastava, R., Gupta, U., & Choubey, U. B. (2009). FRP: Research, Education and Application in India and China in Civil Engineering. In *INFORMATION PAPER International Journal of Recent Trends in Engineering* (Vol. 1, Issue 6).
- Simsir, C. C., Aschheim, M. A., & Abrams, D. P. (2004). Out-of-plane dynamic response of unreinforced bearing walls attached to flexible diaphragms. *Proceedings of 13th World Conference on Earthquake Engineering*, 2045, 15. <https://www.researchgate.net/publication/265197391>
- Šipoš, T. K., Hadzima-Nyarko, M., Miličević, I., & Grubišić, M. (2018). Structural Performance Levels for Masonry Infilled Frames. *16th European Conference on Earthquake Engineering*, 1–13. <https://www.researchgate.net/publication/325908891>
- Smiroldo, F., Kallioras, S., Sommacal, G., Bournas, D., Piazza, M., & Giongo, I. (2023). Full-scale testing of masonry-infilled RC frames retrofitted with cross-laminated timber panels. *Engineering Structures*, 294(August), 116789. <https://doi.org/10.1016/j.engstruct.2023.116789>
- Soleymani, A., Najafgholipour, M. A., Johari, A., & Dooshabi, A. (2024). The diagonal shear behavior of masonry walls fabricated with historical lime-based mortar and retrofitted with near surface mounted method. *Structures*, 59, 1–17. <https://doi.org/10.1016/j.istruc.2023.105795>
- STANDARD, I. (2003). *Timber structures — Joints made with mechanical fasteners — Quasi-static reversed-cyclic test method*.
- Statista. (2024). *Statista - Geography & Nature*. [Www.Statista.Com. https://www.statista.com/statistics/267017/strongest-earthquakes-worldwide-since-1900/](https://www.statista.com/statistics/267017/strongest-earthquakes-worldwide-since-1900/)
- Stauffer, J. D., Woodward, C. B., & White, K. R. (2006). Nonlinear Ultrasonic Testing with Resonant and Pulse Velocity Parameters for Early Damage in Concrete. *ACI MATERIALS JOURNAL*, 102, 4–7.
- Stavridis, A. (2009). *Analytical and experimental study of seismic performance of reinforced concrete frames infilled with masonry walls*. UNIVERSITY OF CALIFORNIA.
- Stavridis, A., Koutromanos, I., & Shing, P. B. (2011). Shake-table tests of a three-story reinforced concrete frame with masonry infill walls. *Earthquake Engineering and Structural Dynamics*, 41, 1089–1108. <https://doi.org/10.1002/eqe.1174>

- Stavridis, A., & Shing, P. B. (2010). Finite-Element Modeling of Nonlinear Behavior of Masonry-Infilled RC Frames. *Journal of Structural Engineering (United States)*, 136, 285–296. <https://doi.org/10.1061/ASCEST.1943-541X.116>
- T. Zimmermann, A. S. and R. W. (2011). Structures Congress 2011 © ASCE 2011 1736. *Structures Congress*, 1736–1747.
- T.P. Ganesana, M. Lakshmipathy, V. Thirumurugan, K. S. S. (2015). *Experimental studies on the effects of different interface materials on the behaviour of infilled frames* (pp. 1–10). <https://www.researchgate.net/publication/316990338>
- Tasnimi, A. A., & Mohebkhah, A. (2011). Investigation on the behavior of brick-infilled steel frames with openings , experimental and analytical approaches. *Engineering Structures*, 33(3), 968–980. <https://doi.org/10.1016/j.engstruct.2010.12.018>
- Tetta, Z. C., & Bournas, D. A. (2016). TRM vs FRP jacketing in shear strengthening of concrete members subjected to high temperatures. *Composites Part B*, 106, 190–205. <https://doi.org/10.1016/j.compositesb.2016.09.026>
- Torrise, G S Crisafulli, F J, P. A. (2012). An innovative Model for the In-Plane Nonlinear Analysis of Confined Masonry and Infilled Frame Structures A.Pavese. *15th World Conference on Earthquake Engineering (15WCEE)*, 1–10. <http://www.confinedmasonry.org/>
- Trapani, F. Di, Shing, P. B., Asce, M., & Cavaleri, L. (2018). *Macroelement Model for In-Plane and Out-of-Plane Responses of Masonry Infills in Frame Structures*. 144(2). [https://doi.org/10.1061/\(ASCE\)ST.1943-541X.0001926](https://doi.org/10.1061/(ASCE)ST.1943-541X.0001926)
- Triantafillou, T. C., Karlos, K., Kapsalis, P., & Georgiou, L. (2018). Innovative Structural and Energy Retrofitting System for Masonry Walls Using Textile Reinforced Mortars Combined with Thermal Insulation: In-Plane Mechanical Behavior. *Journal of Composites for Construction*, 22(5), 1–15. [https://doi.org/10.1061/\(ASCE\)CC.1943-5614.0000869](https://doi.org/10.1061/(ASCE)CC.1943-5614.0000869)
- Vemuri, J., Ehteshamuddin, S., & Kolluru, S. (2018). Numerical simulation of soft brick unreinforced masonry walls subjected to lateral loads. *Cogent Engineering*, 5(1), 1–21. <https://doi.org/10.1080/23311916.2018.1551503>
- Verderame, G. M., Balsamo, A., Ricci, P., Di Domenico, M., & Maddaloni, G. (2019). Experimental assessment of the out-of-plane response of strengthened one-way spanning masonry infill walls. *Composite Structures*, 230.

<https://doi.org/10.1016/j.compstruct.2019.111503>

- Verderame, G. M., Balsamo, A., Ricci, P., & Domenico, M. Di. (2019). Experimental assessment of the out-of-plane response of strengthened one-way spanning masonry in fill walls. *Composite Structures*, 230(May), 111503. <https://doi.org/10.1016/j.compstruct.2019.111503>
- Vladimir G. Haach Graça Vasconcelos and Paulo B. Lourenço. (2010). Experimental Analysis of Reinforced Concrete Block Masonry Walls Subjected to In-Plane Cyclic Loading. *Journal of Structural Engineering (United States)*, 136, 452–462. <https://doi.org/10.1061/ASCEST.1943-541X.0000125>
- Wang, F. (2023). Experimental Research on Seismic Performance of Masonry - Infilled RC Frames Retrofitted by Using Fabric - Reinforced Cementitious Matrix Under In - Plane Cyclic Loading. *International Journal of Concrete Structures and Materials*, 17(1), 1–19. <https://doi.org/10.1186/s40069-023-00594-4>
- Wang, G., Li, Y., Zheng, N., & Ingham, J. M. (2017). Testing and modelling the in-plane seismic response of clay brick masonry walls with boundary columns made of precast concrete interlocking blocks. *Engineering Structures*, 131, 513–529. <https://doi.org/10.1016/j.engstruct.2016.10.035>
- Wang, L., Tang, Z., Li, Y., & Qian, K. (2019). Seismic behavior of masonry-infilled precast concrete frames considering effects of opening. *Construction and Building Materials*, 211, 756–770. <https://doi.org/10.1016/j.conbuildmat.2019.03.287>
- Wang, X., Ghiassi, B., Oliveira, D. V., & Lam, C. C. (2017). Modelling the nonlinear behaviour of masonry walls strengthened with textile reinforced mortars. *Engineering Structures*, 134, 11–24. <https://doi.org/10.1016/j.engstruct.2016.12.029>
- Wang, Xiaomin, Zhao, W., Kong, J., & Zhao, T. (2020). Numerical Investigation on the Influence of In-Plane Damage on the Out-of-Plane Behavior of Masonry Infill Walls. *Advances in Civil Engineering*, 6276803, 1–16. <https://doi.org/https://doi.org/10.1155/2020/6276803>
- Xianxin Xie, Lingxin Zhang, and Z. Q. (2020). A Critical Review of Methods for Determining the Damage States for the In-plane Fragility of Masonry Infill Walls. *Journal of Earthquake Engineering ISSN:*, 1–23. <https://doi.org/https://doi.org/10.1080/13632469.2020.1835749>
- Yaw-Jeng Chiou, Jyh-Cherng Tzeng, Y.-W. L. (1999). EXPERIMENTAL AND

- ANALYTICAL STUDY OF MASONRY INFILLED FRAMES. *Journal of Structural Engineering*, 125(10), 1109–1117.
- Yekrangnia, M., & Asteris, P. G. (2020a). Multi-strut macro-model for masonry infilled frames with openings. *Journal of Building Engineering*, 32, 101683. <https://doi.org/10.1016/j.jobe.2020.101683>
- Yekrangnia, M., & Asteris, P. G. (2020b). Multi-strut macro-model for masonry infilled frames with openings. *Journal of Building Engineering*, 32. <https://doi.org/10.1016/j.jobe.2020.101683>
- Yuen, Y. P., & Kuang, J. S. (2014). Masonry-infilled rc frames subjected to combined in-plane and out-of-plane loading. *International Journal of Structural Stability and Dynamics*, 14(2), 1–17. <https://doi.org/10.1142/S0219455413500661>
- Yuen, Y. P., & Kuang, J. S. (2015). Nonlinear seismic responses and lateral force transfer mechanisms of RC frames with different infill configurations. *Engineering Structures*, 91, 125–140. <https://doi.org/10.1016/j.engstruct.2015.02.031>
- Zhai, C., Kong, J., & Wang, X. (2012). A finite element model for simulating out-of-plane behavior of masonry infilled RC frames. *Applied Mechanics and Materials*, 166–169, 849–852. <https://doi.org/10.4028/www.scientific.net/AMM.166-169.849>
- Zhou, L., Ni, C., Asce, M., & Chui, Y. (2017). *Testing and Modeling of Wood – Masonry Hybrid Wall Assembly*. 143(2), 1–11. [https://doi.org/10.1061/\(ASCE\)ST.1943-541X.0001654](https://doi.org/10.1061/(ASCE)ST.1943-541X.0001654).
- Zone, R. S. (2023). *Disaster Management, Relief & Civil Defence Department*. Government of Rajasthan.
- Zovkic, J., Sigmund, V., & Guljas, I. (2012). Cyclic testing of a single bay reinforced concrete frames with various types of masonry infil. *EARTHQUAKE ENGINEERING & STRUCTURAL DYNAMICS*, 2263(42), 1131–1149. <https://doi.org/10.1002/eqe>
- Zuo, H., Zhang, W., Wang, B., & Gu, X. (2021). Seismic behaviour of masonry infilled hinged steel frames with openings : experimental and numerical studies. *Bulletin of Earthquake Engineering*, 19(3), 1311–1335. <https://doi.org/10.1007/s10518-020-01040-6>

LIST OF PUBLICATIONS

Journals:-

- Jaya Kumar Bhaskar Dipendu Bhunia, J Karthik, Akash Samadhiya, “A state of the art review on the evolution of the performance of masonry infill walls under lateral loadings”, *Asian Journal of Civil Engineering*, 2022 <https://doi.org/10.1007/s42107-022-00446-8>
- Jaya K Bhaskar Dipendu Bhunia, Nithin Palchuri, “Numerical simulation of RC masonry infill wall system strengthened with textile reinforced concrete”, *Materials Today Proceedings*, ISSN 2214-7853, 2023 <https://doi.org/10.1016/j.matpr.2023.03.657>
- Jaya Kumar Bhaskar, Dipendu Bhunia, Lampros Koutas, “In-Plane Behaviour of Masonry Infill Walls with Openings Strengthened using Textile Reinforced Mortar”, *Structures, Elsevier* (Impact Factor = 4.1, Quartile = Q1, Abstracting and Indexing = Science Citation Index Expanded) – **ACCEPTED**

Conferences:-

- Jaya Kumar Bhaskar, Dipendu Bhunia, "Fortification of Masonry Infilled Walls Susceptible to Earthquakes", Second ASCE India Conference on “Challenges of Resilient and Sustainable Infrastructure Development in Emerging Economies”(CRSIDE) 2020 Kolkata, March 2-4, 2020.
- J Bhaskar, D Bhunia, "Investigation on the Behaviour of Masonry Infilled Walls Strengthened With Fabric Reinforced Cementitious Matrix", 17th World Conference on Earthquake Engineering, 17 WCEE, Sendai, Japan, September 13-18, 2021.
- Jaya K Bhaskar, Dipendu Bhunia, Nithin Palchuri, "Numerical Simulation of RC Masonry Infill Wall System Strengthened with Textile Reinforced Concrete", Second International Conference on "Construction Materials and Structures"(ICCMS) 2022 Calicut, December 14-18, 2022.
- Jaya Kumar Bhaskar, Dipendu Bhunia, Lampros Koutas, "Experimental Investigation On The Performance Of Unreinforced Masonry Infill Walls With Openings Under Seismic Loading", 20th International Conference on Experimental Mechanics, ICEM20, Portugal, 2-7, July 2023.

- Jaya K Bhaskar, Dipendu Bhunia, “In-Plane Behavior of Strengthened Unreinforced Masonry Infill Walls Experimental and Numerical Study”, Engineering for Sustainable Development, IABSE Congress New Delhi, September 20-22, 2023.
- Jaya K Bhaskar, Dipendu Bhunia, “Numerical Validation and Parametric Study of Masonry Infill Wall Strengthened With Textile Reinforced Mortar”, 3rd International Conference On Advances in Concrete, Structural & Geotechnical Engineering (ACSGE), BITS Pilani, Pilani Campus, February 26-28, 2024.

To be Published (Under Review)

- Jaya Kumar Bhaskar, Lampros Koutas, Dipendu Bhunia, “In-Plane Behaviour of Masonry Infill Walls with Opening Retrofitting Using Textile Reinforced Mortar Subjected to Lateral Loads”, *Construction and Building Materials, Elsevier* (Impact Factor = 7.4, Quartile = Q1, Abstracting and Indexing = Science Citation Index Expanded) – **UNDER REVIEW**
- Jaya Kumar Bhaskar, Dipendu Bhunia, “Non-Linear Finite Element Study of Masonry Infill Walls Strengthened with Fiber Reinforced Cementitious Matrix Subjected to In-Plane Loads”, *International Journal Of Concrete Structures And Materials, SpringerOpen* (Impact Factor = 3.4, Quartile = Q1, Abstracting and Indexing = Scopus) – **REVIEWS COMPLETED**

APPENDICES

Appendix 1: Design axial load carrying capacity of the column

- a) Calculation gross c.s.a of column (A_g)

$$\text{Size of column} = 200 \times 140 = 28000 \text{ mm}^2$$

- b) Calculation of area of steel in col

$$\text{Area of bar} = (6) \times \pi/4 \times D^2 = 678.24 \text{ mm}^2$$

- c) Calculation area of concrete in column

w.k.t gross c.s.a = area of concrete in column and area of steel in concrete

$$A_g = A_c + A_{sc}$$

$$A_c = A_g - A_{sc}$$

$$A_c = 28000 - 678.24 = 27321.76 \text{ mm}^2$$

- d) $P_u = (0.4 \times 20 \times 27321.76) + (0.67 \times 415 \times 678.24) = 2374.32 \text{ kN}$

- e) Load carrying capacity of column

For steel grade 500, concrete M20

$$P = (2.7005 p + 8) bD/1500 = \mathbf{199.742 \text{ kN}}$$

Appendix 2: Ductility of the unreinforced and reinforced frames

Ductility = failure displacement (Δ_f)/yield displacement (Δ_y)

$$\Delta_f/\Delta_y \text{ for URS} = (80\% \text{ of } 89 \text{ kN}) = 71.2 \text{ kN} \rightarrow (22.4/13.57) = 1.651$$

$$\Delta_f/\Delta_y \text{ for DRS} = (80\% \text{ of } 147.5 \text{ kN}) = 118 \text{ kN} \rightarrow (14.25/4.8) = 2.97$$

APPENDIX 3: DESIGN REPORT

DESIGN OF LOADING FRAME TO MOUNT THE ACTUATOR

DESIGN REPORT

Done by:

Jaya Kumar Bhaskar

2018PHXF0420P

Research Scholar

Department of Civil Engineering

BITS Pilani – 333031

Checked by:

1. Prof. Dipendu Bhunia, Professor, Dept. of Civil Engg. BITS Pilani – 333031
2. Dr. Lampros Koutas, Assistant Professor, University of Thessaly, 38334, Volos, Greece

Approved by:

1. Prof. Dipendu Bhunia, Professor, Dept. of Civil Engg. BITS Pilani – 333031



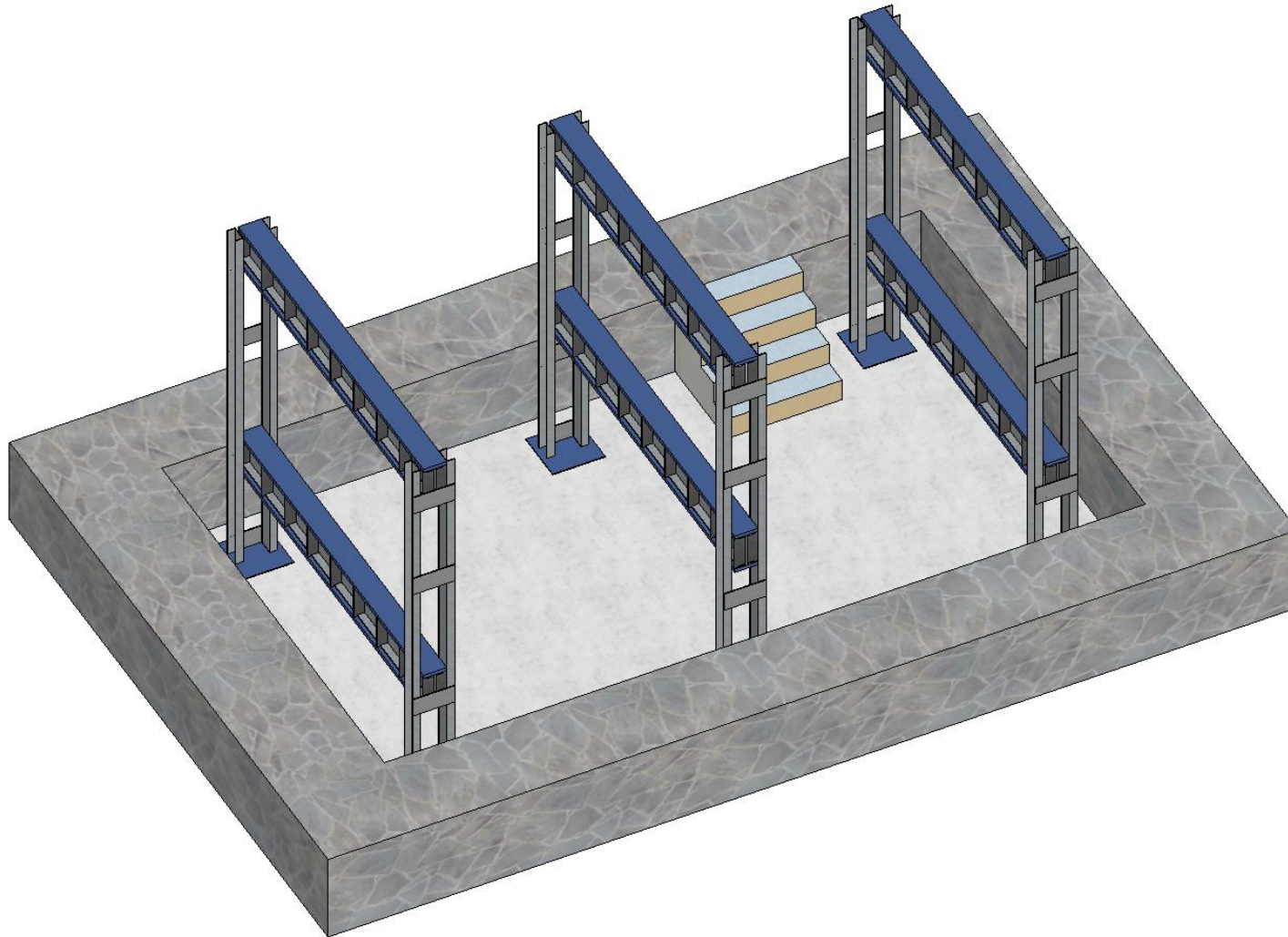
BIRLA INSTITUTE OF TECHNOLOGY AND SCIENCE, PILANI – 333031

September 2020

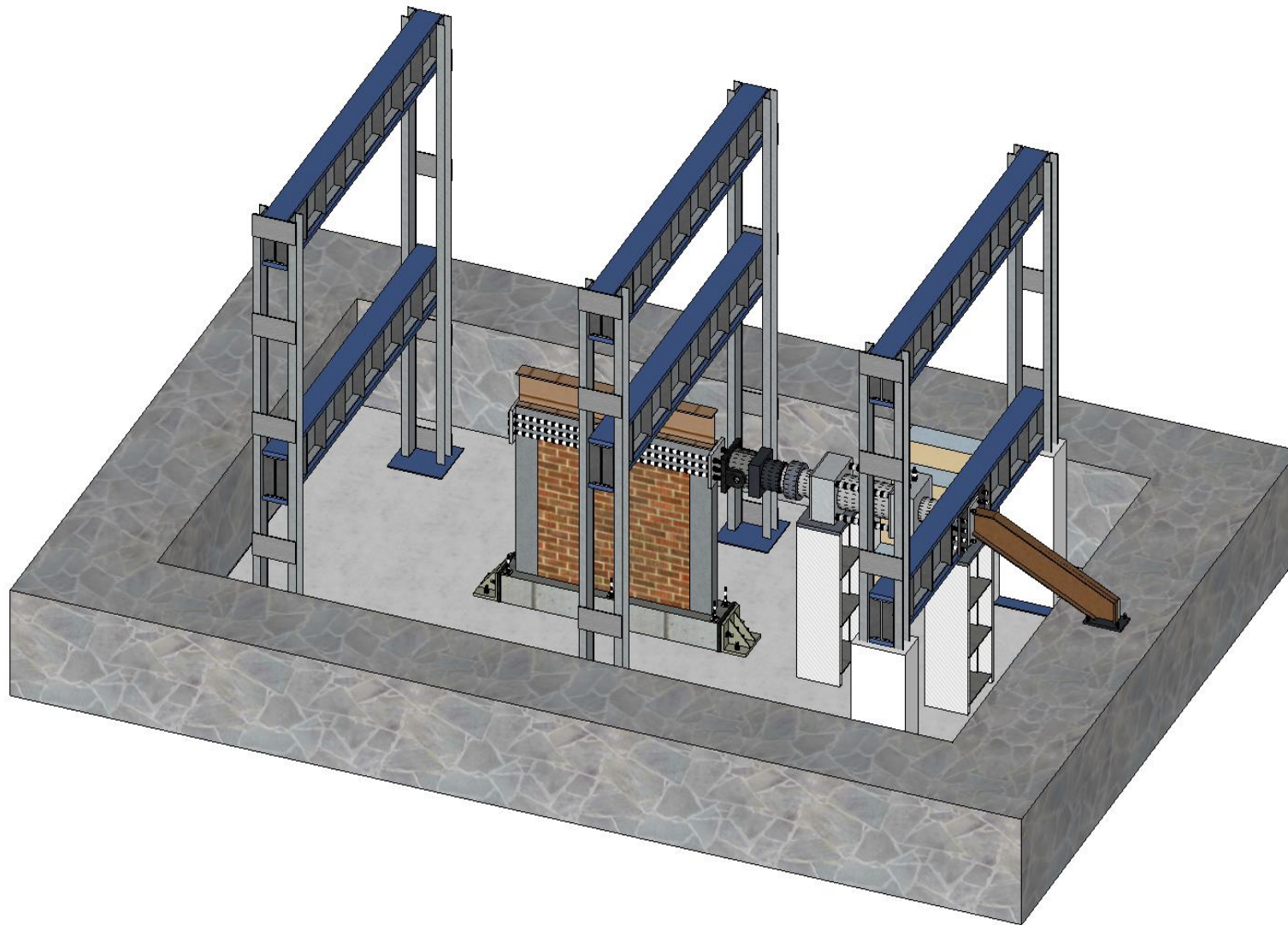
I. DRAWING AND DESIGN DETAILS

RAW MATERIAL: Mild Steel		QUANTITY: XX		DEPARTMENT OF CIVIL ENGINEERING BITS PILANI, 333031.
RAW MATERIAL SIZE: XX		WEIGHT: ____ in KG		
	NAME	DATE	SIGN	
DRAWN	Jaya Kumar Bhaskar	-	-	
CHECKED	Dipendu Bhunia Lampros Koutas	-	-	
APPROVED	Dipendu Bhunia	-	-	
DIMENSIONS ARE DENOTED IN RED COLOUR	NO THICK LINES USED IN THE DIAGRAM	SCALE USED IN AUTOCAD – 1 : 100		PAGE NUMBER
HIDDEN PORTIONS ARE DENOTED USING RED AND PINK DASHED LINES	φ - DIAMETER TKS - Thickness	TITLE: SPECIFIED UNDER CONTENTS FOR EACH FIGURE		
ALL DIMENSIONS ARE IN mm IN AUTOCAD	ALL DIMENSIONS ARE IN mm IN SKETCHUP MAKE	ALL DIMENSIONS ARE IN m IN STAAD Pro.		

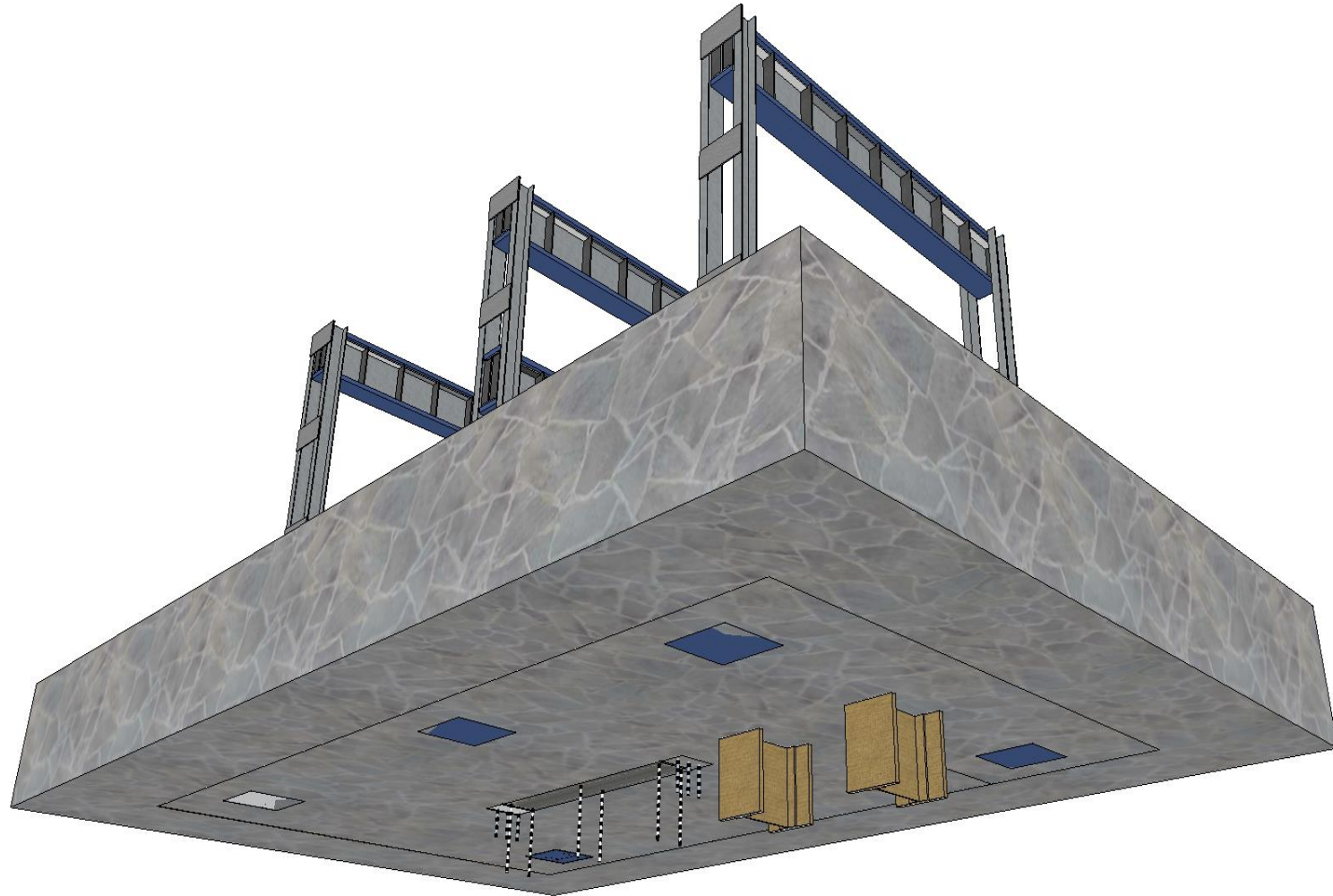
II. SKETCHUP MAKE - WHOLE EXPERIMENTAL SETUP IN LABORATORY



LOADING FRAME BEFORE THE INSTALLATION OF THE ACTUATOR - TOP VIEW



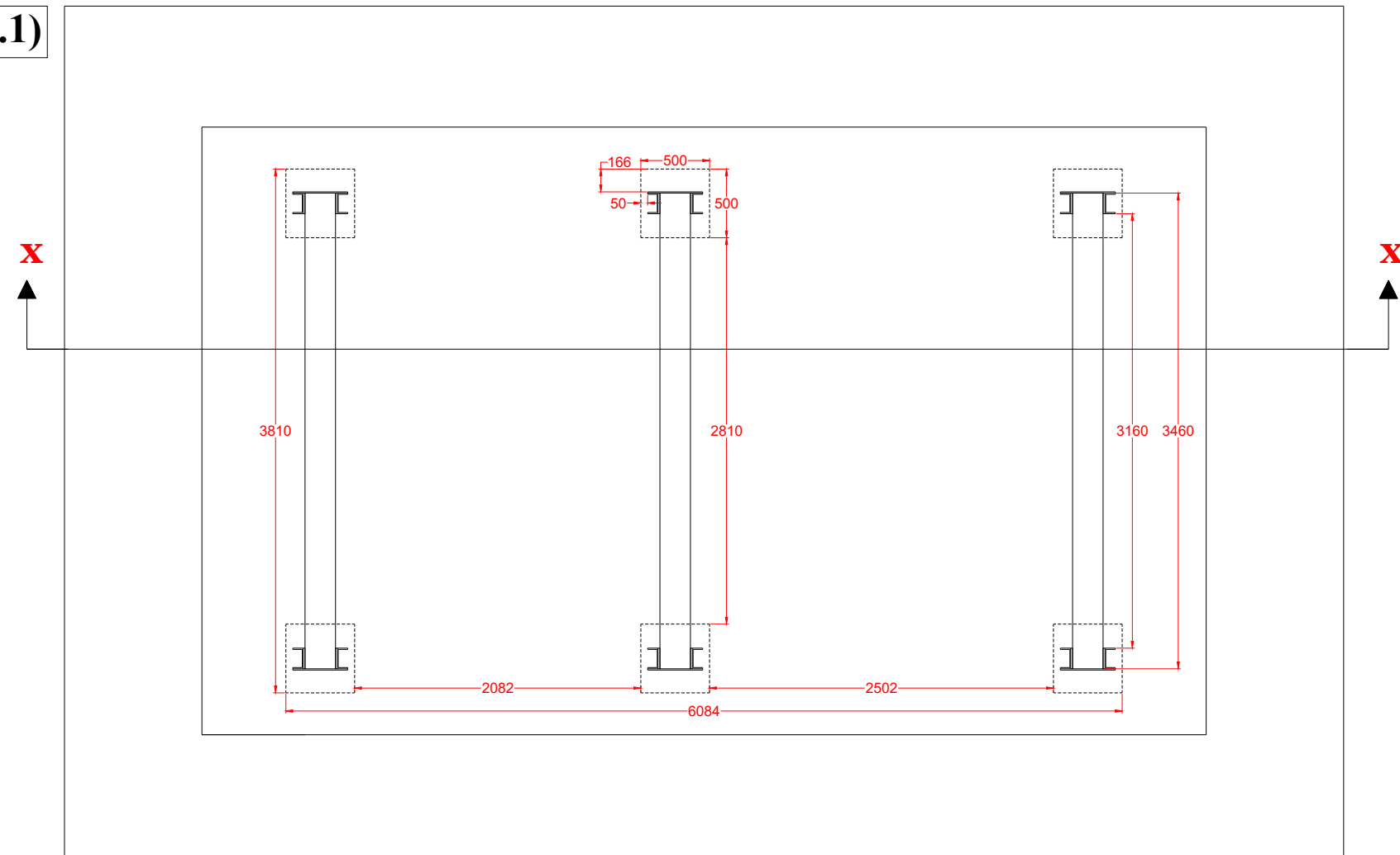
LOADING FRAME AFTER THE INSTALLATION OF THE ACTUATOR (EXPERIMENTAL SETUP) - TOP VIEW



LOADING FRAME AFTER THE INSTALLATION OF THE ACTUATOR - BOTTOM VIEW

1.1)

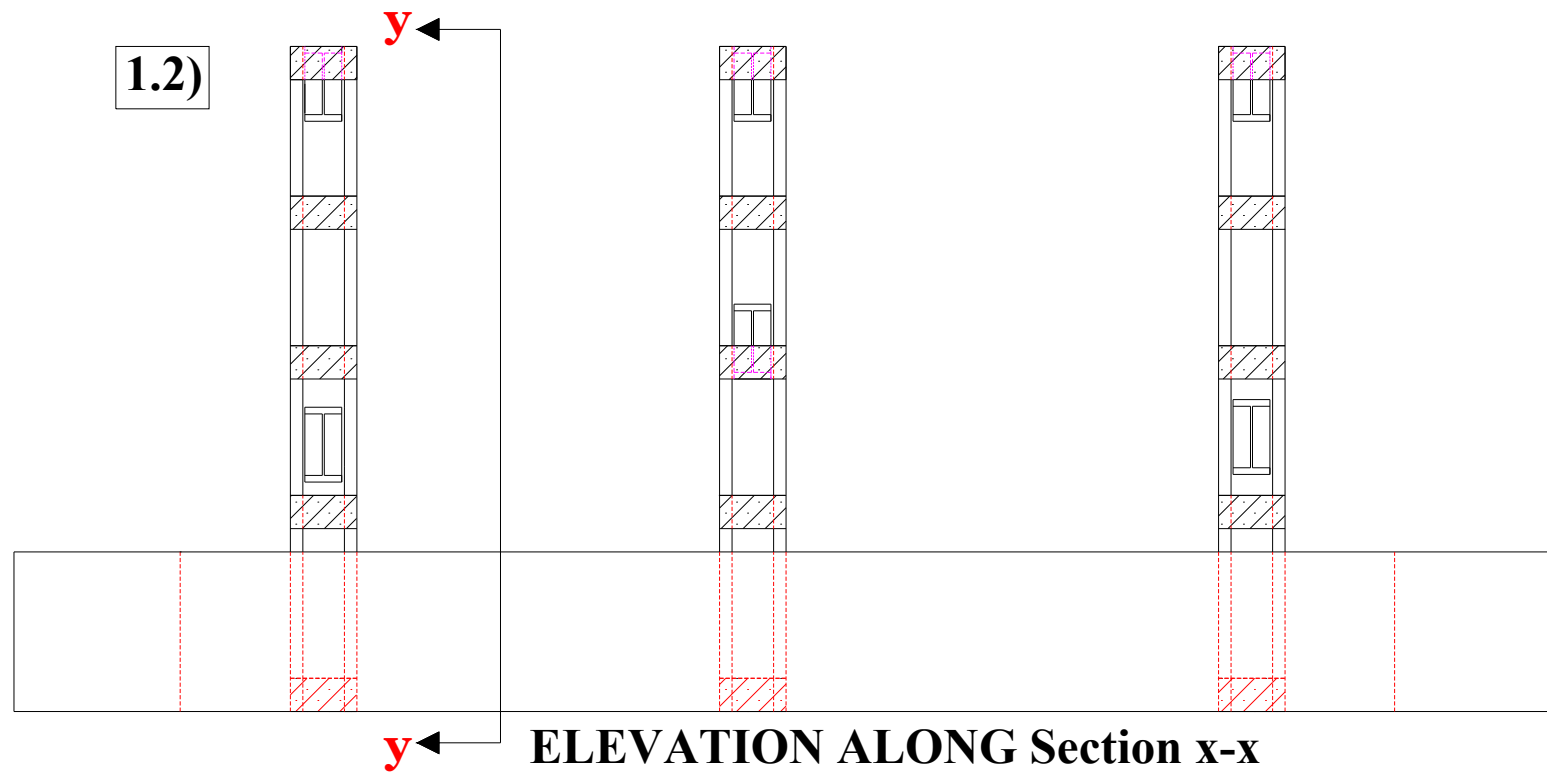
ALL DIMENSIONS ARE IN mm
SCALE 1:100



1. EXISTING LOADING
FRAME
IN LABORATORY

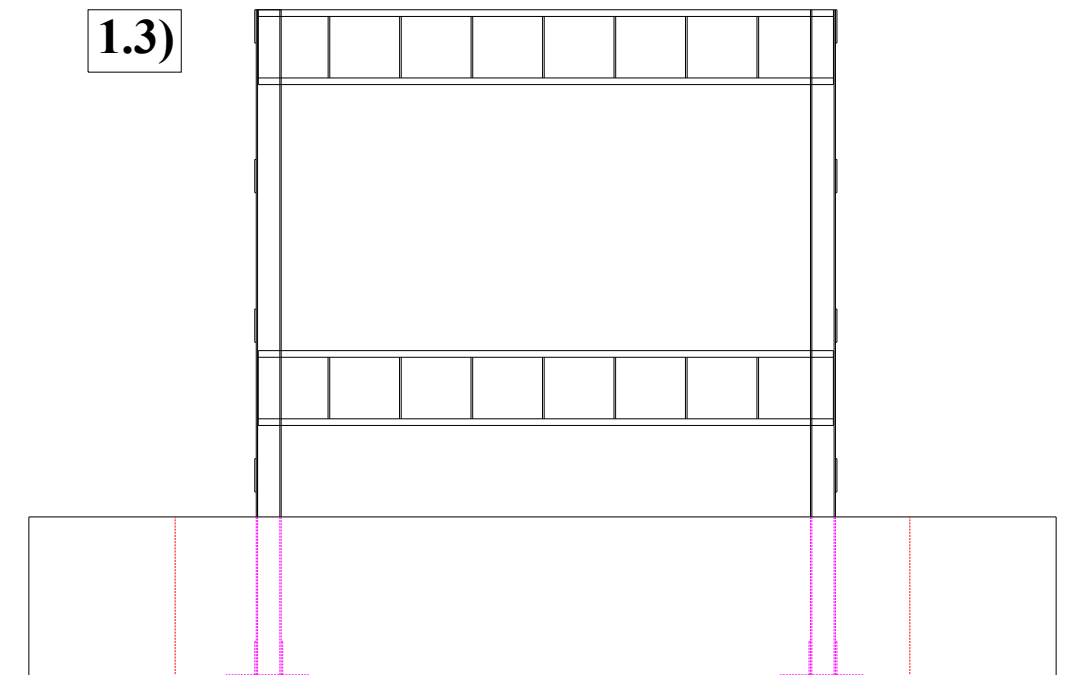
PLAN

1.2)



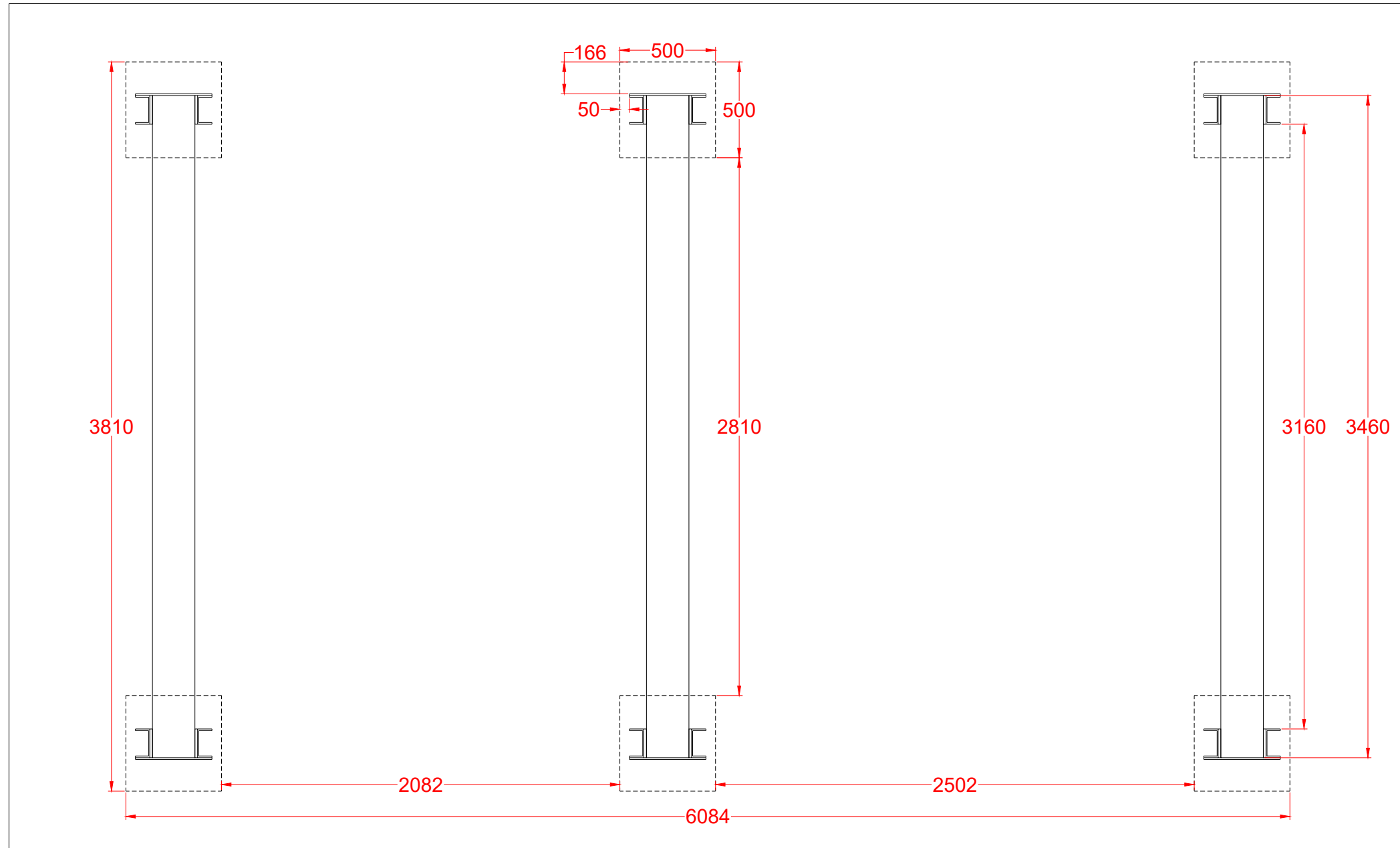
ELEVATION ALONG Section x-x

1.3)



VIEW ALONG Section y-y

1.1)



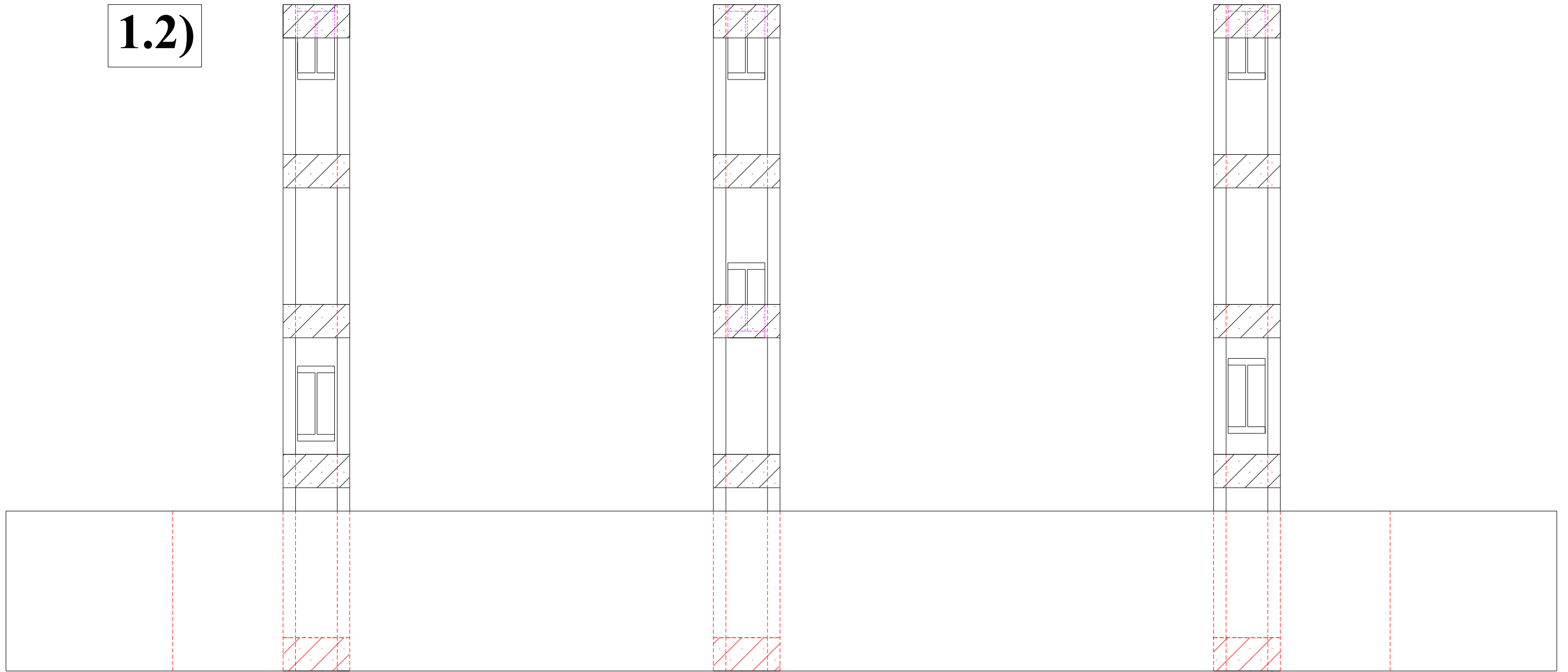
PLAN

PRODUCED BY AN AUTODESK STUDENT VERSION

ALL DIMENSIONS ARE IN mm

SCALE 1:100

1.2)

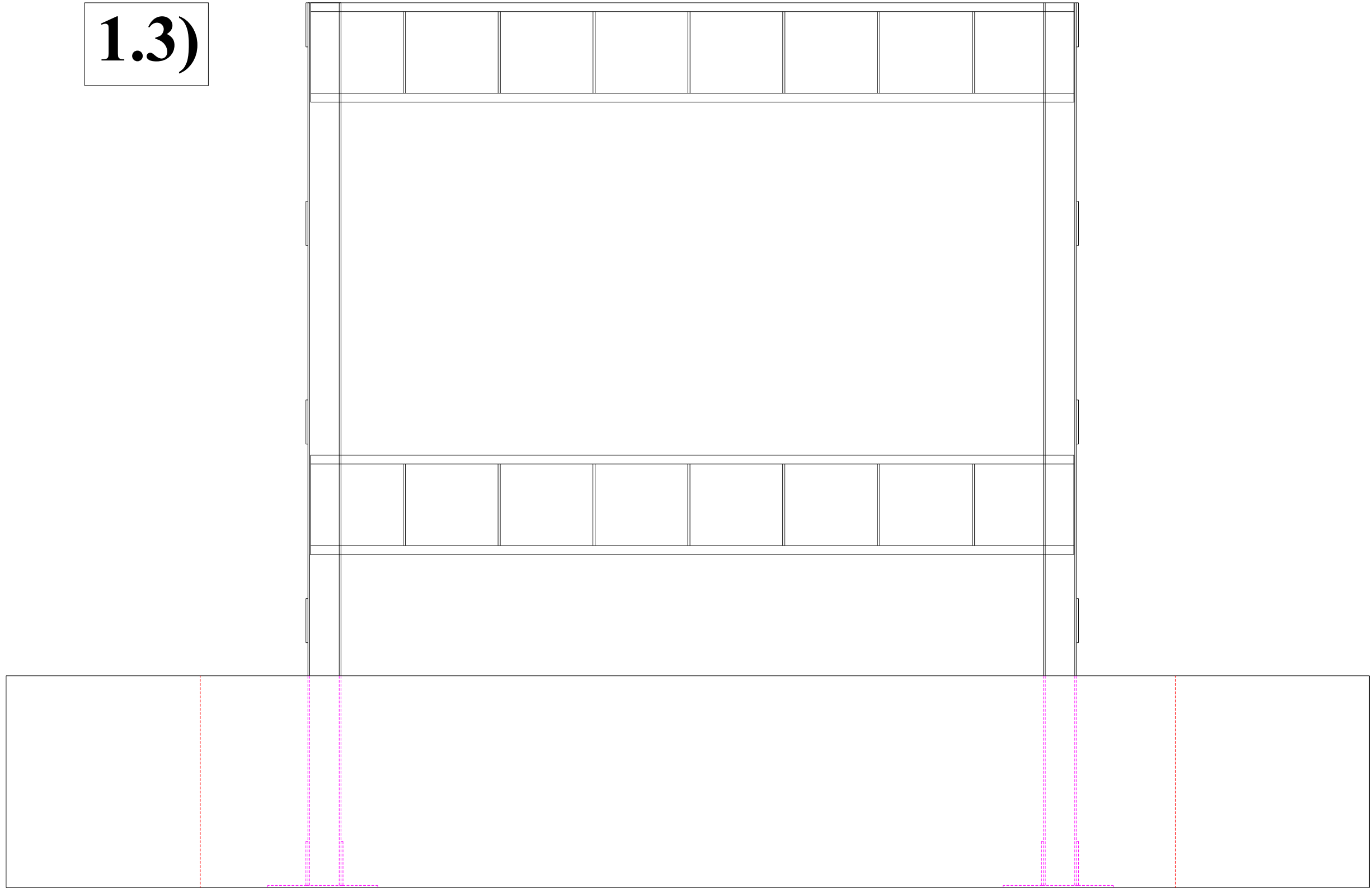


ELEVATION ALONG section x-x

ALL DIMENSIONS ARE IN mm

SCALE 1:100

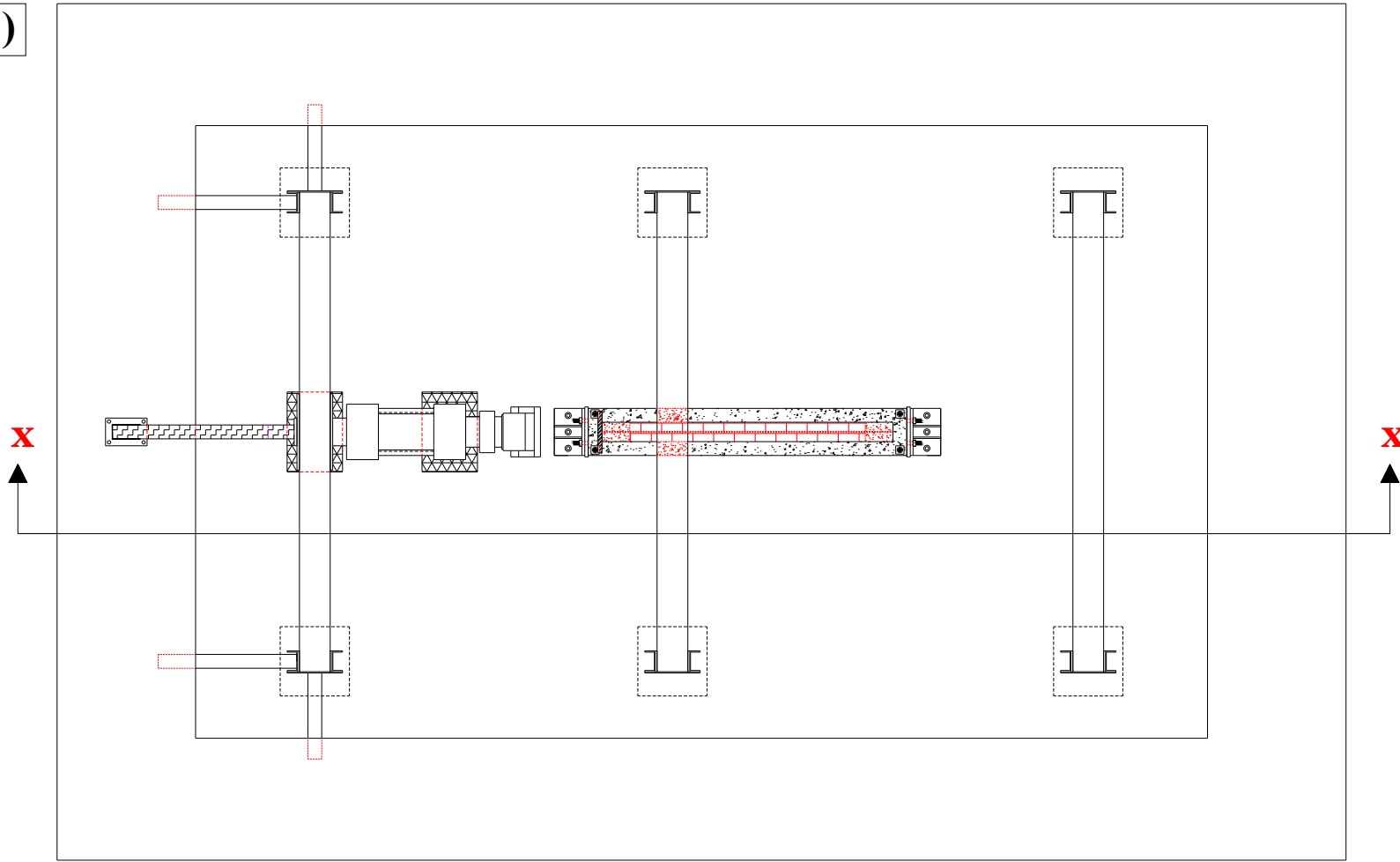
1.3)



VIEW ALONG section y-y

ALL DIMENSIONS ARE IN mm
SCALE 1:100

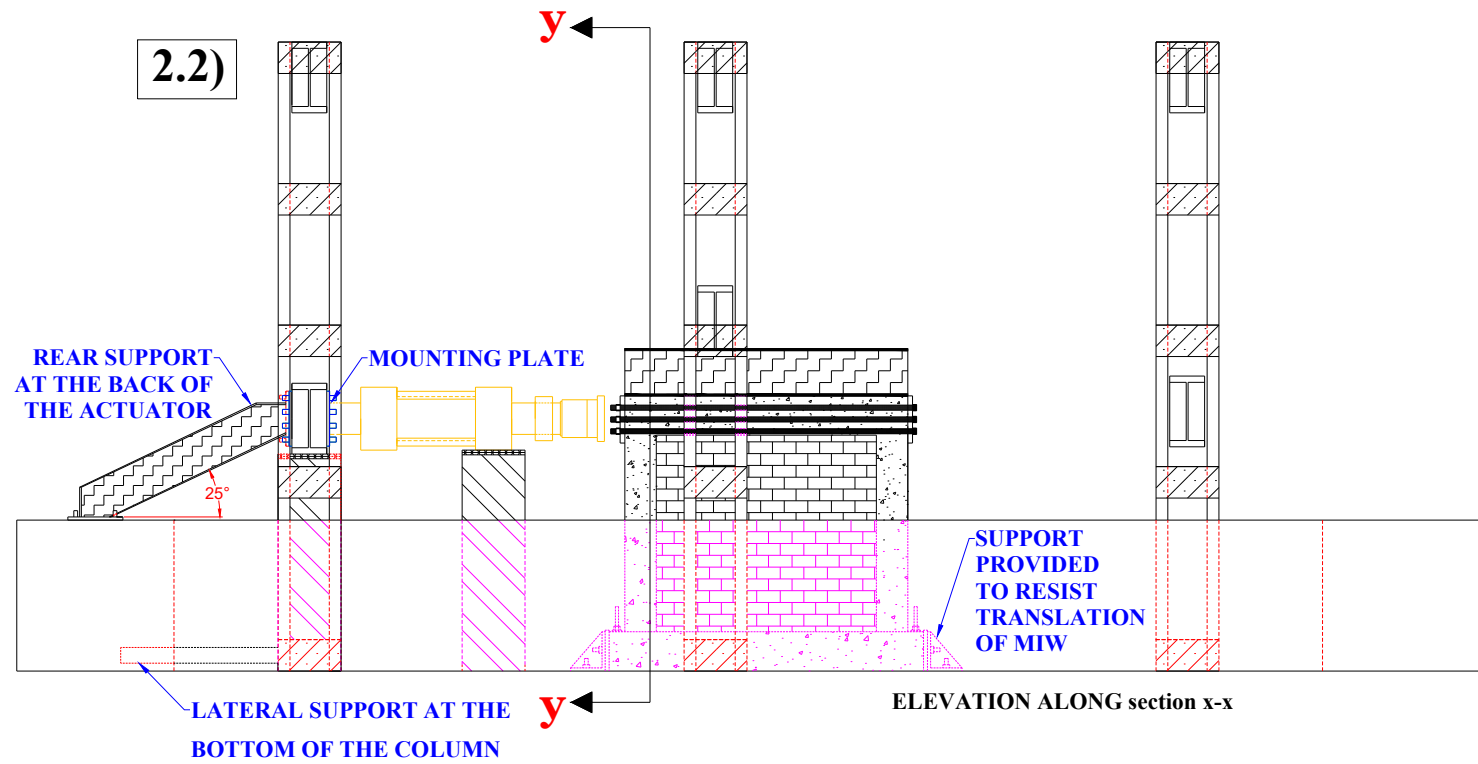
2.1)



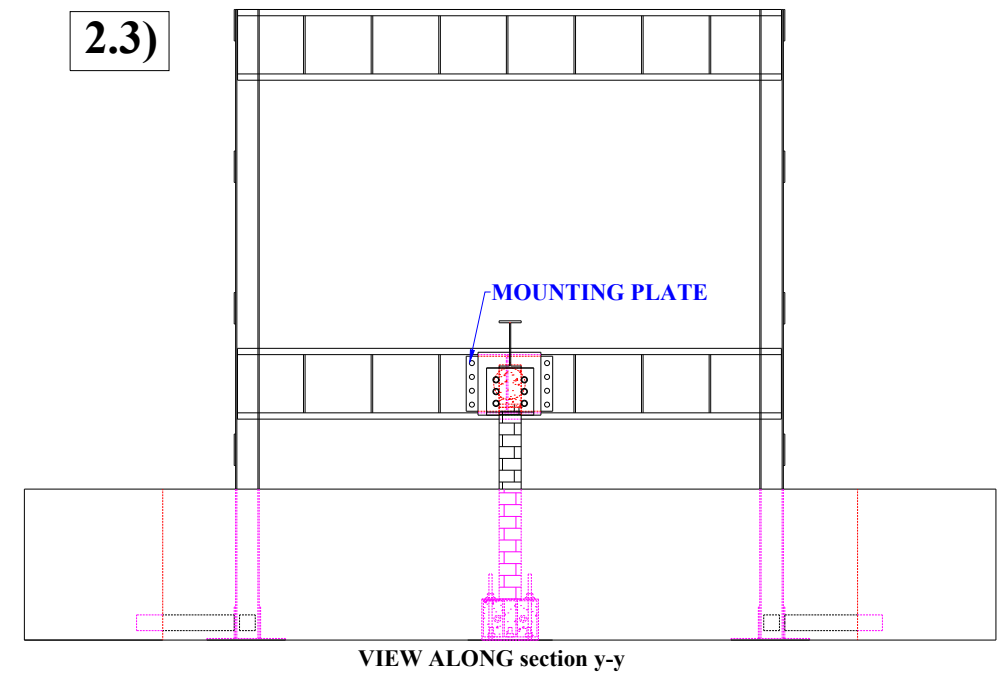
ALL DIMENSIONS ARE IN mm
SCALE 1:100

2. LOADING ON TO THE SPECIMEN WITH STEEL BEAM ABOVE MIW

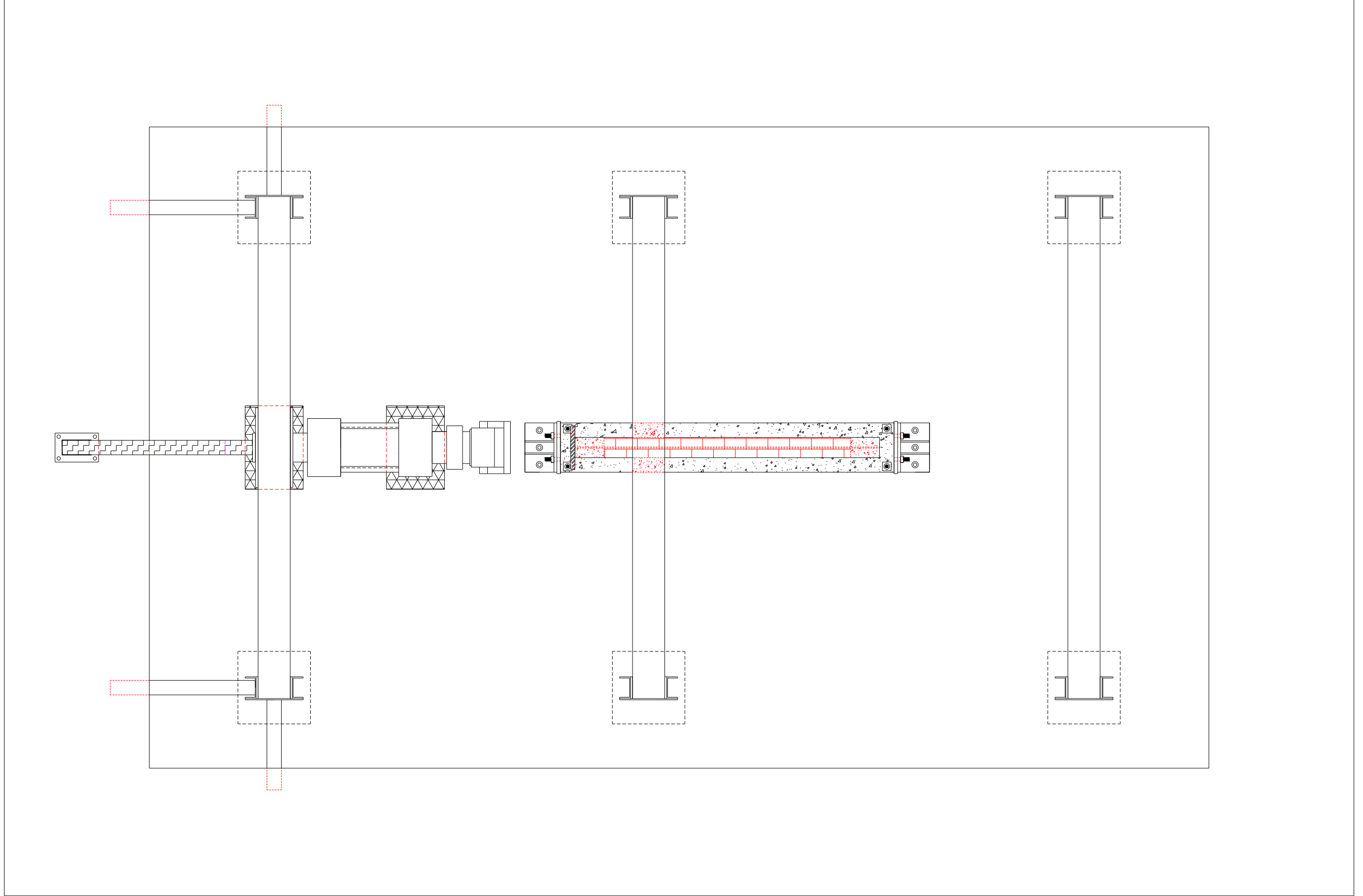
2.2)



2.3)

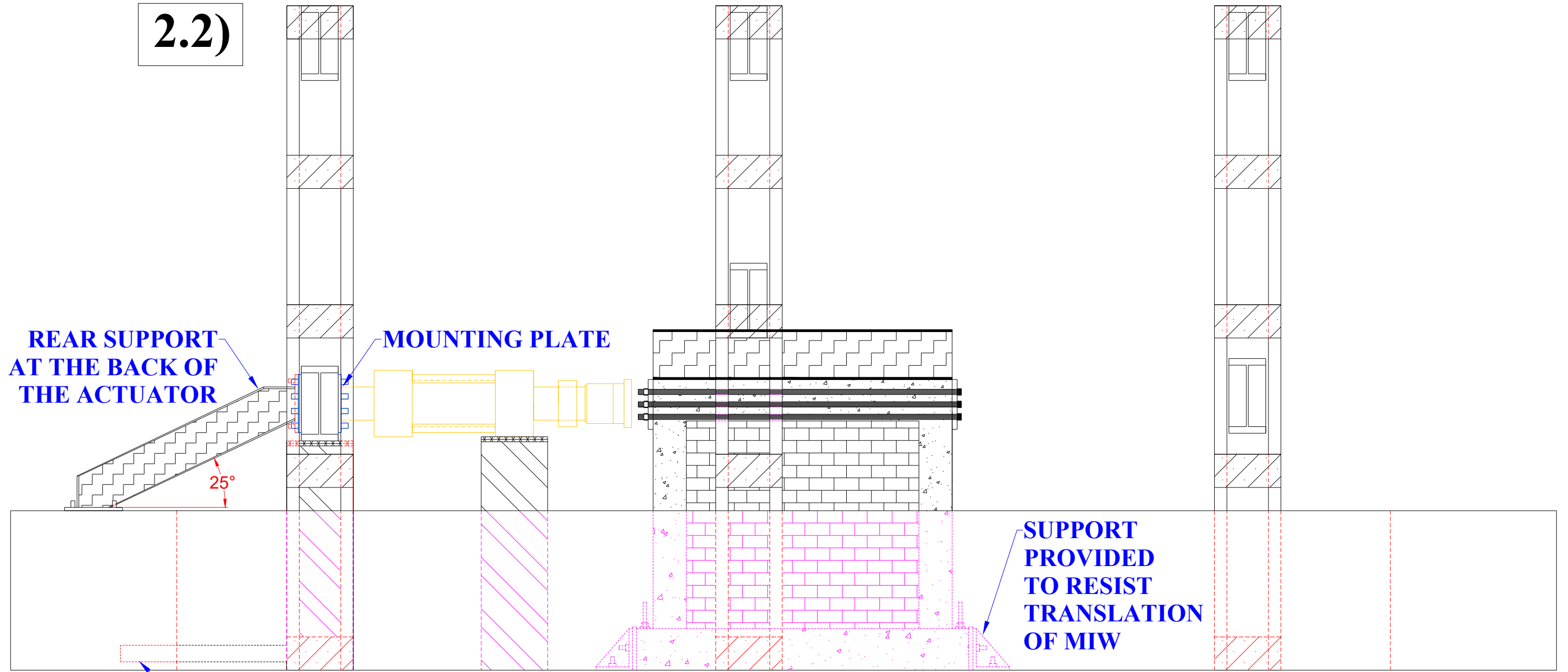


2.1)



PLAN

2.2)



REAR SUPPORT
AT THE BACK OF
THE ACTUATOR

MOUNTING PLATE

25°

SUPPORT
PROVIDED
TO RESIST
TRANSLATION
OF MIW

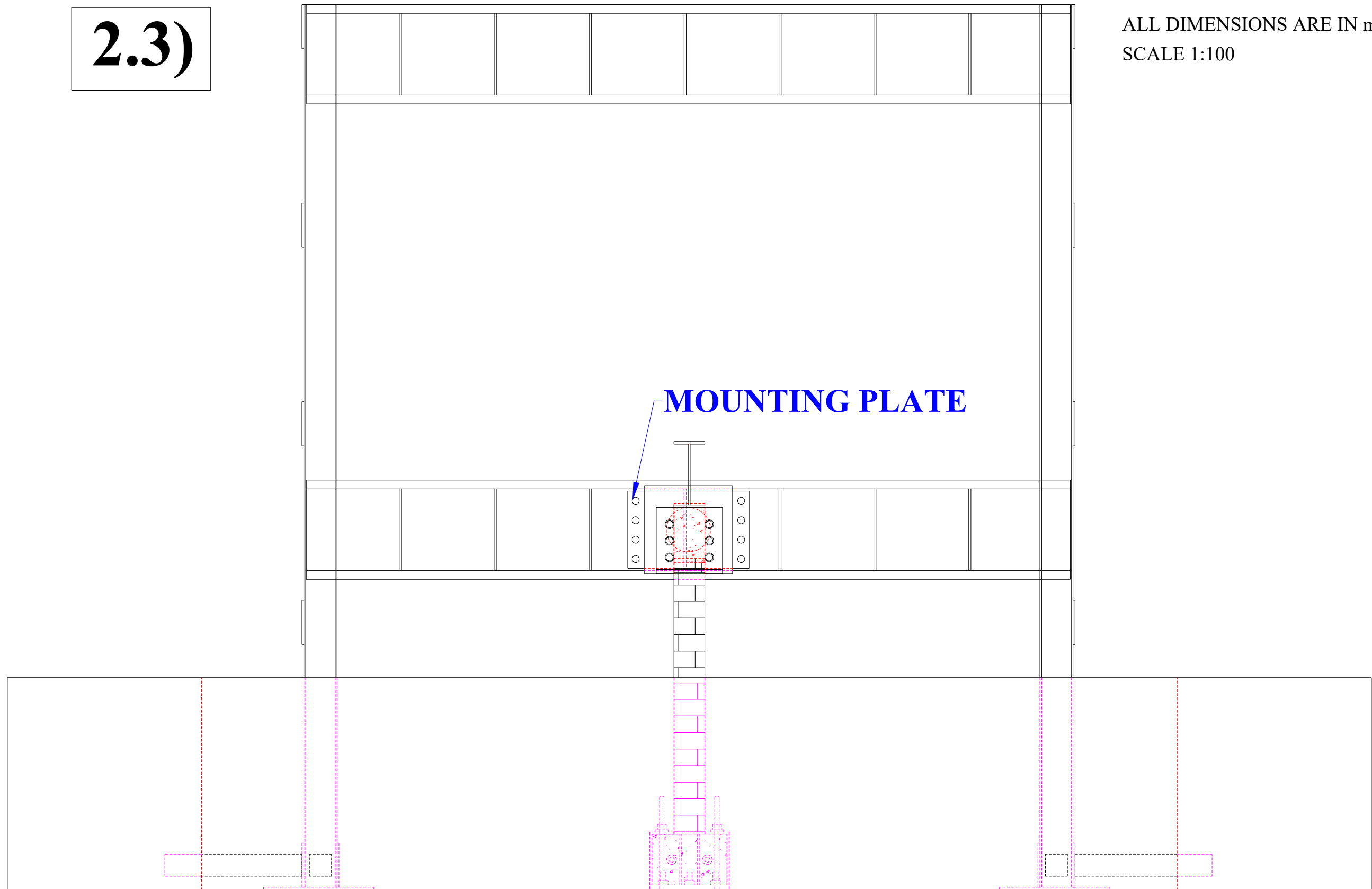
LATERAL SUPPORT AT THE
BOTTOM OF THE COLUMN

ELEVATION ALONG section x-x

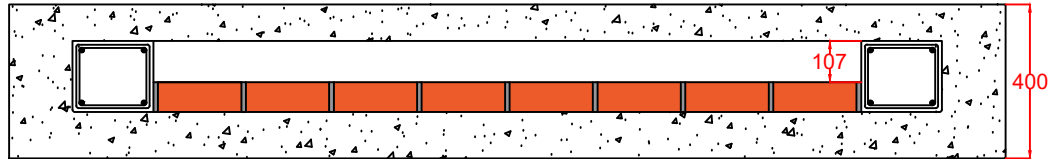
ALL DIMENSIONS ARE IN mm
SCALE 1:100

2.3)

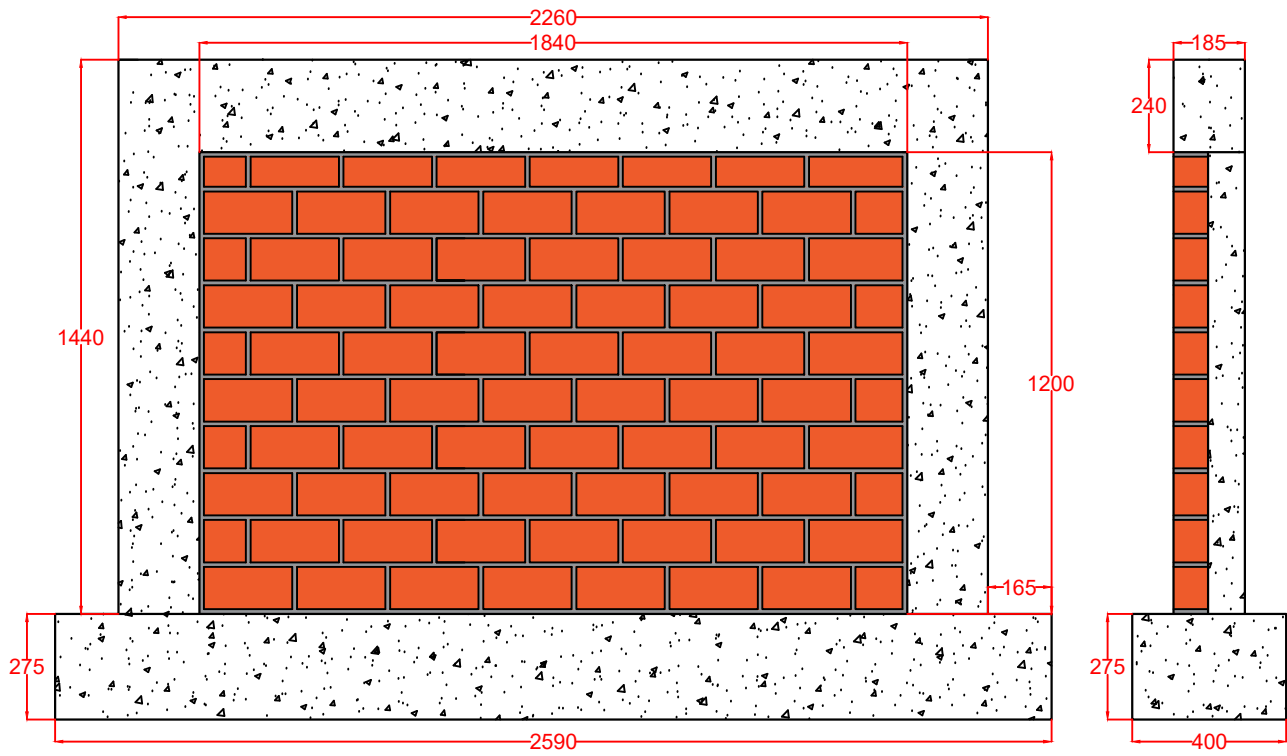
ALL DIMENSIONS ARE IN mm
SCALE 1:100



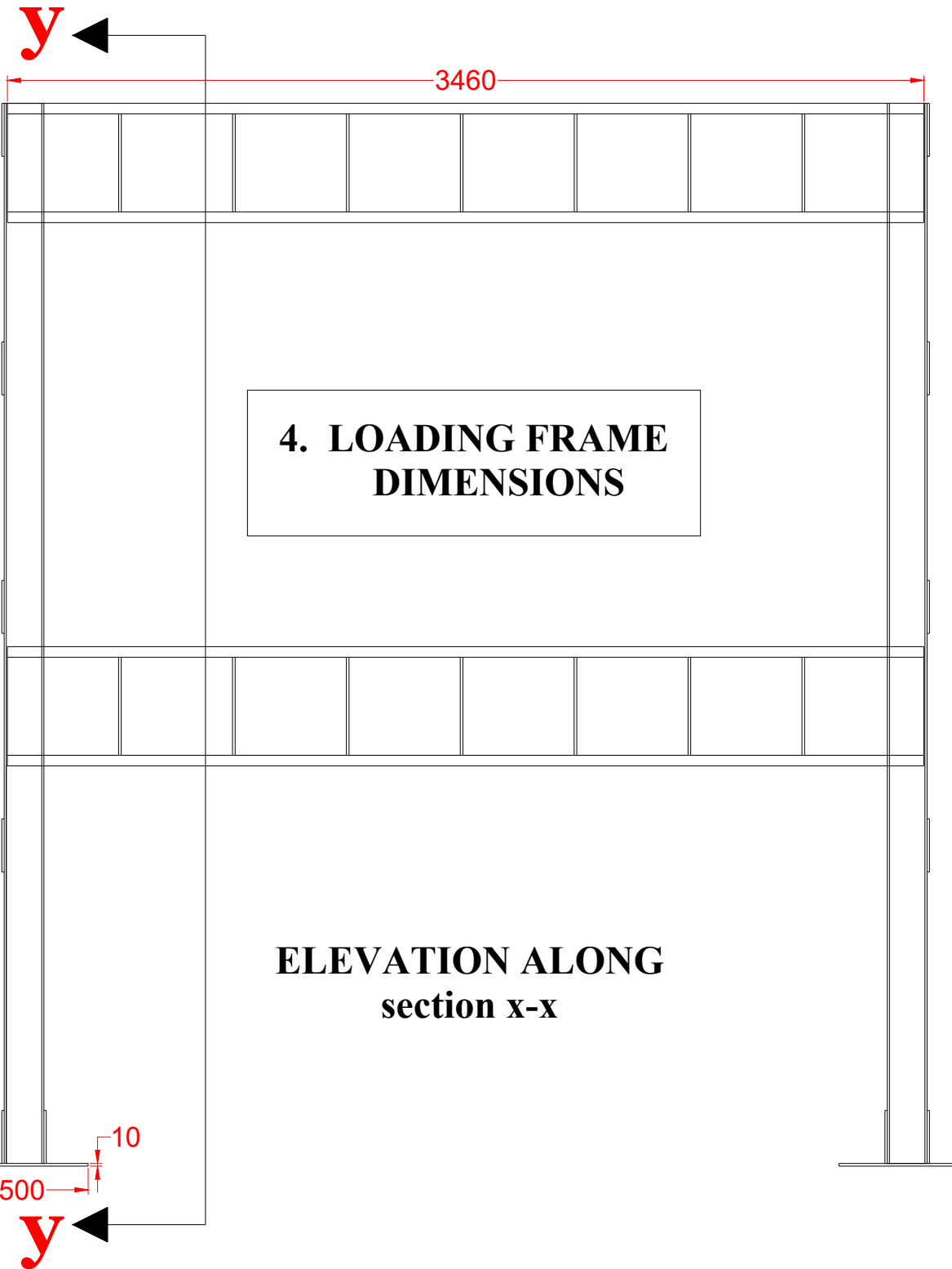
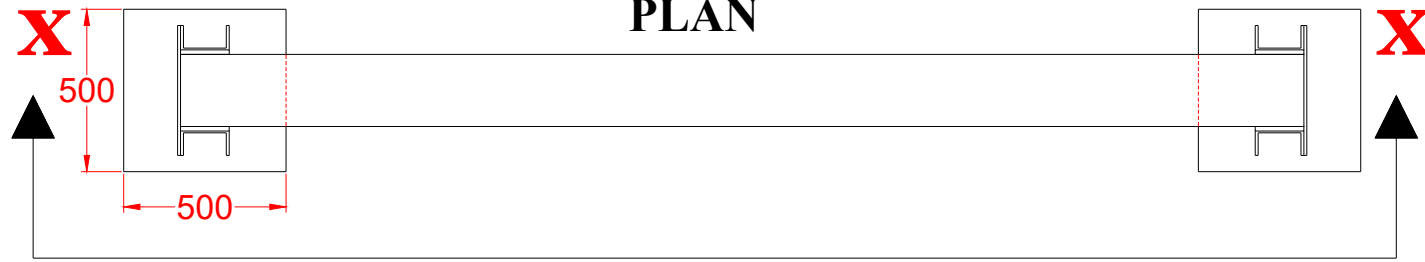
VIEW ALONG section y-y



3. DIMENSIONS OF TYPICAL MASONRY INFILL WALL (MIW)

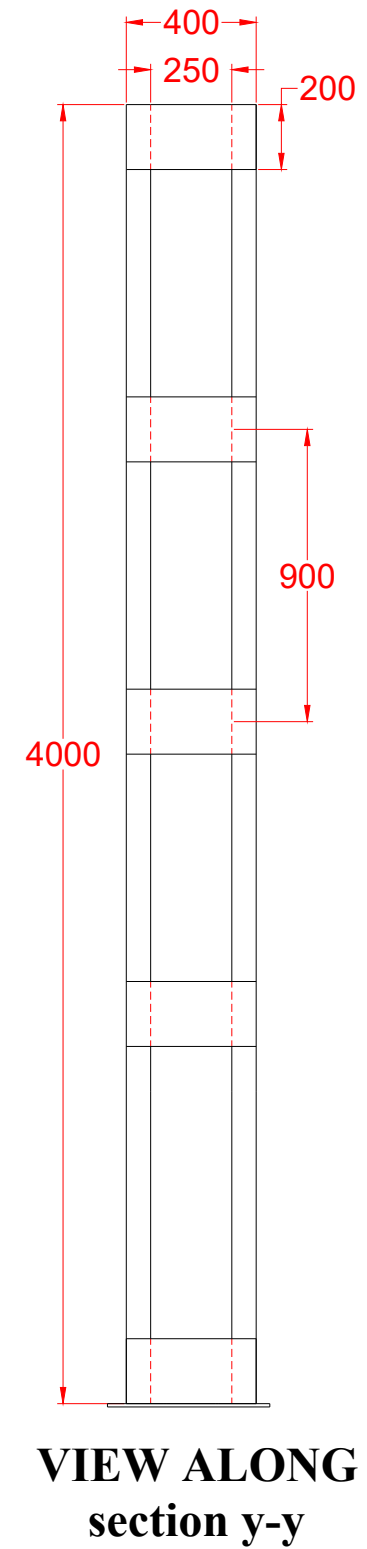


PRODUCED BY AN AUTODESK STUDENT VERSION
PLAN



4. LOADING FRAME
DIMENSIONS

ELEVATION ALONG
section x-x



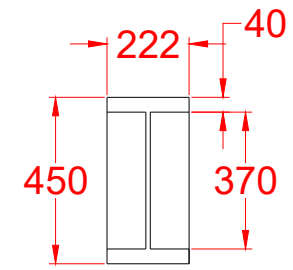
VIEW ALONG
section y-y

ALL DIMENSIONS ARE IN mm
SCALE 1:100

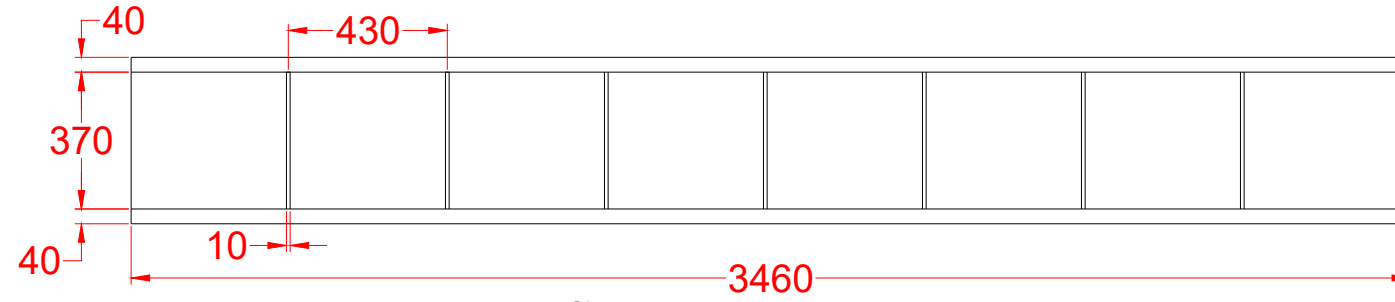
PRODUCED BY AN AUTODESK STUDENT VERSION

PRODUCED BY AN AUTODESK STUDENT VERSION

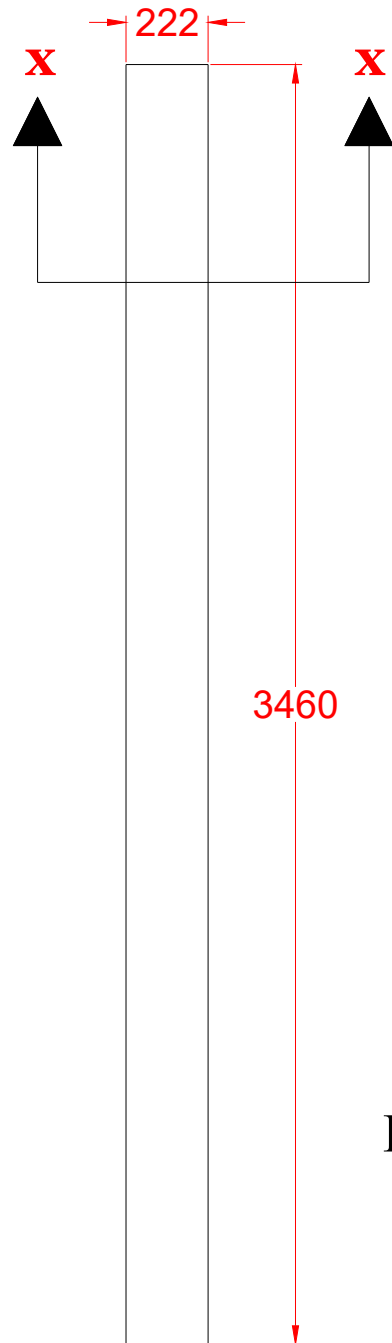
PRODUCED BY AN AUTODESK STUDENT VERSION



**VIEW ALONG
section x-x**



SIDE VIEW



ELEVATION

**5. PLATE GIRDER
DIMENSIONS**

ISMB 350

COVER PLATE DIMENSIONS -

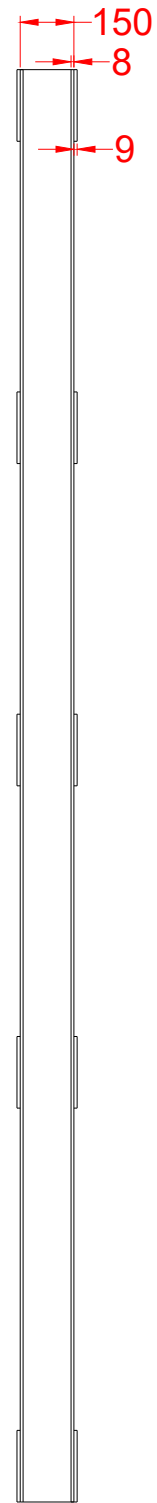
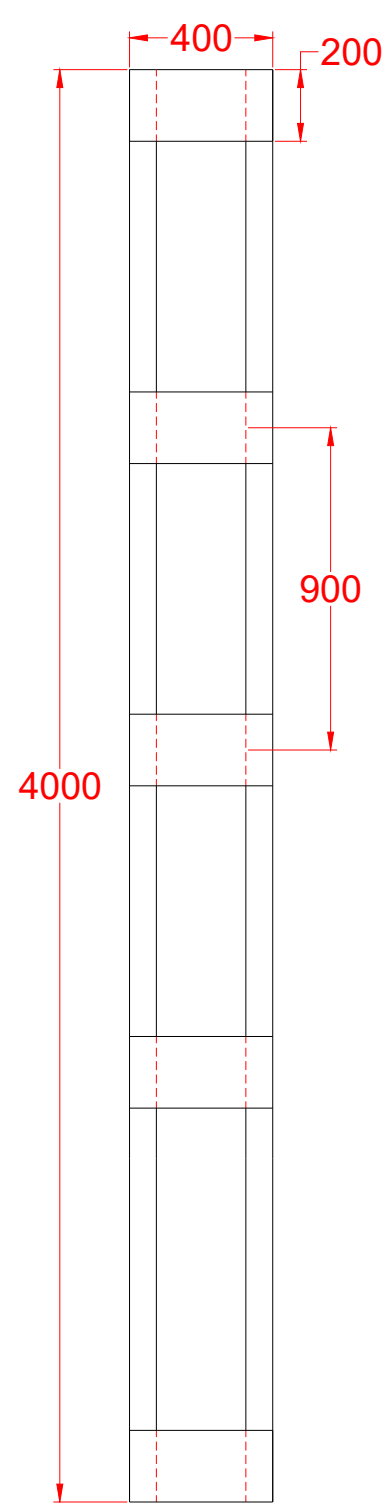
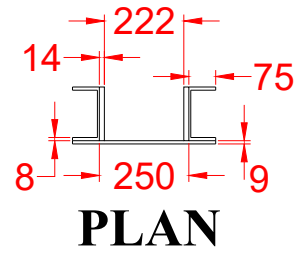
TOP PLATE WIDTH = 222 mm

TOP PLATE TKS = 40 mm

BOTTOM PLATE SIZE SAME

AS TOP PLATE

ALL DIMENSIONS ARE IN mm
SCALE 1:100

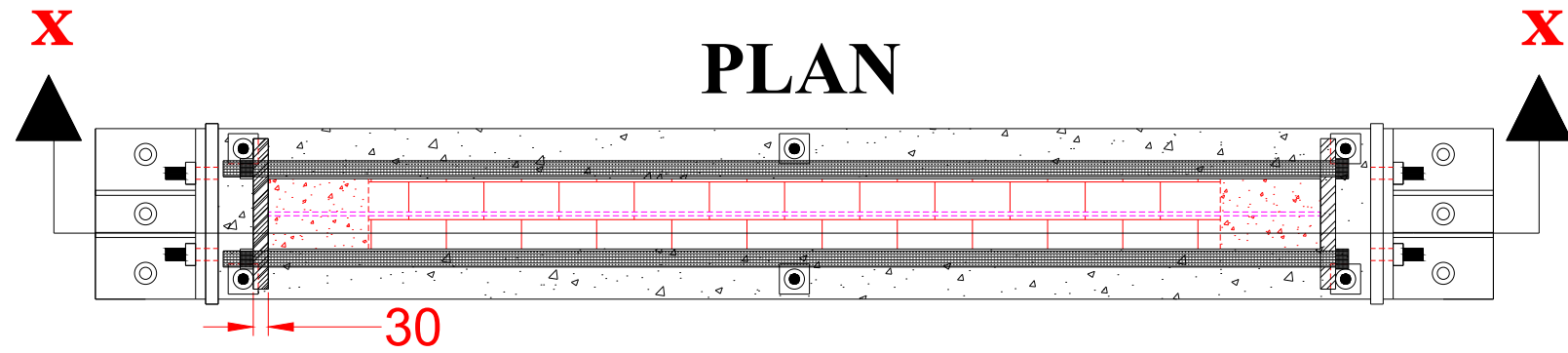


6. COLUMN DIMENSIONS

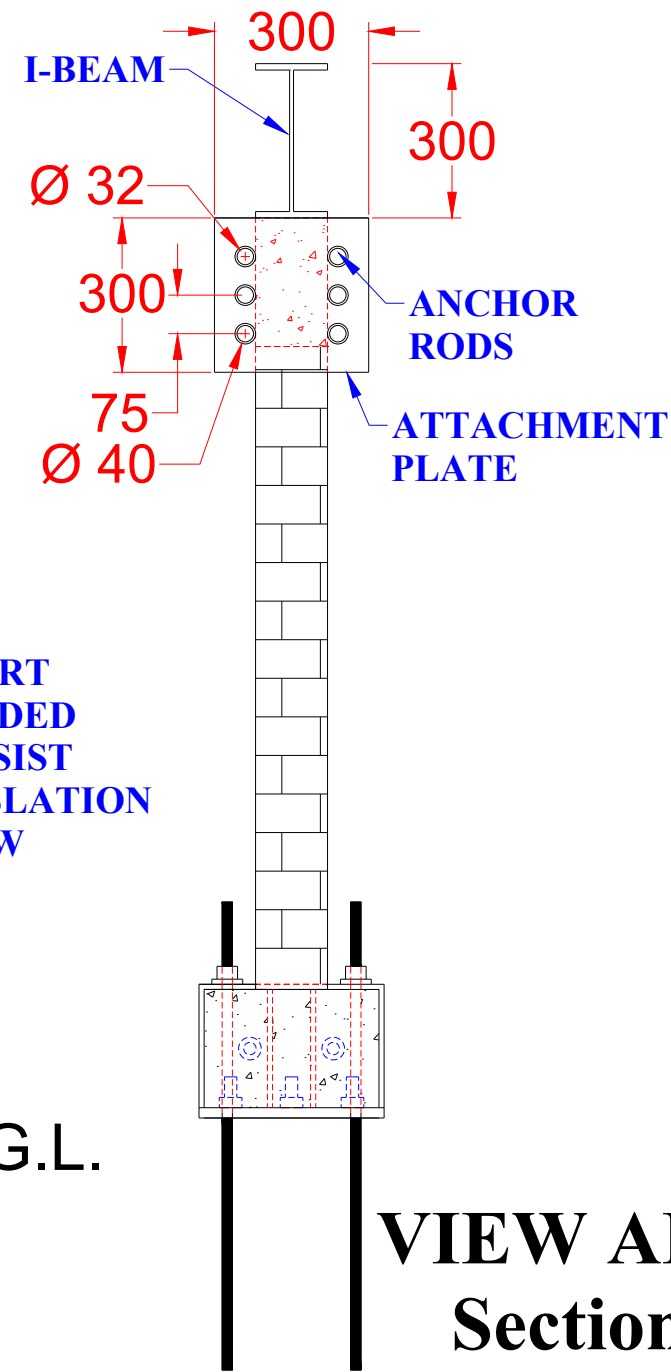
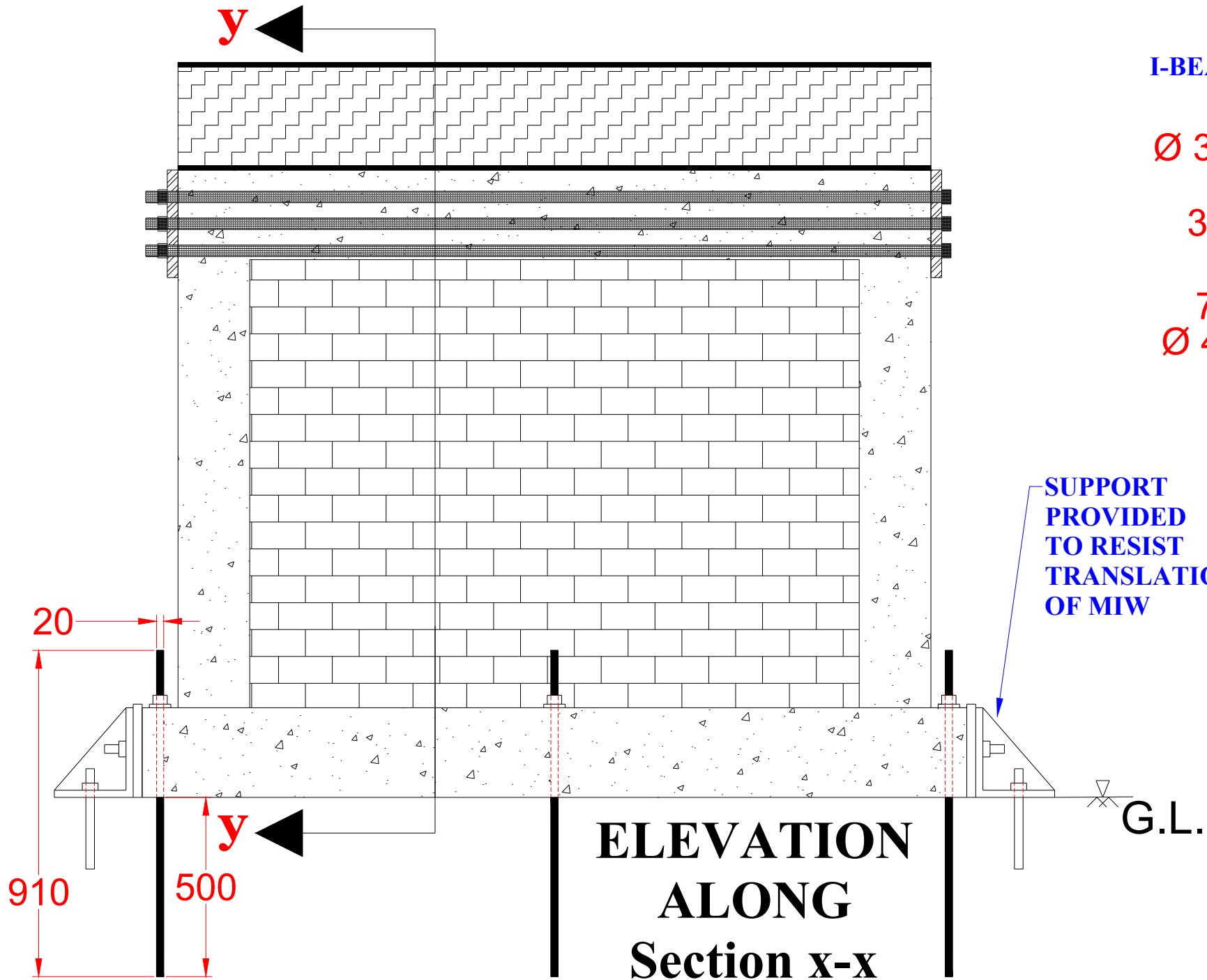
ISMC 150
BACK-TO-BACK
SPACING = 250 mm
FLANGE WIDTH = 75 mm
FLANGE TKS = 8 mm
WEB TKS = 5 mm

BATTEN PLATE DETAILS -
WIDTH = 400 mm
DEPTH = 200 mm
TKS = 9 mm
SPACING = 900 mm c/c

ALL DIMENSIONS ARE IN mm
 SCALE 1:100

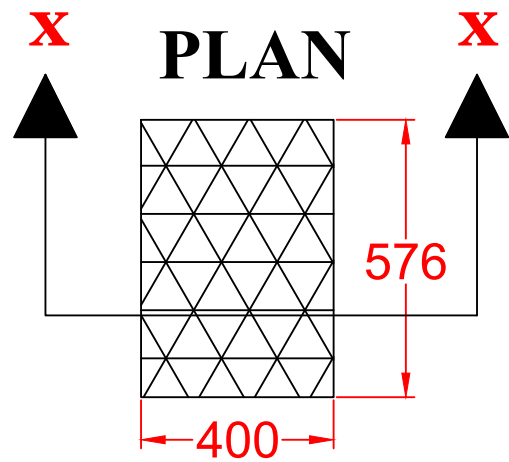


7. LOADING ON TO THE SPECIMEN WITH STEEL BEAM ABOVE MIW (TEST SPECIMEN SETUP)

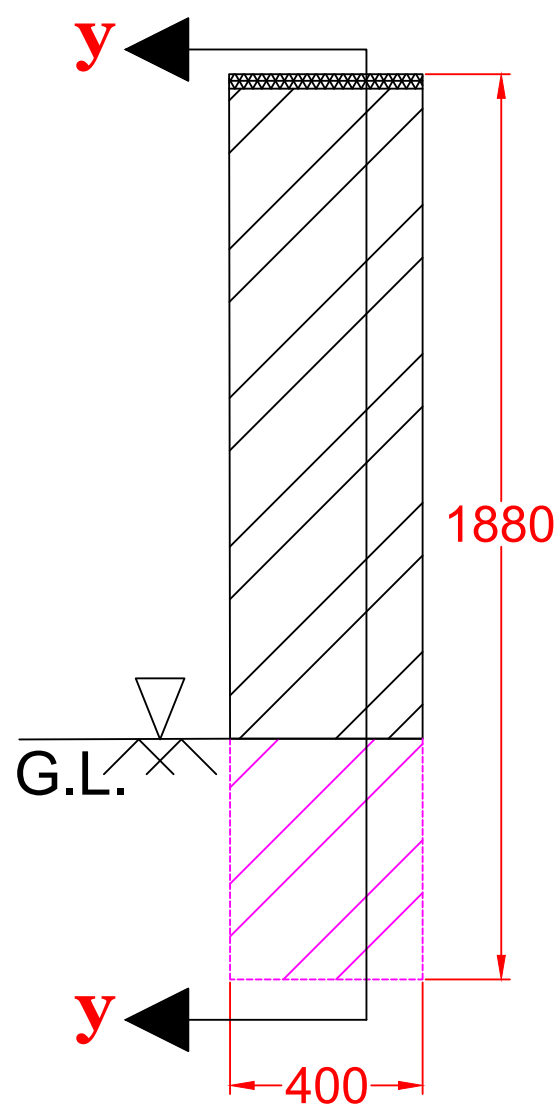


- R.C. FRAME DETAILS -**
- CONCRETE GRADE = M 20
- BRICK DETAILS -**
- BRICK GRADE = FIRST CLASS
- BRICK SIZE = 23 x 10.8 x 8 cm
- I-BEAM DETAILS -**
- ISMB 300
- FLANGE WIDTH = 140 mm
- FLANGE TKS = 12.5 mm
- WEB TKS = 7.5 mm
- ATTACHMENT PLATE DETAILS -**
- WIDTH = 300 mm
- DEPTH = 300 mm
- TKS = 30 mm
- ANCHOR RODS DETAILS -**
- LENGTH = 2250 mm
- DIAMETER = 32 mm
- CENTER-TO-CENTER DISTANCE = 75 mm

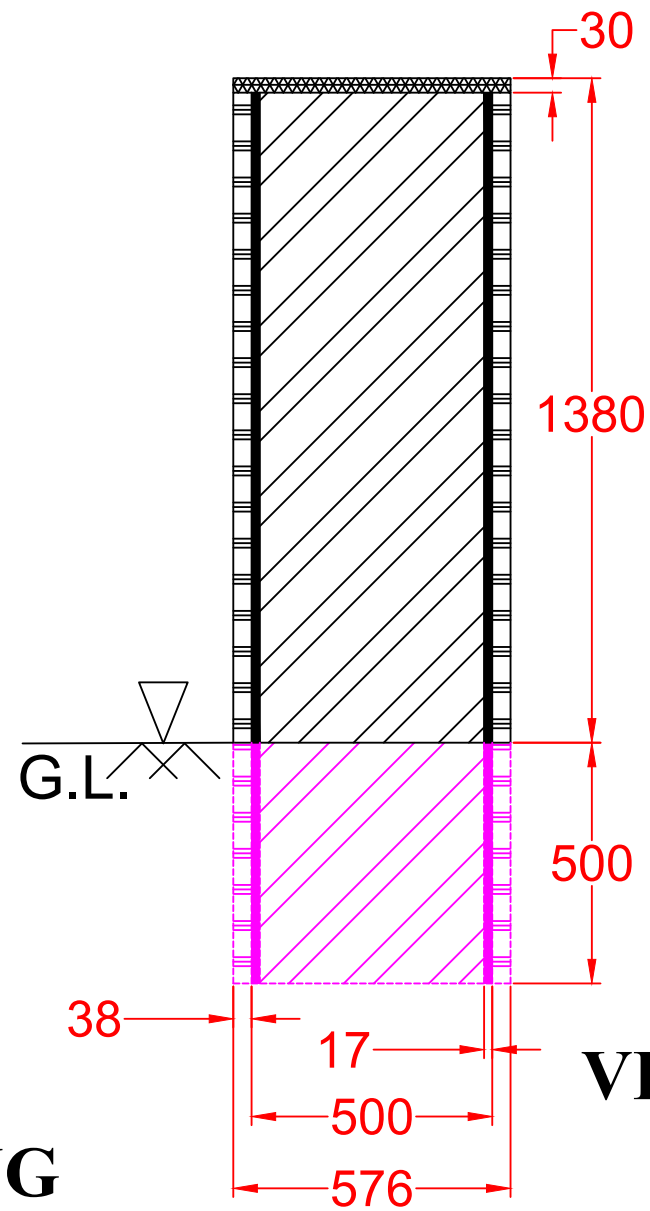
ALL DIMENSIONS ARE IN mm
SCALE 1:100



8. EXTRA COLUMN BELOW BEAM



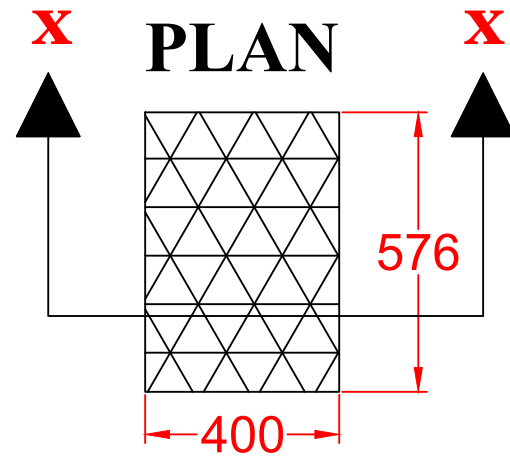
ELEVATION ALONG section x-x



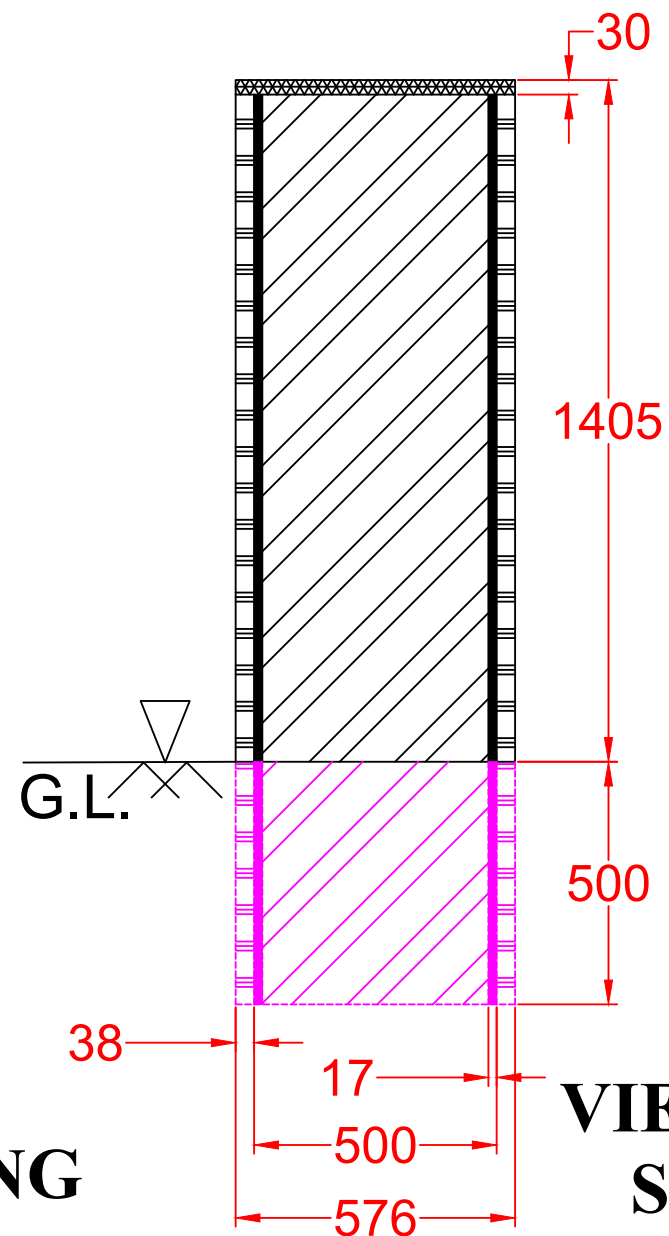
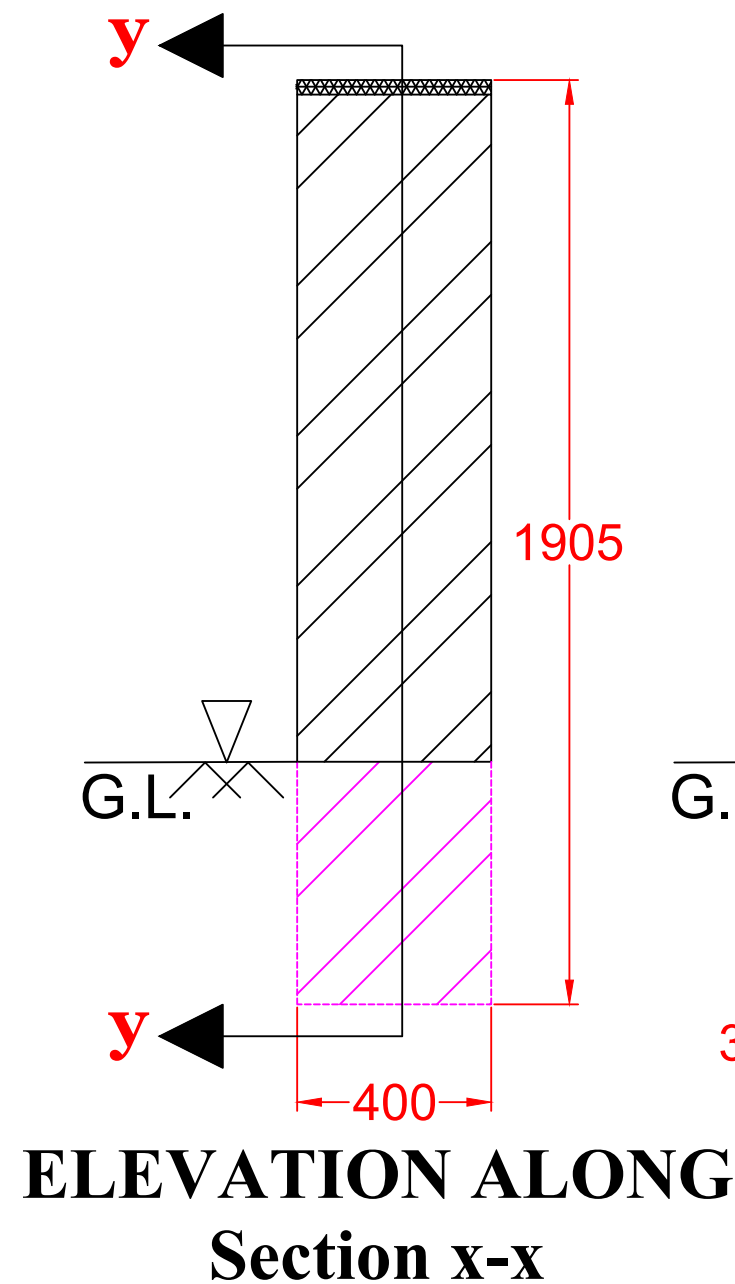
VIEW ALONG section y-y

ISWB 500 with COVER PLATES
COVER PLATE DIMENSIONS -
TOP PLATE WIDTH = 400 mm
TOP PLATE TKS = 38 mm
BOTTOM PLATE SIZE SAME AS TOP PLATE
G.L. = GROUND LEVEL

ALL DIMENSIONS ARE IN mm
 SCALE 1:100



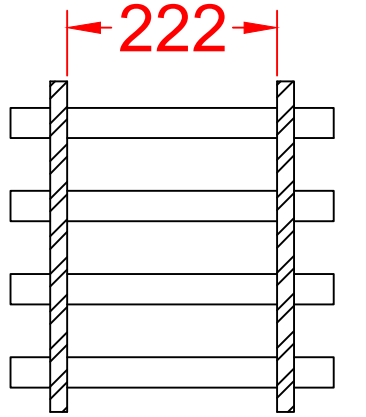
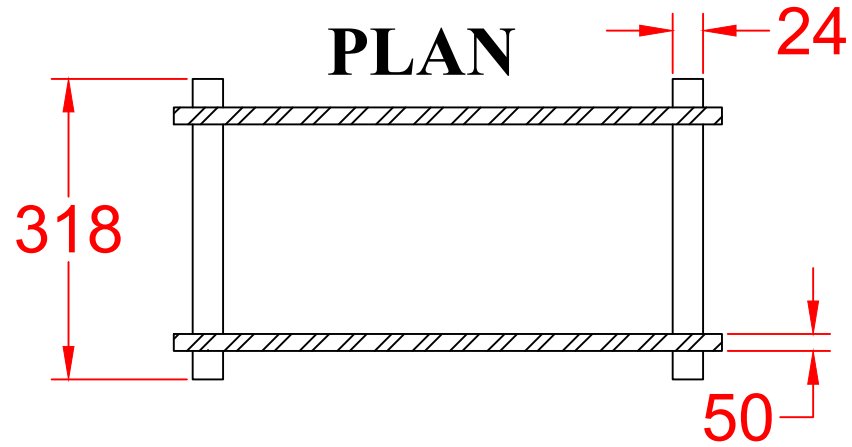
**9. EXTRA COLUMN
BELOW ACTUATOR**



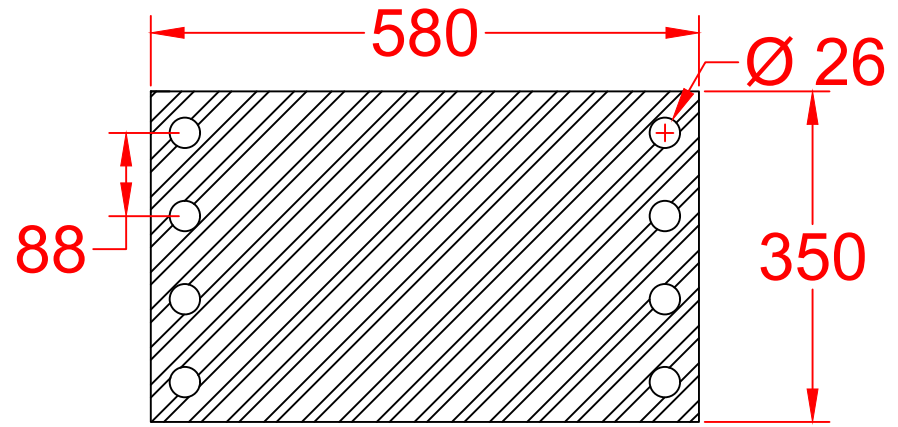
ISWB 500 with COVER PLATES
COVER PLATE DIMENSIONS -
TOP PLATE WIDTH = 400 mm
TOP PLATE TKS = 40 mm
BOTTOM PLATE SIZE SAME
AS TOP PLATE
G.L. = GROUND LEVEL

ALL DIMENSIONS ARE IN mm
 SCALE 1:100

10. MOUNTING PLATE

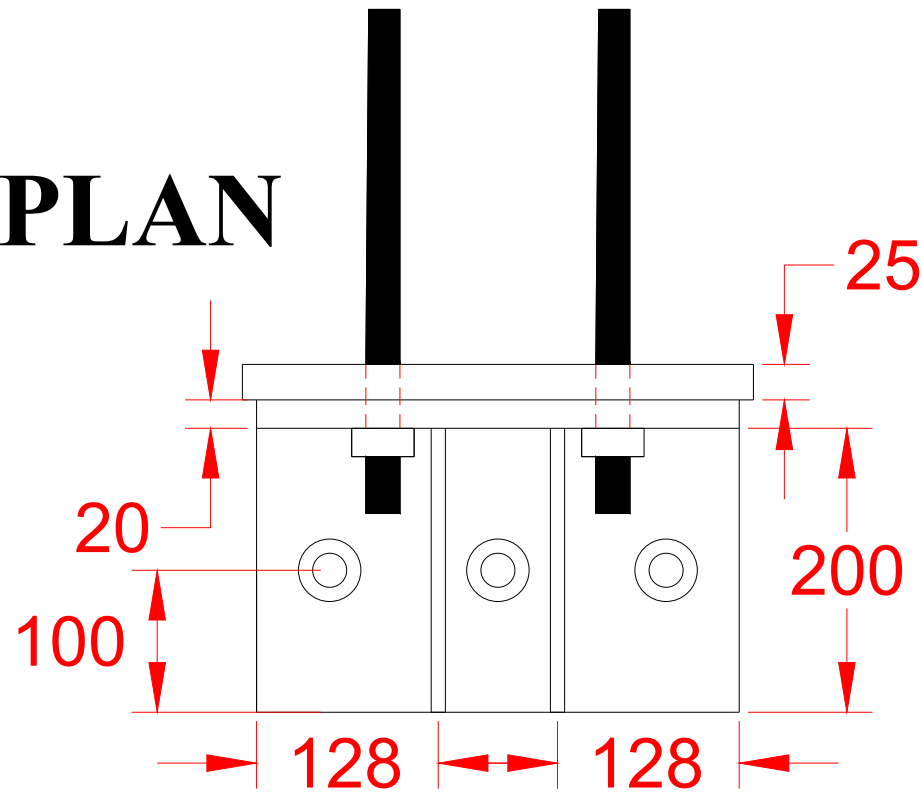


SIDE VIEW

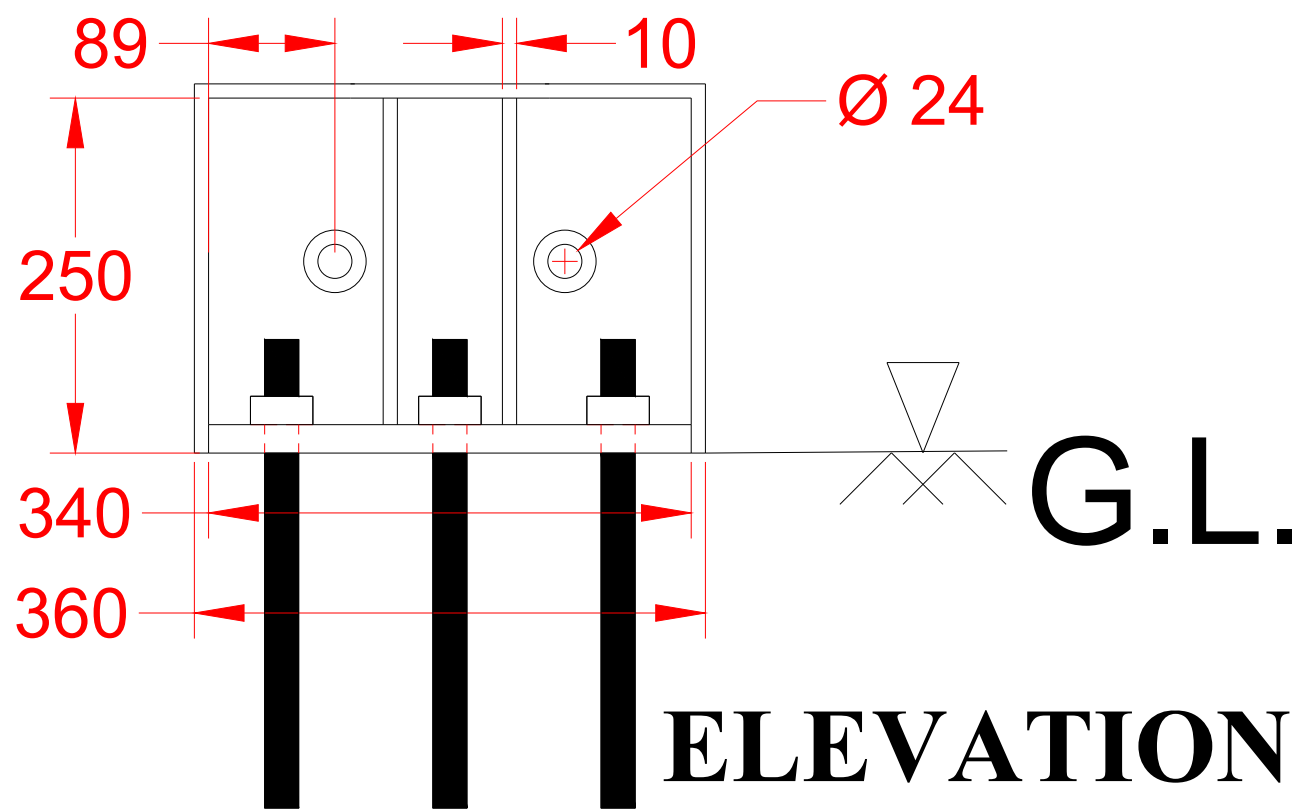


ELEVATION

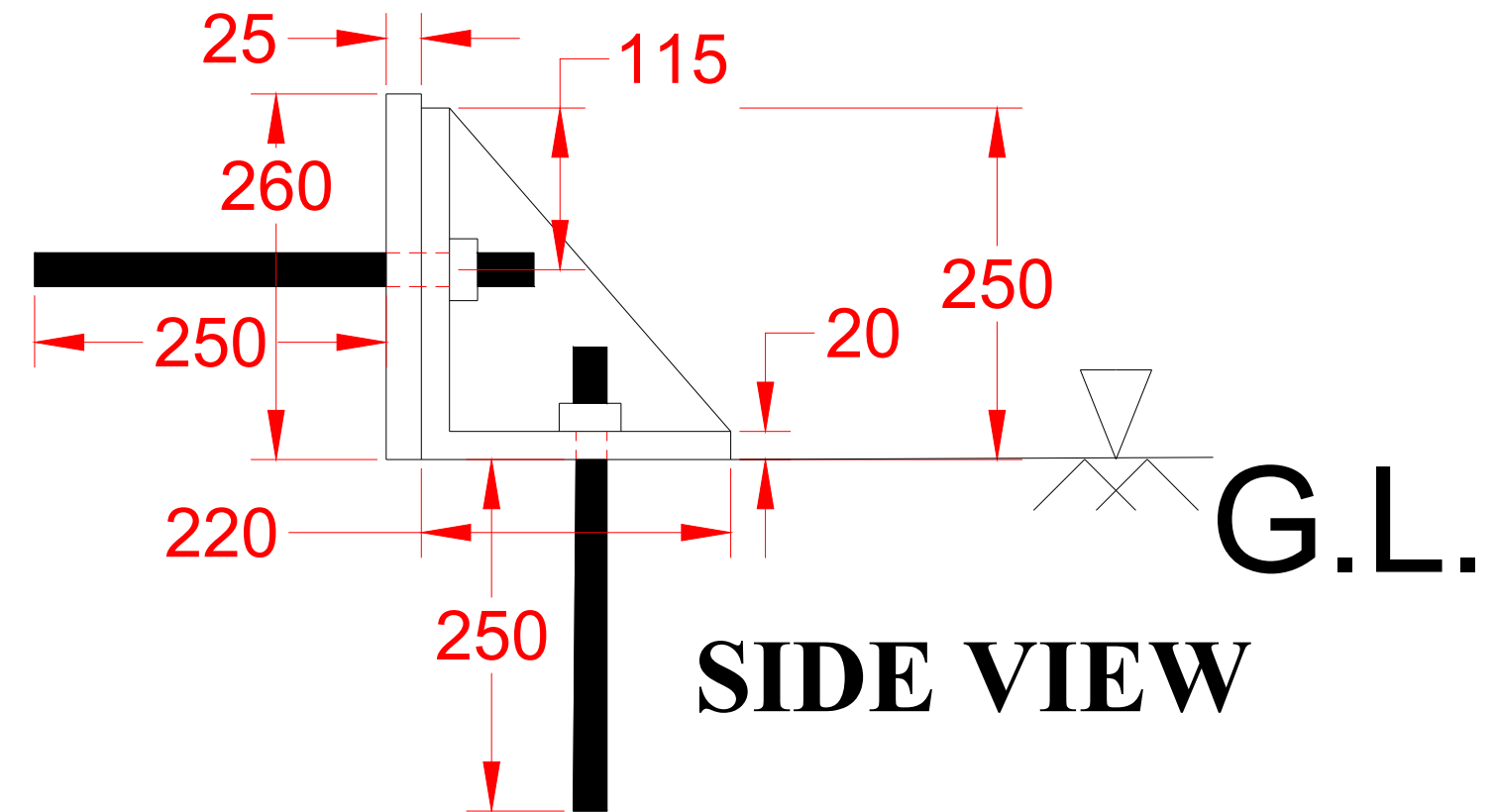
PLAN



**11. SUPPORT PROVIDED
TO RESIST
TRANSLATION OF MIW**

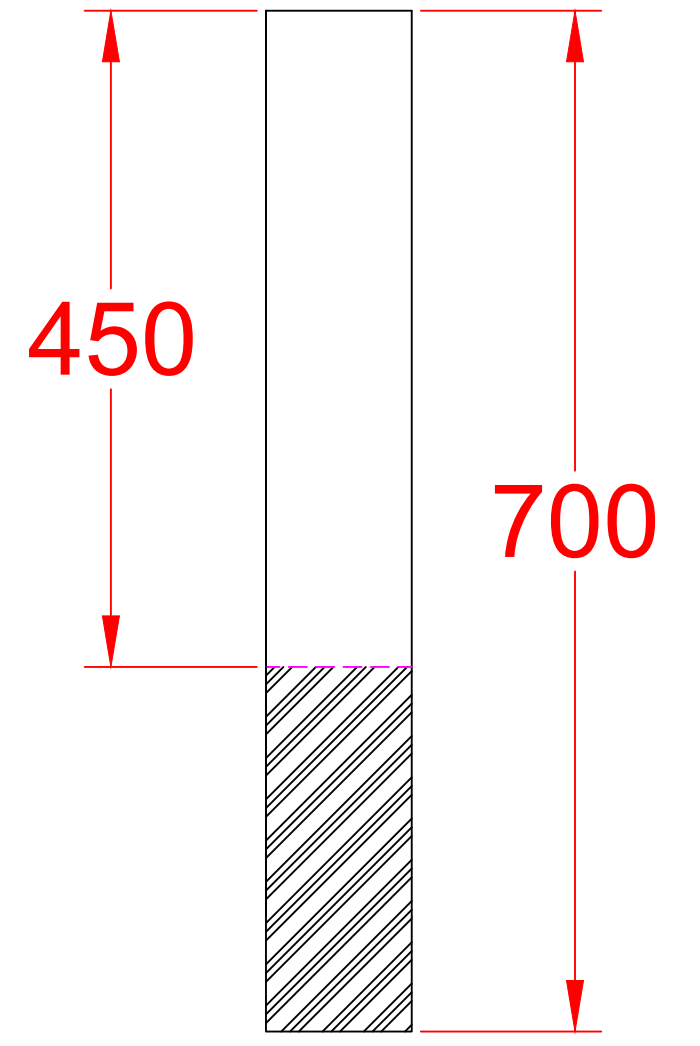
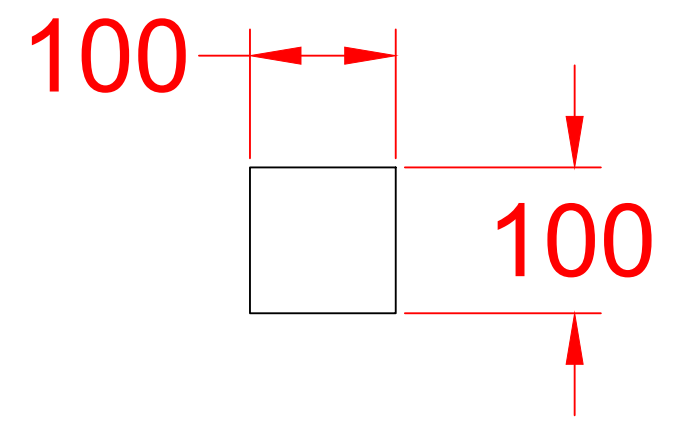
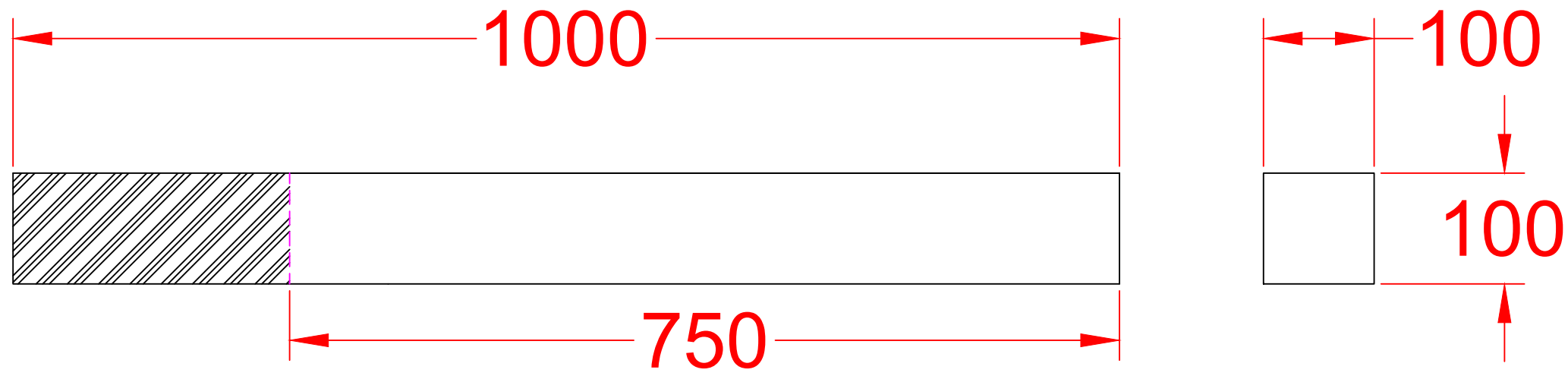


ELEVATION



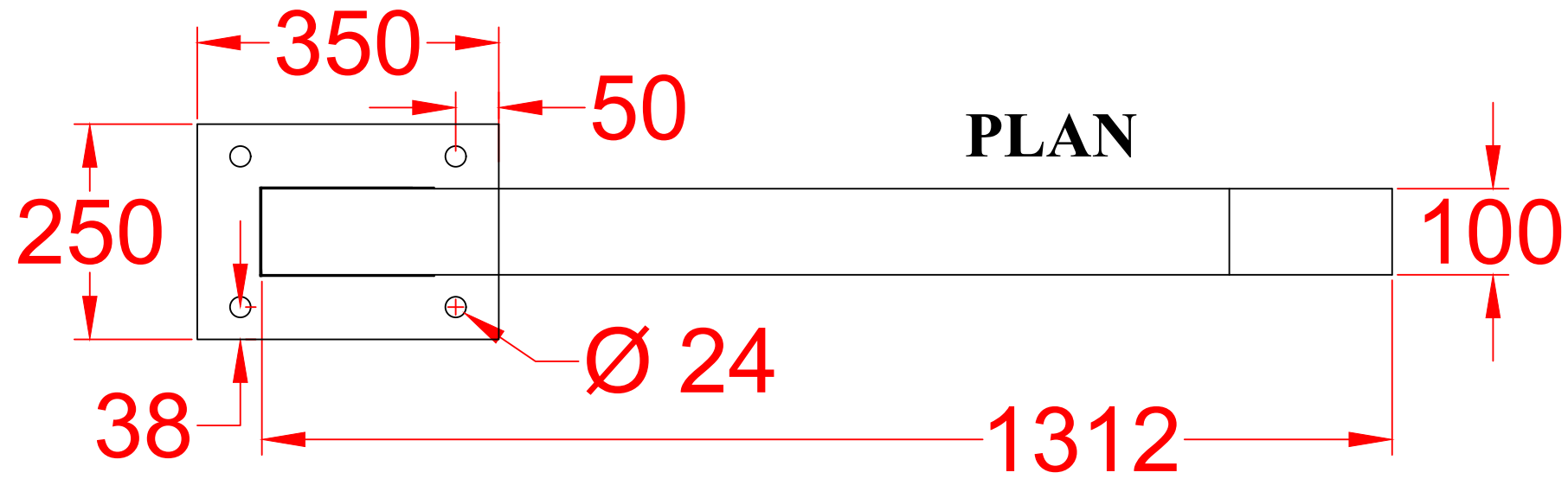
SIDE VIEW

ALL DIMENSIONS ARE IN mm
SCALE 1:100



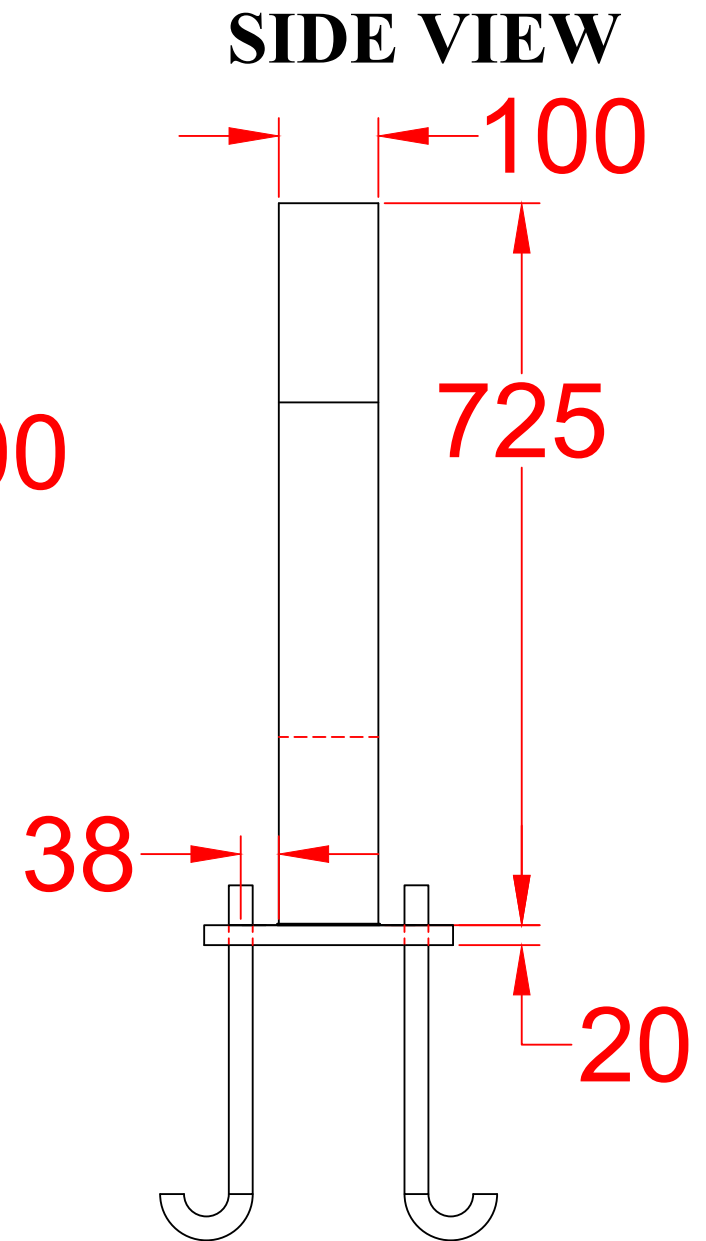
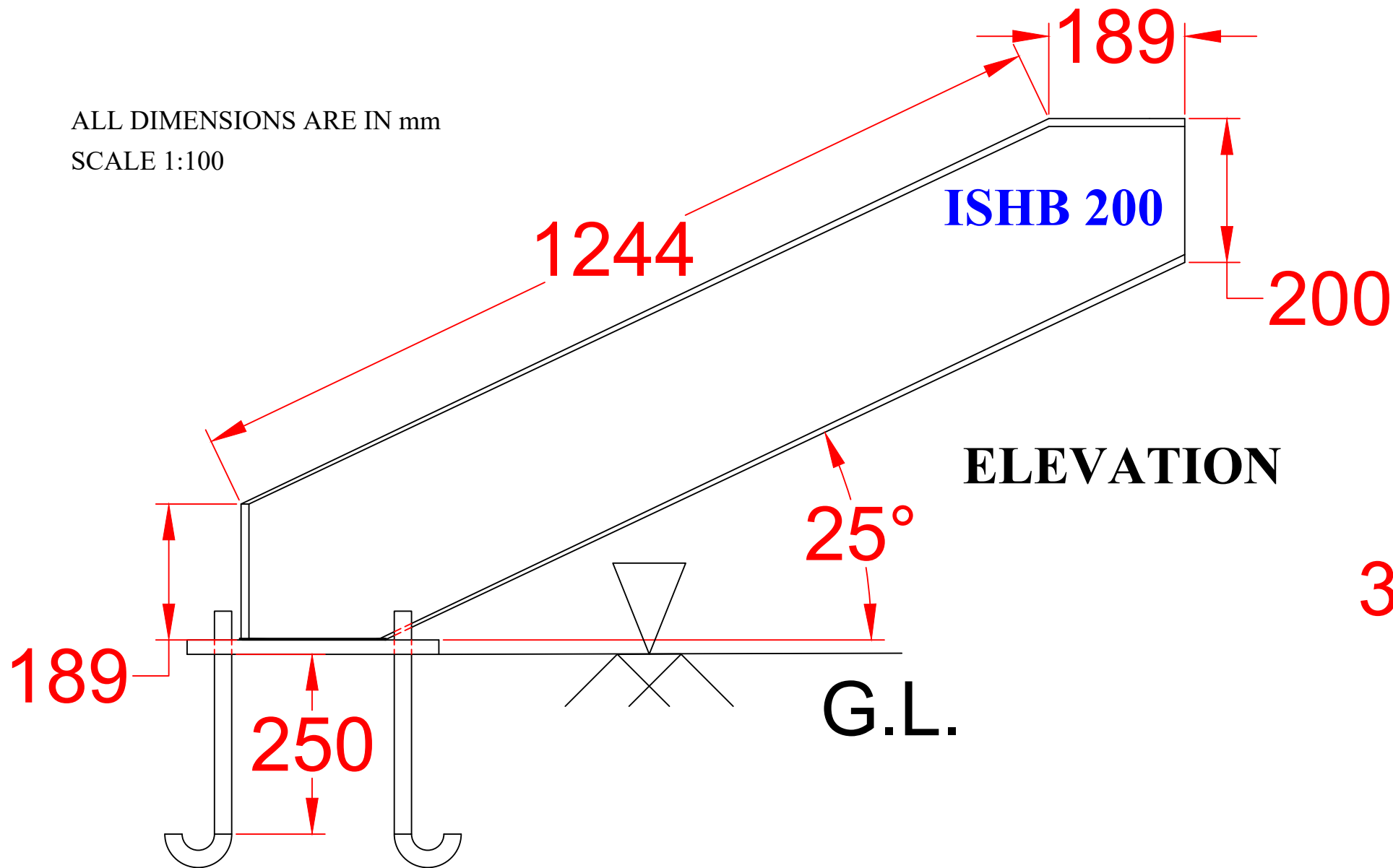
12. LATERAL SUPPORT AT THE BOTTOM OF THE COLUMN

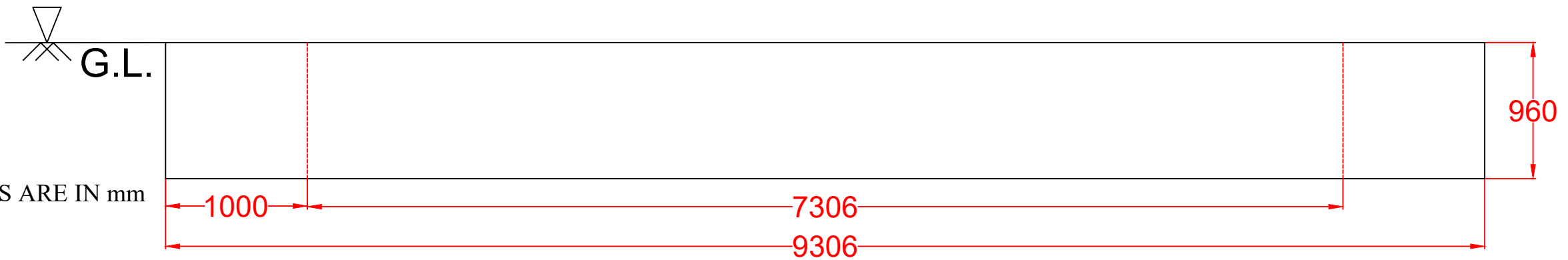
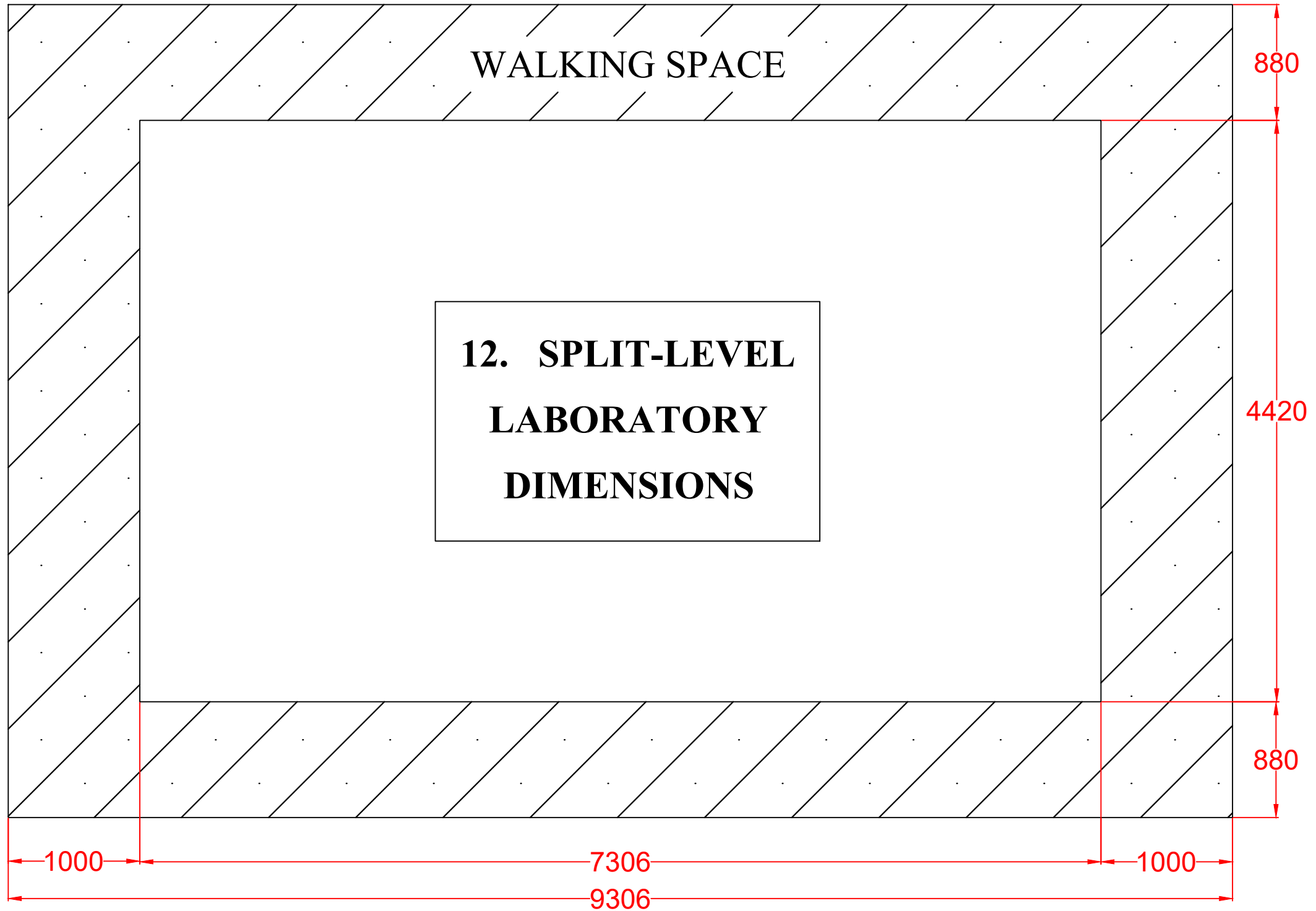
ALL DIMENSIONS ARE IN mm
SCALE 1:100



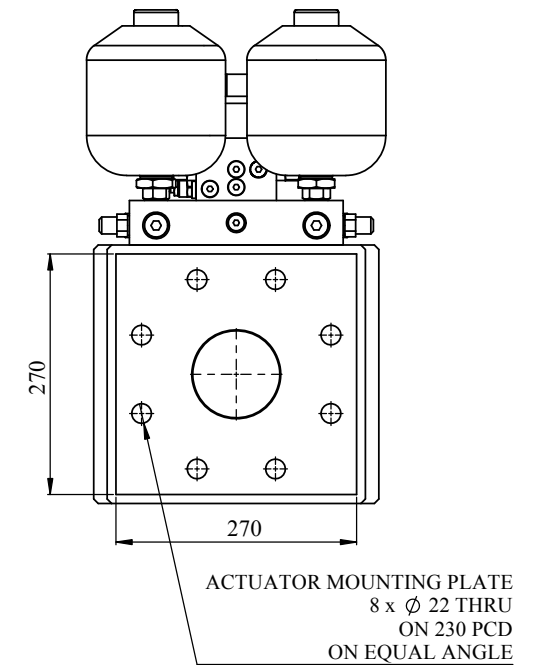
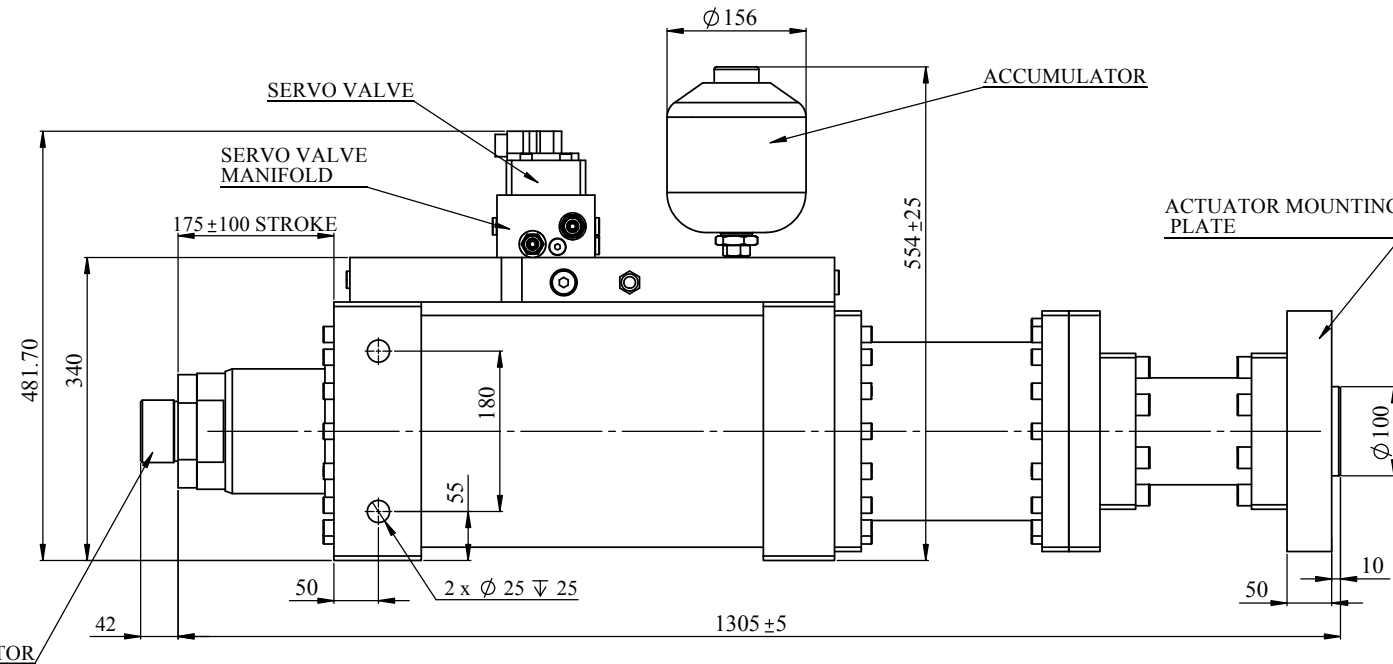
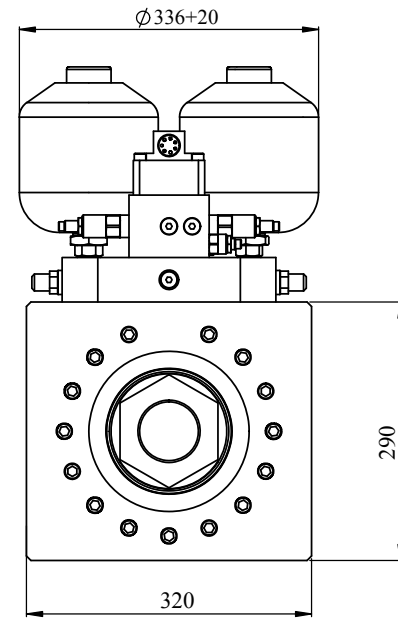
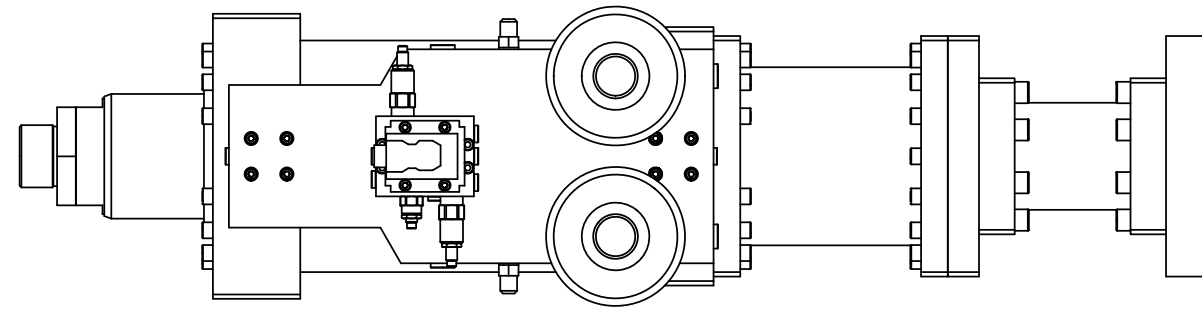
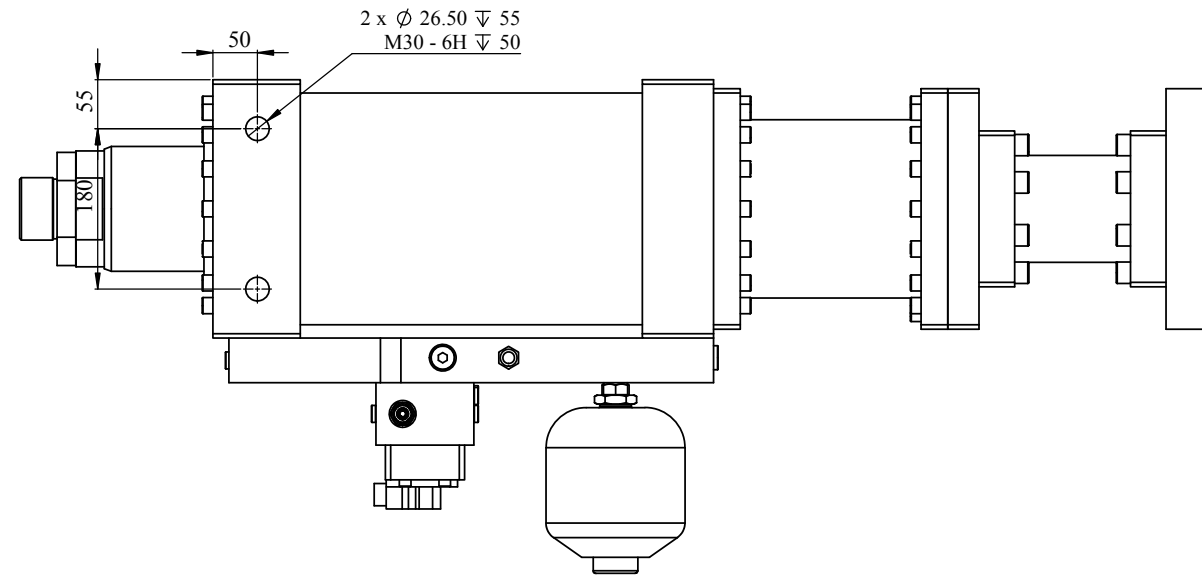
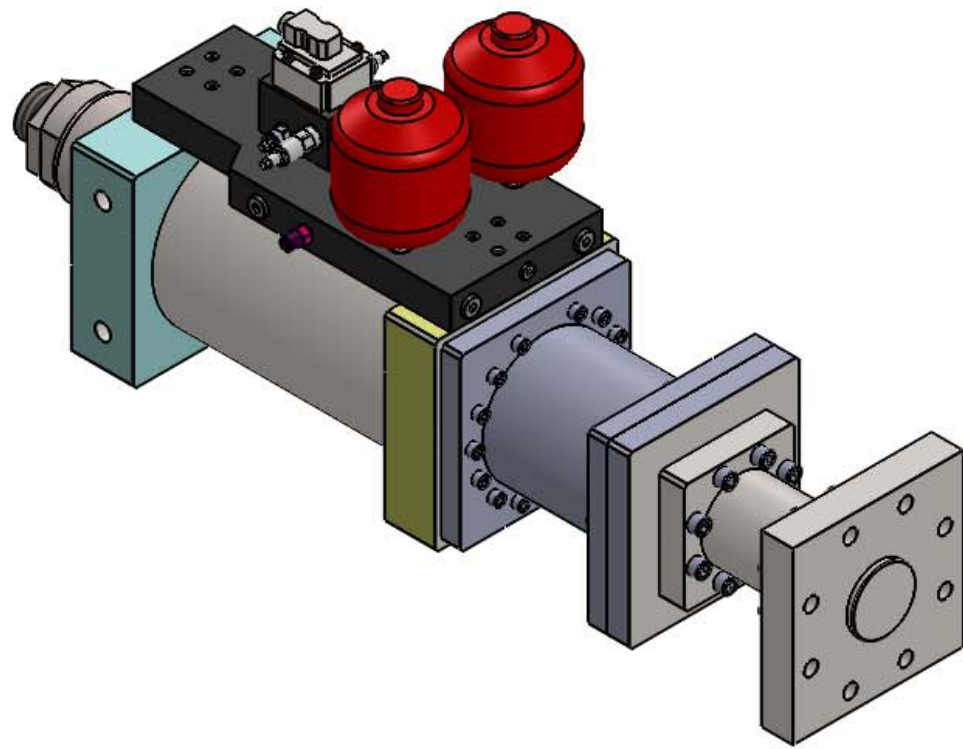
13. REAR SUPPORT FOR THE BEAM

ALL DIMENSIONS ARE IN mm
SCALE 1:100





ALL DIMENSIONS ARE IN mm
SCALE 1:100



TECHNICAL SPECIFICATION :	
CYLINDER SIZE	Ø210XØ140X200MM
WORKING PRESSURE	140 BAR (210 BAR WITH SERVO VALVE)
CYLINDER TYPE	SERVO-HYDRAULIC DOUBLE ACTING DOUBLE ENDED
MOUNTING	REAR FLANGE
TESTING PRESSURE	210 BAR(315 BAR WITH SERVO VALVE)
FREQUENCY	15Hz FOR ±0.1 MM
CAPACITY	250 kN

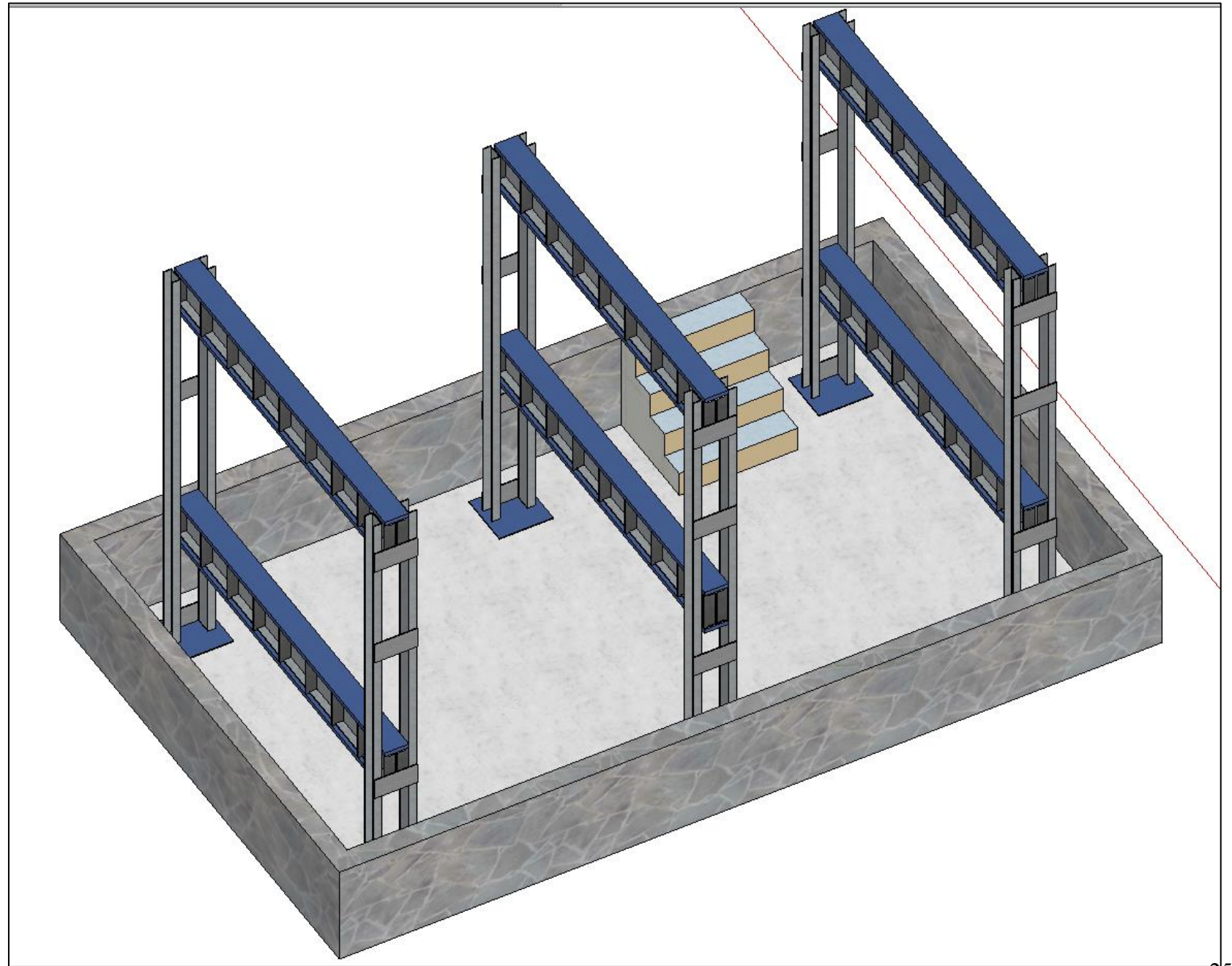
RAW MATERIAL: M.S.	QTY : 01 NO.	OA NUMBER : SH-6566/1920
RAW MATERIAL SIZE: XX	WEIGHT: -- KG	SUPREME INSTRUMENTS SOLUTIONS. NEW DELHI - 110059
DRAWN P.Y.S.	06.01.2020	
CHECKED S.V.K.	06.01.2020	
APPV'D S.N.S.	06.01.2020	
UNSPECIFIED TOLERANCES FOR MACHINING MEDIUM IS - 2102 - 1993		SCALE : -- SHEET : 1 of 1
ANGLE : ±0.5° RADI: 0.5 R SURFACE ROUGHNESS 3.2		ALL DIMENSIONS ARE IN MM
OVER 0.3 06 30 120 315 1000		TITLE:- GA DRAWING FOR SERVO ACTUATOR Ø210XØ140X200MM@140 BAR
UP TO 06 30 120 315 1000 2000		DRAWING NO.: SCH-1006-00-00
TOLERANCE ±0.1 ±0.2 ±0.3 ±0.5 ±0.8 ±1.2		REV: 0A

REV	DESCRIPTION	ECR NO.	BASE LINE	REV. BY.	APP. BY.	DATE

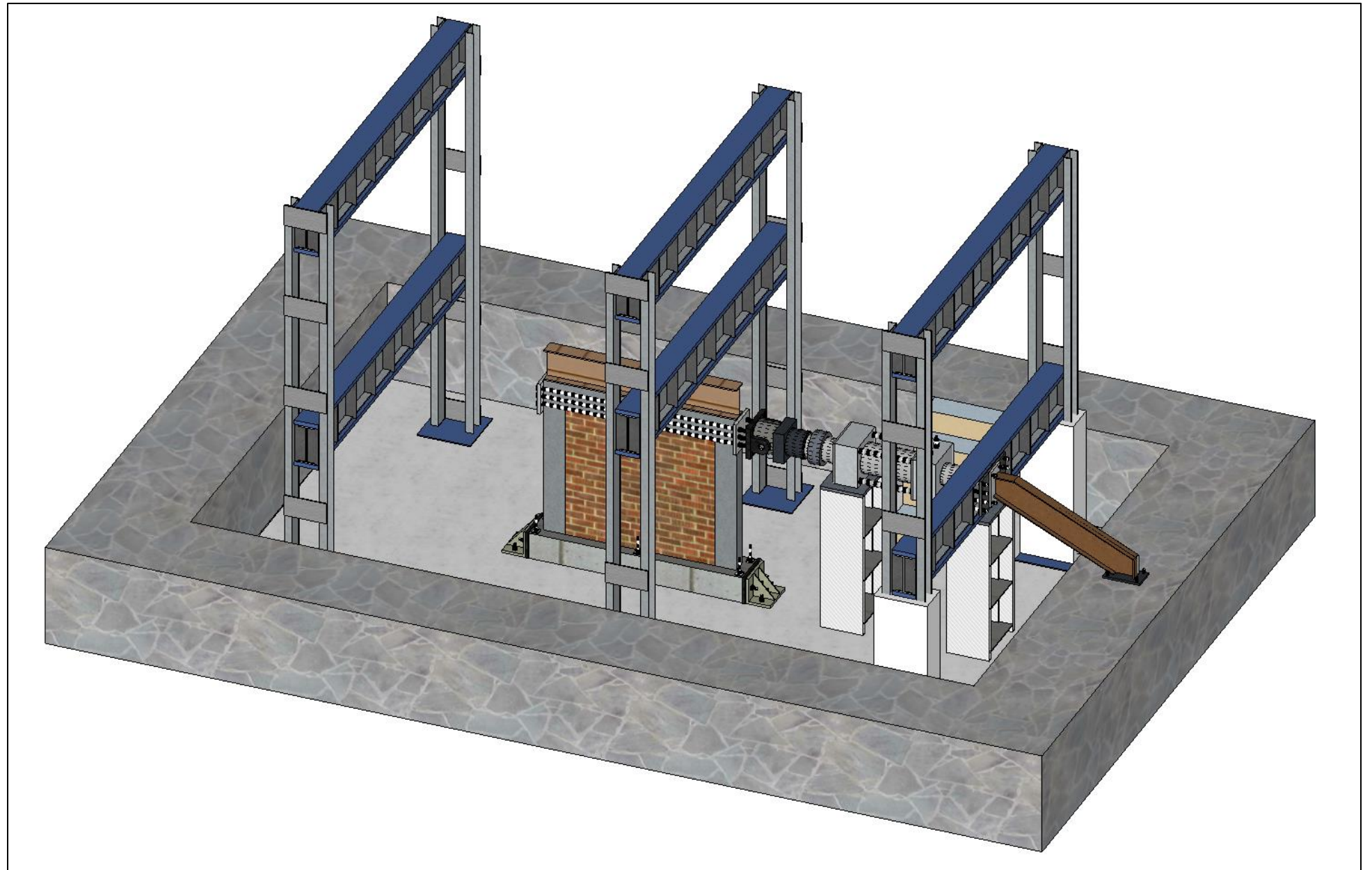
EXISTING LOADING FRAME



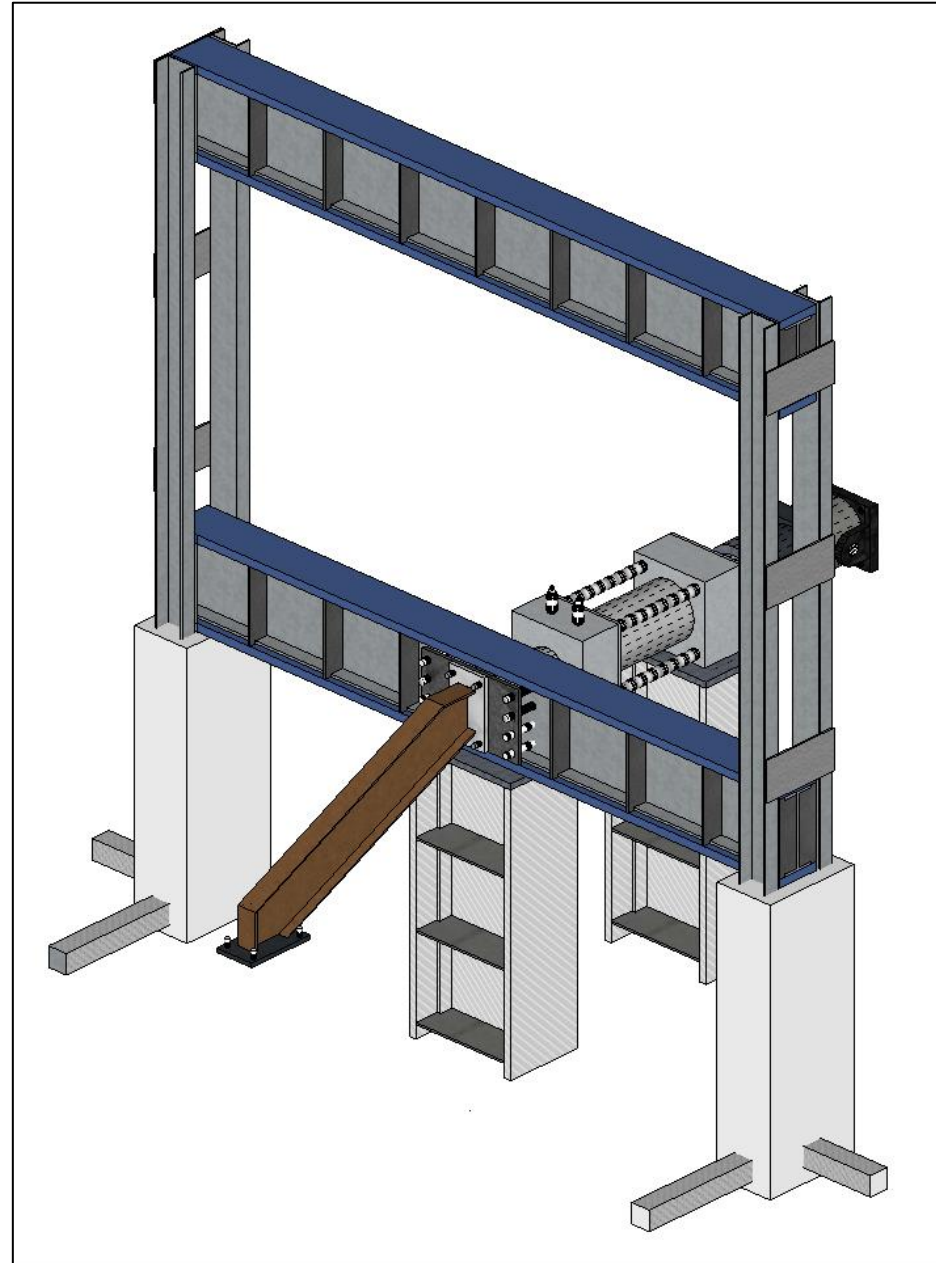
Existing Loading Frame in Laboratory



**New Loading
Frame With
Actuator**



**Loading Frame to be
Modelled In
STAAD Pro**



IV. DESIGN OF LOADING FRAME IN STAAD Pro.

STAAD.Pro V8i (SELECTseries 4) - [new validated structure - Whole Structure]

File Edit View Tools Select Geometry Commands Analyze Mode Window Help

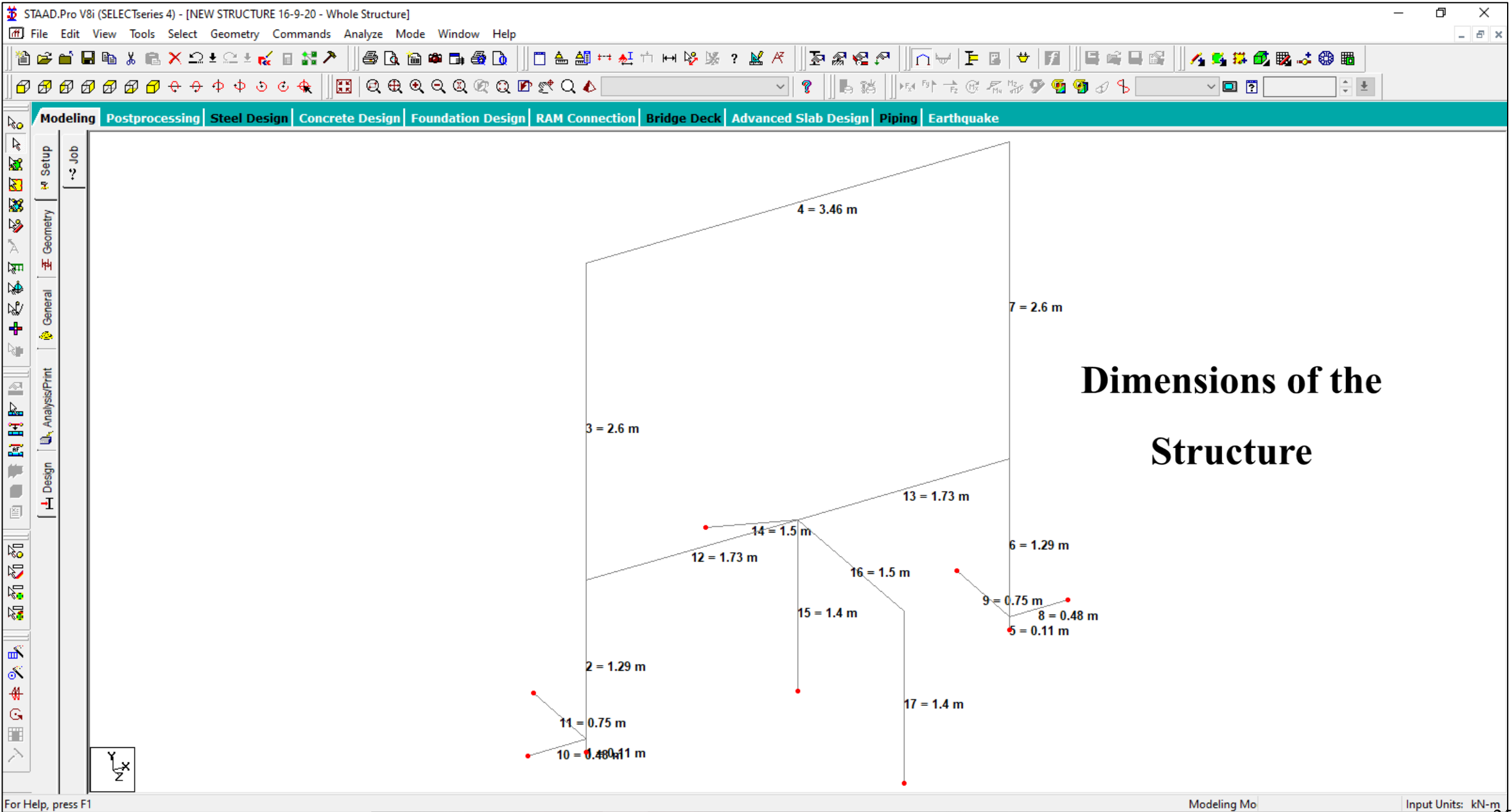
Modeling Postprocessing Steel Design Concrete Design Foundation Design RAM Connection Bridge Deck Advanced Slab Design Piping Earthquake

Skeleton Structure

Load 1

For Help, press F1

Modeling Mo Load 1 : DEAD Input Units: kN-m



STAAD.Pro V8i (SELECTseries 4) - [new validated structure - Whole Structure]

File Edit View Tools Select Geometry Commands Analyze Mode Window Help

Modeling Postprocessing Steel Design Concrete Design Foundation Design RAM Connection Bridge Deck Advanced Slab Design Piping Earthquake

Material Properties of the Members

Properties - Whole Structure

Section Beta Angle

Ref	Section	Material
1	ISMC150 D	STEEL
2	ISMB350 TB	STEEL
3	ISWB500 TB	STEEL
4	Cir 0.30	STEEL
5	Rect 0.50x0.30	CONCRETE
6	Rect 0.10x0.10	STEEL
7	ISHB200	STEEL

Highlight Assigned Geometry

Assignment Method

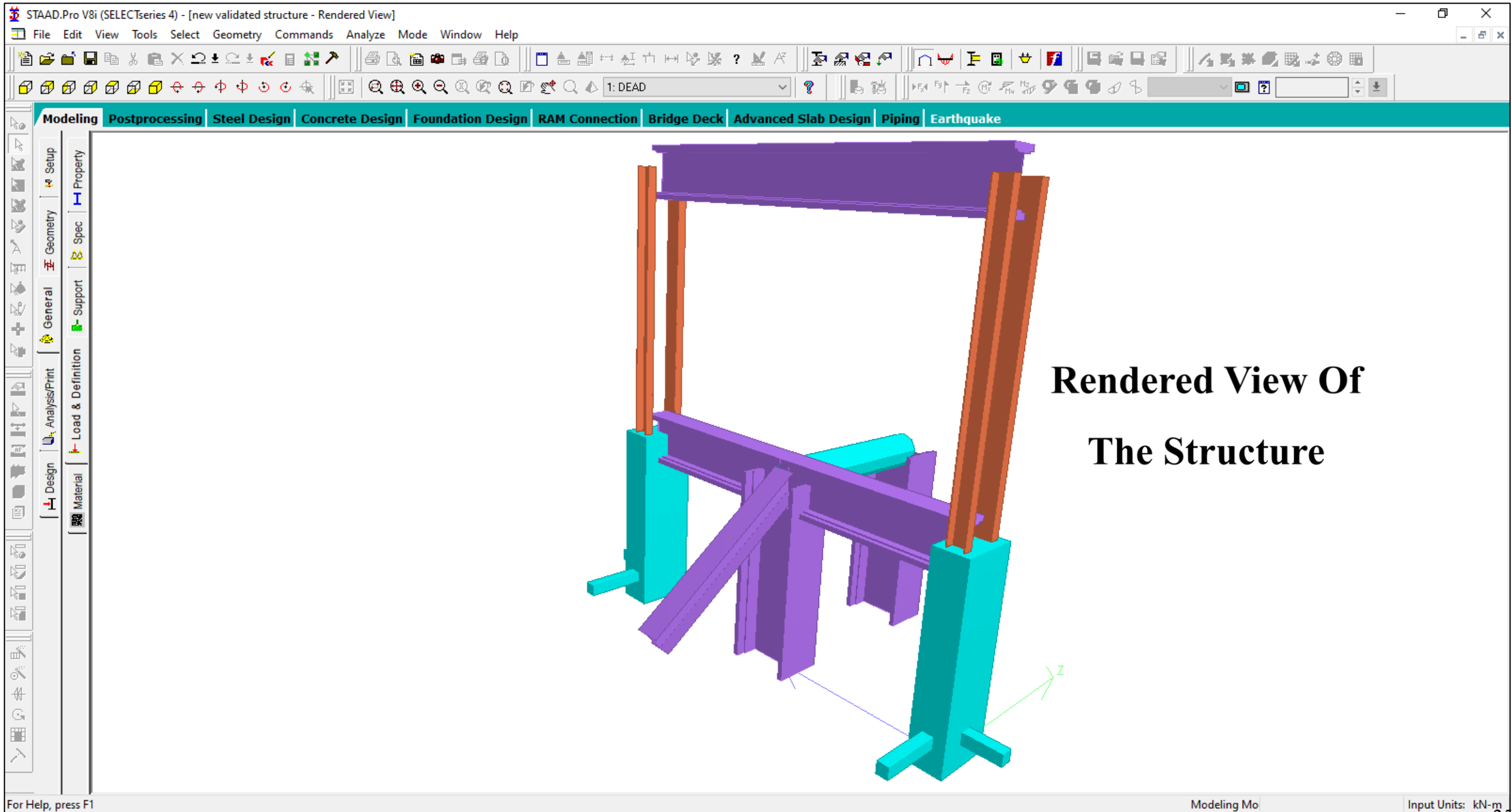
Assign To Selected Beams
 Use Cursor To Assign

Assign To Edit List
 Assign To View

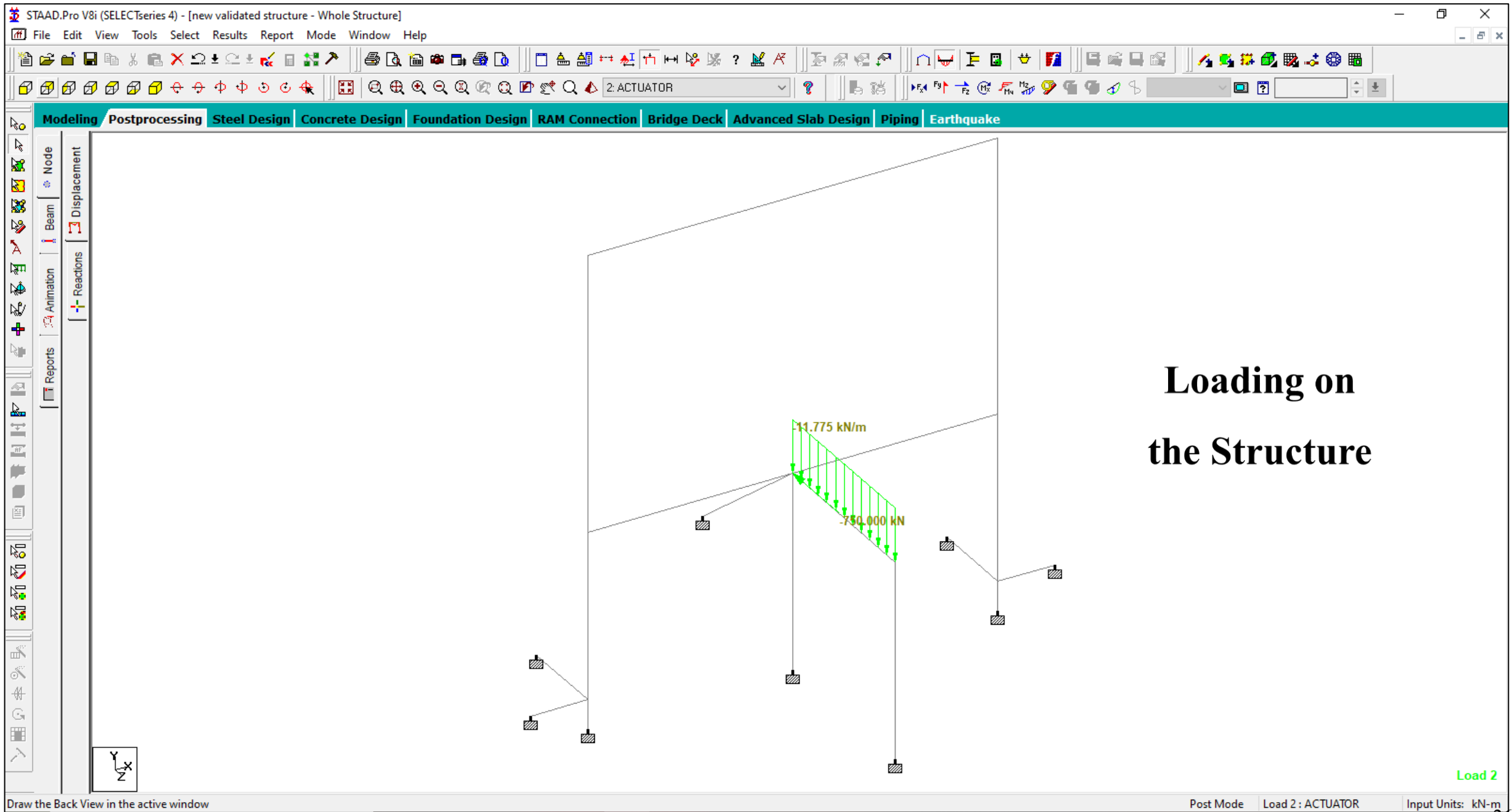
For Help, press F1

Modeling Mo: Load 1 : DEAD

Input Units: kN-m



Rendered View Of The Structure



Loading on the Structure

Load 2

Draw the Back View in the active window

Post Mode Load 2 : ACTUATOR Input Units: kN-m

STAAD.Pro V8i (SELECTSeries 4) - [new validated structure - Whole Structure]

File Edit View Tools Select Geometry Commands Analyze Mode Window Help

Modeling Postprocessing Steel Design Concrete Design Foundation Design RAM Connection Bridge Deck Advanced Slab Design Piping Earthquake

Design Input for Steel

Steel Design - Whole Structure

Current Code: IS800

- JOINT COORDINATES
- MEMBER INCIDENCES
- DEFINE MATERIAL START
- MEMBER PROPERTY INDIAN
- MEMBER PROPERTY INDIAN
- MEMBER PROPERTY INDIAN
- MEMBER PROPERTY INDIAN
- MEMBER PROPERTY INDIAN
- CONSTANTS
- SUPPORTS
- LOAD 1 LOADTYPE Dead TITLE DEAD
- LOAD 2 LOADTYPE Live TITLE ACTUAT
- PERFORM ANALYSIS
- PARAMETER 1
- CHECK CODE
- PARAMETER 2
- STEEL MEMBER TAKE OFF
- PARAMETER 3
- SELECT
- PARAMETER 4
- STEEL TAKE OFF
- START CONCRETE DESIGN
- FINISH

Highlight Assigned Geometry

Toggle Assign

Select Parameters... Define Parameters... Commands...

Assignment Method

Assign To Selected Beams

Assign To View

Use Cursor To Assign

Assign To Edit List

Select Group/Deck

Assign Close Help

Open an existing structure file

Modeling Mo: Load 1 : DEAD Input Units: kN-m

STAAD.Pro V8i (SELECTSeries 4) - new validated structure

File Edit View Tools Select Geometry Commands Analyze Mode Window Help

Modeling Postprocessing Steel Design Concrete Design Foundation Design RAM Connection Bridge Deck Advanced Slab Design Piping Earthquake

new validated structure - Whole Structure

Design Input for Concrete

Concrete Design - Whole Structure

Current Code: IS456

- MEMBER PROPERTY INDIAN
- MEMBER PROPERTY INDIAN
- MEMBER PROPERTY INDIAN
- CONSTANTS
- SUPPORTS
- LOAD 1 LOADTYPE Dead TITLE DEAD
- LOAD 2 LOADTYPE Live TITLE ACTUAT
- PERFORM ANALYSIS
- PARAMETER 1
- CHECK CODE
- PARAMETER 2
- STEEL MEMBER TAKE OFF
- PARAMETER 3
- SELECT
- PARAMETER 4
- STEEL TAKE OFF
- START CONCRETE DESIGN
 - CODE INDIAN
 - FC 20000
 - DESIGN COLUMN
 - CONCRETE TAKE
 - END CONCRETE DESIGN
- FINISH

Highlight Assigned Geometry

Toggle Assign

Select Parameters... Define Parameters... Commands...

Assignment Method

Assign To Selected Beams

Assign To View

Use Cursor To Assign

Assign To Edit List

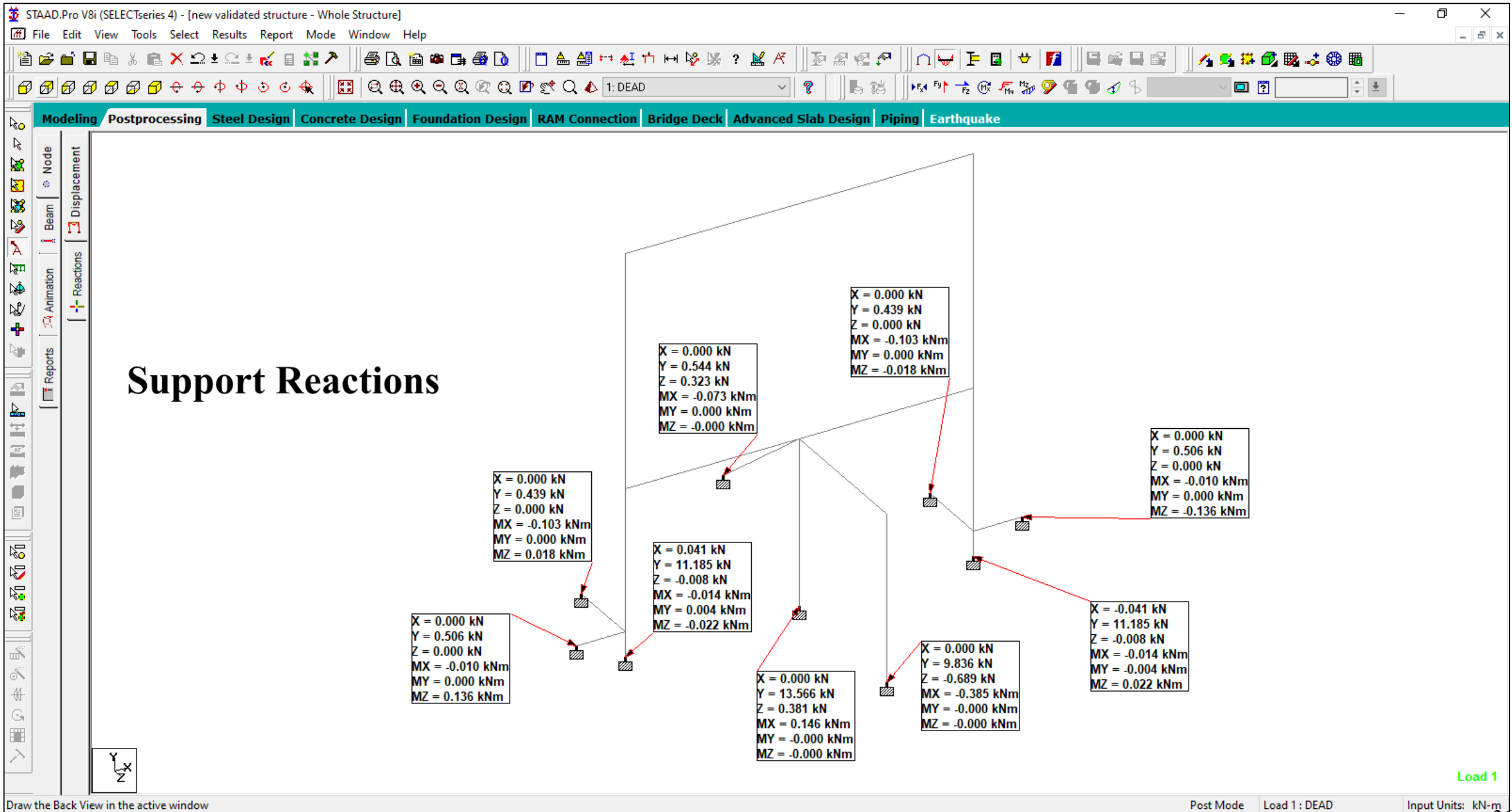
Select Group/Deck

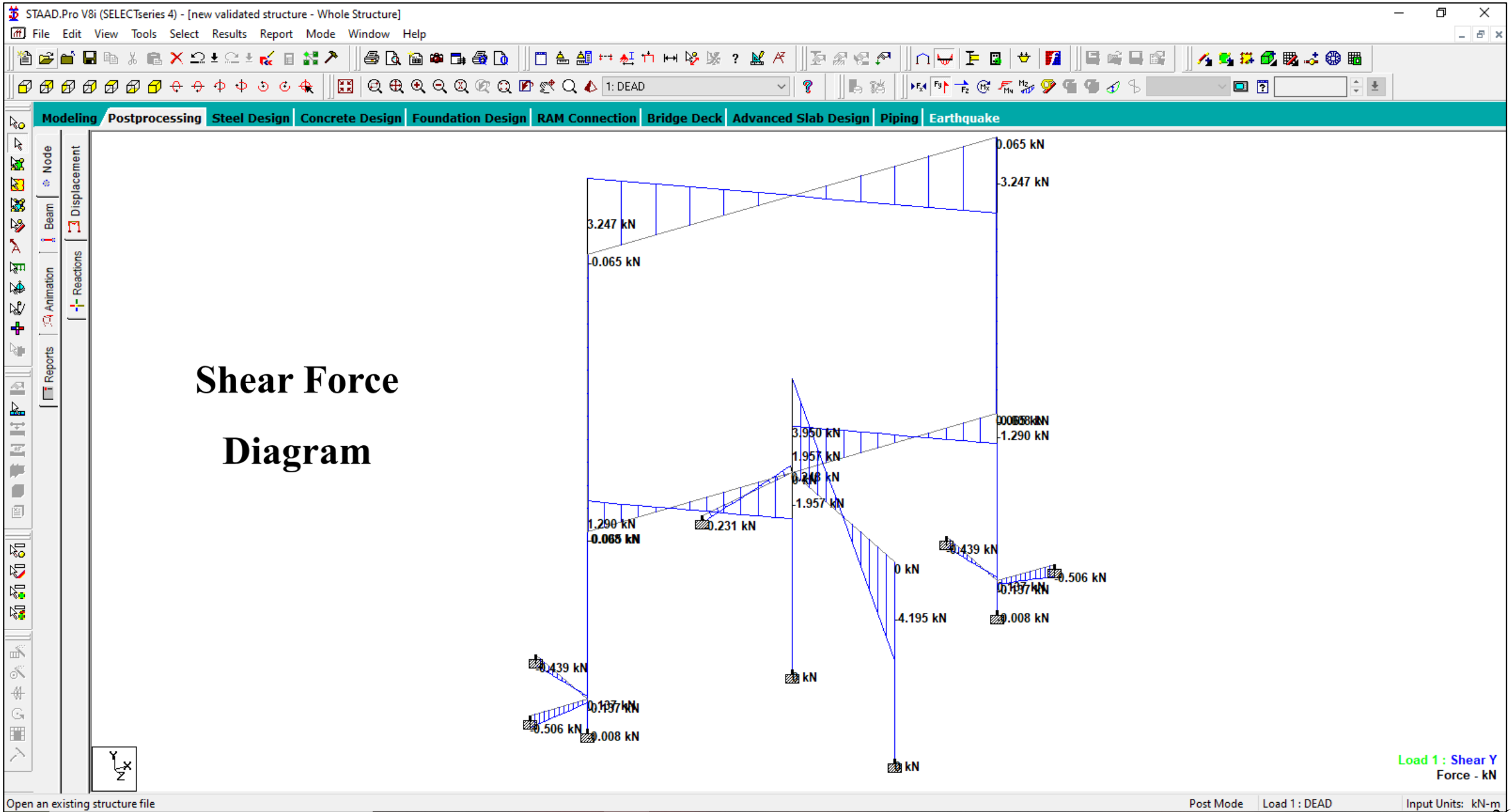
Assign Close Help

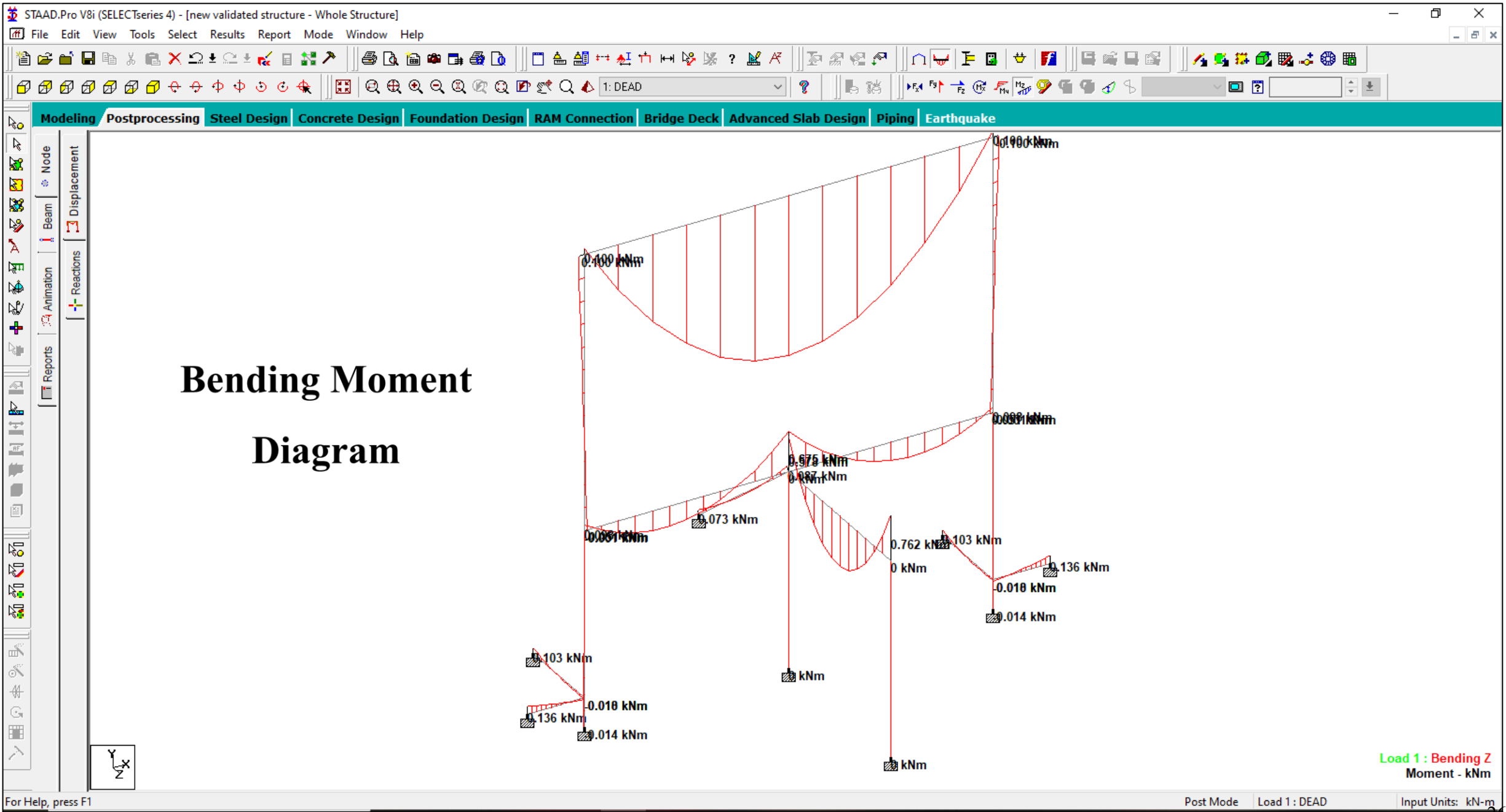
Load 1

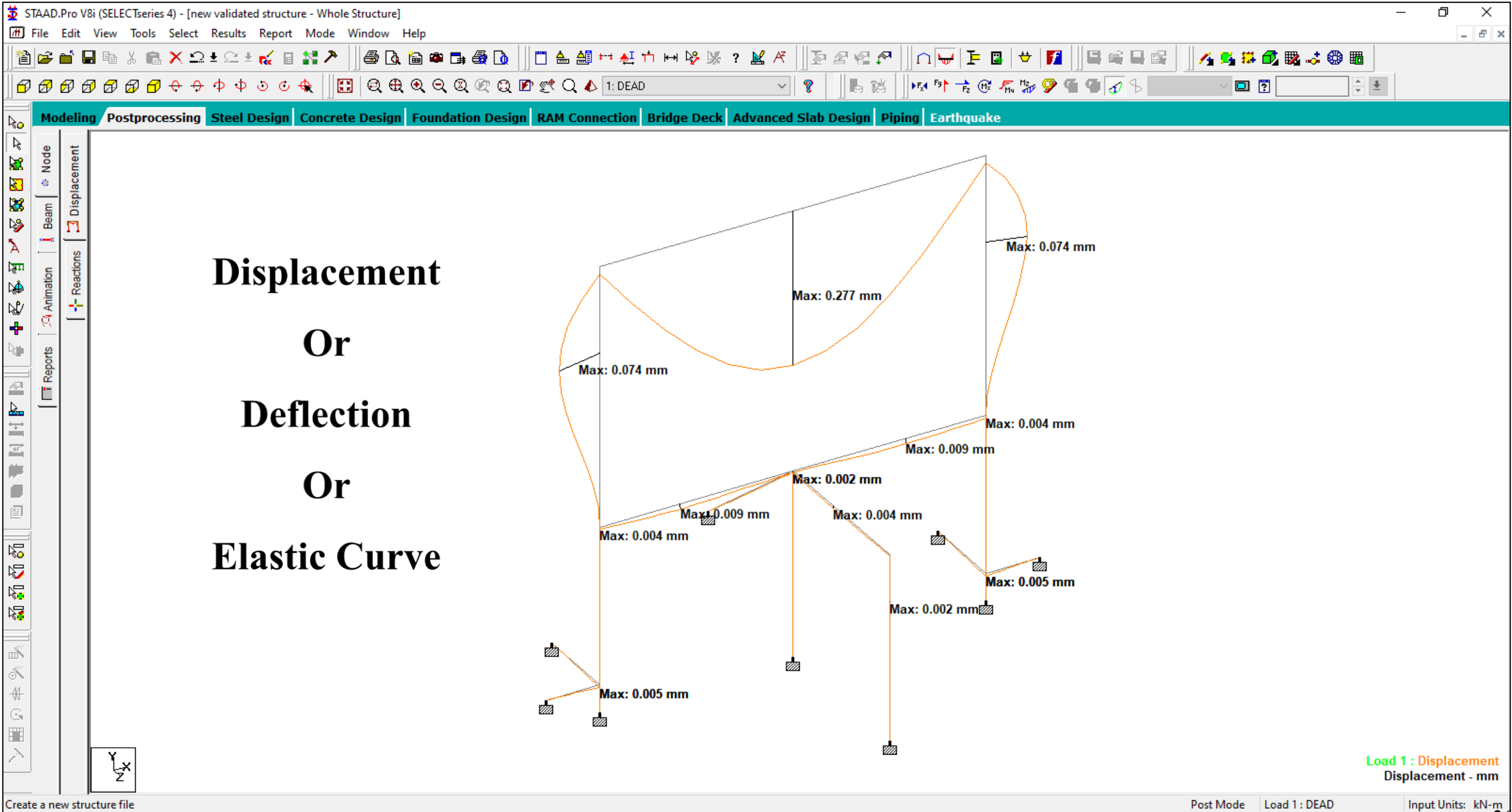
Draw the end elevation in the active window

Modeling Mo Load 1 : DEAD Input Units: kN-m









new validated structure.anl - STAAD Output Viewer

File Edit View Help

WARNING

RESULTS

STEEL DESIGN
STEEL TAKE OFF
STEEL DESIGN
STEEL TAKE OFF
CONCRETE DESIGN

NOTES

ALL UNITS ARE - KN METE (UNLESS OTHERWISE Noted)

MEMBER	TABLE	RESULT/ FX	CRITICAL COND/ MY	RATIO/ MZ	LOADING/ LOCATION
1	PRI SMAT		(INDIAN SECTIONS)		
		PASS	IS-7.1.2	0.011	2
		1.84 T	0.25	22.50	0.00
2	D ISMC150		(INDIAN SECTIONS)		
		PASS	IS-7.1.1(A)	0.008	1
		3.25 C	0.00	0.10	2.34
3	TB ISMB350		(INDIAN SECTIONS)		
		PASS	SHEAR-Y	0.009	1
		0.06 C	0.00	0.10	0.00
4	PRI SMAT		(INDIAN SECTIONS)		
		PASS	IS-7.1.2	0.011	2
		1.84 T	-0.25	22.50	0.00
5	D ISMC150		(INDIAN SECTIONS)		
		PASS	IS-7.1.1(A)	0.008	1
		3.25 C	0.00	-0.10	2.34
6	TB ISWB500		(INDIAN SECTIONS)		
		PASS	IS-7.1.2	0.436	2
		141.59 T	-156.07	0.00	0.00
7	TB ISWB500		(INDIAN SECTIONS)		
		PASS	IS-7.1.2	0.429	2
		142.69 T	-153.62	0.00	0.00
8	PRI SMAT		(INDIAN SECTIONS)		
		PASS	IS-7.1.2	0.280	2
		159.06 T	0.00	116.07	0.00
9	TB ISMB350		(INDIAN SECTIONS)		
		PASS	IS-7.1.2	0.142	2
		0.45 T	16.00	2.57	1.73

-----< PAGE 3 Ends Here >-----

STAAD SPACE -- PAGE NO. 4

Steel Design Output

a) All members are passing under the given loading conditions.

b) C stands for Compression
T stands for Tension

F_x = Axial Force

M_y = Moment in y-direction

M_z = Moment in z-direction

Contd...

new validated structure.anl - STAAD Output Viewer

File Edit View Help

WARNING RESULTS

STEEL DESIGN
STEEL TAKE OFF
STEEL DESIGN
STEEL TAKE OFF
CONCRETE DESIGN

ALL UNITS ARE - KN METRE (UNLESS OTHERWISE Noted)

MEMBER	TABLE	RESULT/ FX	CRITICAL COND/ MY	RATIO/ MZ	LOADING/ LOCATION
10	TB ISMB350		(INDIAN SECTIONS)		
		PASS	IS-7.1.2	0.142	2
		0.45 T	16.00	2.57	0.00
11	ST ISHB200		(INDIAN SECTIONS)		
		PASS	IS-7.1.1(B)	0.819	2
		505.14 C	0.00	-6.35	1.66
12	PRI SMAT		(INDIAN SECTIONS)		
		PASS	IS-7.1.1(A)	0.004	1
		0.00 T	0.00	0.10	0.75
13	PRI SMAT		(INDIAN SECTIONS)		
		PASS	IS-7.1.1(A)	0.005	1
		0.00 T	0.00	0.14	0.48
14	PRI SMAT		(INDIAN SECTIONS)		
		PASS	IS-7.1.1(A)	0.004	1
		0.00 T	0.00	0.10	0.75
15	PRI SMAT		(INDIAN SECTIONS)		
		PASS	IS-7.1.1(A)	0.005	1
		0.00 T	0.00	0.14	0.48

***** END OF TABULATED RESULT OF DESIGN *****

63. PARAMETER 2
64. CODE INDIAN
65. STEEL MEMBER TAKE OFF ALL

-----< PAGE 4 Ends Here >-----

NOTES

Total Page: 12 CAP NUM

Steel Design Output

a) All members are passing under the given loading conditions.

b) C stands for Compression
T stands for Tension

Fx = Axial Force

My = Moment in y-direction

Mz = Moment in z-direction

new validated structure.anl - STAAD Output Viewer

File Edit View Help

WARNING

RESULTS

STEEL DESIGN
STEEL TAKE OFF
STEEL DESIGN
STEEL TAKE OFF
CONCRETE DESIGN

72. START CONCRETE DESIGN
73. CODE INDIAN
74. FC 20000 MEMB 1 4
75. DESIGN COLUMN 1 4

-----< PAGE 8 Ends Here >-----

STAAD SPACE -- PAGE NO. 9

=====

C O L U M N N O. 1 D E S I G N R E S U L T S

M20 Fe415 (Main) Fe415 (Sec.)

LENGTH: 1665.0 mm CROSS SECTION: 300.0 mm X 500.0 mm COVER: 40.0 mm

** GUIDING LOAD CASE: 2 END JOINT: 1 TENSION COLUMN

REQD. STEEL AREA : 1200.00 Sq.mm.
REQD. CONCRETE AREA: 148800.00 Sq.mm.
MAIN REINFORCEMENT : Provide 12 - 12 dia. (0.90%, 1357.17 Sq.mm.)
(Equally distributed)
TIE REINFORCEMENT : Provide 8 mm dia. rectangular ties @ 190 mm c/c

SECTION CAPACITY BASED ON REINFORCEMENT REQUIRED (KNS-MET)

Puz : 1712.70 Muz1 : 89.42 Muy1 : 49.04

INTERACTION RATIO: 0.26 (as per Cl. 39.6, IS456:2000)

SECTION CAPACITY BASED ON REINFORCEMENT PROVIDED (KNS-MET)

WORST LOAD CASE: 2
END JOINT: 1 Puz : 1760.20 Muz : 101.19 Muy : 54.94 IR: 0.23

=====

NOTES

Concrete Design Output

Contd...

Total Page: 12 CAP NUM

new validated structure.anl - STAAD Output Viewer

File Edit View Help

WARNING RESULTS

STEEL DESIGN
STEEL TAKE OFF
STEEL DESIGN
STEEL TAKE OFF
CONCRETE DESIGN

NOTES

```

      C O L U M N   N O .       4   D E S I G N   R E S U L T S

      M20                      Fe415 (Main)          Fe415 (Sec.)

      LENGTH:  1665.0 mm   CROSS SECTION:  300.0 mm X  500.0 mm   COVER:  40.0 mm

      ** GUIDING LOAD CASE:    2   END JOINT:    5   TENSION COLUMN

-----< PAGE 9 Ends Here >-----

      STAAD SPACE                      -- PAGE NO.    10

      REQD. STEEL AREA   :    1200.00 Sq.mm.
      REQD. CONCRETE AREA:  148800.00 Sq.mm.
      MAIN REINFORCEMENT : Provide  12 - 12 dia. (0.90%,  1357.17 Sq.mm.)
                          (Equally distributed)
      TIE REINFORCEMENT  : Provide  8 mm dia. rectangular ties @ 190 mm c/c

      SECTION CAPACITY BASED ON REINFORCEMENT REQUIRED (KNS-MET)
      -----
      Puz :   1712.70   Muz1 :    89.42   Muy1 :    49.04

      INTERACTION RATIO: 0.26 (as per Cl. 39.6, IS456:2000)

      SECTION CAPACITY BASED ON REINFORCEMENT PROVIDED (KNS-MET)
      -----
      WORST LOAD CASE:    2
      END JOINT:    5   Puz :   1760.20   Muz :   101.19   Muy :    54.94   IR: 0.23
      =====

      *****END OF COLUMN DESIGN RESULTS*****

      76. CONCRETE TAKE
      77. END CONCRETE DESIGN

-----< PAGE 10 Ends Here >-----

```

Total Page: 12 CAP NUM

Concrete Design Output

new validated structure.anl - STAAD Output Viewer

File Edit View Help

WARNING

RESULTS

STEEL DESIGN
STEEL TAKE OFF
STEEL DESIGN
STEEL TAKE OFF
CONCRETE DESIGN

NOTES

STEEL TAKE-OFF

PROFILE	LENGTH (METE)	WEIGHT (KN)
D ISMC150	4.67	1.528
TB ISMB350	6.92	12.987
TB ISWB500	3.33	11.281
ST ISHB200	1.66	0.606
PRISMATIC STEEL	3.96	10.035
TOTAL =		36.437

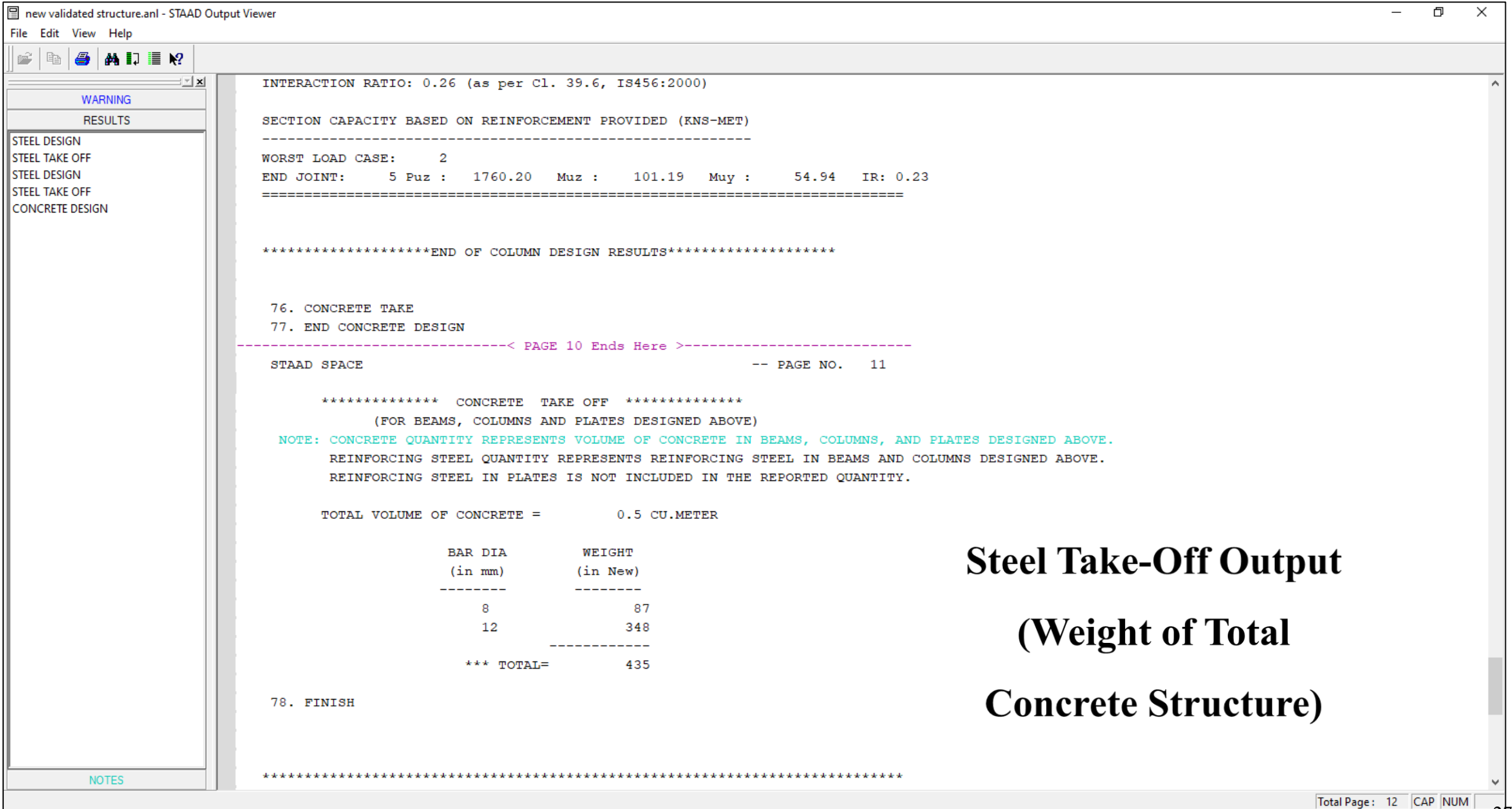
TOTAL VOLUME OF PRISMATIC STEEL SECTIONS = 0.13 CUBIC METE

MEMBER	PROFILE	LENGTH (METE)	WEIGHT (KN)
2	D ISMC150	2.34	0.764
3	TB ISMB350	3.46	6.493
5	D ISMC150	2.34	0.764
6	TB ISWB500	1.66	5.641
7	TB ISWB500	1.66	5.641
8	PRI SMAT	1.50	8.145
9	TB ISMB350	1.73	3.247
10	TB ISMB350	1.73	3.247
11	ST ISHB200	1.66	0.606
12	PRI SMAT	0.75	0.576
13	PRI SMAT	0.48	0.369
14	PRI SMAT	0.75	0.576
15	PRI SMAT	0.48	0.369
TOTAL =		36.437	

Total Page: 12 CAP NUM

Steel Take-Off Output

(Weight of Total Steel Structure)



- WARNING
- RESULTS
- STEEL DESIGN
- STEEL TAKE OFF
- STEEL DESIGN
- STEEL TAKE OFF
- CONCRETE DESIGN

INTERACTION RATIO: 0.26 (as per Cl. 39.6, IS456:2000)

SECTION CAPACITY BASED ON REINFORCEMENT PROVIDED (KNS-MET)

WORST LOAD CASE: 2

END JOINT: 5 Puz : 1760.20 Muz : 101.19 Muy : 54.94 IR: 0.23

=====

*****END OF COLUMN DESIGN RESULTS*****

76. CONCRETE TAKE
77. END CONCRETE DESIGN

-----< PAGE 10 Ends Here >-----

STAAD SPACE -- PAGE NO. 11

***** CONCRETE TAKE OFF *****
(FOR BEAMS, COLUMNS AND PLATES DESIGNED ABOVE)

NOTE: CONCRETE QUANTITY REPRESENTS VOLUME OF CONCRETE IN BEAMS, COLUMNS, AND PLATES DESIGNED ABOVE.
REINFORCING STEEL QUANTITY REPRESENTS REINFORCING STEEL IN BEAMS AND COLUMNS DESIGNED ABOVE.
REINFORCING STEEL IN PLATES IS NOT INCLUDED IN THE REPORTED QUANTITY.

TOTAL VOLUME OF CONCRETE = 0.5 CU.METER

BAR DIA (in mm)	WEIGHT (in New)
8	87
12	348

*** TOTAL=	435

78. FINISH

Steel Take-Off Output

(Weight of Total Concrete Structure)

BIOGRAPHIES

Biography of Jaya Kumar Bhaskar (Scholar)



Jaya Kumar Bhaskar received his Bachelor of Engineering from Price Shri Venkateswara Padmavathy Engineering College, Chennai, India, in 2013 and Master of Technology from SRM University, Chennai, India, in 2017. Initially, he worked as a Site Engineer at Ramya Properties and Developers, Chrompet, Chennai, India from June 2013 to August 2013. He then joined as a Project Assistant Level – II in the Council of Scientific and Industrial Research – Structural Engineering Research Centre (CSIR-SERC), Chennai, India, from September 2013 to June 2015. He has also worked as an Assistant Professor at Visvodaya Engineering College, Kavali, Andhra Pradesh, India, for a brief period from July 2017 to January 2019.

He has enrolled in his doctoral studies at the Department of Civil Engineering, BITS Pilani, under the guidance of Prof. Dipendu Bhunia, BITS Pilani. Dr. Lampros Koutas, Assistant Professor at the University of Thessaly, Greece, became his Co-Supervisor. During his tenure as a research scholar, he has published two technical papers in peer-reviewed journals (three journals yet to be submitted) and has presented papers at three national and international conferences. He also designed a loading frame of 1000 kN in the Advanced Structural Laboratory in the Department of Civil Engineering, BITS Pilani, to mount a Servo-Hydraulic Actuator of 250 kN capacity to carry out the experiments as a part of his research thesis.

Biography of Prof. Dipendu Bhunia (Supervisor)



Prof. Dipendu Bhunia is a professor at the Department of Civil Engineering, BITS Pilani, Pilani Campus. He obtained his B.E and M.E from IEST Shibpur, Howrah (earlier Bengal Engineering College), and completed his PhD from IIT Roorkee in 2010. He is the Faculty-in-Charge of the Estate Management Unit BITS Pilani. His research interests include performance-based seismic design, earthquake-resistant design of structures, concrete technology, and structural health monitoring. He has guided two PhD students and is currently supervising four PhD candidates. His research collaborators include La Trobe University, Australia; University of Thessaly, Greece; Trinity College, Dublin; and Ireland-India concrete research initiative. He has completed research projects funded by diverse bodies, such as the Ministry of Steel Department of Science and Technology (DST), totaling over one million INR. To his credit, he has 75 publications in the top-tier journals and reputed conferences. He has been a member/ secretary/ coordinator of the organizing committees of several conferences and workshops conducted by BITS Pilani and AICTE. He has delivered invited lectures in organizations such as NITTR Chandigarh, NIT Trichy, Trinity College Dublin, Bokaro Steel Plant (SAIL), VNIT Nagpur, Indian Concrete Institute, NIT Warangal, and Jadavpur University. He has been a member of several academic and professional bodies, such as the Indian Society for Earthquake Technology (ISET), Indian Association of Structural Engineers (IStructE), Indian Society for Wind Engineering (ISWE), American Concrete Institute (ACI), American Society of Civil Engineers (ASCE), and Indian Concrete Institute (ICI).

Biography of Dr. Lampros Koutas (Co-Supervisor)



Dr. Lampros Koutas is an assistant professor at the Department of Civil Engineering at The University of Thessaly, Greece, and a Concrete Technology and Reinforced Concrete Structures Lab member in the same department. He has held his current position since October 2018.

His qualifications include a Diploma in Civil Engineering, an MSc in Seismic Design of Structures and a PhD in Civil Engineering from The University of Patras (Greece). He has worked as a Post-Doctoral Research Associate at the Dept. of Civil and Structural Engineering of The University of Sheffield and at the Dept. of Civil Engineering of The University of Nottingham.

He has extensively worked on projects related to composite materials (such as FRP TRM) to retrofit existing reinforced concrete and masonry structures. He has built expertise in using textile-fiber composites in structural and earthquake engineering applications. He has published more than 35 papers in International Journals and Conferences.

He is a member of the fib Task Group 5.1, “FRP Reinforcement for Concrete Structures”, and the RILEM MCC Committee on “Mechanical Characterization and Structural Design of Textile Reinforced Concrete”. He has also reviewed more than 200 papers in 27 International Journals, while he is a member of the International Editorial Board of the ASCE Journal of Composites for Construction.